Far-Infrared Spectroscopy of Weakly Bound Hydrated Cluster Molecules

Andersen, Jonas

Publication date:
2015

Document Version
Publisher's PDF, also known as Version of record

Far-Infrared Spectroscopy of Weakly Bound Hydrated Cluster Molecules

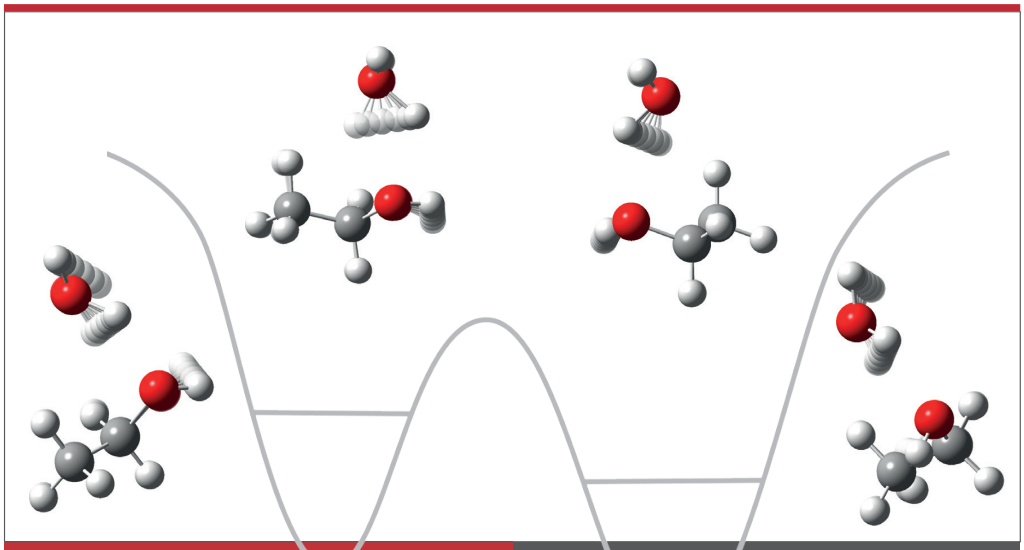

Jonas Andersen
November 2015

PhD thesis

DTU Chemistry
Department of Chemistry

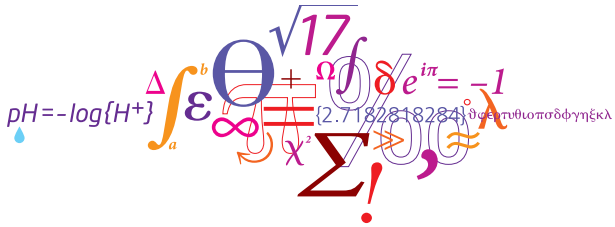

Far-Infrared Spectroscopy of Weakly Bound Hydrated Cluster Molecules

A dissertation presented by

Jonas Andersen, M. Sc.

to

The Department of Chemistry

in partial fulfilment of the requirements

for the degree of

Doctor of Philosophy

in the subject of

Chemistry

Kongens Lyngby 2015

Technical University of Denmark
Department of Chemistry
Kemitorvet, Building 207,
2800 Kongens Lyngby, Denmark
Phone +45 45 25 24 19
www.kemi.dtu.dk

Abstract

The thermodynamic properties of condensed phases, the functionality of many materials and the molecular organization in biological organisms are all governed by the classes of non-covalent interactions that occur already on the microscopic scale between pairs of molecules. A detailed investigation of the intermolecular interactions between prototypical molecular assemblies are valuable for accurate descriptions of larger supramolecular systems such as materials, gas hydrates and biological macromolecules.

The aim of this PhD dissertation is to investigate intermolecular interactions for a series of medium-sized molecular clusters with water by means of far-infrared and terahertz neon matrix isolation spectroscopy. The embedding of non-covalent cluster molecules in solid cryogenic neon matrices at 2.8 K ensures a high sensitivity for *direct* spectroscopic observations of the large-amplitude intermolecular vibrational bands of the cluster molecules in the challenging far-infrared and terahertz spectral regions. A key parameter in the validation of the performance of theoretical predictions for weak non-covalent intermolecular interactions is the dissociation energy D_0 that depends heavily on the class of large-amplitude intermolecular vibrational modes for an accurate estimation of the zero-point vibrational energy.

The spectroscopic observation of intermolecular vibrational modes for the weak van der Waals complex of carbon dioxide and water provides crucial observables for characterization of the shallow potential energy surface spanned between the two molecular subunits. The combination of thick matrices and isotopic substitution of the water subunit allows observation of three intermolecular vibrational modes corresponding to 75 % of the predicted intermolecular zero-point vibrational energy. The combination with high-level electronic structure calculations has enabled a (semi)-empirical value for the dissociation energy D_0 of 738 ± 15 cm^{-1} for the weak van der Waals complex.

The weak intermolecular interactions between unsaturated hydrocarbons and water are investigated by combined infrared and terahertz absorption spectroscopy studies. The hydrogen bond interaction of either C-H $\cdots$ O or O-H $\cdots$ π character can be revealed by the nature of the large-amplitude intermolecular vibrational modes. Two high-frequency librational modes for the water/ethylene dimer reveal an intermolecular O-H $\cdots$ π hydrogen bond, while the single intermolecular acceptor wagging mode for the acetylene/water dimer reveals a C-H $\cdots$ O hydrogen bond. The spec-

troscopic observations in combination with electronic structure calculations enable (semi)-empirical dissociation energies D_0 of 786 ± 25 cm^{-1} for the acetylene/water dimer and 589 ± 25 cm^{-1} for the water/ethylene dimer.

For the first time the embedding of methanol in cryogenic neon matrices allow observation of the intermolecular hydrogen bond donor OH librational mode and the perturbed OH torsional mode of the acceptor molecule for the methanol dimer by far-infrared spectroscopy. The donor OH librational band is blue-shifted by more than 300 cm^{-1} relative to the torsional mode of the methanol monomer. The far-infrared spectroscopy study of mixed alcohol/water complexes embedded in cryogenic neon matrices combined with partial isotopic substitution of individual subunits and annealing of the neon matrix, for the first time allow an unambiguous assignment of the intermolecular high-frequency out-of-plane donor OH librational modes and low-frequency in-plane donor OH librational modes. The vibrational assignments based on isotopic red-shifts *directly* confirm that water is the hydrogen bond donor in mixed binary complexes with methanol, ethanol, isopropanol and *t*-butanol with dissociation energies D_0 of 16.82 $kJ{\cdot}mol^{-1}$, 18.69 $kJ{\cdot}mol^{-1}$, 19.98 $kJ{\cdot}mol^{-1}$ and 20.89 $kJ{\cdot}mol^{-1}$, respectively, for the most stable conformation. The interaction between ethanol and water represents one of the simplest cases of adaptive aggregation where a subunit is forced into its less stable conformation upon complexation. Partial isotopic substitution of the ethanol subunit allows observation of the intermolecular librational modes of two conformations of the ethanol/water dimer with water as the hydrogen bond donor. The weaker cooperative secondary C-H $\cdots$ O hydrogen bond causes a significant blue-shift of the intermolecular low-frequency in-plane donor OH librational mode, which has proven an excellent spectroscopic probe for this interaction. The strength of the primary hydrogen bond manifests itself by the red-shift of the intramolecular donor OH stretching mode and the absolute band origin of the highly localized intermolecular out-of-plane donor OH librational mode. The latter large-amplitude intermolecular out-of-plane donor OH librational mode turns out to be a *direct* probe for the strength of the hydrogen bond interaction, similar to the Badger-Bauer rule.

The hydrogen bond donor/acceptor properties of the alcohol/water interactions can be reversed by substituting hydrogens with fluor, as shown for the interaction between the most simple fluorinated alcohol 2,2,2-trifluoroethanol and water. The nature of the intermolecular interaction is characterized by observation of one high-frequency donor OH librational mode and four intermolecular acceptor vibrational modes for the hydrogen bonded complex of 2,2,2-trifluoroethanol and water. The "high" interaction energy for the most stable geometry of the mixed complex allows this weakly bound cluster to be isolated in supersonic jet expansions, revealing a small spectral blue-shift from gas phase to the cryogenic neon matrix environment of less than 1% for the donor OH librational band. Small spectral blue-shift from gas phase to the cryogenic neon matrix environment are likewise observed for the donor OH librational mode of homodimers of methanol, ethanol, isopropanol and *t*-butanol isolated

in supersonic jet expansions and embedded in cryogenic neon matrices. The experimental observations demonstrate that neon matrix isolation spectroscopy at 2.8 K can provide accurate spectroscopic observables for a series of weakly bound cluster molecules, which allow for accurate assessment of the potential energy surfaces for weakly bound cluster molecules.

Resumé

De termodynamiske egenskaber af kondenserede faser, de mekaniske egenskaber af mange materialer og den molekylære organisering af biologiske systemer er alle kontrolleret af de ikke-kovalente vekselvirkninger mellem molekyler, der allerede forekommer ved den parvise interaktion mellem molekyler på det mikroskopiske niveau. Detaljerede studier af de intermolekylære vekselvirkninger for prototypiske molekylære klynger er værdifulde for nøjagtige beskrivelser af større supramolekylære systemer som materialer, gashydrater og biologiske makromolekyler.

Formålet med denne ph.d.-afhandling har været at studere intermolekylære vekselvirkninger for en serie af mellemstore molekylære klynger med vand ved brug af fjern-infrarød og terahertz neon matrixisolationsspektroskopi. Fastfrysningen af svagt bundne molekylære klynger i inerte matricer af neon ved 2.8 K medfører en høj spektroskopisk følsomhed der muliggør *direkte* spektroskopiske observationer af intermolekylære vibrationssvingninger med store amplituder i de udfordrende fjern-infrarøde og terahertz spektralområder. En nøgleparameter for at kunne validere de teoretiske forudsigelser for de svagt bundne molekylære klynger er dissociationsenergien D_0, der afhænger kraftigt af klassen af intermolekylære vibrationssvingninger for et nøjagtigt estimat af den vibrationelle nulpunktsenergi.

De spektroskopiske observationer af de intermolekylære vibrationssvingninger for det svagt bundne van der Waals kompleks af kuldioxid og vand bidrager med essentielle observable for karakteriseringen af den intermolekylære potentialeoverflade der udspændes af de to molekyler. Kombinationen af høj optisk densitet, tykke matricer og isotopsubstitution af vand muliggør observationen af tre intermolekylære vibrationssvingninger, der tilsammen karakteriserer 75 % af den teoretiske vibrationelle nulpunktsenergi. En (semi)-empirisk dissociationsenergi D_0 på 738 ± 15 cm^{-1} for det svage van der Waals kompleks er baseret på høj-niveau beregninger af elektronstrukturen og spektroskopiske observationer af de intermolekylære vibrationssvingninger.

De svage hydrogenbindinger mellem umættede kulbrinter og vand er undersøgt ved kombineret infrarød og terahertz absorptionsspektroskopi. Hydrogenbindinger af enten C-H $\cdots$ O eller O-H $\cdots$ π karakter kunne påvises*direkte* ved observation af de intermolekylære vibrationssvingninger. To høj-frekvente librationssvingninger for det binære kompleks af ethen og vand afspejler en O-H $\cdots$ π hydrogenbinding, mens en enkelt intermolekylær acceptor vibrationssvinging afspejler en C-H $\cdots$ O hydrogenbin-

ding for det binære kompleks af ethyn og vand. De spektroskopiske observationer kombineret med højt-niveau elektronstrukturberegninger resulterer i en (semi)-empirisk dissociationsenergi D_0 på 786 $\pm$ 25 cm^{-1} for det binære kompleks af ethyn og vand og 589 $\pm$ 25 cm^{-1} for det binære kompleks af ethen og vand.

Den intermolekylære donor OH librationssvinging og hindrede acceptor torsionssvingning er for første gang blevet observeret for dimeren af methanol ved at fange det hydrogen-bundne kompleks i inerte matricer af neon. Donor librationssvingingen er blåforskudt med mere end 300 cm^{-1} i forhold til torsionssvingningen i det isolerede methanolmolekyle. Det fjerninfrarøde spektroskopiske studie af blandede alkohol/vand klynger fastfrosset i inerte neon matricer kombineret med delvis isotopsubstitution og kontrolleret opvarmining af matricen, har for første gang tilladt en utvetydig tilordning af både den højfrekvente donor OH librationssvingning og lavfrekvente donor OH librationssvinging. De vibrationelle tilordninger baseret på isotopiske rødforskydninger bekræfter *direkte* at vand er hydrogenbindingsdonor i blandede binære molekylære klynger med methanol, ethanol, isopropanol og *t*-butanol med estimerede bindingsenergier på henholdsvis 16.82 $kJ{\cdot}mol^{-1}$, 18.69 $kJ{\cdot}mol^{-1}$, 19.98 $kJ{\cdot}mol^{-1}$ og 20.89 $kJ{\cdot}mol^{-1}$ for det mest stabile kompleks. I den mest stabile konformation af det binære kompleks af ethanol og vand skifter konformationen af ethanol fra *trans* til *gauche* under dannelsen af den intermolekylære hydrogenbinding. Delvis isotopsubstitution af ethanol i ethanol/vand komplekset muliggør observation af to forskellige konformerer af det svagt bundne kompleks med vand som hydrogenbindingsdonor. Den svage kooperative sekundære hydrogenbinding forårsager en blåforskydning af den lavfrekvente donor OH librationssvingning, som har vist sig at være en fremragende spektroskopisk sensor for denne hydrogenbinding. Bindingsenergien af den intermolekylære hydrogenbinding afspejles i en rødforskydning af den intramolekylære donor OH strækningsvibrationssvinging og ved en blåforskydning af den intermolekylære isolerede højfrekvente donor OH librationssvingning. Den sidstnævnte intermolekylære donor OH librationssvingning har vist sig at være en *direkte* sensor for bindingsenergien af den intermolekylære hydrogenbinding, svarende til Badger-Bauer reglen.

Et modsat donor/acceptor hydrogenbindingsforhold kan opnås ved substitution af hydrogen med fluor, illustreret ved det binære kompleks af den mest simple flourerede alkohol, 2,2,2-trifluoroethanol, og vand. Dette modsatte hydrogenbindings donor/acceptor forhold er blevet observeret for en enkelt højfrekvent donor OH librationssvinging og fire intermolekylære acceptor vibrationssvingninger for det binære kompleks af vand med 2,2,2-trifluoroethanol. Den "stærke" bindingsenergi for den mest stabile konformer af det blandede kompleks muliggør studier af dette kompleks i adiabatiske ekspansioner, hvor en lille blåforskydning på mindre end 1% er observeret fra gasfase til det inerte neon matrix miljø. Denne lille blåforskydning er ligeledes blevet observeret for en række homodimerer af methanol, ethanol, isopropanol og *t*-butanol isoleret i gas fase og i neon matricer. De eksperimentelle observationer demonstrerer at neon matrixisolationsspektroskopi bidrager med nøjagtige spektroskopiske

observable for en serie af svagt-bundne molekylære klynger, der muliggør validering af teoretiske potentiale overflader for svagt bundne molekylære klynger.

Preface and Acknowledgements

This dissertation is submitted in partial fulfilment of the requirements for the degree of Doctor of Philosophy from the Technical University of Denmark (DTU). The dissertation is based on experimental work from September 2012 to November 2015 under the supervision of main supervisor Associate Professor René Wugt Larsen and co-supervisor Associate Professor Kenny Ståhl. The project was funded by the Technical University of Denmark.

First and foremost, I would like to express my sincere gratitude towards my two supervisors Associate Professor Kenny Ståhl and Associate Professor René Wugt Larsen, for their help, advice, guidance and support during my time as a PhD student at DTU.

I would like to thank Associate Professor René Wugt Larsen for introducing me to the fascinating world of low-temperature chemistry and physics, and for introducing me to the advanced spectroscopic methods used in this study. I highly appreciate the numerous discussions on scientific as well as non-scientific matters during the previous three years. I would like to thank Associate Professor Kenny Ståhl for help and support during my studies

I am grateful to Professor Per Uvdal, Associate Professor Emeritus Bengt Nelander, Beam-line Manager Anders Engdahl and Beam-line Scientist Jimmy Heimdal for the collaboration at the MAX IV Laboratory, University of Lund for the past three years. I highly appreciate the many good times at the synchrotron facility. Additional thanks to Jimmy Heimdal for assistance with the CCSD(T)-F12 calculations at LUNARC.

I am grateful to Professor Dr. Martin Suhm for letting me visit his group at the Georg-August Universität in Göttingen, Germany. I would like to thank PhD student Matthias Heger and Dr. Franz Kollipost for introducing me to the *filet*-jet setup and for the collaboration on alcohol dimers. It has been a pleasure to visit Göttingen.

I would like to thank the students, faculty and staff at the Department of Chemistry for giving me an inspiring and dynamic workplace. To PhD Phillip Malcho, postdoc Christian Engelbrekt and PhD student Peter L. Thomassen - a thank you for the numerous discussions during the inevitable coffee breaks. The discussions often got diverted from scientific matters.

I am grateful for a generous allocation of computational resources at the High Performance Computing services associated with the DTU Computing Center and the STENO cluster at the Department of Chemistry.

I acknowledge grants from the Danish Center for Synchrotron Studies (DANSCATT) for far-infrared experiments at beamline 02B1-1 at the Canadian Light Source Facility in Saskatoon, Saskatchewan, Canada and X-ray diffraction experiments at beamline I811 at the MAX IV Laboratory, University of Lund, Sweden. I acknowledge a travel grant from the Idella Foundation to cover the experimental stays at the Georg-August Universität in Göttingen, Germany. I acknowledge support from the Otto Mønsted Foundation for my participation in the 62^{nd} Pacific Conference on Spectroscopy and Dynamics in Pacific Grove, California, USA.

In closing, I would like to thank my family and friends for their love and support. To my brother Mads and my parents Birgitte and Stig - for the life lessons and for the everlasting love and support. I am forever grateful.

Jonas Andersen, M. Sc.
Kongens Lyngby, Denmark, 30-November-2015

Enclosed Peer-Reviewed Journal Publications

---

1. **Communication: THz absorption spectrum of the CO_2 - H_2O complex: Observation and assignment of intermolecular van der Waals vibrations**, J. Andersen, J. Heimdal, D. W. Mahler, B. Nelander, and R. Wugt Larsen, *The Journal of Chemical Physics 140, 091103 (2014)*

2. **The effect of hydrogen bonding on torsional dynamics: A combined far-infrared jet and matrix isolation study of methanol dimer**, F. Kollipost, J. Andersen, D. W. Mahler, J. Heimdal, M. Heger, M. A. Suhm, and R. Wugt Larsen, *The Journal of Chemical Physics 141, 174314 (2014)*

3. **The influence of large-amplitude librational motion on the hydrogen bond energy for alcohol-water complexes**, J. Andersen, J. Heimdal, and R. Wugt Larsen, *Physical Chemistry Chemical Physics 17, 23761–23769 (2015)*

4. **Spectroscopic identification of ethanol-water conformers by large-amplitude hydrogen bond librational modes**, J. Andersen, J. Heimdal, and R. Wugt Larsen, *The Journal of Chemical Physics, accepted, (2015)*

Contents

Chapter 1

Introduction

The unlimited number of chemical and biological systems, their macroscopic properties and functionalities, the many natural phenomena people encounter on a daily basis, are demonstrations of the collective behavior of atoms and molecules governed by a subtle interplay between several different types of intermolecular interactions on the microscopic level. That is why, for a better understanding of the many physical, chemical and biological processes, and optimization of various applications relevant to biotechnological-, chemical-, pharmaceutical-, and petrochemical-industries it is necessary to study the interactions between molecules.

Besides the well-established covalent bonding between atoms, another class of interactions exists between atoms and molecules. These are known as non-covalent interactions. Many chemical and biological processes occur in condensed phase where non-covalent interactions play a significant role in liquids, solvation phenomena, the secondary structure of biological macromolecules, molecular recognition, supramolecular chemistry and crystal packing. [1]. The molecular conformation, a result of the weak intermolecular interaction with the environment and the weak intramolecular interaction, determines the reactivity and functionality of biomolecules [2]. For a large number of chemical and biological phenomena, such as molecular recognition, molecular transport through biological membranes, drug-receptor matching, virus detection and enzyme catalysis, not only the conformation of the involved molecules are important but also the interactions with the surrounding environment. Thus, in real chemical and biological systems, the conformational shape and reactivity properties are governed by a subtle balance between intra- and inter-molecular interactions. The thermodynamic behavior of condensed bulk phases, described by phase diagrams, diffusion rates, viscosities and fluid dynamics are mainly caused by the weak non-covalent interactions.

Highly advanced quantum-chemical methodologies have been developed to describe the non-covalent interactions with high accuracy. As the electronic structure calculations scale extremely fast with the number of electrons, highly accurate description of the previously mentioned systems of relevance to the sciences of energy, materials and

life is almost out of reach even with modern super computers. Spectroscopic studies of gas-phase isolated fundamental weakly bound finite-sized molecular complexes provide important observables that allow for robust assessment of the performance of the developed quantum-chemical methodologies and provide valuable experimental observables for many macroscopic systems.

1.1 Intermolecular Interactions

The formation of a chemical bond is a quantum chemical phenomenon of the interaction between two atoms resulting in the formation of a molecule. The covalent bond between atoms is formed by sharing an electron pair between two atoms leading to a minimization of the total energy of this system and a covalent bond energy is in the order of 400 kJ·mole^{-1} [3].

In isolated molecules the negatively charged electron shell shields off the positively charged molecular core, leading to a neutral system. When molecules are close to each other, the electron shell experiences not only the influence from their own positively charged molecular core but also the presence of electron shells from surrounding molecules. This presence leads to a deformation and redistribution of the electron charge within the molecules, resulting in an incomplete shielding of the positively charged molecular cores and the appearance of locally charged molecular species. Molecules thus interact with each other by electrostatic forces acting between positively charged molecular cores and negatively charged electron shells. The non-bonding interactions are referred to as non-covalent interactions to distinguish the interaction from covalent chemical bonds, and can be either *attractive* or *repulsive*. The *attractive* forces are classified as *electrostatic, induction* and *dispersion*, while the *repulsive* interactions are caused by the Pauli exclusion principle [4]. The *repulsive* intermolecular interaction arise when two molecules are close to each other. It can be explained by the Pauli exclusion principle, which prohibit electrons from one molecule to penetrate the occupied molecular orbitals of the other molecule. The consequence is that electrons of the same spin are kept apart by a repulsive exchange interaction. The exchange interaction, E_{exch} can be formulated as

$$E_{exch} = A \cdot e^{-\frac{2r}{a_0}} \tag{1.1}$$

where a_0 is the Bohr radius of the hydrogen atom, A an empirical constant and r the intermolecular distance.

Permanent charge distributions can be expanded as a series of multipole moments, such as dipoles and quadrupoles. Two molecules interact with each other through the interaction of the static multipole moments of their charge distribution. That is why

this type of intermolecular interaction is referred to as *electrostatic*, and the resulting energy term is denoted E_{el} and can be defined as:

$$E_{el} = \frac{q_A q_B}{|\mathbf{r}|} + \frac{q_A|\mu_B|}{\mathbf{r}^2} + \frac{q_B|\mu_A|}{\mathbf{r}^2} + \frac{\mu_A \cdot \mu_B}{|\mathbf{r}|^3} + \frac{q_A Q_B}{|\mathbf{r}|^3} + \frac{q_B Q_A}{|\mathbf{r}|^3} + \frac{\mu_A \cdot Q_B}{\mathbf{r}^4} + \frac{\mu_B \cdot Q_A}{\mathbf{r}^4} + \frac{Q_A Q_B}{|\mathbf{r}|^5} + ... \tag{1.2}$$

where q, μ, Q and $\mathbf{r}$ stand for the electric charge, electric dipole moment, electric quadropole moment and the position vector of the second molecule, B, relative to the first molecule, A. The electrostatic energy thus depends both on the magnitude and orientation of the multipoles, which causes the molecules to be oriented in a way that minimizes the overall electrostatic interaction energy. The magnitude of the higher-order terms in the multipole expansion decreases rapidly with the intermolecular distance, due to the inverse power law, and the interaction energy can be described fairly accurate by including only the first terms in the multipole expansion. However, some molecules do not have low-rank multipoles due to symmetry and higher-order terms have to be included.

The *induction* interaction between two molecules originates from the interaction between a permanent dipole in one molecule with the induced dipole moment in the other molecule. The magnitude of the induced dipole moment depends on the magnitude of the permanent dipole moment, the distance between the two molecules and the polarizability α of the molecule for which the dipole moment is induced. The potential energy of the induction interaction, E_{ind}, can be written as:

$$E_{ind} = -\frac{1}{2}\alpha_B \left(\frac{q_A^2}{\mathbf{r}^4} + f_1(\mu_A, \mu_B)\frac{\mu_A^2}{\mathbf{r}^6} + f_2(\mu_A, \mu_B)\frac{Q_A^2}{\mathbf{r}^8} \right) \tag{1.3}$$

The molecule with the permanent multipole is denoted A, and the molecule with induced dipole moment is denoted B. The functions f_1 and f_2 depend on the relative orientation of the two molecules.

The *dispersion* interactions constitute the last attractive intermolecular interaction. The interaction arises from the mutual polarization of the constant fluctuating electron density distribution of the molecules A and B. They were first described by London, and have since then also been known as London interactions. The potential energy of dispersion interactions, E_{disp} can be written as

$$E_{disp} = -\frac{C_6}{\mathbf{r}^6} - \frac{C_8}{\mathbf{r}^8} - \frac{C_{10}}{\mathbf{r}^{10}} - ... \tag{1.4}$$

C_6, C_8 and C_10 are empirical constants and $\mathbf{r}$ is the position vector of molecule B relative to molecule A. The interaction is the weakest among the attractive interactions, but gains significant importance in nonpolar molecular complexes where it is the only

attractive interaction of the three attractive interactions, e.g. in complexes of noble-gas atoms or hydrocarbons. The importance of this class of non-covalent interactions increases with the number of electrons for the molecular system. The dispersion interaction can likewise be realized as an intramolecular force; linear unsaturated hydrocarbons of a moderate length prefer a fully extended all *trans* conformation, but will fold at a certain length due to weak dispersion forces [5].

The net effect of the intermolecular interactions is co-operative subtle balance between the *repulsive* and *attractive* interactions, resulting in a weak intermolecular interaction that differs from the strong covalent bonds between atoms. The total intermolecular interaction can be described as:

$$E_{int} = E_{el} + E_{ind} + E_{disp} + E_{exch} \tag{1.5}$$

The balance between the attractive and repulsive potentials often leads to an equilibrium configuration at which net interaction energy has a minimum, as illustrated in Figure 1.1.

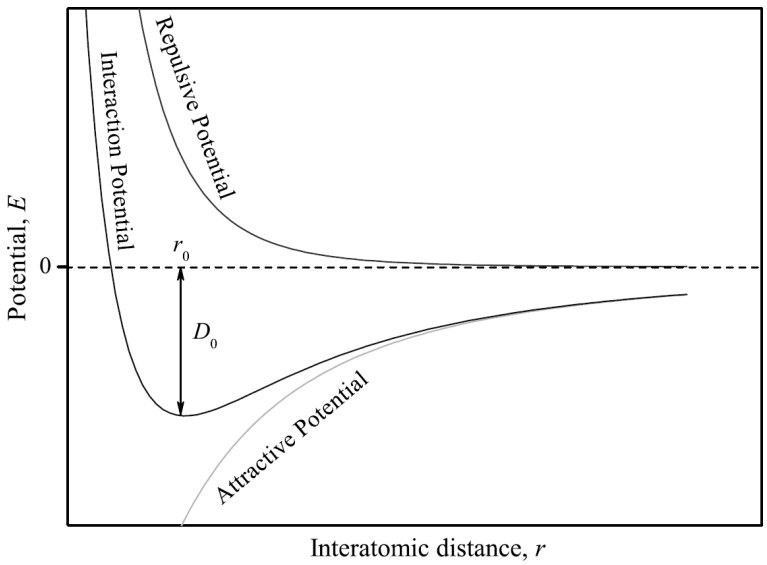

Figure 1.1: A schematic representation of the repulsive, attractive and total intermolecular interaction.

The combination of the different weak intermolecular interactions leads to many different bonding patterns and it is difficult to make a clear distinction between the different types of interactions. In general, the van der Waals interaction is used to

describe intermolecular interactions such as dispersion interactions, dipole-dipole interactions and induced dipole-dipole interactions. A "general" interaction energy of 8 kJ·mole^{-1} [3] has been reported for the class of intermolecular van der Waals interactions, however, the many combinations of intermolecular interactions make this a very crude generalization.

Another class of intermolecular interactions is the strong intermolecular hydrogen bond. Hydrogen bonds are one of the most important types of weak non-covalent interactions, and is responsible for many properties in liquids as well as chemical and biological systems. A hydrogen bond has a general motif of X-$H \cdots Y$, where the X-H group is the proton donor and Y the acceptor. Usually, X is an electronegative atom such as oxygen, nitrogen, chlorine or fluorine and Y is most typically an atom possessing an available lone pair of electrons. The hydrogen acceptor can also be a π-electron cloud, such as those in aromatic rings and between carbon atoms in carbon-carbon double and triple bonds. This type of hydrogen bond interaction is highly important in determination of the secondary structure of biological macromolecules. IUPAC [6] has defined several criteria for a hydrogen bond, including:

- *The forces involved in the formation of a hydrogen bond include those of an electrostatic origin, those arising from charge transfer between the donor and acceptor leading to partial covalent bond formation between H and Y, and those originating from dispersion.*
- *The atoms X and H are covalently bonded to one another and the XH bond is polarized, the $H \cdots Y$ bond strength increasing with the increase in electronegativity of X.*
- *The $XH \cdots Y$ angle is usually linear (180°) and the closer the angle is to 180°, the stronger is the hydrogen bond and the shorter is the $H \cdots Y$ distance.*
- *The length of the XH bond usually increases on hydrogen bond formation leading to a red shift in the infrared XH stretching frequency and an increase in the infrared absorption cross-section for the X-H stretching vibration. The greater the lengthening of the X-H bond in X-$H \cdots Y$, the stronger is the $H \cdots Y$ bond. Simultaneously, new vibrational modes associated with the formation of the $H \cdots Y$ bond are generated.*

Hydrogen bonds weaken the covalent bonding between X-H leading to an elongation of the bond and a red-shift of the donor X-H stretching vibration. One can argue that a charge transfer takes place from the electron lone pair or the π-electron cloud from the proton acceptor to the antibonding orbitals of the proton donor. This causes an increase in electron density of the antibonding orbitals and thus a weakening and elongation of the X-H chemical bond [7]. The size of the red-shift is thus a direct indication of the strength of the intermolecular interaction.

The traditional strong hydrogen bonds, such as a N-H $\cdots$ O and O-H $\cdots$ O typically have interactions energies of 20 - 40 kJ·mole^{-1} [3]. The class of weak hydrogen bond including C-H $\cdots$ O and O-H $\cdots$ π interactions has smaller binding energies in the range of 2 to 20 kJ·mole^{-1} [3].

The extended disordered intermolecular hydrogen bond networks found in strongly associating liquids such as liquid water and liquid alcohols determine to a large extend their unique physical and chemical properties. The low interaction energies for the class of intermolecular hydrogen bonds allow the hydrogen bonds to freely associate and dissociate under ambient conditions making it an important class of intermolecular interactions for the study of intermolecular energy transfer [8].

Water is of fundamental importance to life on Earth. The oceans cover about 70 % of the Earth's surface and the abundance of water varies between 1 and 2% in the atmosphere. The remaining atmosphere consists of more than 99% non-polar molecules such as N_2 and O_2. As diatomic linear molecules do not absorb infrared radiation, water molecules and hydrated cluster molecules have a great effect on the green house effect on Earth and the radiative transfer through planetary atmospheres [9]. Water is not a simple liquid, it possesses strong intermolecular polar hydrogen bonds that are responsible for the many unique macroscopic properties. The increased melting and boiling points are higher than for comparable molecules, due to the unique dual hydrogen bond donor/acceptor properties of the water molecule. In solid face a single water molecule creates hydrogen bonds with four other water molecules, thus creating an extended crystal structure. The number of hydrogen bonds are slightly less in liquid water due to the continuously association and dissociation of hydrogen bonds between water molecules. Under the right conditions gas phase water molecules can create cluster molecules such as dimers, trimers, etc.

The exploration of intermolecular interactions, the structure and the binding preferences of small water clusters provide a key for understanding bulk water in solid and liquid states. The combination of *ab initio* quantum chemical calculations and high-resolution spectroscopy have been successful in describing such structures [10], as illustrated by the determination of the prototypical O-H $\cdots$ O hydrogen bonding in the water dimer. The structure of the water dimer has been determined by rotational spectroscopy by Dyke and Muenter [11], revealing a hydrogen bonded cluster of C_s symmetry, as illustrated in Figure 1.2a.

The formation of an intermolecular hydrogen bond results in a red-shift of the donor O-H stretching mode as observed for the water dimer by Huang and Miller [12] and by Page *et al.* [13]. Figure 1.2b illustrates the red-shifted donor OH stretching mode for the water dimer that provides an *indirect* qualitative description of the intermolecular binding energy [14]. The class of large-amplitude intermolecular vibrations has been characterized by vibration-rotation-tunneling spectroscopy by the

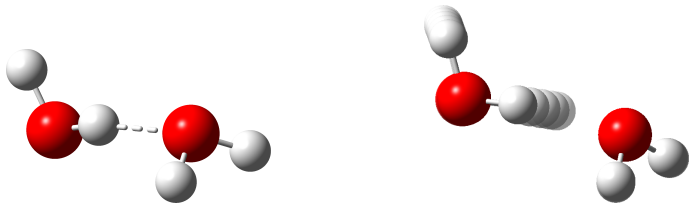

(a) Minimum energy geometry of the water dimer

(b) Normal mode illustration of the red-shifted symmetric donor OH stretching for the water dimer.

Figure 1.2: Minimum energy geometry of the water dimer (a) at the MP2/aug-cc-pVQZ level of theory and a normal mode illustration of the red-shifted symmetric donor OH stretching of the water dimer (b).

group of Saykally [15] and several far-infrared and terahertz absorption spectroscopy studies of water embedded in cryogenic neon matrices by Ceponkus *et al.* [16–20] and by Bouteiller and Perchard [21, 22]. A normal mode illustration of two of the assigned intermolecular vibrations are illustrated in 1.3. The spectroscopic observables based on rotational microwave spectroscopy, mid-infrared spectroscopy for perturbed monomer fundamental vibrations and combined far-infrared and terahertz spectroscopy for characterization of the class of large-amplitude intermolecular vibrations allow for validation of a high-level theoretical potential energy surface by Shank *et al.* [23] and ultimately comparison with the experimentally determined dissociation energy D_0 of 1105 $\pm$ 10 cm^{-1} [24] for the hydrogen bonded water dimer.

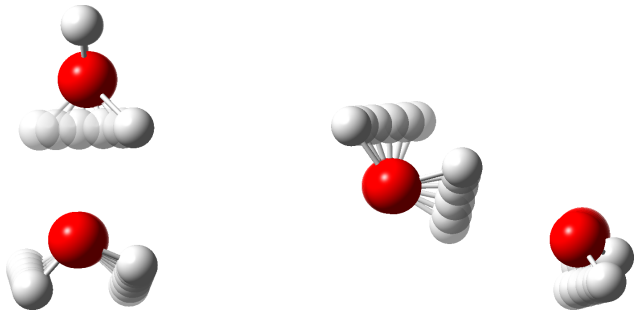

(a) out-of-plane bending mode

(b) in-plane bending mode

Figure 1.3: Normal mode illustrations of two intermolecular vibrations for the water dimer following the notation by Ceponkus *et al.* [18]

The interaction energy in the water dimer, the so-called two-body term, has been shown to account for approximate 80 % of the intermolecular interaction for the water hexamer. An accurate description of the interaction energy of the water dimer is

thus a very important step towards an accurate description of liquid water properties [25].

1.2 Weakly Bound Cluster Molecules

Weakly bound cluster molecules held together by non-covalent interactions can be viewed as finite-sized pieces of the condensed phases of matter. From both an experimental and theoretical perspective, the finite-size of the molecular clusters are of great advantage in simplifying the system, allowing accurate molecular level characterization of intermolecular interactions. The ability to prepare molecular clusters by adding one molecule at a time help to explore how the structures as well as the dynamics change with the size, ranging from gas phase isolated small clusters towards the bulk limit. The most detailed information can be gained for binary complexes, dimers, where the intermolecular potential energy surfaces can be characterized accurately by vibrational spectroscopy. Studies of larger molecular complexes beyond dimers provide information about many-body interactions, which are essential for describing bulk systems in more details.

Theoretical methodologies have been developed for accurate and quantitatively description of weak intermolecular interactions and can, in principle, provide all desired properties of the investigated molecular clusters entirely from first principles. Thus experimental observations of the weak non-covalent interactions are of paramount importance to the validation of the theoretical methodologies.

The intermolecular potential energy surface is a function of the geometry of the involved monomers and the intermolecular interactions. The flexibility of the intermolecular interaction may cause the potential energy surface to have several minima, corresponding to local minimum energy conformations. A key parameter in the validation of the theoretical predictions is the dissociation energy D_0 of the non-covalent interaction, which depends on the theoretical dissociation energy D_e and the zero-point vibrational energy for the weakly bound molecular cluster that requires accurate and reliable band origins, especially for the class of large-amplitude intermolecular vibrations that are difficult to predict by theory due to their anharmonic character. The dissociation energy D_e for the molecular complex can be expressed by the "supermolecule" approach, in which the dissociation energy is the difference between the energy of the molecular cluster (the "supermolecule") and the isolated monomers. The experimental observation of the large-amplitude intermolecular vibrational bands in the challenging far-infrared and terahertz provides a *direct* probe of the potential energy surface that can be used to validate the theoretical predictions.

The motions of a molecule of N atoms can be described by $3N$ degrees of freedom

in relation to the cartesian coordinates (x, y, z). The degrees of freedom describe the rotational, translational and vibrational motions of a molecule. Three degrees of freedom are necessary for describing translational motion and three degrees of freedom for describing the rotational motion for non-linear molecules, leaving $3N - 6$ degrees of freedom for vibrational modes. For a linear molecule the number of vibrational modes become $3N - 5$ as only two cartesian axes are necessary for describing rotational motion. Three translational and three rotational degrees of freedom of a subunit in a molecular cluster are converted into a new class of intermolecular vibrational degrees of freedom upon complexation. These intermolecular vibrations involve large-amplitude motions of the subunits with respect to each other and the corresponding vibrational transition will typically appear in the far-infrared and tera-hertz regions. For a detailed description of vibrational spectroscopy readers are referred to leading textbooks [26–29].

A simple potential energy landscape is shown Figure 1.4 for a case with two potential energy minima. The potential energy landscape could correspond to the two conformations of the mixed methanol/water dimer, but could also represent a potential energy surface for a biological macromolecule in its folded and unfolded conformation. The unfolded geometry corresponds to a local minima (to the left in Figure 1.4). In order for the molecule to be trapped in its global folded minima (to the right in Figure 1.4) it must overcome the energy barrier between the minima.

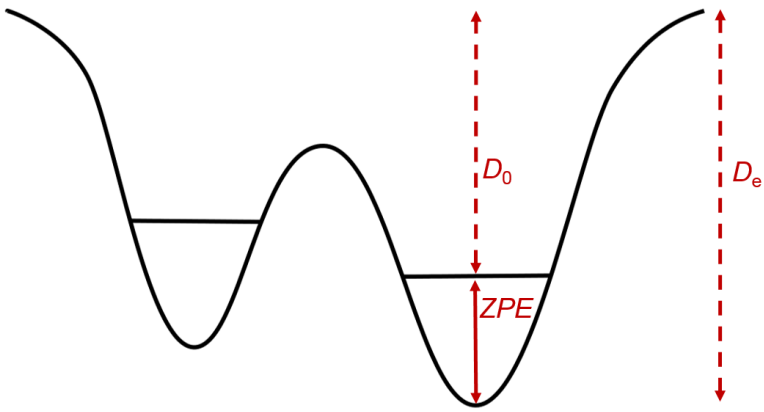

Figure 1.4: The dissociation energy (D_e), the dissociation energy (D_0) and the zero-point vibrational energy (ZPE) illustrated for an anharmonic potential with two potential energy minima.

Several challenges exist for experimental observations of weak intermolecular com-

plexes. For instance, the structures of weakly bound molecular clusters are not directly observable and can only be determined by pure rotational spectroscopy and high spectral resolution. Microwave [30] and vibration-rotation-tunneling [31] resolved terahertz laser spectroscopic studies of weakly bound cluster molecules isolated in supersonic jet expansions have helped to determine many important molecular clusters.

Spectroscopic studies of the vibrational energy levels are necessary for a quantitative investigation of the intermolecular potential energy surface, either by *indirect* observation of perturbed monomer vibrational fundamental transitions in the mid-infrared region or by *direct* observation of the large-amplitude intermolecular vibrational transitions in the far-infrared and terahertz regions. Fourier transform spectroscopy [32, 33] owing to the multiplex advantage complements the more selective and restricted laser spectroscopy methods, e.g. cavity ring down laser spectroscopy (CRDLAS) [34–36] and tunable diode laser spectroscopy (TD-LAS) [37].

The minima on the potential energy surface correspond to different conformations of the weakly bound molecular cluster. Each minima are characterized by a "local" force field and a corresponding set of vibrational modes, which allow for experimental observation and characterization. The results obtained from vibrational spectroscopy, the band origins and intensity, thus allow for determination of the global energy minimum and possible higher energy minima in combination with theoretical first principles predictions. A particularly sensitive probe of intermolecular hydrogen bonding is the large-amplitude donor librational motions of the central hydrogen atom in the hydrogen bond. The librational motion strongly depends on the cluster size, symmetry and hydrogen bond strength [38–40]. These librational motions can be observed in the region below 800 cm^{-1} [39]. The large-amplitude and thereby highly anharmonic vibrational motion of the librational modes will therefore have a significant impact on both the intermolecular zero-point vibrational energy and the vibrational spectra of a molecular complex [32].

1.3 The Experimental Approach

Studying species that are unstable under ambient conditions, such as ions, radicals and weakly bound clusters, one must attempt to trap them in conditions where the species can be studied to gain insight into the electronic and molecular structure. Conditions are sought after where the experimental results can be directly compared with theoretical predictions, i.e. isolated molecules at low temperatures. Due to the Boltzmann distribution of populated energy levels, only the ground state energy level will be populated at low temperatures and favor the observation of fundamental transitions, as illustrated in Figure 1.5, where the molecule is cooled to the absolute minimum temperature to the right. The low temperature makes it easier to assign precise fundamental vibrational band origins without overlapping hot bands. The hot bands at increased temperatures shift the band origins of the vibrational bands and thereby increase the uncertainty of the experimental assignments.

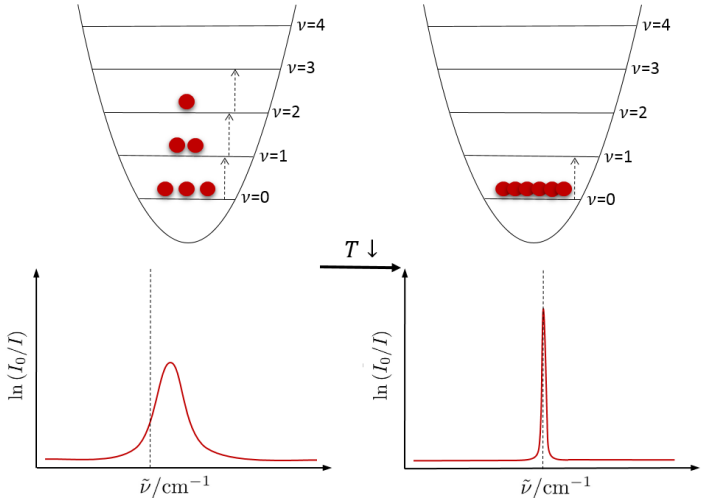

Figure 1.5: The vibrational transitions from populated energy levels and the corresponding band profile at very low temperature (to the right) and at an increased temperature (to the left).

Several experimental approaches based on complementary infrared and terahertz spectroscopy can be used to reach those conditions. One technique that probes the molecules in the vibrational and rotational ground state is the high-throughput supersonic jet expansions, where temperatures below 20 K can be reached. The technique is efficient when one wants to study monomers and molecular clusters in gas phase by spectroscopy. The sample gas is diluted with an inert rare gas and adiabatically

expanded through a nozzle into vacuum. The difference in pressures between the sample region and the vacuum region causes an acceleration of the molecules when they are expanded into vacuum. The first stage of the process is characterized by a high number of collisions and high velocity of the gas in the direction of the expansion. In the second stage, the molecules gain a narrow velocity distribution equal to the velocity of the carrier gas due to the high number of collisions and "freeze" the internal degrees of freedom. This leads to a significant reduction of the population in the rotational and vibrational excited levels and simplifies the recorded spectrum. As there are no collisions between the sample gas molecules after the first stage of the expansion, given the very narrow velocity distribution, the weakly bound molecular assemblies formed in the first stage will survive long enough to be observed [32]. The *filet* experi-mental approach developed in Göttingen, used in this study, is described in detail in the cited references [41, 42]. The vibrational transitions of the sample molecules are probed by a single optical path of 60 cm of a gas mixture that consists of 99 % helium carrier gas and approximately 1% sample. The spectroscopic sensitivity of this Fourier transform infrared spectroscopy and supersonic jet approach becomes smaller in the far-infrared and terahertz regions where the emission from conventional blackbody radiation sources is drastically lowered.

An alternative and more sensitive approach to study weakly bound molecular assemblies is to trap the species in a cryogenic environment of solid inert noble gas. This method ensures a higher optical density of the weakly bound molecular clusters and allow for the samples to be probed over a longer period of time relative to the many short pulses in the supersonic jet spectroscopy approach. The method is known as “Matrix Isolation” and was first used by G. Pimentel [43–45], who together with G. Porter [46] pioneered the matrix isolation field. The method refers to a technique in which the sample gas is mixed with a large excess of a typically inert host gas and condensed on a cold surface to ensure rapid phase transition from gas to solid. Ideally, one ends up with each sample molecule immobilized and encapsuled by one or more layers of the inert host material. The sample molecules are thus “isolated” from other sample molecules in the “Matrix” of the host gas. One tries to create an environment that provides a minimum of interaction with the investigated sample and noble gases such as argon or neon are the best choices. In many cases heavier noble gases such as krypton and xenon and even nitrogen, methane or oxygen have been used as matrix gas. As all atomic and homonuclear diatomic gases except *para*-hydrogen are transparent in the infrared and terahertz region they represent an ideal matrix host material for matrices.

Mid-infrared absorption spectroscopy has been used for many decades to study intermolecular interactions. The intermolecular interactions are *indirectly* investigated for the involved subunits and the perturbed force fields are easily observable for strongly bound cluster molecules. Far-infrared and terahertz spectroscopy below 600 cm^{-1} provides *direct* information on intermolecular interactions given that the large-amplitude intermolecular vibrational modes of weakly bound clusters molecules are

observed in this region. The combination of far-infrared spectroscopy for *direct* observations of the large-amplitude intermolecular vibrations and the matrix isolation approach to compensate for the poor radiation sources by a higher optical density is an attractive tool for studying weakly bound molecular complexes.

An essential factor in making cryogenic matrices of good optical property is the packing of the matrix. The packing often depends on the temperature and the speed of the deposition. The matrix must be rigid at all times during deposition to prevent diffusion and change of the sample, which is the case if the temperature is below one third of the melting temperature (T_m). The matrix becomes semi-rigid when the temperature increases above 1/3 of T_m and reordering of the matrix takes place including build up of larger molecular clusters, as small molecules such as water can move inside the solid matrix [47].

A certain amount of diffusion is always present during deposition of the matrix. As hot gas hits the surface of the cold matrix the temperature increases slightly and diffusion occurs. Increased diffusion can be avoided if the temperature of the matrix stays below 1/3 of T_m during deposition.

Several possibilities exist for the placement of a molecule in a matrix. One is the placement of a molecule in an interstitial site, i.e. between close packed matrix atoms in an inert lattice. This option is only possible for very small species such as monoatomic ions and a more likely possibility is the substitutional site where one or more matrix atoms are substituted with a sample molecule [48].

Another important point is the degree of isolation of the matrix isolated species, where the probability of interaction depends among other things on the ratio between matrix and sample gas, the size of the substitutional site and the purity of the matrix gas. For instance, a 1% impurity of nitrogen would result in 12 % of all sites in the matrix having at least one nitrogen molecule in the surroundings [47].

The matrix material influences the observed vibrational transitions, depending on the free volume of the substitutional site inside the matrix material and the dispersion interaction between the sample molecule and the matrix material. The size of the cavity in the matrix even allows smaller molecules to rotate freely, with the spectral shift from gas phase depending on the host matrix. Larger noble gases such as xenon and krypton have a large effect on the vibrations, whereas helium, *para*-hydrogen and neon perform much better [18].

Matrix isolation using *para*-hydrogen as host material should provide more free space for guest molecules than noble gas matrices. Consequently, the perturbations caused by the interactions with the *para*-hydrogen matrix are small and the isolated cluster molecules should behave almost as in the gas phase. It remains to be seen whether the larger cavity in the *para*-hydrogen crystal provides a better matrix material for

studying the large-amplitude librational transitions in the far-infrared and terahertz regions. The smallest band shifts are observed in Helium Nanodroplet Spectroscopy, however, this action spectroscopy approach is restricted by the availability of lasers at all wavelengths - especially in the challenging but highly rewarding far-infrared and terahertz regions.

The rotational transitions are hindered for larger molecules, making it possible to observe the vibrational band centers directly. These band positions are slightly shifted from gas phase values depending on how perturbing the matrix host environment is.

A highly unwanted feature for matrix environments such as argon and nitrogen is the appearance of site effects, i.e. molecules are trapped in different sites in the matrix environment. The different environment will result in several bands appearing for the same intramolecular vibrational transition as the geometry is slightly perturbed depending on the site. Strongly perturbing matrix environments such as N_2 will have site effects, but more importantly the matrix environment can change the weak interactions between molecules, as seen for the methanol/water interaction in a nitrogen matrix observed by Perchard [49] relative to the gas phase [50] and cryogenic neon [51] observations.

The intermolecular vibrations can be regarded as hindered rotation of an entire subunit. Deploying a matrix that is as non-perturbing as possible to allow for almost free large-amplitude vibrations is important to observe the gas phase intermolecular vibrations.

The ideal situation is to observe gas phase isolated clusters trapped in the vibrational ground state. In supersonic jet expansions the weakly bound cluster molecules are relaxed into the vibrational ground state. However, when dealing with weak molecular clusters, weak absorbers and a region with limited intensity of light, matrix isolation spectroscopy seems an ideal compromise.

1.3.1 Fourier Transform Infrared Spectroscopy

Infrared spectroscopy studies the interaction between molecules and electromagnetic radiation in the infrared region. The absorbance of energy can cause molecular vibrational and rotational transitions that can be studied using spectrometers. Traditional spectrometers used a dispersive element to select the wavelength of the ingoing beam to sample. Modern spectrometers are based on the Michelson interferometer developed in the 1880's. Instead of a wavelength scan with the dispersive element which was the case of the old traditional spectrometers, each interferometer scan generates an interferogram that contains information for the entire spectrum acquired simultaneously. By Fourier transformation the interferogram is converted to the frequency

domain for the recorded wavelengths, which combined with a suitable background generates an absorbance spectrum. The Fourier transform infrared spectrometer uses beamsplitters and mirrors to direct the light from the light source through the sample to the detectors, as illustrated in Figure 1.6. The amount of light from the

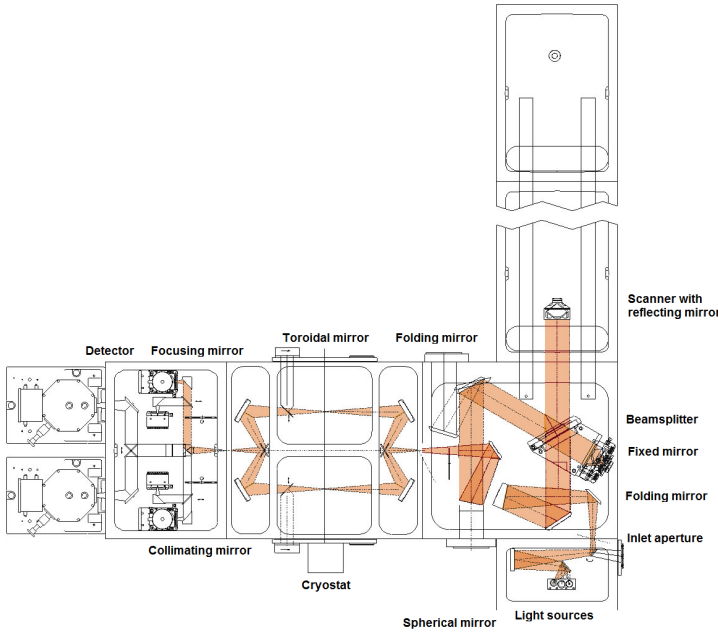

Figure 1.6: The optical path of the Bruker IFS 120 at the MAX IV Laboratory modified for matrix isolation experiments.

light source is controlled by an aperture. The radiation from the infrared light source is divided into two equal parts by the beamsplitters. One part of the beam is reflected to the stationary mirror, while the other part of the beam is transferred to the movable mirror. Ideally, the beamsplitter should divide the beam into two equal parts. The divided beams recombine after reflection from the mirrors back to the beamsplitter. The beam is then split again with one part transferred back to the light source and the other part transferred through the sample to the detector. The arrangement of the movable and stationary mirrors results in a constructive or deconstructive interference between the reflected waves caused by the difference in the travelled distance. The optical path retardation determined by the relative position of the movable mirror is called the retardation δ. If two waves are in phase, where $\delta = n\lambda, n = 0, 1, 2, ...$, constructive interference occurs and a double amplitude of the original split beam is observed, with λ being the wavelength of light. If the two waves are a half-wavelength out of phase ($\delta = n\lambda/2, n = 1, 3, 5, ...,$) deconstructive

interference occurs and no intensity is observed. Phase differences between the two extremes results in partial interference. A plot of the light output as a function of the retardation is called an interferogram [26]. For a monochromatic light source the interferogram can be represented by a cosine wave as

$$I(\delta) = B(\tilde{\nu}) \cos\left(\frac{2\pi\delta}{\lambda}\right) = B(\tilde{\nu}) \cos(2\pi(\tilde{\nu})\delta) \tag{1.6}$$

where $I(\delta)$ is the light that reaches the detector as a function of the retardation and $B(\tilde{\nu})$ a constant that corresponds to the light source, beamsplitter efficiency and detector response. It depends on the wavenumber ($\tilde{\nu}$) of the light, corresponding to $1/\lambda$. For a broad band light source, (1.6) can be extended to

$$I(\delta) = \int_{-\infty}^{+\infty} B(\tilde{\nu}) \cos(2\pi(\tilde{\nu})\delta) d\tilde{\nu} \tag{1.7}$$

At zero retardation, δ=0, all light frequencies interfere constructively. The interferogram thus has maximum amplitude at this point and is denoted the centerburst. As the mirror moves away from the centerburst the interferogram intensity decays. The wider the bandwidth of the incident light, the faster the decay. Therefore an infinitely broadband lightsource, e.g. the white light generated from a synchrotron storage ring, will generate an interferogram with only one centerburst. The interferogram is converted from the time domain of the measured cosine signals to the frequency domain by Fourier transformation. As the interferogram is symmetric around the centerburst, the Fourier transformation can be written as

$$B(\tilde{\nu}) = 2 \int_{0}^{+\infty} I(\delta) \cos(2\pi(\tilde{\nu})\delta) d\delta \tag{1.8}$$

In practice the scanner mirror can only move a certain length, and the Fourier transformation occurs from 0 to the maximum retardation. Thus the transformed single-beam spectrum has a finite resolution. The resolution, or the difference between two neighbouring frequencies, is inversely proportional to the maximum scanner retardation $\Delta\tilde{\nu} = 1/\delta_{max}$. To double the resolution the scanner thus has to move twice the original distance. However, each point in the interferogram contains both signal and noise, thus an increased resolution will result in increased noise in the spectra.

Fourier transform spectroscopy offers several advantages over the traditional dispersive instruments. The multiplex or Fellgett advantage arises from the fact that each detector scan contains information from all wavelengths in the input light. For a fixed number of scans of the detector the elements are sampled more often in the Fourier Transformed (FT) instrument than in the dispersive instrument. This relates to a better signal-to-noise ratio in the same scanning time or an equal signal-to-noise ratio in less time. The fast-scanning possibility thus makes it possible to use signal averaging to reduce the level of random noise in the spectrum. The Jacquinot advantage is related to the high light throughput in the FT instrument. No slits are

used in the optical path, thus more light can reach the detector. If the experiment is limited by the noise of the detector response, higher light throughput will lead to a better signal-to-noise ratio. However, too much light can cause the detector to become saturated and respond nonlinearly [26]. Another advantage, the Connes advantage, is the highly repeatable spectral wavelengths. The internal He-Ne laser provides the control of the sampling of the interferogram, and the spectral frequency is thus directly related to the stability of the laser [52].

1.3.2 The Matrix Isolation Setup

The Matrix Isolation setup at the MAX IV Laboratory, University of Lund, consists of a Bruker HR120 spectrometer, a small immersion helium cryostat and transfer optics. The cryostat has been modified for matrix isolation experiments by employing a rotatable outer shroud, an oxygen free high conductivity copper mirror and resistive heaters. The outer shroud is mounted with two optical windows, CsI and TPX, and a valve for the matrix deposition system. TPX, polymethylpentene, windows are optically transparent in UV, visible and terahertz regions with an optical cut-off at 500 cm^{-1} and 80-90 % transmission and longer wavelengths. The CsI window has an effective cut-off at 160 cm^{-1}, but is optically clear at higher wavenumbers. The transfer optics consists of four reflecting mirrors and two focusing mirrors that are placed symmetrically around the center of the cold head. The mirrors project the beam to a focus outside the spectrometer, with the focal point being the surface of the mirror where the matrix is deposited. The mirrors closest to the light source are left untouched, while the mirrors on the detector side are adjusted according to the position and thickness of the matrix and the rotation of the cryostat.

The infrared absorption spectrum is recorded with the Bruker HR120 spectrometer with an available spectral range from 5 cm^{-1} in the terahertz region to 50,000 cm^{-1} in the UV/visible region at a maximum resolution of 0.00125 cm^{-1}. For matrix isolation experiments up to four different spectral regions are explored for the same matrix. The mid-infrared region spectra are recorded from 4,500 cm^{-1} to 600 cm^{-1} at 0.1 cm^{-1} resolution using a globar lightsource, a Ge/KBr beamsplitter and a liquid nitrogen cooled HgCdTe detector. The Ge/KBr beamsplitter has an optical band pass from 7,800 cm^{-1} to 370 cm^{-1}. Two different HgCdTe detectors are employed in the experiments, a liquid nitrogen cooled broadband HgCdTe detector with a spectral range of 500 cm^{-1} to 5,000 cm^{-1} is used for experiments involving carbon dioxide, acetylene and ethylene and a liquid nitrogen cooled narrowband HgCdTe with an available spectral range from 600 cm^{-1} to 5,000 cm^{-1} for all other experiments.

Near-infrared spectra are recorded from 8,500 cm^{-1} to 1,850 cm^{-1} at 0.5 cm^{-1} resolution using a tungsten lamp, a CaF_2 beamsplitter and a liquid nitrogen cooled InSb detector. The CaF_2 beamsplitter is optical transparent from 1,200 cm^{-1} to 15,000

cm^{-1} while the InSb detector operates in the spectral region from 10,000 cm^{-1} to 1,850 cm^{-1}.

Far-infrared spectra are recorded from 600 cm^{-1} to 160 cm^{-1} using a globar lightsource, a 6μ multilayer mylar beamsplitter and a liquid helium cooled Si bolometer employing an optical filter from 650 cm^{-1} to 150 cm^{-1}. Terahertz spectra are recorded from 300 cm^{-1} (9 THz) to 30 cm^{-1} (0.9 THz) using a globar lightsource, a 6μ multilayer mylar beamsplitter and a liquid helium cooled Si bolometer employing a low pass optical pass filter at 370 cm^{-1}. The liquid helium bolometer operates at 4.2 K in the spectral region from 650 cm^{-1} and below. The multilayer silver coated 6μ mylar beamsplitter is optical transparent in the region from 680 cm^{-1} to 30 cm^{-1}. An overview of the experimental properties are given in Table 1.1.

Table 1.1: Experimental properties for the near-infrared (NIR), mid-infrared (MIR), far-infrared (FIR) and terahertz (THz) regions.

Spectral region (cm^{-1})		Lightsource	Beamsplitter	Detector	Resolution (cm^{-1})
NIR	8,500 - 1,850	W lamp	CaF_2	InSb	0.5
MIR	4,500 - 600	globar	Ge/KBr	HgCdTe	0.1
FIR	600 - 160	globar	6μ mylar	Si bol.[a]	1
THz	300 - 30	globar	6μ mylar	Si bol.[a]	1

[a] Si bolometer

The high conductivity oxygen free copper mirror has been gold plated for better reflection of the light beam. A 3 mm deep cavity with a diameter of 10 mm has been drilled into the mirror to support the thick matrices. Without this cavity in the gold plated copper mirror, the matrices would fall off once a certain thickness is reached. The temperature of the mirror is measured with a Lake Shore silicon diode, and the temperature of the mirror is kept stable within 0.1 K by feedback electronics and resistive heaters.

The matrix deposition system is attached to the cryostat by the valve on the rotatable shroud. The deposition system consists of three separate inlet tubes, two sample gas inlets and a matrix gas inlet. The matrix gas inlet is precooled with liquid nitrogen before the matrix gas is deposited on the mirror, this procedure minimizes the heat load on the cryostat and makes it possible to deposit thicker matrices faster. The deposition speed is kept constant by keeping the temperature of the mirror constant and varying the matrix gas flow by adjusting the needle valve to the matrix gas volume. The sample gases are introduced via separate inlets, which allow partial isotopic substitution of individual subunits. The sample gas flow is adjusted by a needle valve for each sample volume and is left untouched during deposition. The entire deposition system is attached to the cryostat and pumped until the pressure is $5.0 \cdot 10^{-7}$ mbar. At this point the deposition is precooled with liquid nitrogen

and the pressure drops to $\simeq 1.0 \cdot 10^{-7}$ mbar. The valve on the rotatable shroud can now be opened to the 2.8 K cold cryostat and the matrix deposition system placed at a fixed position 10 mm from the cavity in the gold plated copper mirror. 0.008 mole neon is deposited before 0.02 mole neon is deposited with open needle valves to the sample volumes. An extra 0.008 mole neon is deposited before the matrix deposition system can be withdrawn and the valve closed. The deposition of 0.02 at 3.5 K mole neon takes about an hour. The entire cryostat is lowered into the spectrometer and put under vacuum to remove gas phase transitions from water, carbon dioxide etc., which is highly crucial for obtaining high quality spectra.

The temperature of the mirror is kept stable at 2.8 K before and after deposition of the matrix by pumping on the liquid helium reservoir in the cryostat. The resistive heaters attached to the mirror makes it possible to adjust the temperature of the mirror and the matrix. By increasing the temperature the matrix becomes softer, which allow small molecules to move around inside the matrix and build up larger clusters. Such annealing experiments are a method to build up larger cluster entities and determine whether the observed band belongs to a monomer or a molecular cluster. By changing the temperature one varies the Boltzmann distribution which makes it possible to study hot bands, ground state splittings etc.

In the study of weak absorbers in a part of the electromagnetic radiation spectrum with no high-intensity lightsources, one needs to utilize the maximum amount of light. The spectrometer at the MAX IV Laboratory is attached to the storage ring, but since it is not possible to resolve the rotational fine structure of the molecular complexes one can compromise with the resolution of the recorded spectrum and instead increase the aperture and use the internal globar light source to allow more light to hit the sample. Optimizing the experimental conditions is thus a fine balance between the thickness of the cryogenic matrix due to the type of absorber and the investigated spectral region.

1.4 Water Embedded in Cryogenic Noble Gas Matrices

The importance of the non-covalent intermolecular interaction with the Earth's universal solvent, water, can be revealed by the many theoretical and experimental studies of both the water monomer and the water dimer. The theoretical studies have investigated the intermolecular potential energy surface by Density Functional Theory, *ab initio* calculations and Symmetry Adapted Perturbation Theory [53–63]. The water monomer and dimer have been investigated experimentally in cryogenic matrices of argon [64–69], krypton [68, 69], xenon [68], nitrogen [70, 71], oxygen and nitrogen [72], neon [16, 18–22, 67, 73–75], *para*-hydrogen [16, 76], helium [77–80] and

in gas phase [12, 13, 15, 81–91].

Discrete rotation-vibration transitions for the three fundamental vibrations appear as water rotates almost freely inside the confinement of a matrix [16, 67]. The mid-infrared absorption spectrum of water embedded in a cryogenic neon matrix is shown in Figure 1.7, the spectrum reveals a series of rovibrational transitions for which the fundamental vibrational band origins can be estimated. The band origin for the asymmetric stretching fundamental, ν_3, is estimated at 3759.5 cm^{-1}, the symmetric stretching fundamental, ν_1, at 3665.4 cm^{-1} and the bending fundamental, ν_2, at 1595.4 cm^{-1}. The spectrum likewise reveals a red-shifted symmetric donor OH stretching vibrational mode at 3590.5 cm^{-1} for the water dimer.

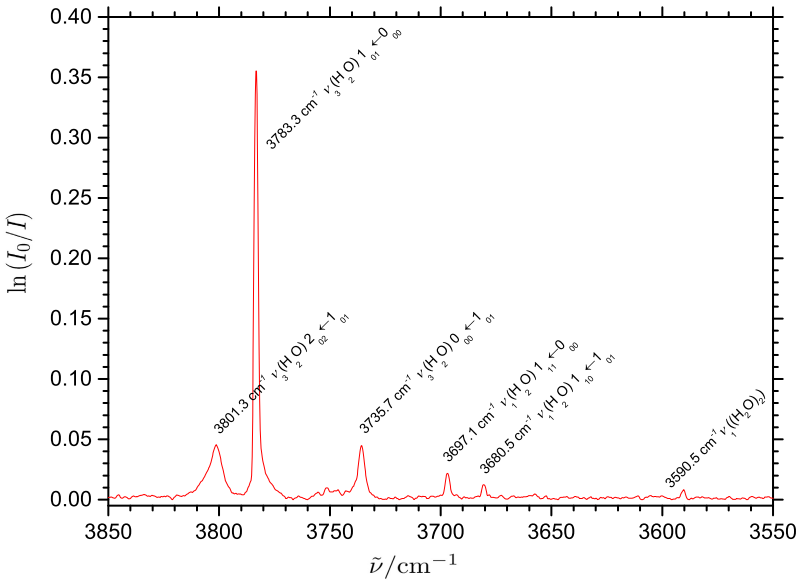

Figure 1.7: Mid-infrared absorption spectrum of 0.1 cm^{-1} resolution of water ($Ne:H_2O$) = (1740:1) embedded cryogenic neon matrices at 2.8 K.

Vibrational spectroscopy studies of water embedded in different cryogenic matrix environments [16, 67, 68, 77, 82] reveal different band origins for the water fundamentals. The difference in band origins can be ascribed as interactions of the water monomer with the matrix environment. The estimated band origins for the three vibrational fundamentals of the water monomer are listed in Table 1.2. The spectroscopic observations indicate larger perturbations of the water vibrational fundamentals in argon, krypton and xenon matrices while smaller perturbations are observed in cryogenic

matrices of *para*-hydrogen, neon and helium relative to the gas phase observations.

Table 1.2: Estimated fundamental vibration band origins (units of cm^{-1}) for the three water fundamentals in different cryogenic matrices.

	Ar [67]	**Kr** [68]	**Xe** [68]	**p-H_2** [16]	**Ne**	**He** [77]	**Gas phase** [82]
ν_1	3638.4	3627.0	[a]	3646.0	3665.4	3655.8	3657.1
ν_2	1588.7	1588.3	1586.1	1592.9	1595.4	[a]	1594.6
ν_3	3734.1	3724.3	3717.4	3742.8	3759.5	3755.1	3755.8

[a] Not observed

The water monomer, dimer and trimer have been extensively studied from the terahertz region to the near-infrared region in one of the least perturbing cryogenic matrices of neon by Ceponkus *et al.* [16–20, 67, 73, 74] and Bouteiller and Perchard [21, 22]. The far-infrared and terahertz regions below 600 cm^{-1} is almost completely transparent for cryogenic neon matrices containing water monomers. Below 100 cm^{-1} the terahertz spectra contains both pure rotational transitions for the water monomer and a very intense and broad spectral feature that can be observed at 79.5 cm^{-1}. The strong band is assigned to a rotation-translation coupling (RTC) of the water monomer with the matrix environment [67]. The band appears as the water molecule rotates about a center of interaction caused by the interaction with the matrix environment and not the center of mass [92]. The pure rotational transitions are assigned at 51.0 cm^{-1}, 32.6 cm^{-1} and 15.9 cm^{-1} to the $2_{12} \leftarrow 1_{01}$, $1_{11} \leftarrow 0_{00}$ and $1_{10} \leftarrow 1_{01}$ rotational transitions. Six large-amplitude intermolecular vibrations are introduced upon complexation of the water dimer. Following the notation of Ceponkus *et al.* [19] a high frequency out-of-plane bending mode is observed at 522.4 cm^{-1}, an in-plane bending mode at 309.5 cm^{-1}, an intermolecular stretching mode at 173 cm^{-1}, an acceptor twisting mode at 150.6 cm^{-1}, an acceptor wagging mode at 122.2 cm^{-1} and a donor torsional mode at 92 cm^{-1} are observed in cryogenic neon matrices at 2.8 K [19]. A combined far-infrared and terahertz spectrum of cryogenic neon matrices doped with water is shown in Figure 1.8, showing the assigned transitions for the water monomer [67], dimer [19] and trimer [17]. The spectroscopic observations and assignments of the large-amplitude intermolecular vibrations for clusters of water isotopologues are essential for the study of mixed non-covalent molecular clusters with water in the far-infrared and terahertz regions.

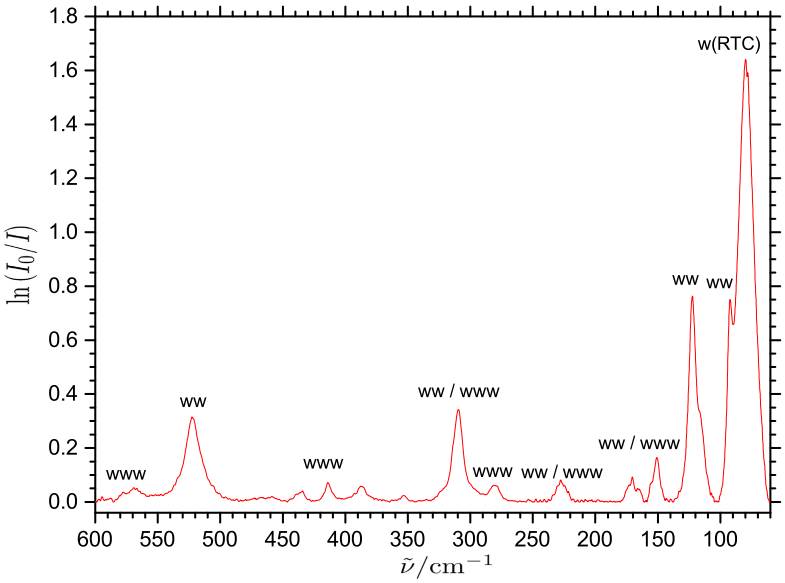

Figure 1.8: Combined far-infrared and terahertz absorption spectra of 1.0 cm^{-1} resolution of water embedded in a cryogenic neon matrix at 2.8 K. The RTC band for the water monomer is denoted w(RTC), ww for intermolecular water dimer vibrational bands and www for the water trimer vibrational bands.

1.5 Exploratory Quantum Chemical Predictions

Quantum chemical predictions are a highly valuable tool for investigating and probing the intermolecular potential energy surfaces for weakly bound cluster molecules. The accuracy of the calculations depends both on the selected method and the size of the basis set. The B3LYP [93–95] method is based on Becket's functional from 1988 that is combined with a correlation functional of Lee, Yang, Parr. It is difficult to accurately describe dispersion forces with the B3LYP functional [96–98], but the description can be improved by adding Grimme's D3 dispersion correction (B3LYP-D3) [99]. A higher-level of electron correlation is achieved with the *ab initio* second order Møller-Plesset Perturbation theory [100]. The root-mean-square force convergence criteria has been set to 10^{-6} (atomic units) for all geometry optimizations at the B3LYP, B3LYP-D3 and MP2 levels of theory. The calculations have applied the augmented correlation consistent polarized basis sets of the form aug-cc-pVnZ (n=D,T,Q,5) developed by Dunning and coworkers [101, 102]. The basis sets are augmented with diffuse functions for a better description of long range interactions. They are designed to converge systematically towards the complete basis limit (CBS) by using empirical extrapolation techniques [103].

To account for shortening of intermolecular distances and thus a strengthening of the intermolecular interaction caused by basis set superposition errors (BSSE) [104], geometry optimizations have included the counterpoise corrections scheme developed by Boys and Bernardi [105].

The electronic energy for the optimized geometries at the B3LYP, B3LYP-D3 and MP2 levels of theory have been further refined by the coupled cluster singles, doubles and perturbative triples method (CCSD(T)) [106, 107] and the explicitly-correlated CCSD(T)-F12 method [108] to further account for electron correlation effects. The CCSD(T)-F12 method is designed to convergence faster towards the limit of a complete basis set.

Harmonic frequency predicted band origins and zero-point vibrational energies have been calculated in the "double-harmonic approximation". The vibrational second order perturbation theory (VPT2) [109–111] has been used to predict anharmonic vibrational frequencies. The VPT2 method is implemented in several quantum chemical software packages, including Gaussian [112, 113].

B3LYP, B3LYP-D3, MP2 and CCSD(T) calculations are performed using the Gaussian suite of programs [114], while CCSD(T)-F12 calculations have been performed using Turbomole [115–117].

Chapter 2

Experimental Results and Discussion

Experimental far-infrared and terahertz results are presented in this section for the study of weakly bound hydrated cluster molecules. The observations and assignments are supported by mid-infrared absorption spectra and theoretical quantum chemical explorations using Density Functional Theory and *ab initio* methods with extensive basis sets. The investigated intermolecular interactions range from weak van der Waals interactions as illustrated by carbon dioxide and water to strong hydrogen bonding as illustrated by the interaction between various alcohols and water. The weak van der Waals interaction between carbon dioxide and water has been published as a communication in Journal of Chemical Physics with the title "THz absorption spectrum of the CO_2-H_2O complex: Observation and assignment of intermolecular van der Waals vibrations". The previously determined dissociation energy D_0 have been updated by including the contribution from observed band origins of perturbed monomer fundamentals in the mid-infrared region.

Hydrophobic interactions are illustrated by the weak hydrogen bond interaction between hydrocarbons and water. The experimental findings of the intermolecular interaction of the water/acetylene complex and the water/ethylene complex have yet to be submitted for publication. The experimental findings show how direct observations of the intermolecular vibrational transitions can determine the nature of the intermolecular hydrogen bond of either a C-H $\cdots$ O or a O-H $\cdots$ π character. A (semi)-empirical dissociation energy D_0 is estimated for the weakly bonded water/ethylene complex by assigning the two observable intermolecular vibrational modes in the challenging terahertz region. Together the two intermolecular vibrational modes account for approximate 70 % of the intermolecular zero-point vibrational energy.

Traditional O-H $\cdots$ O hydrogen bond interactions between water and alcohol are presented in the remaining subsections. Methanol, the simplest alcohol, and the simplest alcohol hydrogen bond in the methanol dimer have been investigated by far-infrared spectroscopy. The results have been published in the Journal of Chemi-

cal Physics with the title "The effect of hydrogen bonding on torsional dynamics: A combined far-infrared jet and matrix isolation study of methanol dimer".

A thorough understanding of the properties for the methanol monomer and the methanol dimer is essential for studying the intermolecular vibrational modes of the mixed methanol/water complex. The large-amplitude intermolecular vibrational modes have likewise been studied for the most simple tertiary alcohol (*t*-butanol) and the findings of both investigated systems published in Physical Chemistry Chemical Physics with the title "The influence of large-amplitude librational motion on the hydrogen bond energy for alcohol-water complexes". The theoretical results have been updated to include larger basis sets for both MP2 and CCSD(T) calculations for methanol/water interaction. The results highlight one of the advantages of the matrix isolation setup, where experiments can be performed with a deuterated subunit without H/D substitution between samples.

The subtle balance between a strong primary O-H $\cdots$ O hydrogen bond and a weaker secondary C-H $\cdots$ O hydrogen bond is investigated by the interaction between ethanol and water. The system is complicated due to two conformers of the ethanol monomer and is a great example of adaptive aggregation where the ethanol subunit change conformation upon complexation. The experimental findings have been accepted for publication in the Journal of Chemical Physics with the title "Spectroscopic identification of ethanol-water conformers by large-amplitude hydrogen bond librational modes".

Far-infrared and terahertz spectroscopic observations are presented for the interaction between water and the most simple secondary alcohol, isopropanol, and the most simple fluorinated alcohol 2,2,2-trifluoroethanol. The latter, represents a case with reversed donor/acceptor relationship as compared to non-fluorinated alcohols caused by the inductive effect of fluor.

Finally, experimental results are presented for alcohol dimers embedded in cryogenic neon matrices and isolated in supersonic jet expansions for the purpose of comparing intermolecular vibrational transitions in gas phase and in cryogenic neon matrices.

The notation on molecular clusters interacting by intermolecular hydrogen bonds mentions the hydrogen bond donor first and the acceptor second. The methanol/water dimer will thus be the dimer with methanol as the hydrogen bond donor and water as the hydrogen bond acceptor.

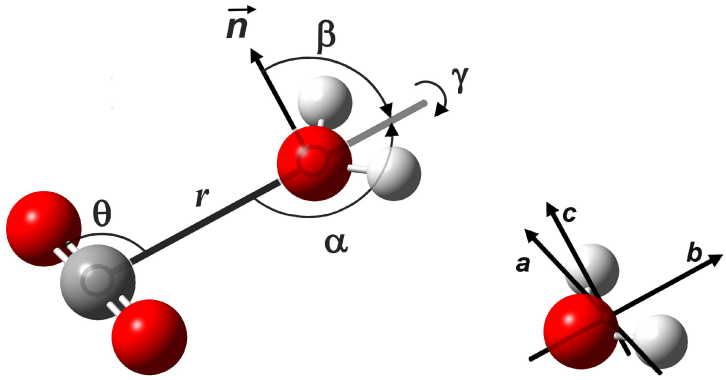

Figure 2.1: The five intermolecular coordinates (r,α,β,γ,Θ) specifying the configuration of the CO_2-water van der Waals complex and the rotational axes (a, b, c) illustrated for a water molecule.

2.1 Weak van der Waals Interaction between Carbon Dioxide and Water

The intermolecular interaction between carbon dioxide and water represents a case with weak van der Waals interaction. The interaction between carbon dioxide and water is responsible for many phenomena in biology, physics and chemistry, including the formation of carbonic acid from carbon dioxide and water [118], transportation of dissolved carbon dioxide in biological tissues and the radiative transfer through the Earth's and other planetary atmospheres [119]. The weak van der Waals heterodimer of carbon dioxide and water have been studied extensively by both experiment and theory. Several studies of the intermolecular potential energy surface have been reported for the weak complex [120–130]. A high level of electron correlation, extensive basis sets and inclusion of basis set superposition errors are necessary to describe the very flat global potential energy minimum. A five dimensional *ab initio* intermolecular potential energy surface reveals a global energy minimum of a planar and T-shaped geometry of C_{2v} symmetry with the oxygen atom from water interacting with the carbon atom from carbon dioxide [131], as illustrated in Figure 2.1. The global intermolecular potential energy minimum of C_{2v} symmetry has been proposed by spectroscopic studies [132–134], whereas a variety of matrix isolation spectroscopic studies with the weakly bound complex embedded in cryogenic nitrogen matrices suggests the existence of another less stable and slightly tilted T-shaped configuration having C_s symmetry [135, 136]. A key parameter for validation of the potential en-

ergy surface is an accurate value for the dissociation energy D_0 which depend on reliable band origins for intramolecular vibrational modes and more importantly for the five intermolecular van der Waals vibrational modes that are introduced upon formation of the complex.

The mid-infrared absorption spectra of several millimeter thick neon matrices doped only with carbon dioxide (CO_2:H_2O:Ne)=(1:0:800) immediately reveal a very intense band at 2347.8 cm^{-1} and a weaker band at 668.0 cm^{-1}. The strong band at 2347.8 cm^{-1} is assigned to the asymmetric stretching mode, ν_3, of carbon dioxide for the regular isotope and at 2282.0 cm^{-1} for the ^{13}C-enriched carbon dioxide sample. The weaker band at 668.0 cm^{-1} is assigned to the degenerate carbon dioxide bending mode, ν_2, and at 649.0 cm^{-1} for ^{13}C-carbon dioxide. The asymmetric stretching modes have previously been observed in neon matrices by Wan *et al.* [137] at identical band positions.

The symmetric stretching mode, ν_1, of carbon dioxide is infrared-forbidden and can not be directly observed. However, the transition energy of ν_1 is similar to the first overtone of the bending mode ($2\nu_2$) and Fermi resonance takes place as the two transitions transform according to the same irreducible representation of the corresponding molecular point group. The ν_1 band of carbon dioxide is observed experimentally at 1284.5 cm^{-1} and $2\nu_2$ at 1387.9 cm^{-1}. The Fermi resonance bands can likewise be observed as combination bands with the strong asymmetric stretching (ν_3) mode. The combination bands $\nu_3 + 2\nu_2$ can be observed at 3713.4 cm^{-1} and $\nu_3 + \nu_1$ at 3611.1 cm^{-1}. These combination bands have previously been observed for carbon dioxide embedded in cryogenic argon matrices at 11 K by Schriver *et al.* [138] while the Fermi resonance bands have been observed by Andrews *et al.* [139] in cryogenic argon matrices and by Suzuki [140] in gas phase. The Fermi coupling between two different states make it difficult to perform high level anharmonic predictions of the vibrational transitions, as the VPT2 calculations require extra treatment for considering near-resonances [141].

The mid-infrared absorption spectra for cryogenic neon matrices containing both water and carbon dioxide (3:1:4000) reveal small perturbations of intramolecular fundamental vibrational transitions upon formation of the weak carbon dioxide/water complex. When carbon dioxide is added to a neon matrix containing water, new bands appear at 3760.4, 3664.8 and 1595.2 cm^{-1}. These bands correspond to the perturbed asymmetric stretching, symmetric stretching and bending fundamentals of the water subunit in the carbon dioxide/water complex and are observed in close proximity of the estimated water fundamentals..

For carbon dioxide a small perturbation is expected for the antisymmetric stretching, however the strong and highly saturated monomer band overlaps the weaker dimer band making it impossible to observe the dimer transition. The natural abundance of ^{13}C of 1.1% make it possible to observe the blue-shift of an unsaturated band. A

small and reproducible blue-shift of 2.2 cm^{-1} is observed of the asymmetric stretching $^{13}CO_2$ fundamental. No new bands have been observed in the spectral region associated with the symmetric stretching fundamental of carbon dioxide.

Stronger perturbation is expected for the degenerate bending mode of carbon dioxide. The $D_{\infty h}$ symmetry of carbon dioxide is broken in the carbon dioxide/water complex and a splitting of the degenerate bending fundamental into two modes is expected. Two new bands that scale with the concentration of carbon dioxide and water in a stoichiometric 1:1 relationship can be observed at 658.7 cm^{-1}, red-shifted by 9.3 cm^{-1} relative to the band origin of the monomer fundamental. Another band can be observed at 672.2 cm^{-1}, blue-shifted by 4.2 cm^{-1}. The red- and blue-shift of the carbon dioxide vibrational bending modes are almost unaffected by isotopic substitution of the hydrogens in the water subunit. The mid-infrared absorption spectra of cryogenic matrices doped with $^{13}CO_2$ and water are shown in Figure 2.2. Two complex bands can be observed at 653.0 cm^{-1} and at 640.2 cm^{-1} for the interaction between $^{13}CO_2$ and water. Besides the dimer bands, several sharp bands are observed in the mid-infrared spectra, these are addressed in section 2.1.1.

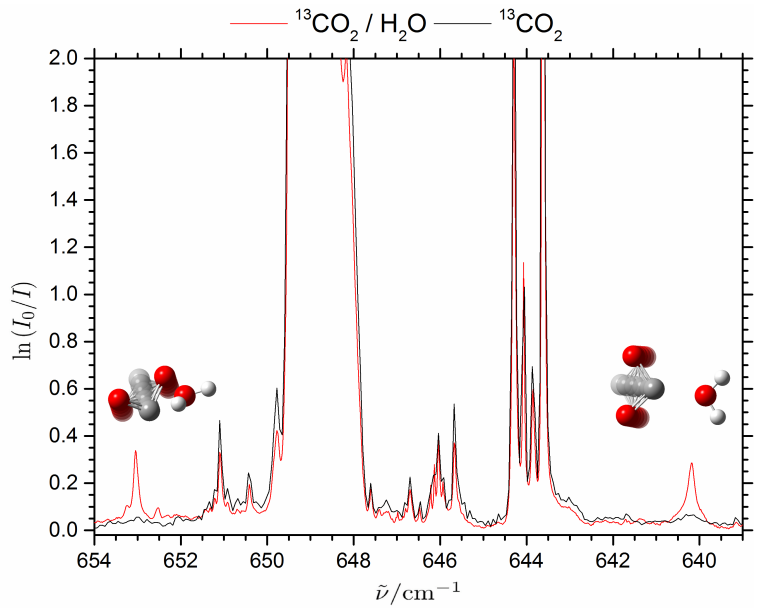

Figure 2.2: Mid-infrared absorption spectra of 0.01 cm^{-1} resolution of cryogenic neon matrices containing $^{13}CO_2$ and a mixture of $^{13}CO_2$ and water. The perturbed carbon dioxide bending fundamentals are indicated by normal mode illustrations.

Table 2.1: Harmonic frequency predictions at the MP2/aug-cc-pVQZ level of theory of vibrational band origins (units of cm^{-1}) and corresponding infrared band strengths (units of $km{\cdot}mol^{-1}$, in parenthesis) for water, carbon dioxide and the weakly bound carbon dioxide/water dimer, including the spectral from monomer to dimer calculated as ω(monomer)-ω(dimer)

	Mode	**ω(monomer)**	**ω(dimer)**	$\Delta\omega$
H_2O	$\omega_1(A_1)$	3839.7 (6.1)	3836.3 (9.9)	3.4
	$\omega_2(A_1)$	1632.4 (73)	1630.2 (76)	2.2
	$\omega_3(B_2)$	3965.5 (78)	3962.3 (87)	3.2
CO_2	$\omega_1(\sigma_g^+)$	1331.9 (0.0)	1334.7 (0.2)	-2.8
	$\omega_2(\pi_u)$	663.3 (46)	667.2 (22)	-3.9
			653.2 (39)	10.1
	$\omega_3(\sigma_u^+)$	2412.2 (582)	2415.3 (564)	-3.1

The mid-infrared experimental findings are supported by theoretical predictions. MP2/aug-cc-pVTZ geometry optimizations without counterpoise corrections were unable to capture a global energy minimum for the carbon dioxide/water complex as the potential energy surface is very flat and shallow near the global minimum. Counterpoise correction or a more extensive basis set is necessary to capture the global energy minimum. Harmonic frequency predictions are carried out at the MP2/aug-cc-pVQZ level of theory. The predicted band origin for the monomer fundamentals are listed in Table 2.1, including the perturbed band origins for the carbon dioxide/water complex and the predicted spectral shift.

The harmonic frequency predictions and description of the class of intermolecular vibrational modes for the carbon dioxide/water complex are listed in Table 2.2. Harmonic frequency predictions for isotopologues of the water/carbon dioxide complex are listed in Table 2.3. Small perturbations are predicted and observed in the mid-

Table 2.2: Harmonic frequency predictions at the MP2/aug-cc-pVQZ level of theory (units of cm^{-1}) and intensities in parenthesis (units of $km{\cdot}mol^{-1}$) for the class of intermolecular vibrational modes for weakly bound carbon dioxide/water van der Waals complex.

Mode	**Description**	**Band Origin**
$\omega_5(A_1)$	intermolecular O$\cdots$C stretching	111.2 (0)
$\omega_6(A_2)$	H_2O torsion	151.2 (0)
$\omega_8(B_1)$	H_2O wagging	101.7 (228)
$\omega_{11}(B_2)$	H_2O rocking	167.6 (25)
$\omega_{12}(B_2)$	CO_2 libration	16.8 (29)

Table 2.3: MP2/aug-cc-pVQZ frequency predictions in the double harmonic approximation of vibrational band origins (units of cm^{-1}) and corresponding infrared band strengths (units of $km \cdot mol^{-1}$, in parenthesis) for isotopologues of the weakly bound dioxide/water dimer.

Mode	CO_2/H_2O	$CO_2/H_2{}^{18}O$	CO_2/HDO	CO_2/D_2O	$^{13}CO_2/H_2O$
ν_1 (A_1)	3836.3 (10)	3828.3 (9.4)	2831.4(23)	2765.3(7.4)	3836.3 (10)
ν_2 (A_1)	1630.2 (76)	1623.3 (75)	1429.5 (63)	1193.9 (42)	1630.2 (76)
ν_3 (A_1)	1334.7 (0.2)	1334.7 (0.2)	1334.7 (0.2)	1334.7 (0.2)	1334.7 (0.2)
ν_4 (A_1)	653.2 (39)	653.2 (39)	653.2 (39)	653.2 (39)	634.8 (37)
ν_5 (A_1)	111.2 (0.4)	107.2 (0.4)	109.1 (0.4)	107.1 (0.4)	110.9 (0.4)
ν_6 (A_2)	151.2 (0.0)	151.2 (0.0)	135.9 (43)	108.3 (0.0)	151.2 (0.0)
ν_7 (B_1)	667.2 (22)	667.2 (22)	667.2 (22)	667.2 (22)	648.2 (21)
ν_8 (B_1)	101.7 (228)	100.8 (225)	83.6 (133)	77.4 (125)	101.7 (228)
ν_9 (B_2)	3962.3 (87)	3946.1 (86)	3902.3 (53)	2903.4 (50)	3962.3 (87)
ν_{10} (B_2)	2415.3 (564)	2415.3 (564)	2415.2(563)	2415.2 (562)	2346.4 (533)
ν_{11} (B_2)	167.6 (25)	165.4(25)	156.0 (14)	148.5 (9)	167.6 (25)
ν_{12} (B_2)	16.8 (29)	16.8 (29)	15.0 (23)	13.7 (18)	16.8 (29)

infrared region, as revealed by the predicted spectral shifts for the perturbed monomer fundamental vibrational modes in Table 2.1. *Direct* observation of the class of intermolecular vibrational modes is thus necessary for the characterization of the intermolecular potential energy surface and an accurate estimation of the dissociation energy D_0. Five intermolecular vibrational transitions are predicted for the carbon dioxide/water complex in the challenging terahertz region. The carbon dioxide librational mode(ω_{12}) is predicted below the optical band gap of the experimental setup, whereas the intermolecular O $\cdots$ C stretching mode(ω_5) has a very low IR intensity. The remaining three librational transitions primarily involve movement of the water subunit; the out-of-plane wagging mode (ω_8), the in-plane rocking(ω_{11}) and the torsional mode (ω_6). The torsional mode of the water subunit is predicted to have zero infrared intensity, however, the torsional mode gains infrared intensity when water is substituted with HDO due to the change in amplitude caused by a slower rotation of deuterium relative to hydrogen, as shown in Table 2.3. The terahertz absorption spectra for several millimeter thick neon matrices containing carbon dioxide, water and mixtures of carbon dioxide and water are shown in Figure 2.3. The terahertz features of neon matrices containing water have been observed and assigned by Ceponkus *et al.* [18–20, 73, 74]. The most imminent features belong to a rotation-translation coupling for water [18] at 79.5 cm^{-1} and water dimer modes at 116.0 cm^{-1} and 122.2 cm^{-1} [19, 20, 73, 74].

Terahertz spectra recorded for neon matrices doped solely with carbon dioxide showed no signs of carbon dioxide-containing cluster entities. In support, high-level theoretical studies of the weakly bound carbon dioxide dimer of C_{2h} symmetry, predict that both infrared active van der Waals vibrational modes, the out-of-plane and geared

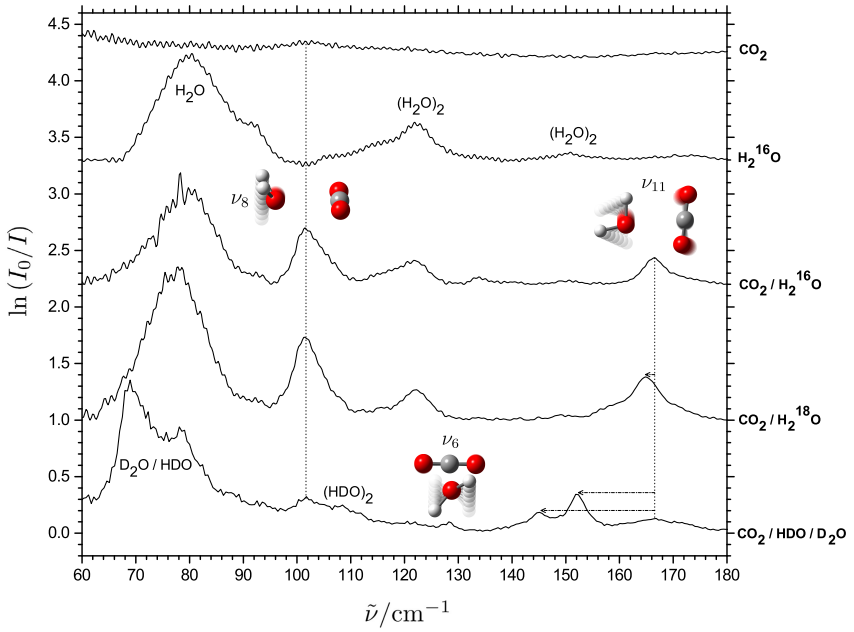

Figure 2.3: A series of terahertz absorption spectra of 1.0 cm^1 resolution collected for cryogenic neon matrices doped with carbon dioxide, water, and 3:1 mixtures of carbon dioxide and isotopically enriched samples of water at 2.8 K. The carbon dioxide/water assignments are indicated by animated normal vibrational mode illustrations. The figure has been reproduced with permission from AIP publishing [142].

intermonomer vibrational transitions, appear around 25 cm^{-1} [143].

Simultaneous doping of the thick neon matrices with both carbon dioxide and water resulted in the appearance of two new bands at 101.6 cm^{-1} and 166.6 cm^{-1} with the high-frequency band being much less intense. The intensity of these bands increased similarly with the concentration of carbon dioxide and water suggesting that the bands belong to a mixed carbon dioxide/water complex with a stoichiometric 1:1 relationship, confirmed by a complementary infrared spectral series.

The observed frequency shifts for carbon dioxide/water-^{18}O bands are very small, however, a series of independent experiments reproduce a small isotopic red-shift of

0.2 cm^{-1} for the low-frequency intermolecular mode observed at 101.4 cm^{-1}. The high-frequency intermolecular mode has an isotopic red-shift of 1.9 cm^{-1} and is observed at 164.7 cm^{-1}, the small reproducible isotopic red-shift is illustrated with an arrow in Figure 2.3.

The intermolecular librational motions all involve movement of the water subunit, as oxygen is placed on the axis of symmetry only the hydrogen atoms move. Deuteration of the water subunit is expected to have a much larger impact on the recorded terahertz spectra than isotopic substitution of oxygen from the water subunit. The rotational motion of water-d_2 is much slower than water, thus larger isotopic frequency red-shifts are expected for both of the water-d_2 modes. A series of terahertz spectra recorded for neon matrices doped with carbon dioxide, water-d_1 and water-d_2 mixtures reproduce a medium strong band at 145.1 cm^{-1} which is assigned to the high-frequency water-d_2 mode for the carbon dioxide/water-d_2 complex as indicated in Figure 2.3. Water-d_1 rotates faster than water-d_2 but slower than water, thus smaller isotopic red-shifts are expected. The water-d_1 mode is observed and assigned at 152.1 cm^{-1}, indicated by arrows in Figure 2.3 for a neon matrix doped with a composition of (CO_2:D_2O:HDO:H_2O) of (18:6:6:1). The strong intermolecular wagging modes for carbon dioxide/water-d_1 and carbon dioxide/water-d_2 are overlapped by the strong rotation-translation coupling transitions for water, water-d_1 and water-d_2 [67].

With different masses for the hydrogen atoms in water-d_1, the torsional motion of the water subunit is predicted to be infrared active. The change of the dipole moment emerges as vibrational motion of the hydrogen atom is much larger than the heavier deuterium atom, supported by an infrared active torsional mode by the MP2/aug-cc-pVQZ harmonic frequency predictions for the carbon dioxide/water-d_1 complex. The band origin for the infrared-forbidden torsional mode for the carbon dioxide/water complex is predicted at 151.2 cm^{-1} and red-shifted to 135.9 cm^{-1} with an infrared intensity of 43 km/mol. A series of independent experiments of cryogenic neon matrices reproduce a weak band at 128.4 cm^{-1}, belonging to the torsional mode of the carbon dioxide/water-d_1 complex. The torsional motion can be described as a hindered rotation around the C_2 symmetry axis which also has the role of the principal b-axis for an isolated water molecule, as illustrated in Figure 2.1. As the ratio of the two harmonic torsional modes is proportional to the square root of the ratio of the B rotational constants for the two isotopic water molecules the band center for the carbon dioxide/water complex can be extrapolated at 140 cm^{-1} from fitted B-values from high-resolution ro-vibrational studies [82].

Comparing the harmonic MP2 predictions and the assigned transitions an immediate correlation appears between the high-frequency intermolecular water rocking mode and the low-frequency intermolecular water wagging mode for the terahertz spectra of cryogenic neon matrices containing both carbon dioxide and water. The straightforward agreement between experiment and theory is most likely caused by a

cancellation of small spectral errors in opposite directions that could originate from anharmonicity effects, mode couplings and matrix perturbations. However, the harmonic frequency predictions suggest straightforward assignments for the out-of-plane water wagging mode ν_8 (B_1) at 101.6 cm^{-1} and the in-plane water rocking mode ν_{11} (B_2) at 166.6 cm^{-1} for the regular carbon dioxide/water complex. The assignments are listed in Table 2.4, and the three observed librational modes illustrated in 2.4.

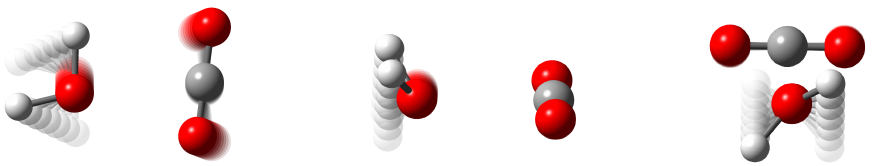

Figure 2.4: The three observed librational modes of the carbon dioxide/water van der Waals complex.

The experimental observations for the weak carbon dioxide/water van der Waals complex make it possible to provide an almost completely empirical estimate of the system's zero-point vibrational energy. Nine out of twelve vibrational modes have been observed by complimentary mid-infrared and terahertz absorption spectra for the weak van der Waals complex of carbon dioxide and water. The ω_3 mode for the carbon dioxide/water complex is infrared forbidden. The intensity of the intermolecular O$\cdots$C stretching mode ω_5 is below the detection limit, while the carbon dioxide librational mode ω_{12} is non-observable as the band is close to the optical band gap in the experimental setup. The intermolecular interaction energy is thus based on the remaining nine vibrational modes, with theoretical contributions from the remaining three non-observed vibrational modes. The very weak interaction between carbon dioxide and water causes small perturbations of intramolecular fundamental vibrations. A closer look at the water fundamentals reveals an almost negligible contribution 0.05 cm^{-1} to the intermolecular zero-point vibrational energy. Perturbation of the carbon dioxide fundamentals provide a contribution of -2.15 cm^{-1} to the intermolecular zero-point vibrational energy, mainly caused by the splitting of the degenerate carbon dioxide bending mode. A combined contribution of -2.1 cm^{-1} to the intermolecular zero-point vibrational energy is estimated from perturbed fundamentals.

According to the harmonic frequency predictions the assigned van der Waals vibrational transitions constitute roughly 75 % of the total intermolecular vibrational zero-point energy contribution to D_0. The contribution from the water wagging mode at 101.6 cm^{-1} and the water rocking mode at 166.6 cm^{-1} are clear, while the band center for torsional mode is extrapolated to 140 cm^{-1} based on the observation for the carbon dioxide/water-d$_1$ complex. The contributions for the O$\cdots$C stretching

mode and the carbon dioxide librational mode are based on the harmonic frequency predictions, which are surprisingly close to the observed values. A total contribution to the intermolecular zero-point vibrational energy of 268.1 cm^{-1} is estimated from the intermolecular van der Waals vibrational transitions, which yields a total (semi)-empirical zero-point vibrational energy of 266 cm^{-1}. The equilibrium dissociation energy D_e value of 1004 cm^{-1} estimated by Makarewicz [131] combined with the experimental observations provides a value of 738 $\pm$ 15 cm^{-1} for the dissociation energy D_0 including uncertainties.

The excellent agreement between MP2/aug-cc-pVQZ harmonic predictions and the observed band origins of the weak van der Waals carbon dioxide/water complex embedded in solid neon matrices is rather surprising. The harmonic frequency predictions are typically blue-shifted relative to the actual anharmonic bands. The present experimental findings thus invite for future high-level anharmonic theoretical investigations of the large-amplitude intermolecular carbon dioxide/water vibrational motions, which may shed light on the subtle balance of potential neon matrix blue-shifts, anharmonicity constants and mode couplings for this weakly bound system.

Table 2.4: The assigned transitions (units of cm^{-1}) for the combined infrared and terahertz absorption spectra for isotopologues of the weak van der Waals complex of carbon dioxide and water embedded in cryogenic neon matrices at 2.8K.

	Mode	Mode Description	CO_2/H_2O	$CO_2/H_2{}^{18}O$	CO_2/HDO	CO_2/D_2O	$^{13}CO_2/H_2O$
CO_2/H_2O	ν_1 (A_1)	sym. H_2O stretching	3664.8	3657.5	2726.4	2676.7	3664.8
	ν_2 (A_1)	in-plane H_2O bending	1595.2	1588.7	1403.6	1178.2	1595.2
	ν_3 (A_1)	sym. CO_2 stretching	[a]	[a]	[a]	[a]	[a]
	ν_4 (A_1)	in-plane CO_2 bending	658.7	658.6	658.5	658.2	640.2
	ν_5 (A_1)	int. O···C stretching	[b]	[b]	[b]	[b]	[b]
	ν_6 (A_2)	int. H_2O torsion	[a]	[a]	128.4	[a]	[a]
	ν_7 (B_1)	out-of-plane CO_2 bending	672.2	672.2	672.2	672.2	653.0
	ν_8 (B_1)	int. H_2O wagging	101.6	101.4	[c]	[c]	101.6
	ν_9 (B_2)	asymmetric. H_2O stretching	3760.4	3746.2	3714.2	2790.5	3760.4
	ν_{10} (B_2)	asymmetric. CO_2 stretching	[d]	[d]	[d]	[d]	2284.2
	ν_{11} (B_2)	int. H_2O rocking	166.6	164.7	152.1	145.1	166.6
	ν_{12} (B_2)	int. CO_2 libration	[b]	[b]	[b]	[b]	[b]
H_2O	ν_1 (A_1)	sym. H_2O stretching	3665.4	3658.0	2727.0	2678.8	3665.4
	ν_2 (A_1)	in-plane H_2O bending	1595.4	1588.9	1404.0	1178.9	1595.4
	ν_3 (B_2)	asymmetric. H_2O stretching	3759.5	3745.7	3713.8	2790.0	3759.5
CO_2	ν_1 (σ_g^+)	sym. CO_2 stretching[e]	1387.9	1387.9	1387.9	1387.9	[b]
			1284.5	1284.5	1284.5	1284.5	[b]
	ν_2 (π_u)	CO_2 bending	668.0	668.0	668.0	668.0	649.0
	ν_3 (σ_u^+)	asymmetric. CO_2 stretching	2347.8	2347.8	2347.8	2347.8	2282.0

[a] Infrared forbidden [b] Not observed [c] Overlapped by rotation-translation coupling transition
[d] Overlapped by monomer asymmetric carbon dioxide stretching [e] Fermi resonance band of ν_1 and $2\nu_2$

2.1.1 The Carbon Dioxide Dimer

The bending region of carbon dioxide reveals beside information about the carbon dioxide monomer and the weak mixed van der Waals dimer with water several extra bands. The recorded mid-infrared spectra of 0.01 cm^{-1} resolution of carbon dioxide ($Ne:CO_2:{}^{13}CO_2$) = (800:1:0), ^{13}-C carbon dioxide (800:0:1) and a mixture of the two (1600:1:1) are shown in Figure 2.5.

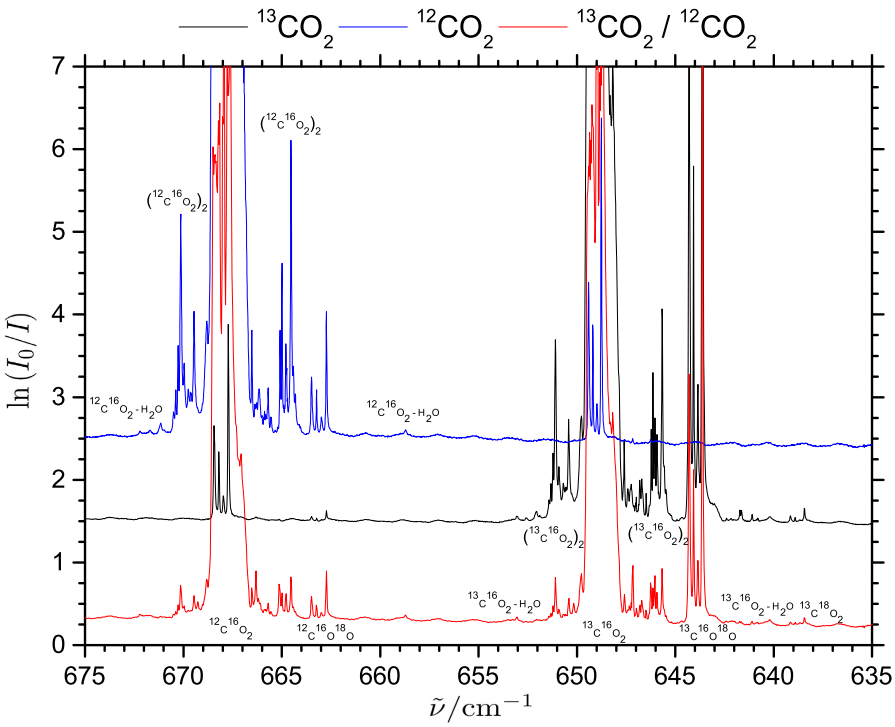

Figure 2.5: Mid-infrared absorption spectra of 0.01 cm^{-1} resolution of cryogenic neon matrices containing pure and mixed carbon dioxide isotopologues in the carbon dioxide bending region.

The mid-infrared spectra reveal a series of sharp bands. The most apparent feature is a splitting of the previously saturated monomeric carbon dioxide degenerate bending mode into a quartet of bands. The splitting of these bands is reproduced for a series of carbon dioxide isotopologues due to the natural abundance of both ^{13}C and ^{18}O. The high-resolution of 0.01 cm^{-1} can reveal possible band shifts during annealing experiments. At 9 K the intensity and band positions of the carbon dioxide quartet

is identical, indicating that no site splitting occurs for the carbon dioxide monomer in cryogenic neon matrices. A physical explanation for the quartet splitting is still to be addressed.

The band center for the carbon dioxide monomer has previously been assigned at 667.4 cm^{-1} in gas phase [140], which tentatively agrees with the center of the quartet bands. A new quartet of bands appear with a band center at 663.1 cm^{-1}, assigned to the bending mode of $^{16}O^{12}C^{18}O$. A more abundant feature with band center of 649.0 cm^{-1} is assigned to $^{16}O^{13}C^{16}O$, verified by designated experiments for isotopically ^{13}C - enriched carbon dioxide. As the isotopically ^{13}C - enriched carbon dioxide also contains increased amounts of ^{18}O it has been possible to assign a band center at 644.0 cm^{-1} for the $^{16}O^{13}C^{18}O$ monomer bending mode and at 638.8 cm^{-1} for $^{13}C18O_2$.

At higher carbon dioxide concentrations several new bands appear in close proximity of the monomer bending fundamental, suggesting the formation of carbon dioxide clusters. The carbon dioxide dimer has previously been observed and assigned at lower resolution studies in argon and nitrogen matrices by Fredin *et al.* [144]. However, both nitrogen and argon matrices contain site splittings, as indicated by the study of Vigasin *et al.* [145]. The slipped parallel global minimum energy structure of the carbon dioxide dimer has been proposed by Bukowski *et al.* [143] and the many spectroscopic studies cited in this paper. The slipped parallel geometry of D_{2h} symmetry, illustrated in Figure 2.6. Minor perturbations are predicted for the asymmetric

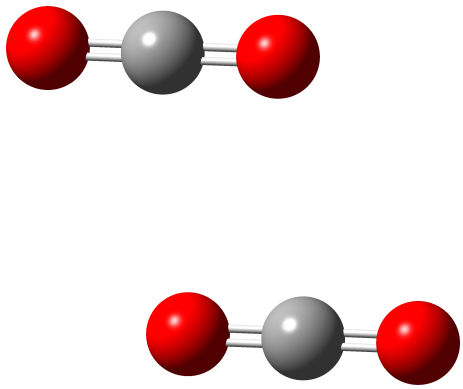

Figure 2.6: The slipped parallel geometry of the carbon dioxide dimer of D_{2h} symmetry.

stretching region for the carbon dioxide dimer by MP2/aug-cc-pVQZ level of theory. Due to the highly intense monomer stretching band, the bending region might serve as a better region for observation of carbon dioxide dimers, especially as the four intermolecular vibrational transitions for the carbon dioxide dimer are predicted below 100 cm^{-1} [143]. The harmonic frequency calculations at the MP2/aug-cc-pVQZ for

the bending modes of the carbon dioxide monomer, the carbon dioxide/water van der Waals complex and the carbon dioxide dimer are listed in Table 2.5.

Table 2.5: MP2/aug-cc-pVQZ predictions in the double harmonic approximation of carbon dioxide bending band origins (units of cm^{-1}) and corresponding infrared band strengths (units of $km \cdot mol^{-1}$, in parenthesis) for carbon dioxide, the carbon dioxide/water complex and the carbon dioxide dimer.

CO_2	CO_2/H_2O	CO_2/CO_2
663.3 (46)	667.2 (22)	664.6 (42)
	653.2 (39)	662.4 (0.0)
		661.2 (0.0)
		659.9 (60)

The two most dominant spectral features that appear in the regular carbon dioxide spectrum is a blue-shifted band at 670.1 cm^{-1} and a red-shifted band at 665.9 cm^{-1}. Similar red- and blue-shifted bands are observed for the $^{13}C16O_2$ dimer at 651.1 cm^{-1} and 645.7 cm^{-1}. The predicted blue- and red-shifted bands and their relative infrared band strengths qualitatively agree with the harmonic frequency predictions allowing a tentatively assignment of the two infrared active bending modes at 670.1 cm^{-1} and 665.9 cm^{-1} for the regular carbon dioxide dimer. An unambiguous assignment of even larger carbon dioxide clusters and the clusters of mixed isotopologues are still to be addressed.

The dissociation energy D_e is predicted to be 484 cm^{-1} by Bukowski *et al.* [143] which translates into a much smaller dissociation energy D_0 when corrected for the zero-point vibrational energy, thus the carbon dioxide dimer is the weakest molecular complex to be observed in this study.

2.2 Weak O-H $\cdots\pi$ and C-H $\cdots$ O Hydrogen Bond Interactions between Hydrocarbons and Water

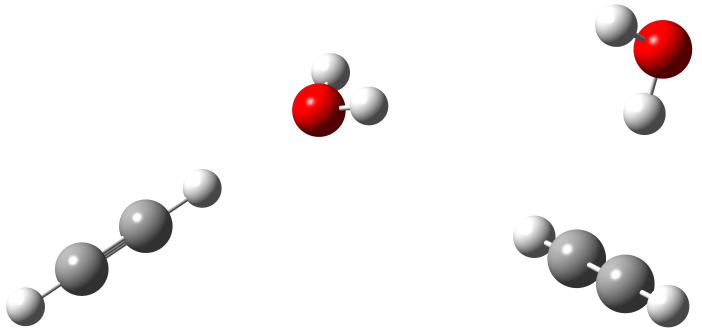

(a) Acetylene/water **(b)** Water/acetylene

Figure 2.7: Minimum geometries of the two conformations of the acetylene/water dimer optimized at the MP2/aug-cc-pVQZ level of theory

Hydrophobic interactions play a highly important role in many chemical and biochemical processes [146–148]. Hydrophobicity, i.e. the repulsion from water, can to a large degree be associated with non-covalent interactions in terms of steric repulsion, dispersion interactions, van der Waals interactions and hydrogen bonding between polar and nonpolar systems. This includes conformations of large nonpolar macromolecules such as polymers, peptides and proteins dispersed in a polar solvent, for which the solvent interaction plays a key factor. The description of the water/hydrocarbon phase equilibrium governed by weak non-covalent interactions is a challenging problem for many refining and petrochemical processes as well as the environmental sciences [149,150]. The many equations of states developed for the description of associating fluids include the effect of intermolecular hydrogen bonding by adding the number of hydrogen bonding "sites" and the related interaction energy per molecule [150]. A study of model systems involving interactions between hydrocarbons and water can thus provide important insights into improving the equations of states ability to describe hydrocarbon/water mixtures by adding the number of "sites" and the related interaction energy.

It is evident that the strong hydrogen bonding that occurs between two electronegative atoms is impossible for hydrocarbons, thus intermolecular hydrogen bond interaction is much weaker for hydrocarbons and water. The question arises whether the hydrocarbon is the hydrogen bond acceptor or donor when interacting with water. For the two most simple unsaturated hydrocarbons involving a multiple carbon-carbon bond, ethylene and acetylene, one can envision an interaction with the delocalized π-electron cloud between the two carbon atoms with the hydrocarbon as the hydrogen

bond acceptor, resulting in a weak O-H $\cdots$ π hydrogen bond [151], as illustrated in Figure 2.7b. For interactions involving the hydrocarbon as the hydrogen bond donor, the weak interaction occurs by formation of an intermolecular C-H$\cdots$ O hydrogen bond, as illustrated in Figure 2.7a. The hybridization of the carbon atom attached to the hydrogen atom will significantly determine the acidity of the hydrogen atom and thus the ability to form hydrogen bonds. Delocalized π-electron clouds are clearly not a prototypical hydrogen bond acceptor, but several studies have reported that the hydrogen bond interaction involves this feature [152–159]. The π-electron cloud associated with formation of a carbon-carbon double or triple bond is involved in the mechanism of catalysts in organic chemistry [160] and in crystal packing by several overlapping π-electron clouds [161].

The argon matrix isolation experiments by Engdahl and Nelander [152,162] on ethylene/water and acetylene/water have been performed in the mid-infrared region without observing the intermolecular large-amplitude vibrational modes with band centers in the far-infrared and terahertz regions. A hydrogen bonded acetylene donor complex was proposed for the acetylene/water interaction [162] while a water donor complex was proposed for the ethylene/water interaction [152]. The interaction between acetylene and water have further been studied experimentally by rotational [163] and optothermal [164] spectroscopy and theory [165,166], while the dimer of ethylene and water has been investigated by rotational spectroscopy [167,168] and theory [169–171].

In order to shed light on the hydrogen bond donor/acceptor properties of the interaction between unsaturated hydrocarbons and water, the combined infrared and terahertz absorption spectra have been studied for cryogenic neon matrices containing ethylene/water and acetylene/water mixtures. The mid-infrared absorption spectra of acetylene ($Ne:H_2O:C_2H_2$) = (1000:1:2) embedded in cryogenic neon matrices immediately revealed strong absorption in the C-H stretching region around 3300 cm^{-1} and in the C-H bending region around 750 cm^{-1}. The strong asymmetric C-H stretching fundamental is observed at 3283.2 cm^{-1}, while the strong acetylene bending mode is observed at 732.0 cm^{-1}. For matrices containing both acetylene and water, a new strong spectral feature can be observed in the C-H stretching region at 3248.7 cm^{-1}. This spectral feature is assigned to the red-shifted C-H stretching fundamental of acetylene in the mixed complex with water. In the matrices embedded with heavy water isotopologues this feature is red-shifted slightly to 3248.3 cm^{-1} indicating a C-H $\cdots$ O hydrogen bond. The symmetric C-H stretching fundamental for the acetylene monomer is infrared forbidden, and non-observable in the infrared absorption experiments. The infrared forbidden asymmetric acetylene bending mode gains infrared intensity upon complexation with water resulting in a splitting of the degenerate mode, with two bands observed at 626.4 cm^{-1} and 620.9 cm^{-1}. A more pronounced blue-shifting is observed for the degenerate symmetric bending mode of acetylene, with two new bands appearing at 772.2 cm^{-1} and 778.1 cm^{-1} blue-shifted by 40.2 and 46.1 cm^{-1}, respectively.

The O-H stretching region of matrices embedded with water show ro-vibrational transitions for the water monomer. A band at 3662.6 cm^{-1} have been observed and assigned to the symmetric OH stretching of the water subunit in the acetylene/water complex. The band position is red-shifted by 2.8 cm^{-1} relative to the monomer fundamental estimated from ro-vibrational transitions. It was not possible to identify a red-shifted asymmetric O-H stretching for the acetylene/water complex. The water bending fundamental have been observed at 1602.4 cm^{-1} for the acetylene/water complex, blue-shifted by 7.0 cm^{-1} relative to the vibrational band center for the water monomer.

For the acetylene monomer no vibrational transitions are observed in the far-infrared and terahertz regions. For matrices doped with both water and acetylene a strong and reproducible spectral feature appears at 145.5 cm^{-1}. The intensity of this band depends on the concentration of both water and acetylene, and can be assigned to an intermolecular vibrational for the mixed acetylene/water complex with a 1:1 stoichiometric relationship by a concentration dependency series. The recorded terahertz absorption spectra of cryogenic neon matrices doped only with acetylene ($Ne:H_2O:C_2H_2$) = (500:0:1), water (1740:1:0), heavy water isotopologues (1400:1:0) and mixtures of acetylene and water isotopologues (1000:1:2) are shown in Figure 2.8. Upon H/D substitution of the water subunit a red-shift is predicted for the intermolecular vibrational mode. The mixed acetylene/water-d_1 intermolecular vibrational mode is observed at 127.8 cm^{-1} isotopically red-shifted by 17.7 cm^{-1} relative to the regular complex. An increased red-shift of 26.4 cm^{-1} is observed for the acetylene/water-d_2 complex with a band center of 119.1 cm^{-1}. The observation of the bands have been reproduced by several independent experiments with varying concentrations.

The less acidic hydrogen atoms in the ethylene molecule might change the hydrogen bond donor/acceptor properties of the hydrocarbon/water interaction, possibly preferring the weak intermolecular O-H $\cdots\pi$ hydrogen bond [152].

The recorded mid-infrared spectra reveal strong monomer absorption in the C-H stretching region at 3106.2 cm^{-1} and at 2990.1 cm^{-1} and a very strong band at 953.4 cm^{-1}. The bands in the C-H stretching region correspond to two asymmetric stretching fundamentals while the very strong band at 953.4 cm^{-1} is assigned to the symmetric out-of-plane C-H bending fundamental. The asymmetric in-plane C-H bending fundamental of ethylene can be observed at 1442.3 cm^{-1}. The cryogenic neon matrix containing both ethylene and water reveals new bands at 3736.7 cm^{-1} and at 3628.2 cm^{-1} corresponding to perturbed fundamental asymmetric- and symmetric- OH stretching bands of the water subunit in the water/ethylene complex. These bands are red-shifted by 22.8 cm^{-1} and 37.2 cm^{-1} relative to the estimated vibrational band origins of the water monomer. A new band is observed in close vicinity of the strong out-of-plane C-H bending of ethylene at 961.2 cm^{-1} blue-shifted by 7.8 cm^{-1} from the monomer. The C-H stretching fundamentals of the ethylene sub-

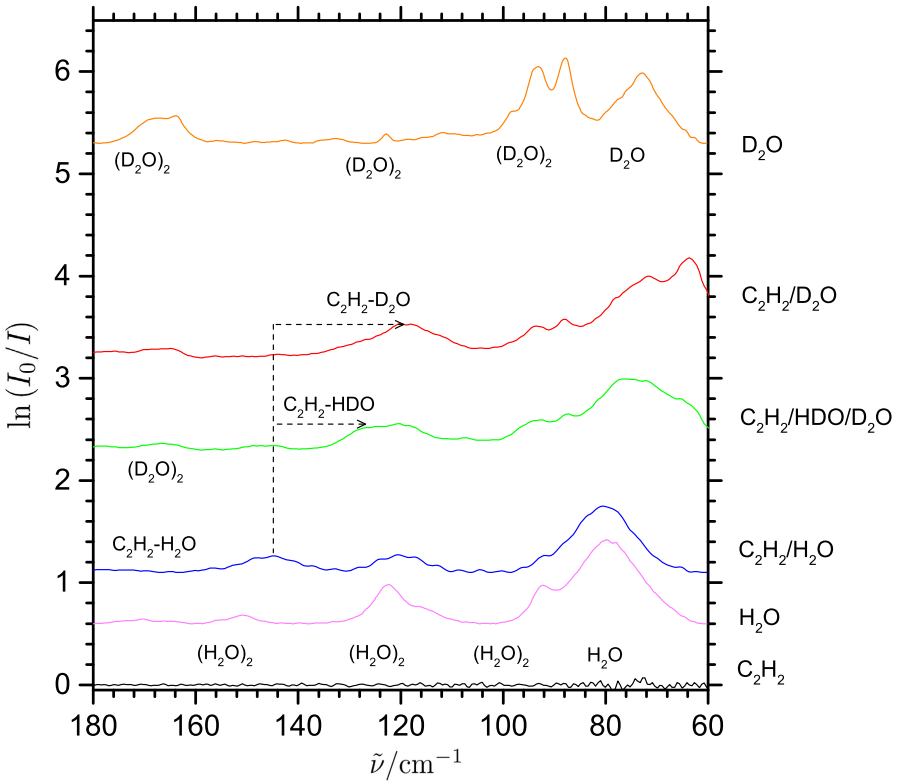

Figure 2.8: Terahertz absorption spectra of 1.0 cm^{-1} resolution for acetylene (Ne:H_2O:C_2H_2) = (500:0:1), water (1740:1:0) and mixtures of acetylene and water including heavy water isotopologues (1000:1:2) in cryogenic neon matrices at 2.8 K

unit are unaffected by the complexation and combined with the observation of the red-shifts of the water fundamental spectral signatures, it indicates that water acts as the hydrogen bond donor in the mixed ethylene/water complex.

The terahertz spectra, shown in Figure 2.9, for thick cryogenic neon matrices doped with ethylene (Ne:H_2O:C_2H_4) = (1100:0:1), water (1740:1:0) and mixtures of ethylene and water with high concentration (1000:1:2) and low concentration (2700:1:2) including heavy water isotopologues (900:1:2) are shown in Figure 2.9. The spectra for cryogenic neon matrices doped with ethylene are completely transparent in the terahertz region. The terahertz spectrum for a matrix doped with a low concentration of ethylene and water immediately reveals a strong and broad band at 187.5 cm^{-1}. A very broad spectral feature with band center at 214.5 cm^{-1} and another very weak

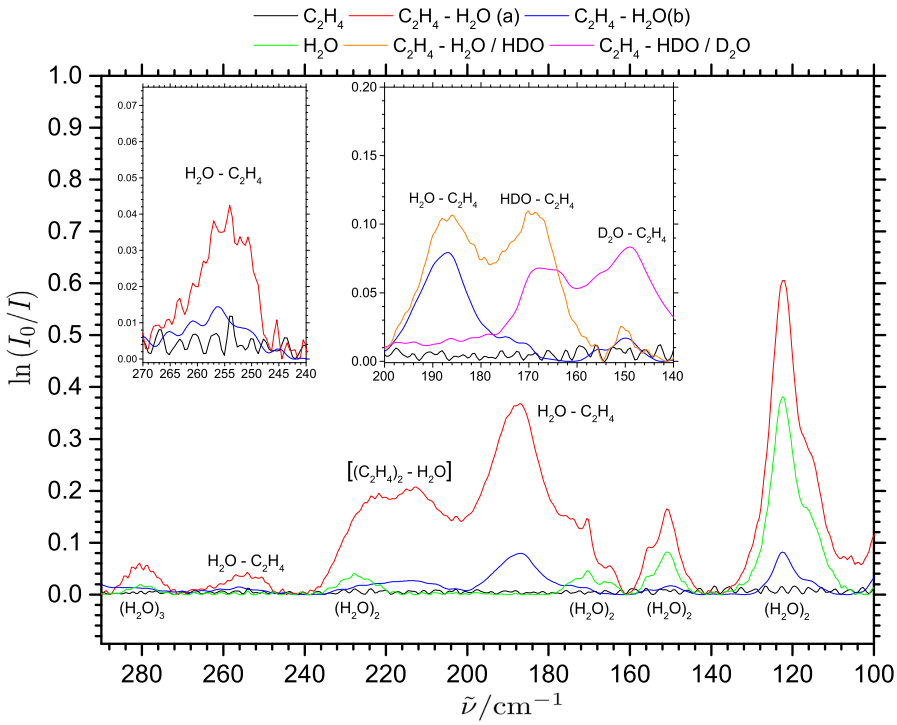

Figure 2.9: Terahertz absorption spectra of 1.0 cm^{-1} resolution of ethylene ($Ne:H_2O:C_2H_4$) = (1100:0:1), water (1740:1:0) and mixtures of ethylene and water with high concentration (1000:1:2) and low concentration (2700:1:2) including heavy water isotopologues (900:1:2) embedded in cryogenic neon matrices at 2.8 K.

spectral feature at 255.0 cm^{-1} are likewise observed as new spectral features. The latter is barely observable and on the detection limit. The intensity of the 187.5 cm^{-1} band scales with both the concentration of ethylene and water suggesting a stoichiometric 1:1 relationship. Isotopic substitution of the water subunit can be used to further support the assignment of this band. Matrices embedded with ethylene, water and water-d_1 reveal a new band at 168.7 cm^{-1} isotopically red-shifted by 18.8 cm^{-1}. This new feature is observable in matrices doped with both water/water-d_1 and water-d_1/water-d_2 suggesting that this band belongs to the water-d_1/ethylene dimer. Matrices containing ethylene and water-d_1/water-d_2 reveal another strong feature at 149.0 cm^{-1} with an isotopic red-shift of 38.5 cm^{-1} relative to the regular complex. This new band is assigned to the dimer of ethylene and water-d_2. At increased concentrations of ethylene and water the absorption of the 255.0 cm^{-1} band at the detection limit starts to increase, following the intensity of the 187.5 cm^{-1}

band. This observation suggests that this band is a higher frequency band for the water/ethylene dimer. The lower infrared intensities for deuterated species make it impossible to observe this band for heavy water isotopologues, as the band is on the detection limit for the regular complex. This weak spectral feature becomes increasingly blurred at higher concentrations, suggesting formation of overlapping larger cluster entities.

Quantum chemical predictions have been used to further support the donor/acceptor properties of the hydrogen bond interaction between hydrocarbons and water and to shed light on the broad spectral feature in the ethylene/water experiments. The interaction between acetylene and water occurs either by formation of an O-H $\cdots\pi$ hydrogen bond resulting in a T-shaped water/acetylene complex or by a C-H$\cdots$O hydrogen bond that results in a Y-shaped acetylene/water complex, as illustrated in Figure 2.7. The harmonic frequency predictions at the MP2/aug-cc-pVQZ level of theory for the weak acetylene/water interacting by a C-H$\cdots$O hydrogen bond are listed in Table 2.6 for monomer fundamentals and perturbed monomer fundamentals in complex. All vibrational modes associated with the weak complex are listed in Table 2.7.

Table 2.6: MP2/aug-cc-pVQZ predictions in the double harmonic approximation of vibrational band origins (units of cm^{-1}) and corresponding infrared band strengths (units of $km{\cdot}mol^{-1}$, in parenthesis) for water with C_{2v} symmetry, acetylene with $D_{\infty h}$ symmetry and the weakly C-H $\cdots$ O bound acetylene/water dimer as well as the calculated shift from monomer to dimer (ω(dimer)-ω(monomer)).

	Mode	ω**(monomer)**	ω**(dimer)**	$\Delta\omega$
H_2O	ω_1 (A_1)	3965.5 (78)	3961.9 (92)	-3.6
	ω_2 (A_1)	1632.4 (73)	1633.4 (68)	2.0
	ω_3 (B_2)	3839.7 (6.1)	3837.7 (12)	-2.0
C_2H_2	ω_1 (σ_g^+)	3530.2 (0.0)	3509.8 (0.1)	-20.4
	ω_2 (σ_g^+)	1975.1 (0.0)	1965.7 (7.6)	-9.4
	ω_3 (σ_u^+)	3442.6 (96)	3397.5 (250)	-45.1
	ω_4 (π_g)	613.6 (0.0)	635.6 (8.7)	22.0
			630.1 (7.8)	16.5
	ω_5 (π_u)	750.3 (198)	813.5 (78)	63.2
			795.2 (75)	44.9

The harmonic frequency predictions suggest a straightforward assignment of the observed band at 145.5 cm^{-1} for the weak C-H $\cdots$ O acetylene/water complex to the predicted in-plane rocking mode at 182.3 cm^{-1}, while the observed mid-infrared monomer perturbations qualitatively agree with the determined geometry. The harmonic frequency predictions for the T-shaped water hydrogen bond donor complex with acetylene reveal red-shifted O-H stretching modes as well as the appearance of

Table 2.7: MP2/aug-cc-pVQZ predictions for the large-amplitude intermolecular vibrational band origins (in units of cm^{-1}) and corresponding infrared band strengths (in units of $km{\cdot}mol^{-1}$, in parenthesis) in the double harmonic approximation for the vibrational spectrum for the C-H $\cdots$ O conformation of the acetylene/water complex at the MP2/aug-cc-pVQZ level.

Vibrational Mode	Description	Band Origin (cm^{-1})
ω_{11}	in-plane H_2O rocking	182.3 (35)
ω_{12}	intermolecular stretching	118.3 (1.4)
ω_{13}	C_2H_2 libration	97.6 (7.8)
ω_{14}	H_2O rocking	56.0 (28.8)
ω_{15}	H_2O wagging	29.4 (224)

two high frequency intermolecular vibrational transitions in the far-infrared and THz region. The two transitions have been predicted at 374.8 cm^{-1} and 171.4 cm^{-1} with intensities of 49 and 71 $km{\cdot}mol^{-1}$, respectively, at the MP2/aug-cc-pVQZ level of theory. The observation of only one transition in far-infrared and terahertz regions directly indicate that the C-H$\cdots$ O hydrogen bonded acetylene/water conformation is the most stable. The vibrational motion of the observed intermolecular vibrational mode can more or less be described as an in-plane rocking mode of the water acceptor subunit in a similar fashion to the in-plane water rocking mode of the weak van der Waals carbon dioxide and water dimer, illustrated in Figure 2.10.

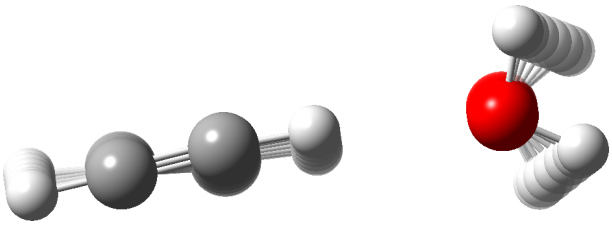

Figure 2.10: Normal mode illustration of the observed intermolecular vibrational mode for the weakly bound acetylene/water complex.

The observation of only one conformation for the hydrogen bond interaction between acetylene and water is supported by calculation of a theoretical dissociation energy D_0. The dissociation energy (D_e) for the weak Y-shaped acetylene-water complex is determined to be 12.5 $kJ{\cdot}mol^{-1}$ or 1043.6 cm^{-1} at the CCSD(T)/aug-cc-pVQZ level of theory for MP2/aug-cc-pVQZ optimized geometries. Subtracting the predicted intermolecular zero-point vibrational energy of 276 cm^{-1} from the harmonic frequency predictions at the MP2/aug-cc-pVQZ level of theory the theoretical disso-

ciation energy (D_0) is determined to be 768 cm^{-1} or 9.2 $kJ{\cdot}mol^{-1}$. Doing the same set of calculations for the T-shaped water/acetylene complex, it results in a dissociation energy D_e of 11.2 $kJ{\cdot}mol^{-1}$ or 934 cm^{-1}, about 100 cm^{-1} smaller than the dissociation energy for the acetylene-water conformation. The zero-point vibrational energy is predicted at 398 cm^{-1}, which translates into a dissociation energy D_0 of 536 cm^{-1}. The large difference in the dissociation energy D_0 of 232 cm^{-1} between the two different conformers of the acetylene/water dimer emphasizes the preference of acetylene as the hydrogen bond donor.

The dissociation energy, D_0, of several isotopologues of acetylene and water have been predicted to investigate whether or not the hydrogen bond donor/acceptor properties for the most stable geometry could change upon deuteration. The results listed in Table 2.8 indicate that acetylene always is the hydrogen bond donor when interacting with water, even for fully deuterated water and regular acetylene where the acetylene/water complex is least stable.

Table 2.8: Dissociation energy D_0 of isotopologues for the two conformations of acetylene and water at the CCSD(T)/aug-cc-pVQZ level of theory using MP2/aug-cc-pVQZ geometry optimizations and harmonic frequencies for calculation of the intermolecular zero-point vibrational energy.

	C_2H_2/H_2O	H_2O/C_2H_2	C_2D_2/H_2O	H_2O/C_2D_2
D_e	12.5	11.2	12.5	11.2
ZPE	3.3	4.8	3.0	4.7
D_0	9.2	6.4	9.5	6.5

	C_2H_2/D_2O	D_2O/C_2H_2	C_2D_2/D_2O	D_2O/C_2D_2
D_e	12.5	11.2	12.5	11.2
ZPE	3.0	3.7	2.7	3.6
D_0	9.5	7.5	9.8	7.6

In a similar fashion the geometry optimization and subsequent harmonic frequency calculation have been performed for the water monomer, the ethylene monomer and the O-H $\cdots\pi$ conformation of the water/ethylene dimer. The monomer fundamentals and fundamental band origins for the mixed water/ethylene dimer are listed in Table 2.9 at the MP2/aug-cc-pVQZ level of theory. A conformational search for a C-H $\cdots$ O hydrogen bonded ethylene/water dimer, similar to the acetylene/water dimer, at the same level of theory was unsuccessful. For the ethylene dimer it has previously been shown that the minimum energy global configuration is an "edge-on" D_{2d} structure with overlapping π-electron clouds by experiment [172] and theory [173] at the CCSD(T)/CBS level of theory, suggesting that ethylene prefers to interact via the delocalized π-electron cloud. The harmonic frequency calculations for the water/ethylene dimer including librational transitions are listed in Table 2.10. The largest

spectral shift of the intramolecular modes is observed for the water monomer, with bathochromic shifts of -45.3 cm^{-1} and -63.8 cm^{-1} for the asymmetric and symmetric water O-H stretching fundamental, which qualitatively supports the mid-infrared experimental findings.

Table 2.9: MP2/aug-cc-pVQZ harmonic frequency predictions (units of cm^{-1}) and corresponding infrared band strengths (units of $km{\cdot}mol^{-1}$, in parenthesis) for water, ethylene and perturbed intramolecular modes of the water/ethylene dimer, including the calculated shift from monomer to dimer as ω(dimer)-ω(monomer).

	Mode	**ω(monomer)**	**ω(dimer)**	$\Delta\omega$
H_2O	ω_1 (A_1)	3965.5 (78)	3937.2 (156)	-28.3
	ω_2 (A_1)	3839.7 (6.1)	3791.2 (126)	-48.5
	ω_3 (B_2)	1632.4 (73)	1637.2 (40)	4.8
C_2H_4	ω_1 (A_g)	3193.4 (0.0)	3191.4 (0.2)	-2.0
	ω_2 (A_g)	1680.3 (0.0)	1674.7 (0.3)	-5.6
	ω_3 (A_g)	1381.3 (0.0)	1380.8 (0.0)	-0.5
	ω_4 (A_u)	1072.9 (0.0)	1078.0 (0.0)	5.1
	ω_5 (B_{1g})	3267.5 (0.0)	3268.2 (0.2)	0.7
	ω_6 (B_{1g})	1249.4 (0.0)	1250.7 (0.0)	1.3
	ω_7 (B_{1u})	979.9 (91)	993.5 (101)	13.5
	ω_8 (B_{2g})	963.9 (0.0)	974.0 (0.0)	10.1
	ω_9 (B_{2u})	3293.8 (12)	3293.9 (6.2)	0.1
	ω_{10} (B_{2u})	823.3 (0.0)	824.2 (0.0)	0.9
	ω_{11} (B_{3u})	3177.2 (9.2)	3176.6 (4.6)	-0.4
	ω_{12} (B_{3u})	1481.4 (9.2)	1482.7 (10.2)	1.3

The predicted class of intermolecular vibrational transitions, listed in Table 2.10 consist of a high-frequency out-of-plane donor OH librational mode ω_{16} at 345.1 cm^{-1}, an in-plane water librational mode ω_{17} at 239.6 cm^{-1}, an intermolecular stretching mode ω_{18} at 109.0 cm^{-1}, an out-of-plane water rocking mode ω_{19} at 79.3 cm^{-1}, an ethylene wagging mode ω_{20} at 67.4 cm^{-1} and finally a water torsion mode ω_{21} at 42.7 cm^{-1}. From these six intermolecular vibrational transitions two medium infrared active librational modes are predicted in the observable terahertz region, ω_{16} and ω_{17}, while the infrared intensity of the intermolecular stretching mode, ω_{18}, make it unobservable. The remaining transitions fall in a region dominated by the rotation-translation coupling band and pure rotational transitions for the water monomer [67].

The harmonic frequency predictions suggest assignments of the two observed bands at 255.0 cm^{-1} and 187.5 cm^{-1} to the high-frequency donor OH librational mode ν_{16} and the in-plane water librational mode ν_{17} for the O-H $\cdots\pi$ hydrogen bonded water/ethylene complex. These assignments suggest that both large-amplitude librational modes are highly anharmonic. The animated normal mode vibrational motions

Table 2.10: Harmonic frequency predictions of the large-amplitude intermolecular vibrational band origins (units of cm^{-1}) and corresponding infrared band strength (units of $km \cdot mol^{-1}$, in parenthesis) for the weakly bound O-H $\cdots\pi$ conformation of the water/ethylene dimer at the MP2/aug-cc-pVQZ level of theory.

Mode	Description	Band Origin (cm^{-1})
ω_{16}	out-of-plane donor OH libration	345.1 (37)
ω_{17}	in-plane H_2O libration	239.6 (84)
ω_{18}	intermolecular H $\cdots$ π stretching	109.0 (1)
ω_{19}	out-of-plane H_2O rocking	79.3 (37)
ω_{20}	C_2H_4 wagging	67.4 (17)
ω_{21}	H_2O torsion	42.7 (82)

for the observed bands are illustrated in Figure 2.11.

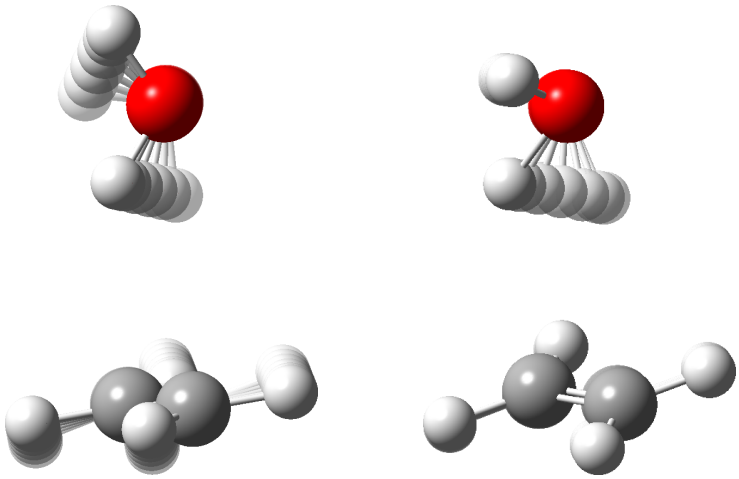

(a) The low-frequency in-plane water librational mode

(b) The high-frequency out-of-plane donor OH librational mode

Figure 2.11: Normal mode illustration of the two observed intermolecular librational modes of the weak O-H $\cdots\pi$ water/ethylene conformation of the water/ethylene dimer.

To verify the assignment of the regular water/ethylene complex, harmonic frequency predictions for ethylene interacting with heavy water isotopologues have been performed and the harmonic frequency predictions of the intermolecular librational band origins are listed in Table 2.11. The predicted isotopic red-shifts for the ω_{17}

are in qualitative agreement with the observed isotopic red-shifts of 18.8 cm^{-1} for ethylene/water-d_1 and 38.5 cm^{-1} for ethylene/water-d_2 as illustrated by the insert in Figure 2.9. The harmonic frequency predictions reveal a large difference for the harmonic band origin for the high-frequency out-of-plane donor OH librational mode, ω_{16} for the two conformations of ethylene and water-d_1. This band has not been observed in the terahertz region for heavy water isotopologues, making it impossible to directly distinguish between a hydrogen- or deuterium bonded water-d_1/ethylene conformation. The mid-infrared observations reveal a perturbed O-D stretching indicating that water-d_1 and ethylene interacts by a deuterium bond.

Table 2.11: MP2/aug-cc-pVQZ quantum chemical predictions in the double harmonic approximation for bands centers (units of cm^{-1}) and corresponding infrared band strength (units of km·mol^{-1}, in parenthesis) for the two observed librational modes for isotopologues of the O-H$\cdots\pi$ ethylene/water dimer.

	$\mathbf{H_2O/C_2H_4}$	$\mathbf{DOH/C_2H_4}$	$\mathbf{HOD/C_2H_4}$	$\mathbf{D_2O/C_2H_4}$
ω_{16}	345.1 (37)	344.6 (42)	249.4 (16)	248.8 (21)
ω_{17}	239.6 (84)	205.2 (50)	204.4 (52)	184.2 (35)

Investigations of larger molecular clusters can possibly shed light on the broad spectral feature that appears at higher concentration of ethylene and water. The broad spectral feature with a band center of 214.5 cm^{-1} grows in intensity when the concentration of the dopants are increased in the matrix. At higher concentrations the broad feature splits into two overlapping bands with band centers of 222.3 cm^{-1} and 213.6 cm^{-1}. Harmonic frequency calculations of larger mixed ethylene/water cluster entities are consulted to investigate these new spectral features. The most likely situation is the appearance of a mixed ternary complex. The minimum energy conformation at the MP2/aug-cc-pVTZ level of theory for the ethylene/water/ethylene ternary complex with two C-H $\cdots\pi$ hydrogen bonds is predicted to have two very strong intermolecular vibrational bands at 315.5 cm^{-1} and 320.8 cm^{-1} with intensities of 87 km·mol^{-1} and 111 km·mol^{-1} respectively. The water/water/ ethylene ternary complex show strong absorptions at 301.0 cm^{-1} with intensity of 162 km·mol^{-1}, and another strong band at 250.1 cm^{-1} with intensity of 79 km·mol^{-1} as well as two high frequency features predicted at 501.2 and 612.4 cm^{-1}. The ternary water/water/ethylene complex has been observed by Engdahl and Nelander [152] while Thompson *et al.* [174] have observed the ethylene/water/ethylene ternary complex. Both observations of the ternary complexes of ethylene and water were made in cryogenic argon matrices.

Both ternary complexes are predicted to be stronger than the water/ethylene dimer with dissociation energies D_0 of 13.8 kJ·mol^{-1} for the ethylene/water/ethylene ternary complex and 25.2 kJ·mol^{-1} for the ternary water/water/ethylene complex using coun-

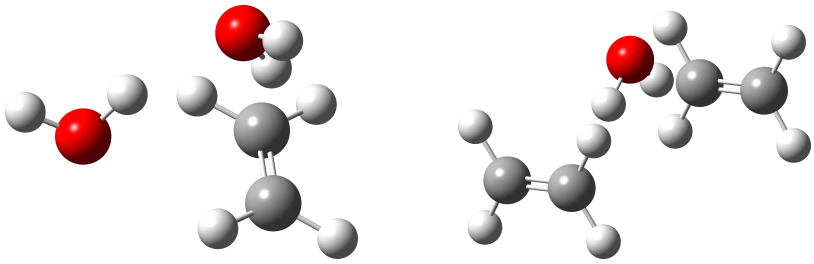

(a) The water/water/ethylene ternary complex

(b) The ethylene/water/ethylene ternary complex

Figure 2.12: Minimum geometries of the ternary complexes of water and ethylene optimized at the MP2/aug-cc-pVTZ level of theory.

terpoise corrected geometry optimizations and harmonic frequency calculations at the MP2/aug-cc-pVTZ level of theory and CCSD(T)/aug-cc-pVTZ for the calculation of the dissociation energy D_e. By employing the scale factor determined from the assignments of the water/ethylene dimer and the harmonic frequency predicted band origins to compensate for the anharmonicity, the two predicted bands for the ethylene/water/ethylene trimer shift into the range of the two observed bands. A higher concentration of ethylene than water is used in the experiments and it is highly unlikely that the observed trimers include two water molecules, although this cluster entity is predicted to be much stronger. The far-infrared region revealed no new bands that could lead to an assignment of mixed water/water/ethylene trimer, thus the two bands observed at 222.3 cm^{-1} and 213.6 cm^{-1} are tentatively assigned to the ethylene/water/ethylene trimer.

The dissociation energy D_e at the CCSD(T)/aug-cc-pVQZ level of theory is determined to be 11.1 $kJ{\cdot}mol^{-1}$ or 935 cm^{-1} for the ethylene/water dimer. Combined with MP2/aug-cc-pVQZ harmonic zero-point vibrational energies the theoretical dissociation energy D_0 is determined at 518 cm^{-1}. A semi-empirical estimation of the zero-point is made from the harmonic predictions of perturbed intramolecular fundamental vibrational transitions that contribute -24 cm^{-1} to the intermolecular zero-point vibrational energy. From the four intermolecular vibrational transitions that have not been observed 149 cm^{-1} is added to the intermolecular zero-point vibrational energy from the harmonic frequency predictions, while an empirical contribution of 221 cm^{-1} is added from the two observed librational transitions resulting in a total intermolecular zero-point vibrational energy of 347 cm^{-1}. From the theoretical dissociation energy D_e a semi-empirical dissociation energy D_0 of 589 $\pm$ 15 cm^{-1} is estimated including uncertainties. The experimental observations of the two librational modes that correspond to approximately 70 % of the intermolecular zero-point vibrational energy thus have a significant impact on the determined dissociation energy D_0.

The intermolecular zero-point vibrational energy is estimated to be the upper limit based on the contribution from harmonic frequency shifts. The semi-empirical dissociation energy is therefore estimated to be the lower limit for the true dissociation energy D_0.

The observations between water and unsaturated hydrocarbons in the form of ethylene and acetylene provide direct observations of the intermolecular potential energy surface of two weakly bound molecular clusters. The nature of the intermolecular vibrational modes directly illustrates whether a hydrocarbon and water interact by formation of a C-H $\cdots$ O hydrogen bond resulting in observation of a single intermolecular vibrational mode in the terahertz region or by formation of an O-H $\cdots\pi$ hydrogen bond in which two high-frequency librational transitions are observed. The determined dissociation energies D_0 reveal a hydrogen bond interaction energy for the C-H $\cdots$ O hydrogen bonded acetylene/water complex of 768 $\pm$ 25 cm^{-1}, similar to the dissociation energy of the weak van der Waals complex of carbon dioxide and water of 738 $\pm$ 25 cm^{-1}, while the dissociation energy of the O-H $\cdots\pi$ hydrogen bonded water/ethylene dimer of 589 $\pm$ 15 cm^{-1} is smaller.

2.3 Semi-Empirical Vibrational Zero-Point Energies

The total zero-point vibrational energy has a significant impact of the dissociation energy D_0 of weakly bound molecular clusters as evident by the investigated weakly bonded clusters of acetylene, ethylene, carbon dioxide and water. The main constituents of the zero-point vibrational energy are the red-shifted donor O-H or C-H stretching for hydrogen-bond interactions and more importantly the appearance of several large-amplitude intermolecular vibrational transitions for the interactions between hydrocarbons. The intermolecular zero-point vibrational energy for the carbon dioxide/water dimer is almost completely characterized by intermolecular vibrational transitions. The intermolecular vibrational modes often involve movement of both subunits in large-amplitude and highly anharmonic motions that are notoriously difficult to predict by computational chemistry. The spectroscopic observations of the intermolecular vibrational modes can be *directly* used to characterize the intermolecular potential energy surface. The harmonic MP2 frequency band origin predictions are often blue-shifted relative to the true anharmonic values, which result in a zero-point vibrational energy that is overestimated and a dissociation energy D_0 that is underestimated. The dissociation energy D_e at the CCSD(T)/aug-cc-pVQZ level of theory and the zero-point vibrational at the MP2/aug-cc-pVQZ level of theory are listed in Table 2.12 for the weakest studied complexes of acetylene/water, carbon dioxide/water and water/ethylene. The dissociation energies D_0 are determined from a theoretical dissociation energy D_e combined with a theoretical or experimentally

corrected (semi-empirical) intermolecular zero-point vibrational energy for the three different mixed complexes.

Table 2.12: The electronic dissociation energy D_e and the dissociation energy D_0 at the CCSD(T)/aug-cc-pVTZ level of theory combined with a theoretical or (semi)-empirical MP2/aug-cc-pVQZ zero-point vibrational energies for the most stable mixed complexes of water with acetylene, ethylene and carbon dioxide (in units of cm^{-1}).

	D_e	ZPE_{tot}^{calc}	$D_{0_{tot}}^{calc}$	ZPE_{tot}^{exp}	$D_{0_{tot}}^{exp}$
C_2H_2/H_2O	1044	276	768	257	786 ± 15
CO_2/H_2O[a]	1004	274	730	266	738 ± 15
H_2O/C_2H_4	935	417	518	347	589 ± 15

[a] see ref. [131]

Three different weak intermolecular interactions are represented by the mixed hydrated molecular clusters; a weak C-H $\cdots$ O hydrogen bond, a weak O-H $\cdots\pi$ hydrogen bond and a weak van der Waals interaction. Even though the intermolecular interactions are of a different character and the resulting dissociation energies D_e are of similar value, the dissociation energies D_0 are very different when corrected for the zero-point vibrational energies.

For the weak van der Waals interaction between carbon dioxide an almost negligible contribution from perturbed intramolecular vibrational modes accounts to approximate 2 cm^{-1}, thus the intermolecular zero-point vibrational energy is almost solely characterized by the five large-amplitude intermolecular vibrational modes. *Direct* spectroscopic observations of the intermolecular vibrational modes is thus crucial for an accurate determination of the interaction energy. Three out of five large-amplitude intermolecular vibrational modes were observed and assigned, these three intermolecular vibrational modes together correspond to roughly 75% of the intermolecular zero-point vibrational energy. When combined with the theoretical dissociation energy D_e by Makarewicz [131] a (semi)-empirical dissociation energy of 738 ± 15 cm^{-1} can be estimated including experimental and theoretical uncertainties. The small difference between the theoretical and experimental zero-point vibrational energies is rather surprising. It can perhaps best be explained by a fortuitous cancellation of errors, especially as the harmonic frequency band origins are blue-shifted and the zero-point vibrational energies are overestimated for all other studied hydrated molecular clusters.

For the interaction between acetylene and water a single intermolecular vibrational mode has been observed for the C-H$\cdots$O hydrogen bond interaction, nevertheless the zero-point vibrational energy contribution from that intermolecular vibrational

mode alone increases the stability of weakly bound complex by 18 cm^{-1}. Only a single high-frequency intermolecular vibrational mode is predicted for the class of intermolecular vibrational modes for the acetylene/water dimer, with the remaining four intermolecular vibrational modes predicted below 100 cm^{-1}. The net result is a low intermolecular zero-point vibrational energy and in turn a higher dissociation energy D_0. That is, however, not the case for the interaction between ethylene and water where two librational transitions are predicted at 345 cm^{-1} and 240 cm^{-1} for the O-H $\cdots\pi$ interaction, significantly increasing the intermolecular zero-point vibrational energy when compared to the to C-H $\cdots$ O interaction of acetylene and water. The two observed large-amplitude intermolecular vibrational modes correspond to 70% of the total intermolecular zero-point vibrational energy. The terahertz absorption observations at 255 cm^{-1} and 188 cm^{-1} for the two intermolecular vibrational modes significantly affect the zero-point vibrational energy and in turn increase the dissociation energy from a theoretical value of 518 cm^{-1} to a (semi)-empirical value of 589 cm^{-1}.

The highly anharmonic donor librational transition for water/ethylene involves movement over the delocalized π-electron cloud. The motion highly resembles the out-of-plane donor OH librational mode for the interaction between water/alcohols and alcohol dimers, where it for the methanol dimer has been shown experimentally that the anharmonic contribution accounts for 100 cm^{-1} [40]. For the shallow potential energy surfaces for the mixed complexes of water with ethylene, acetylene and carbon dioxide VPT2 calculations are unreliable and often fail. The harmonic frequency calculations are thus the only option for non-specialists, and future work of anharmonic predictions for weakly bonded molecular clusters are highly needed.

2.4 Strong O-H ··· Hydrogen Bonding between Alcohol and Water

Intermolecular hydrogen bonding between alcohols and water is of general interest. It ranges from fundamental microscopic aspects related to conformational isomerism, hydrogen bond donor/acceptor preferences and the large-amplitude hydrogen bond vibrational motion introduced upon complexation to more applied macroscopic aspects related to hydrophobic effects and the optimization of experimental separation technologies of bulk alcohol/water mixtures and bio-fuels. The blue-shifted hydrogen bonded donor torsional mode can be described as an almost genuine localized displacement of the hydrogen bonded hydrogen atom, and not as torsional or rotational. The displacement of the hydrogen atom thus directly probes the anharmonic hydrogen bond potential and may be regarded as one of the most sensitive markers of hydrogen bonding [40].

The intermolecular interactions have previously been demonstrated to be responsible for macroscopic thermodynamic anomalies [175] such as negative heats of mixing [176, 177] and negative excess volumes [178, 179] of bulk alcohol/water mixtures. The anomalies can be explained by combined infrared and Raman spectroscopy of isolated clusters of alcohol and water [50, 180], and depend strongly on the relative hydrogen bond energies of mixed alcohol/water complexes versus the pure complexes of alcohols and water [181, 182].

Internal rotation or torsional motion are present for alcohols due to the flexibility of the alcohol group. A thorough study of the investigated alcohol monomer is necessary for the understanding of the properties for the mixed alcohol/water clusters and alcohol clusters. Methanol, the most simple alcohol, is one of the most important molecules for studying torsional motion. The torsional vibration is a large-amplitude motion that involves counter-rotation of two parts of the molecule with respect to each other. For methanol the alcohol group will rotate with respect to the methyl group. The coupling between the anharmonic torsional motion and other vibrational modes is known to accelerate the intermolecular energy transfer [183, 184] and is highly important for the general development of molecular force fields for flexible molecules [185].

The hydrogen bonded methanol dimer, which involves the most simple organic hydrogen bond, has been studied by spectroscopy [186–191], and by theory [192–196]. A sensitive probe for the hydrogen bond interaction is the red-shifted O-H stretching mode for hydrogen bond donor molecule. A large elongation of the O-H bond distance and significantly increased OH transition dipole moment results in a pronounced red-shift and a large gain in infrared intensity, as described by Badger and Bauer [14]. The intensity increase is related to the interaction energy as described

by Iogansen [197]. The red-shifting and intensity gain combined are one of the key parameters in the IUPAC definition of a hydrogen bond [6]. Several experimental approaches have reported the donor OH stretching mode around 3575 cm^{-1} for the methanol dimer with a spectral red-shift of 111 cm^{-1} from the monomer fundamental [41, 198–201]. A thorough VPT2 analysis by Heger *et al.* have decomposed this band into a harmonic contribution of about 121 cm^{-1} [196] and a diagonal anharmonicity correction of 26 cm^{-1} [202] leaving about -36 cm^{-1} for the combined coupling with other vibrational modes.

2.4.1 The Simplest Organic Hydrogen Bond

The large-amplitude torsional motion of methanol is investigated for the simplest organic hydrogen bond between two methanol molecules. Previous studies of methanol embedded in cryogenic matrices of *para*-hydrogen [203] and neon [204,205] have shown to completely forbid the overall rotational motion of methanol but still allow for the anharmonic internal torsional motion, that is slightly hindered compared to gas phase values. The torsion-vibration splittings caused by the torsional tunneling therefore still exist in cryogenic matrices, however, the standard *A*-*A* and *E*-*E* selection rules are no longer valid in the matrix environments [204]. The torsional fundamental of methanol gives rise to four different sub bands, as illustrated in Figure 2.13.

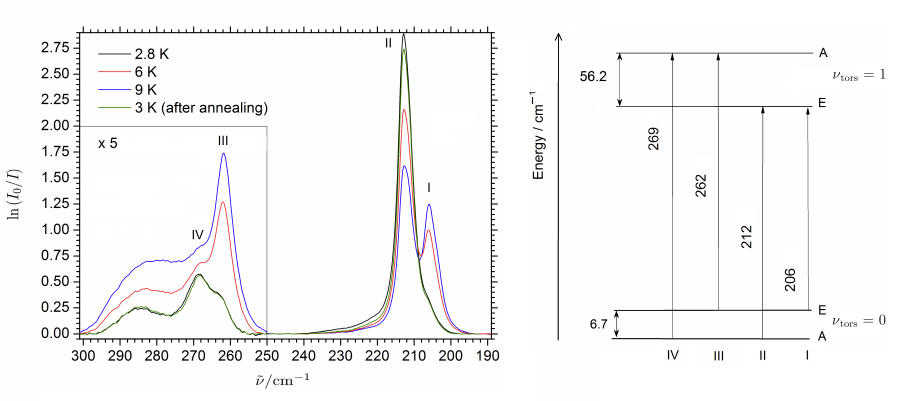

Figure 2.13: Far-infrared absorption spectra of 1.0 cm^{-1} resolution of methanol embedded in cryogenic neon matrices at 2.8 K, 6 K, 9 K and subsequent 3 K after annealing. The figure is reprinted with permission from AIP publishing [40].

The ground state splitting caused by the torsional tunneling is reduced from gas phase values of 9.1 cm^{-1} to 6.7 cm^{-1}, whereas the splitting of the first excited torsional state is reduced from 86.5 cm^{-1} to 56.2 cm^{-1} [204]. These splittings can be

revealed in a neon matrix by varying the population of each energy state by annealing experiments. The recorded far-infrared absorption spectrum of 1.0 cm^{-1} resolution of methanol at 2.8 K, 6 K, 9 K and subsequent cooling to 3 K are shown in Figure 2.13. The temperature effect highlights the ground state and first excited state splittings. The transitions that originate from the A sub-level of the ground state to the A and E sub-level of the first excited torsional state are observed at 212 cm^{-1} and 269 cm^{-1} respectively and are favored at cold temperatures. By annealing, the E-E and E-A transitions gain intensity as the E-sub level of the ground state becomes more populated at higher temperatures and can be observed at 206 cm^{-1} and 262 cm^{-1}. These bands are red-shifted by 6.7 cm^{-1} compared to the cold transitions, which is the vibrational ground state splitting. Another band is also present in the record far-infrared absorption spectra for matrices containing methanol. The band at 286 cm^{-1} is reproducible and depends more on the concentration than the four monomer components, this points to a dimer origin as methanol trimers can be ruled out in matrices containing methanol in the ‰ region which is supported by the lack of OH-stretching trimer bands, that previously have been observed in supersonic jet expansions [201].

The entire far-infrared absorption spectrum of 1.0 cm^{-1} of methanol embedded in a cryogenic neon matrix is shown in Figure 2.14. For the black methanol spectrum, a strong band is observed at 446 cm^{-1} and a weaker band at 507 cm^{-1} in the upper far-infrared region. The broad bands have previously been assigned by Perchard [204] to the overtones of the torsional fundamental from the A-sub level. A small and varying band at approximate 525 cm^{-1} is assigned to a methanol-water complex, which shall be discussed in detail in section 2.4.2. A strong band appears at 558 cm^{-1} for matrices with higher concentration of methanol. The concentration dependency of this band matches the concentration dependency of the 286 cm^{-1} band and is thus assigned to the donor OH librational band for the methanol dimer. The band position of 558 cm^{-1} is slightly off the values observed on supersonic jet expansions at 551 cm^{-1} and 567 cm^{-1} [40]. The spectral resolution of 4 cm^{-1} and overlapping vibrational transitions from larger methanol clusters make it difficult to confidently assign the donor librational band for the methanol dimer, and the methanol dimer in the supersonic jet expansions is thus assigned at 560 ± 10 cm^{-1}. The normal mode illustrations for the two observed librational motions are shown in Figure 2.15.

Isotopic substitution of methanol is used to support the proposed assignment of the methanol dimers. The recorded far-infrared absorption spectra of 1.0 cm^{-1} resolution of methanol and methanol-d_1 embedded in cryogenic neon matrices at 2.8 K are shown together in Figure 2.14, including inserts for methanol-d_3 and methanol-d_4 in the region of the donor OH/OD librational modes. The inevitable H/D exchange in the inlet tubing during deposition makes it difficult to study methanol-d_1 without regular methanol impurities.

The torsion-vibration splitting of methanol-d_1 is smaller than for regular methanol

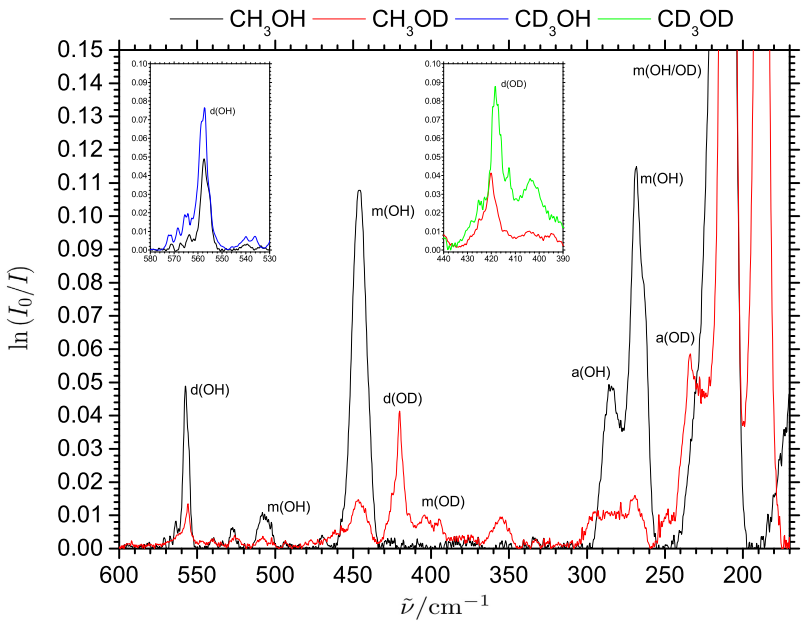

Figure 2.14: Far-infrared absorption spectra of 1.0 cm^{-1} resolution of methanol and methanol isotopologues embedded in cryogenic neon matrices at 2.8 K. The label m, a and d refer to a monomer, dimer donor and dimer acceptor transition respectively, while the (OH)/(OD) refer to the alcohol group.

due to the slower tunneling of the heavier deuterium atom resulting in a much smaller vibrational ground state splitting. The vibrational splitting of the first excited torsional state must thus be very close to the difference between the two observed bands at 187.5 and 205.5 cm^{-1}. The small H/D exchange during deposition does not prevent clear assignment of the donor OD librational band at 420.1 cm^{-1} and the acceptor OD torsion at 234.3 cm^{-1} that appears as a shoulder on the torsional *A-A* transition of methanol-d_1. For methanol-d_3 with a completely deuterated methyl group several monomer bands are observed in the OH torsional region in accordance with the observations by Perchard [204]. The strong monomer bands are slightly red-shifted due to the heavier isotopes and can be observed at 196.8 cm^{-1}, 202.7 cm^{-1}, 251.5 cm^{-1} and 260 cm^{-1} for the *E-E, A-E, E-A* and *A-A* transitions. Two new reproducible spectral features appear at higher methanol-d_3 concentrations, a feature at 557.3 cm^{-1} and a feature at 285.8 cm^{-1}. These two new bands are observed in close vicinity of the regular dimer and can be assigned to the donor OH librational mode at 557.3 cm^{-1} and the acceptor OH torsional mode at 285.3 cm^{-1} for the methanol-d_3 homodimer. A small but reproducible isotopic red-shift of 0.2 cm^{-1} is observed for

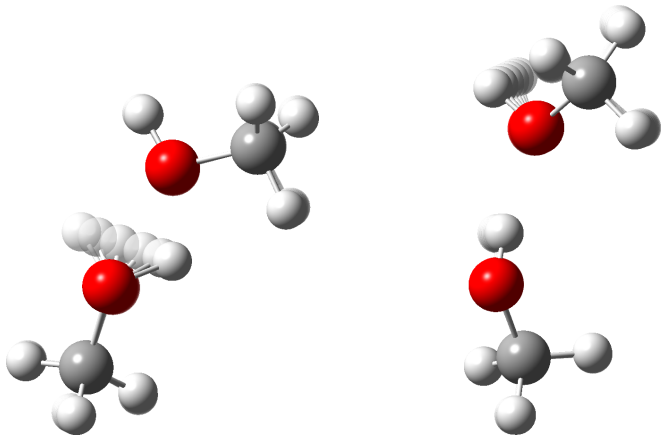

(a) The high-frequency donor OH librational mode

(b) The low-frequency acceptor OH torsional mode

Figure 2.15: Normal mode illustrations of the high-frequency donor OH librational mode and the low-frequency acceptor OH torsional mode for the methanol dimer.

the donor librational transition for methanol-d_3 relative to regular methanol. For the fully deuterated methanol-d_4, the monomer transitions are in accordance with the bands observed by Perchard [204]. A new reproducible feature is observed at 418.9 cm^{-1} and assigned to the donor OD librational mode of the methanol-d_4 dimer. The acceptor torsional mode is overlapped by a broad monomer transition with band center of 220 cm^{-1} and is not assigned. The assignments for the acceptor OH/OD torsional mode and donor OH/OD librational mode for the homodimers of regular methanol and methanol isotopologues are listed in Table 2.13.

Table 2.13: The observed band origins (in units of cm^{-1}) for the acceptor OH/OD torsional mode and the donor OH/OD librational mode of homodimers of methanol, methanol-d_1, methanol-d_3 and methanol-d_4 embedded in cryogenic neon matrices at 2.8 K.

	$(CH_3OH)_2$	$(CH_3OD)_2$	$(CD_3OH)_2$	$(CD_3OD)_2$
acceptor torsion	285.8	234.3	285.8	[a]
donor libration	557.5	420.1	557.3	418.9

[a] Not assigned due to monomer overlap

2.4.2 Hydrogen Bonding between Alcohols and Water

A very limited amount of experimental spectroscopic data are reported in the literature for mixed binary alcohol-water complexes. Rotational spectroscopic studies of adiabatically cooled mixed complexes of water with methanol [206] and *t*-butanol [207] have unraveled the structure of the conformers where the water subunit acts as the hydrogen bond donor. The conformations in which the alcohol subunit acts as the hydrogen bond donor were not detected under the cold conditions of the molecular beam studies. Recent combined infrared and Raman investigations have observed red-shifted OH-stretching bands for mixed complexes of water with methanol and ethanol observed in supersonic jet expansions [50, 180]. The observed vibrational spectral signatures support the hydrogen bond donor/acceptor relationships found in the previously mentioned rotational microwave studies [206,207]. A few other experimental studies of this vibrational OH-stretching manifold have been reported for mixed water complexes with methanol and ethanol embedded in cryogenic matrices of nitrogen and argon [208,209]. In the most perturbing matrix environment of nitrogen a reversed donor/acceptor relationship has been observed although severe site effects blurred the OH-stretching signatures of the alcohol donor subunits. This opposite donor/acceptor relationship observed in cryogenic nitrogen matrices has been explained by weak cooperative attractive interactions between the OH groups and the N_2 host molecules [49]. The strength, directionality and anharmonicity of the intermolecular interactions can be probed by the large-amplitude intermolecular OH vibrational modes in the challenging far-infrared region of the electromagnetic spectrum, as shown for the methanol dimer in the previous section. The mixed water complexes with the simplest primary alcohol, methanol, and the simplest tertiary alcohol, *t*-butanol, are the systems of choice as conformational isomerism is absent. The minimum energy conformations of methanol interacting with water optimized at the MP2/aug-cc-pVTZ level of theory is illustrated in Figure 2.16 while the *t*-butanol/water conformations are shown in Figure 2.17 at the same level of theory.

The recorded far-infrared absorption spectra of 1.0 cm^{-1} resolution of several millime-

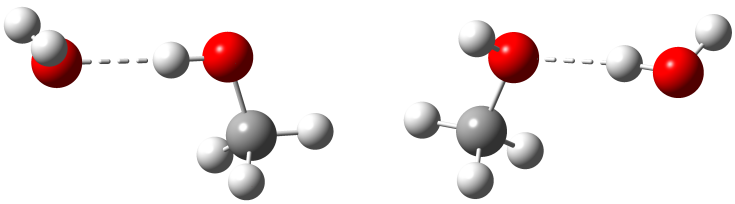

(a) Methanol/water **(b)** Water/methanol

Figure 2.16: Minimum energy geometries of the two conformations of the mixed methanol/water dimer.

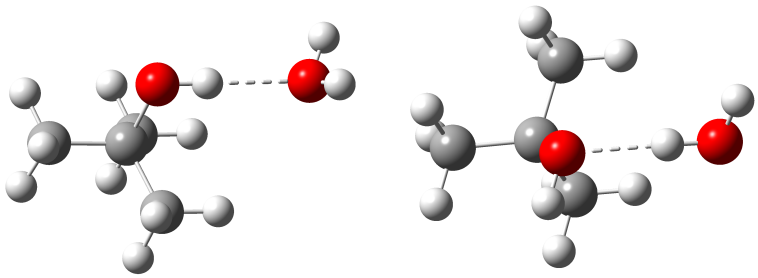

(a) *t*-butanol/water **(b)** Water - *t*-butanol

Figure 2.17: Minimum energy geometries of the two conformations of the mixed *t*-butanol/water dimer.

ter thick cryogenic neon matrices doped with pure water (H_2O:Ne) = (1:2000), pure methanol with traces of water (CH_3OH:H_2O:Ne) = (3:1:13000) and different isotopic water/methanol mixtures (CH_3OH:H_2O:Ne)=(3:2:6000) at 2.8 K are shown in Figure 2.18. The torsional coupling of the vibrational ground state and the corresponding torsional vibrational transition of the methanol monomer results in transitions at 206 cm^{-1}, 212 cm^{-1}, 262 cm^{-1} and 269 cm^{-1}, with overtones observed at 447 and 507 cm^{-1}, as determined in the previous section. The methanol dimer donor OH librational mode was observed at 558 cm^{-1} and the OH acceptor torsional transition at 286 cm^{-1} [40]. Assignment of the librational features of methanol-water was at first not possible with dedicated concentration dependency series. The band at 527.3 cm^{-1} is overlapped by the water dimer band at 522.4 cm^{-1}. Upon annealing to 9 K the intensity of this band increased significantly without returning to the initial state after subsequent cooling to 2.8 K. This points to a build up of molecular clusters in the soft matrix driven by diffusion. As minor traces of water are always present in the inlet system the appearance of this band with increased intensity after annealing suggests a mixed methanol/water complex. The overlap between the out-of-plane donor OH librational mode of the water dimer at 522.4 cm^{-1} suggests that water is the hydrogen bond donor in the mixed methanol/water complex.

Partial H/D isotopic substitution, illustrated by the three inserts in Figure 2.18 of the individual subunits, eased the assignment of the donor/acceptor relationship between alcohol and water. The isotopic substitution of water with water-d_2 introduces a significant isotopic red-shift from 527.3 cm^{-1} to 397.6 cm^{-1}, confirming that water acts as the hydrogen bond donor. The observed band origin for the water-d_2 - methanol band is close to the water-d_2 dimer out-of-plane donor librational mode at 393.2 cm^{-1} [73]. Isotopic H/D substitution on the alcohol group of methanol introduces a minor red-shift of 4 cm^{-1} for the out-of-plane donor OH librational mode confirming a hydrogen bond acceptor role of the methanol subunit. The red-shift of the in-plane donor OH librational band is around 13 cm^{-1} and thus slightly larger

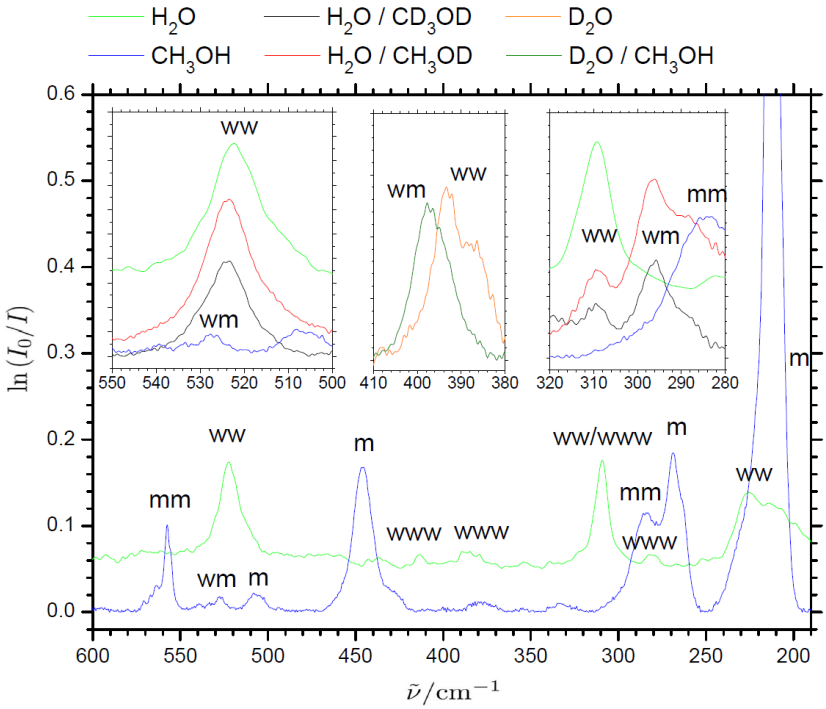

Figure 2.18: Far-infrared absorption spectra of 1.0 cm^{-1} resolution of cryogenic neon matrices doped with pure water (H_2O:Ne) = (1:2000), pure methanol with traces of water (CH_3OH:H_2O:Ne)=(3:1:13000) and different isotopic water/methanol mixtures (CH_3OH:H_2O:Ne)=(3:2:6000) at 2.8 K

than the out-of-plane mode. A closer look at the normal mode illustrations in Figure 2.19 reveal that the high-frequency out-of-plane donor OH librational mode is an almost localized and genuine motion of the hydrogen atom not involving the dangling OH group on the water molecule. The low-frequency in-plane donor OH librational mode can be pictured as a hindered overall c-axis rotation of the water subunit. The large-amplitude motion of the in-plane OH librational motion of the whole water molecule thus has a more significant effect on the center of mass, and is thus more affected by isotopic substitution of the methanol subunit. All observed out-of-plane and in-plane OH librational modes for the water/methanol complexes including isotopic substitutions are listed in Table 2.14.

The far-infrared spectra of t-butanol embedded in cryogenic neon matrices is dominated by complex alcohol and methyl torsional motions for the t-butanol monomer below 300 cm^{-1}. Initial strong features are observed at 208.5 cm^{-1} and 231.7 cm^{-1}, while minor features appear at 254.4 cm^{-1}, 274.3 cm^{-1} and 277.1 cm^{-1}. The simi-

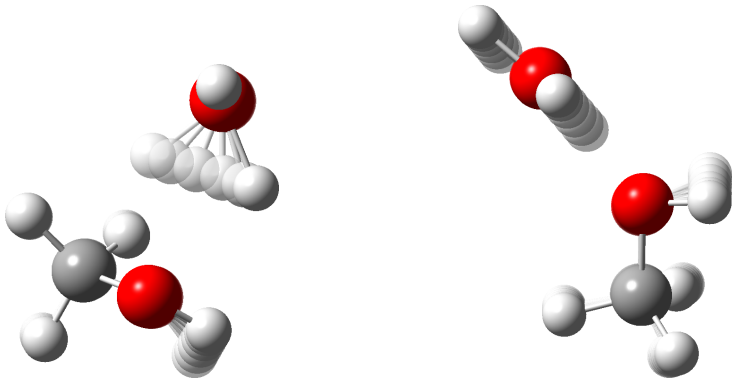

(a) The high-frequency out-of-plane donor OH librational mode

(b) The low-frequency in-plane donor OH librational mode

Figure 2.19: Normal mode illustrations of the high-frequency out-of-plane donor OH librational mode and the low-frequency in-plane donor OH librational mode for the water/methanol dimer.

larities between methanol and *t*-butanol suggests that the two strong low lying features are OH torsional transitions while the bands appearing at higher frequencies involve methyl torsion. A complete analysis of the torsional modes of the *t*-butanol monomer is outside the scope of this study. In addition to the torsional transitions, the monomer of regular *t*-butanol in contrast to methanol exhibits several intramolecular skeletal fundamental transitions in the far-infrared spectral region [210]. The far-infrared absorption spectra of 1.0 cm^{-1} resolution are shown in Figure 2.20 in the region from 300 cm^{-1} to 600 cm^{-1} for several millimeter thick cryogenic neon matrices doped with pure water (H_2O:Ne) = (1:2000), *t*-butanol with small traces of H_2O ($C(CH_3)_3OH$:H_2O:Ne) = (4:1:4000) and different isotopic *t*-butanol/water mixtures ($C(CH_3)_3OH$:H_2O:Ne) = (5:2:3000) at 2.8 K. In the region from 300 cm^{-1} to 600 cm^{-1} the neon matrices doped solely with *t*-butanol reveal two CCC bending fundamentals at 343.4 cm^{-1} and 356.0 cm^{-1}. The symmetric CCO bending fundamental is assigned at 420.2 cm^{-1}, while the two stronger asymmetric CCO bending fundamentals are assigned between 450 cm^{-1} and 475 cm^{-1}. A higher mixing ratio was used to study the *t*-butanol/water complexes as compared to methanol. Infrared spectra recorded in the mid-infrared region was used to eliminate any formation of mixed trimers of water and *t*-butanol based on observations in the O-H stretching region.

As for methanol, two new bands appear in close vicinity of the water OH librational modes for matrices doped simultaneously with water and *t*-butanol. This observation again indicates that the water subunit acts as the hydrogen bond donor in the mixed complexes with *t*-butanol and supports the findings of Evangelisti *et al.* by

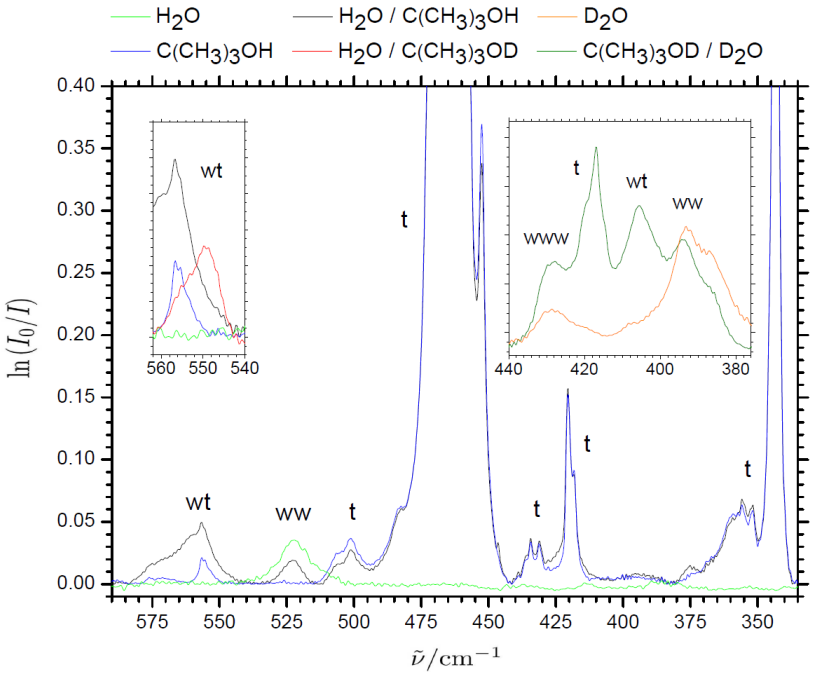

Figure 2.20: Far-infrared absorption spectra of 1.0 cm^{-1} resolution of cryogenic neon matrices doped with pure water (H_2O:Ne) = (1:2000), pure *t*-butanol with traces of H_2O ($(CH_3)_3CHOH$:H_2O:Ne) = (4:1:4000) and different isotopic water/*t*-butanol mixtures ($(CH_3)_3CHOH$:H_2O:Ne) = (5:2:3000) at 2.8 K

rotational microwave spectroscopy [207]. A strong feature is observed at 556.6 cm^{-1}, blue-shifted approximately 35 cm^{-1} relative to the out-of-plane librational mode for the water dimer. This feature is assigned to the out-of-plane librational mode of the mixed *t*-butanol/water complex. A lower lying feature at 318.2 cm^{-1} is assigned to the in-plane donor OH librational band for the mixed complex and this band appears as a shoulder on the water dimer transition at 309.1 cm^{-1}. Isotopic H/D substitution confirmed the donor/acceptor relationship between water and methanol. Isotopic H/D substitution of the alcohol group (*t*-butanol-d_1) and the entire alcohol (*t*-butanol-d_{10}) introduced a minor red-shift of 7.5 cm^{-1} for the donor OH librational band indicating that water is the hydrogen bond donor and that *t*-butanol is the hydrogen bond acceptor. The high-frequency donor OH librational band for the water-d_2 complex with *t*-butanol is expected in the region of the strong CCO bending fundamental around 420.2 cm^{-1}, assuming the band origin ratio of 1.33 observed for the methanol-water complex. The high-frequency out-of-plane OD librational transition is located at 393.2 cm^{-1} for the water-d_2 dimer and the strong shear librational band of water-d_2 trimer is located around 428 cm^{-1} [17]. Nevertheless, independent

Table 2.14: The observed high-frequency out-of-plane ($\nu_{\mathrm{lib},1}$) and low-frequency in-plane donor ($\nu_{\mathrm{lib},2}$) OH (OD) librational band origins (cm^{-1}) for isotopic water complexes and isotopic mixed complexes of water with methanol or *t*-butanol embedded in cryogenic neon matrices at 2.8 K.

Donor-Acceptor	$\nu_{\mathrm{lib},1}$	$\nu_{\mathrm{lib},2}$	Donor-Acceptor	$\nu_{\mathrm{lib},1}$	$\nu_{\mathrm{lib},2}$
H_2O-H_2O	522.4[a]	309.1[a]	D_2O-D_2O	393.2[a]	233.5[a]
H_2O-CH_3OH	527.3	[b]	D_2O-CH_3OH	397.6	[c]
H_2O-CH_3OD	523.7	296.2	D_2O-CH_3OD	395.0	[c]
H_2O-CD_3OD	523.9	295.9	D_2O-CD_3OD	[c]	[c]
H_2O-$C(CH_3)_3OH$	556.6	318.2	D_2O-$C(CH_3)_3OH$	427.7	[d]
H_2O-$C(CH_3)_3OD$	548.9	298.1	D_2O-$C(CH_3)_3OD$	[e]	242.4
H_2O-$C(CD_3)_3OD$	549.0	[f]			

[a] Ceponkus *et al.* [73] [b] Overlapped with $(H_2O)_2$
[c] Overlapped with $(D_2O)_2$ [d] Overlapped with $C(CH_3)_3OH$
[e] Overlapped with $C(CH_3)_3OD$ [f] Overlapped with $C(CD_3)_3OD$

experiments reproduced a new distinct spectral feature at 427.7 cm^{-1} on the high-frequency shoulder of the symmetric CCO bending fundamental band of *t*-butanol. The intensity of this band clearly increases upon annealing to 9 K without subsequent relaxation when the matrix is cooled to 2.8 K. The soft and flexible neon matrix at 9 K makes it possible for water molecules to move inside the matrix and will thus trigger the formation of complexes. The higher concentration of *t*-butanol, combined with a higher mass and almost no diffusion, make *t*-butanol a more likely collision partner for water molecules that move around in the matrix, thus the formation of mixed complexes are favoured. The significant intensity gain of the 427.7 cm^{-1} band relative to the water-d_2 dimer band after annealing supports the assignment of the high-frequency donor OD librational band for water-d_2 with *t*-butanol.

The in-plane low-frequency OD librational transition at 242.4 cm^{-1} is proposed for the mixed complex of water-d_2 with *t*-butanol-d_1. The out-of-plane donor OH librational mode is highly localized, whereas the low-frequency in-plane librational mode might couple with the intramolecular skeletal motions of the *t*-butanol subunits.

The observed librational features indicate a stronger hydrogen bond interaction between water and *t*-butanol than between water and methanol. An inductive effect of the bulky alkyl groups of *t*-butanol improves the acceptor quality of the oxygen atom. A more stiff hydrogen bond and a more hindered internal rotational motion increases the band origins for the donor OH librational modes when the hydrogen bond acceptor changes from water to methanol to *t*-butanol. It has previously been demonstrated by a far-infrared jet study that alkylation strengthens and stiffens the hydrogen bond interaction between alcohol molecules [39].

Ab initio calculations with high degrees of electron-correlation of the electronic dissociation energy have been used to study the dissociation energy of the molecular complexes. Molecular geometries were optimized at the MP2/aug-cc-pVTZ or MP2/aug-cc-pVQZ level of theory including the counterpoise correction scheme of Boys and Bernardi, with subsequent single point energies calculated using CCSD(T). Harmonic frequency calculations were performed to determine the intermolecular zero-point vibrational energy. The dissociation energy of the most stable methanol-water conformer and the energy difference between methanol as hydrogen bond donor or acceptor are listed in Table 2.15 for the combined *ab initio* quantum chemical methodologies. Additional Density Functional Theory calculations are available in the paper "The influence of large-amplitude librational motion on the hydrogen bond energy for alcohol-water complexes", and are not included in Table 2.15. The benchmark level of theory available for both the methanol/water dimer and the larger *t*-butanol/water dimer applies the MP2/aug-cc-pVTZ level of theory for geometry optimizations and the CCSD(T)-F12/aug-cc-pVTZ level of theory for an improved determination of the electronic dissociation energy D_e. The benchmark energy at the MP2/aug-cc-pVTZ/CCSD(T)-F12/aug-cc-pVTZ level of theory for the most stable methanol-water conformer agrees with the highest level of theory MP2/aug-cc-pVQZ/CCSD(T)/CBS within 1.02 and 0.01 kJ·mol^{-1} for the dissociation energy D_e and the energy difference between the conformers. The benchmark level of theory is thus expected to provide reliable results for the complexes between water and the more bulky *t*-butanol for which the MP2/aug-cc-pVQZ level of theory is inaccessible.

Table 2.15: The electronic dissociation energy D_e for the most stable hydrogen bonded complex of water with methanol or *t*-butanol and the difference of electronic dissociation energy between the two different conformers ΔE_e predicted from several combined quantum chemical methodologies for geometry and electronic energy calculations.

Geometry Optimization[a]	**Electronic Energy**	D_e/kJ·mol^{-1}	ΔE_e/kJ·mol^{-1}
	Water/Methanol		
MP2/aug-cc-pVTZ	MP2/aug-cc-pVTZ	25.06	3.10
MP2-CP/aug-cc-pVTZ[b]	MP2/aug-cc-pVTZ	22.71	2.88
MP2-CP/aug-cc-pVTZ[b]	CCSD(T)/aug-cc-pVTZ	25.01	2.82
MP2-CP/aug-cc-pVTZ[b]	CCSD(T)-F12/aug-cc-pVTZ	24.62	2.65
MP2/aug-cc-pVQZ	MP2/aug-cc-pVQZ	24.54	3.06
MP2-CP/aug-cc-pVQZ[b]	MP2/aug-cc-pVQZ	23.36	2.91
MP2-CP/aug-cc-pVQZ[b]	CCSD(T)-F12/aug-cc-pVTZ	24.66	2.65
MP2-CP/aug-cc-pVQZ[b]	CCSD(T)-F12/aug-cc-pVQZ	24.20	2.68
MP2-CP/aug-cc-pVQZ[b]	CCSD(T)/aug-cc-pVDZ	25.67	2.90
MP2-CP/aug-cc-pVQZ[b]	CCSD(T)/aug-cc-pVTZ	24.74	2.82
MP2-CP/aug-cc-pVQZ[b]	CCSD(T)/aug-cc-pVQZ	24.29	2.75
MP2-CP/aug-cc-pVQZ[b]	CCSD(T)/aug-cc-pV5Z	23.92	2.67
MP2-CP/aug-cc-pVQZ[b]	CCSD(T)/CBS	23.60	2.64
	Water/*t*-butanol		
MP2/aug-cc-pVTZ	MP2/aug-cc-pVTZ	30.09	6.90
MP2-CP/aug-cc-pVTZ[b]	MP2/aug-cc-pVTZ	26.75	6.31
MP2-CP/aug-cc-pVTZ[b]	CCSD(T)/aug-cc-pVTZ	30.06	6.65
MP2-CP/aug-cc-pVTZ[b]	CCSD(T)-F12/aug-cc-pVTZ	29.29	6.52

[a] RMS force criterion set to 10^{-6} (atomic units) for all geometry optimizations
[b] CP = Counterpoise Correction applied

The predictions at the benchmark level of theory CCSD(T)-F12/aug-cc-pVTZ, listed in Table 2.15, confirms that *t*-butanol is a superior hydrogen bond acceptor to methanol. The electronic dissociation energy is predicted to be 4.67 kJ·mol^{-1} larger than the corresponding mixed complex with methanol.

The related dissociation energy D_0 and the zero-point vibrational energy must be discussed before reaching further conclusions. The dissociation energy D_e obtained at the benchmark level of theory is combined with the zero-point vibrational energy obtained in the double harmonic approximation at the MP2/aug-cc-pVTZ level of theory. The calculated dissociation energy D_0 determined for the regular complex and heavy isotopologues of water, methanol and *t*-butanol are listed in Table 2.16. The change of vibrational zero-point energy upon intermolecular hydrogen bond formation is difficult to predict computationally. In particular, it is difficult to estimate the large-amplitude and highly anharmonic OH librational modes. For the methanol dimer the anharmonic contribution of the donor OH librational transition is in the order of 100 cm^{-1} [40]. The benchmark harmonic band origin of 660 cm^{-1} combined with the anharmonic contribution provides a theoretical band center of 560 cm^{-1} in excellent agreement with both the observed out-of-plane donor OH librational mode at 557.5 cm^{-1} in cryogenic neon matrices and the 560 $\pm$ 10 cm^{-1} band center in a supersonic jet expansion [40]. An anharmonic VPT2 analysis [112] for the mixed complex of water with methanol at the MP2/aug-cc-pVTZ level predicts an overall anharmonicity of 18% for the high-frequency donor OH librational transition, similar to the predicted anharmonicity effect in the order of 15-20 % for the methanol dimer [40]. A complete anharmonic VPT2 analysis for the mixed complexes of methanol/water and especially *t*-butanol/water would stretch the reliability of the computational approach.

The vibrational zero-point energy contributions have a significant effect on the resulting ground-state energies D_0 of the mixed alcohol-water complexes, as listed in Table 2.16. The vibrational zero-point energy accounts for between 5.6 and 8.4 kJ·mol^{-1} for the mixed complexes with *t*-butanol depending on the isotope of *t*-butanol and the hydrogen bond donor/acceptor role. The sum of experimental anharmonic zero-point energy accounts for up to 5.2 kJ·mol^{-1} or minimum 60 % of the total vibrational zero-point energy when water is the hydrogen bond donor. The last major contribution to the vibrational zero-point energy is the red-shifted donor OH-stretching mode. When water is the hydrogen bond donor the zero-point energy is slightly larger due to two OH donor librational modes, whereas a single donor OH librational mode is present when water is the hydrogen bond acceptor. The benchmark energy difference prediction ΔE_e of 6.5 kJ·mol^{-1} for the two conformers of the water complex with *t*-butanol is converted into a smaller 4.2 - 5.3 kJ·mol^{-1} difference between the resulting D_0-values depending on the isotopic variants when the zero-point vibrational contributions are incorporated.

In terms of the more simple mixed complexes of water and methanol, the total har-

Table 2.16: The electronic dissociation energy D_e for MP2/aug-cc-pVTZ optimized geometries with CCSD(T)-F12/aug-cc-pVTZ[a] single point energies, the total change of harmonic vibrational zero-point energy upon complexation ΔZPE_{tot}^{calc} at the MP2/aug-cc-pVTZ level of theory and the resulting absolute dissociation energy D_0 for mixed isotopic hydrogen bonded donor-acceptor complexes together with the observed (anharmonic) contribution to the zero-point energy from the class of donor OH librational modes ΔZPE_{lib}^{exp} (all values in units of kJ·mol^{-1}).

	H_2O-CH_3OH	**CH_3OH-H_2O**	**H_2O-CH_3OD**	**CH_3OD-H_2O**
D_e	24.62[a]	21.98[a]	24.62[a]	21.98[a]
ΔZPE_{tot}^{calc}	7.80	6.59	7.40	5.65
ΔZPE_{lib}^{exp}	**5.0**		**4.9**	
D_0	16.82	15.39	17.22	16.33

	H_2O-CD_3OD	**CD_3OD-H_2O**	**D_2O-CH_3OH**	**CH_3OH-D_2O**
D_e	24.62[a]	21.98[a]	24.62[a]	21.98[a]
ΔZPE_{tot}^{calc}	7.52	5.90	6.25	5.85
ΔZPE_{lib}^{exp}	**4.9**		**[3.8]**[b]	
D_0	17.10	16.08	18.37	16.13

	H_2O-$C(CH_3)_3OH$	**$C(CH_3)_3OH$-H_2O**	**H_2O-$C(CH_3)_3OD$**	**$C(CH_3)_3OD$-H_2O**
D_e	29.29[a]	22.77[a]	29.29[a]	22.77[a]
ΔZPE_{tot}^{calc}	8.40	6.34	8.29	5.94
ΔZPE_{lib}^{exp}	**5.2**		**5.1**	
D_0	20.89	16.43	21.00	16.83

	H_2O-$C(CD_3)_3OD$	**$C(CD_3)_3OD$-H_2O**	**D_2O-$C(CH_3)_3OH$**	**$C(CH_3)_3OH$-D_2O**
D_e	29.29[a]	22.77[a]	29.29[a]	22.77[a]
ΔZPE_{tot}^{calc}	8.06	5.74	6.77	5.57
ΔZPE_{lib}^{exp}	**5.1**		**[4.0]**[b]	
D_0	21.23	17.04	22.52	17.20

[a] Electronic dissociation energies D_e calculated at the CCSD(T)-F12/aug-cc-pVTZ level based on optimized geometries at the MP2/aug-cc-pVTZ level.

[b] Includes the observed band origin of the high-frequency donor OD librational mode and an anharmonically predicted band origin for the low-frequency donor OD librational mode.

monic vibrational zero-point energy accounts for between 5.9 - 7.8 kJ·mol^{-1} for the conformers of the mixed methanol/water complexes depending on the isotopologues. The sum of the experimental zero-point energy contributions from the donor OH librational motion alone accounts for up to 5.0 kJ·mol^{-1}, i.e. minimum 65%, of the total vibrational zero-point energy for the conformer where water is the hydrogen bond donor. The energy difference at CCSD(T)/CBS ΔE_e of 2.64 kJ·mol^{-1} between the two methanol/water conformations translates into a smaller 1.0 to 2.2 kJ·mol^{-1} difference between the resulting D_0-values depending on the isotopic substitutions. The quantum chemical predictions are supported by a diffusion Monte Carlo study [211] of the two water/methanol conformers.

The effect of the large-amplitude and anharmonic intermolecular donor OH librational motion on the absolute intermolecular hydrogen bond energy D_0 for mixed alcohol-water complexes demonstrated by the present experimental findings has been explored previously for the pure complexes of water [73, 212]. The far-infrared spectroscopy studies have shown that deuterium-bonded water complexes are more stable than the hydrogen bonded counterparts due to the difference in the total vibrational zero-point energies.

The large-amplitude donor librational modes of the partial isotopically substituted mixed complexes of water and alcohols have been observed and assigned in the challenging far-infrared region. The experimental results are supported by quantum chemical calculations at the benchmark level of theory. The results have shown that water acts as hydrogen bond donor upon complexation with aliphatic alcohols. The contributions from the donor OH librational modes alone, are estimated to be 5.0 - 5.2 kJ·mol^{-1}. A stronger intermolecular hydrogen bond results in a more hindered internal rotational motion and thus an increased band origin for the high-frequency hydrogen bond donor OH librational mode. In the mixed complexes of water with methanol and *t*-butanol this feature acts as a measure of the hydrogen bond acceptor properties of the alcohol molecule. The isotopic substitution allows for manipulation of the overall vibrational zero-point energy due to a significant spectral isotopic red-shift of the donor OH librational modes upon H/D substitution. Nevertheless, the large difference in dissociation energies D_e cannot overcome the change in vibrational zero-point energies and thus change the donor/acceptor properties for the mixed complexes of water with methanol or *t*-butanol.

2.4.3 Adaptive Aggregation between Ethanol and Water

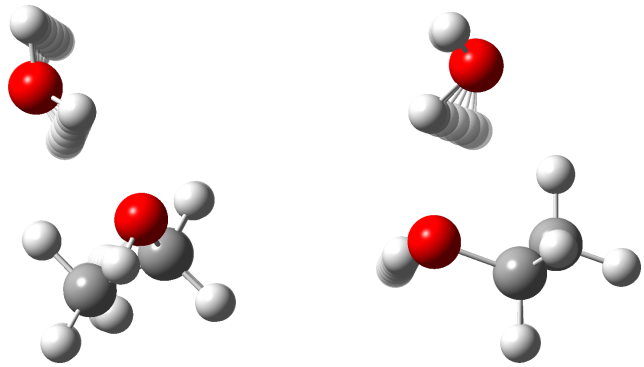

(a) The low-frequency in-plane donor OH librational mode

(b) The high-frequency out-of-plane donor OH librational mode

Figure 2.21: Normal mode illustrations of the observed donor OH librational modes for the hydrogen bonded complex of water and ethanol in the $gauche_+$ conformation.

The ethanol/water interaction is an excellent model system for describing molecular clusters that interact by both traditional O-H · · · O hydrogen bonding and weak C-H · · · O hydrogen bonding. In condensed phase the water/ethanol system has been studied extensively due to the abnormal macroscopic properties. Among these abnormal thermodynamic properties is the release of heat upon mixing of ethanol and water at the macroscopic scale that can be described in terms of microscopic interactions [50]. The energy landscape of the mixed dimer is an equilibrium of the donor/acceptor properties of water and ethanol, already established by the interaction of water with methanol and *t*-butanol, and the trans/gauche conformations of the ethanol monomer.

The water/ethanol complex represents one of the simplest mixed hydrogen bonded molecular systems where internal conformational degrees of freedom influence the hydrogen bond formation. The internal rotating moieties for ethanol consist both of the alcohol group and the methyl group which will greatly affect both the rotational and vibrational spectra. Cryogenic neon matrices have shown to quench the overall rotation of molecules but still allow for the large-amplitude vibrational motions such as torsional motion of an alcohol group. In the mixed ethanol/water complex, the ethanol subunit prefers the *gauche* conformation although the *trans* conformation is the most stable for an isolated ethanol molecule [50, 180]. This is considered one of the most elementary cases of adaptive aggregation, where a flexible molecule is forced into a less stable conformation upon non-covalent binding to optimize the mutual interaction energy [50, 180].

Very limited spectroscopic data is available for the ethanol/water system. The ethanol monomer has previously been studied in cryogenic argon matrices by Barnes and Hallam [213], while the hydrogen bonding interaction between ethanol and water has been studied by rotational spectroscopy [214]. In the rotational spectroscopy study water was determined to be the hydrogen bond donor and ethanol in the *gauche* conformation to be the hydrogen bond acceptor. The results illustrate a cooperative effect between the strong O-H $\cdots$ O hydrogen bond and the weaker C-H $\cdots$ O hydrogen bond. The geometry optimizations of the water/ethanol complexes reveal five local minima energy conformations at the MP2/aug-cc-pVQZ level of theory, the structures are illustrated in Figure 2.22. As evident from the geometry opti-

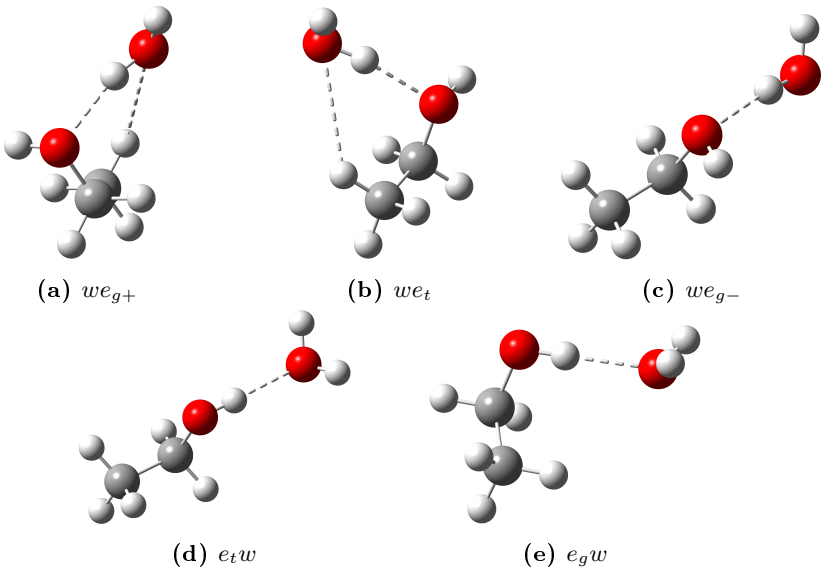

Figure 2.22: Minimum energy geometries of the mixed ethanol/water dimers optimized at the MP2/aug-cc-pVQZ level of theory. w denotes water, e ethanol and the conformation of ethanol are denoted by the subscript of $_{g+}$, $_{g-}$ or $_t$, corresponding to the *gauche*$_+$, *gauche*$_-$ and the *trans*-conformation respectively.

mizations the choice of the conformation of the ethanol subunit and the oxygen lone pair is important. In the *gauche*$_+$ conformation the O-H bond is rotated clockwise or counterclockwise by 120 degrees relative to the *trans* conformation when viewed along the C-C-O axis. A new asymmetric center emerges at the oxygen atom of ethanol caused by the two lone pairs. In one conformation (we_{g-}) water interacts with the lone pair from ethanol that points away from the carbon backbone, which results in a more extended structure. When water interacts with the other lone pair closest to the carbon backbone a more compact structure (we_{g+}) is achieved and a

weak secondary C-H ··· O hydrogen bond is formed between a terminal C-H group from ethanol and one of the available lone pairs from the water oxygen atom. The weak secondary C-H ··· O hydrogen bond can likewise be realized between ethanol in the *trans* conformation and water as the hydrogen bond donor (we_t). Due to rotation of the alcohol group and the two available lone pairs of the oxygen atom in ethanol we_t, we_{g-} and we_{g+} have enantiomeric conformations. These are, however, indistinguishable by vibrational spectroscopy . The intermolecular hydrogen bond distances for MP2/aug-cc-pVQZ optimized geometries are listed in Table 2.17. The far-infrared spectrum of the ethanol monomer has been widely studied due to

Table 2.17: Intermolecular hydrogen bond distances (Å) for minimum energy conformations of the ethanol - water dimers optimized at the MP2/aug-cc-pVQZ level of theory

	$\mathbf{we}_{g+}$	$\mathbf{we}_t$	$\mathbf{we}_{g-}$	$\mathbf{e}_t w$	$\mathbf{e}_g w$
Primary O-H ··· O hydrogen bond	1.901	1.909	1.905	1.955	1.962
Secondary O-H ··· O hydrogen bond	2.695	2.829			

the *trans-gauche* isomerism and the large-amplitude torsional motions of the alcohol and methyl groups [182, 215–220]. The complex splitting of bands due to the flexible ethanol monomer have been studied theoretically [220] and the paper cites several microwave studies to characterize the vibrational ground state and the *trans-gauche* isomerism. For a higher level of detail about the excited energy sub-levels of the ethanol monomer reference is made to the paper by Senent *et al.* and references therein [220]. In the present far-infrared absorption spectrum of ethanol embedded in cryogenic neon matrices (Ne:CH_3CH_2OH) = (1200:1), shown in Figure 2.23, a series of weak and medium-intensity bands are observed beside the strong CCO bending fundamental transition at 419.9 cm^{-1}. A strong and sharp transition arise at 208.9 cm^{-1} with two shoulders at 206.5 cm^{-1} and 202.4 cm^{-1}. The spectra further reveal a broad medium-intense band at 287.4 cm^{-1}, a medium-intense band around 258 cm^{-1} and a weaker band at 243 cm^{-1}. These bands are in agreement with the coupled torsional bands of the alcohol and methyl group [220]. Isotopic H/D substitution of the alcohol group, both in ethanol-d_1 and ethanol-d_6 red-shifts the 287.4 cm^{-1} band to below 200 cm^{-1} thus clearing the important spectral region from 300 cm^{-1} to 600 cm^{-1}.

The far-infrared spectra, shown in Figure 2.24, for cryogenic neon matrices doped with ethanol (Ne:CH_3CH_2OH:H_2O) = (1200:1:0), water (1740:0:1) and a mixture of ethanol and water (7200:4:3) simultaneously reveal new distinct bands in close vicinity of the high-frequency out-of-plane and low-frequency in-plane donor OH libration bands of the water/methanol dimer, the water/*t*-butanol and the water dimer. A weak band appears around 320 cm^{-1} on the shoulder of the low-frequency in-plane water dimer donor OH librational band at 309.1 cm^{-1}. A stronger and more distinct

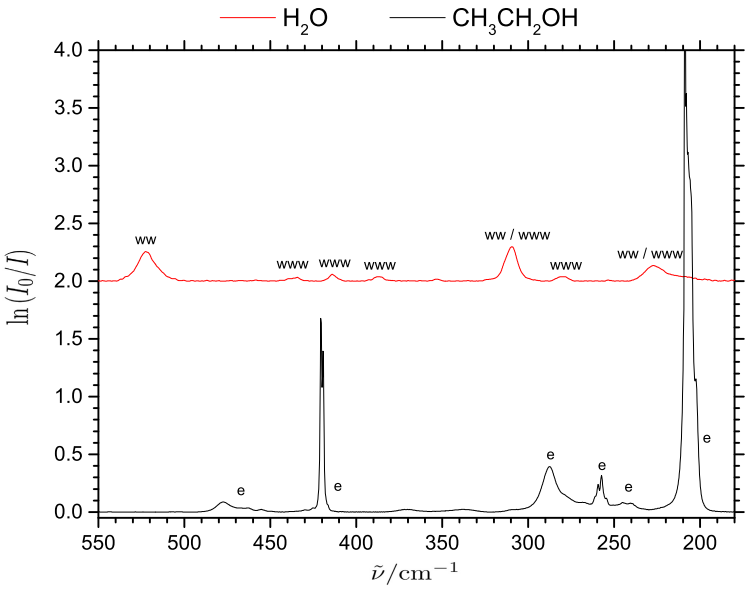

Figure 2.23: Far-infrared absorption spectrum of ethanol (Ne:EtOH:H_2O) = (1200:1:0) and water (1740:0:1) embedded in cryogenic neon matrices at 2.8 K.

feature appears at 551.6 cm^{-1} corresponding to the out-of-plane donor OH librational mode. The size of the blue-shift follows the trend previously observed in the interaction between water and methanol or *t*-butanol. The band origin of 551.6 cm^{-1} suggests a stronger interaction for the water/ethanol interaction than for the water/methanol interaction, but slightly weaker than the water/*t*-butanol interaction. The dual inlet procedure allow for an unambiguous assignment of the donor/acceptor relationship of the interaction between ethanol and water. Isotopic substitution of the water subunit results in an isotopic red-shift from 551.6 cm^{-1} to 412.5 cm^{-1}, confirming the previous hydrogen bond donor/acceptor properties from the methanol and *t*-butanol studies. The low-frequency donor OD in-plane librational mode is shifted to the congested spectral region of monomer bands belonging to the complex methyl and alcohol torsional motions, allowing only a tentative assignment at 239.6 cm^{-1} for this band.

Isotopic substitution of ethanol deposited with regular water can be used to further support the assignment. A small isotopic red-shift of 6 cm^{-1} is observed for the out-of-plane donor OH librational mode for complexes of water/ethanol-d_1 (1630:2:1) and water/ethanol-d_6 (1630:2:1). Contrary to the far-infrared spectra of regular ethanol, the spectra of deuterated ethanol and regular water contain two distinct bands at 545.6 cm^{-1} and 541.1 cm^{-1}. The intensity increase of these bands after annealing suggests that two conformations are present in the matrix. The relative pre- and

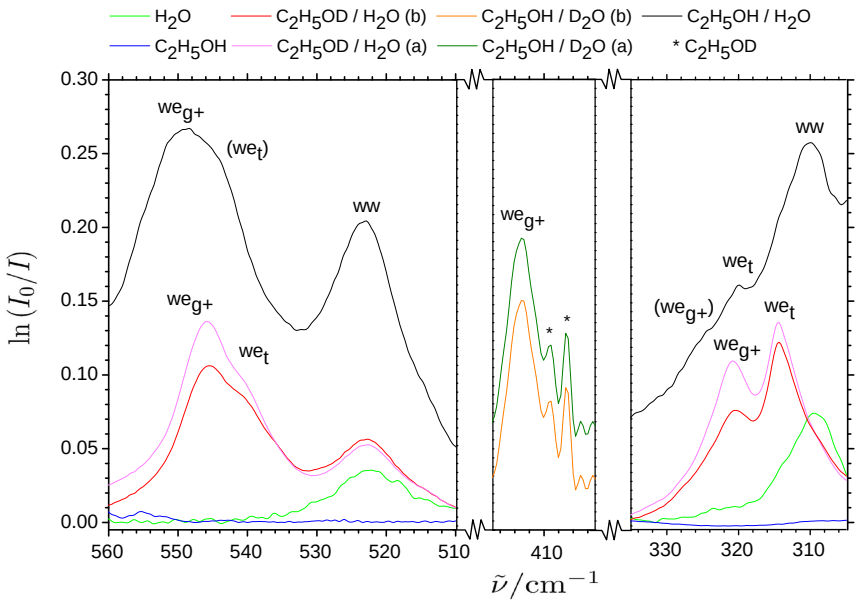

Figure 2.24: Far-infrared absorption spectra of 1.0 cm^{-1} resolution of cryogenic neon matrices doped with pure water (Ne:EtOH:H_2O) = (1740:0:1), pure ethanol(1200:1:0), ethanol - water (7200:4:3), ethanol-D_1-water (1630:2:1), ethanol-D_6-water (1630:2:1) and ethanol-D_2O(1600:2:1) at 2.8 K. Parenthesis of (a) and (b) denote after and before annealing at 9 K.

post-annealing intensity of the two bands differ, with the high-frequency band at 545.6 cm^{-1} being more intense than the low-frequency band at 541.1 cm^{-1}. The most stable conformation of the ethanol-water dimer must be preferred as the matrix becomes softer and small molecules are allowed to move "freely" inside the confinement of the matrix environment. The band at 545.6 cm^{-1} must thus be related to the most stable conformation of the dimer. An identical effect is observed for the low-frequency in-plane donor OH librational modes, where two bands are observed at 320.9 cm^{-1} and 314.7 cm^{-1}. The pre- and post-annealing spectra again reveal a difference in intensity. A more significant increase of the band intensity for the 320.9 cm^{-1} band, allows for an assignment of this band to the most stable conformation. Complete deuteration of ethanol likewise enables observation of two different conformations of the water/ethanol complex. The assignments of the observed librational modes for water/ethanol complexes are listed in Table 2.18. However, in order to assign the observed librational modes for the two different ethanol/water conformers, quantum chemical predictions are consulted.

Table 2.18: The observed high-frequency out-of-plane and low-frequency in-plane donor OH (OD) librational band origins (cm^{-1}) for isotopic water complexes and isotopic mixed complexes of water with ethanol-*trans* (e_t) and ethanol-*gauche*$_+$ (e_{g+}) embedded in cryogenic neon matrices at 2.8 K.

Donor-Acceptor	$\nu_{\text{lib,out-of-plane}}$	$\nu_{\text{lib,in-plane}}$	Donor-Acceptor	$\nu_{\text{lib,out-of-plane}}$	$\nu_{\text{lib,in-plane}}$
H_2O-H_2O	522.4[a]	309.1[a]	D_2O-D_2O	393.2[a]	233.5[a]
H_2O-CH_3OH	527.3	[b]	D_2O-CH_3OH	397.6	[c]
H_2O-CH_3OD	523.7	296.2	D_2O-CH_3OD	395.0	[c]
H_2O-CD_3OD	523.9	295.9	D_2O-CD_3OD	[c]	[c]
H_2O-$CH_3CH_2OH_t$	545.4	320.4	D_2O-$CH_3CH_2OH_t$	[d]	[d]
H_2O-$CH_3CH_2OH_{g+}$	551.6	324.7	D_2O-$CH_3CH_2OH_{g+}$	412.5	239.6
H_2O-$CH_3CH_2OD_t$	541.1	314.7	D_2O-$CH_3CH_2OD_t$	[e]	[d]
H_2O-$CH_3CH_2OD_{g+}$	545.6	320.9	D_2O-$CH_3CH_2OD_{g+}$	[d]	238.2
H_2O-$CD_3CD_2OD_t$	540.1	313.9			
H_2O-$CD_3CD_2OD_{g+}$	545.6	320.9			

[a] Ceponkus *et al.* [73]
[b] Overlapped with water dimer
[c] Overlapped with water-d_2 dimer
[d] Not observed
[e] Overlapped with ethanol-d_1 C-C-O bending

The five different conformers for the interaction between ethanol and water have been investigated using B3LYP, B3LYP-D3, MP2 and subsequent CCSD(T) and CCSD(T)-F12 calculations coupled with Dunning's augmented double, triple and quadruple zeta basis sets. The relative dissociation energies D_0 calculated at the CCSD(T)-F12/aug-cc-pVQZ level of theory with MP2/aug-cc-pVTZ zero-point vibrational energies are illustrated in Figure 2.25.

The quantum chemical results for the two most stable conformers of the water/ethanol dimers are listed in Table 2.19. The computational predictions show that the B3LYP functional underestimates the dissociation energy D_e for the most stable mixed complex of water and ethanol in the *gauche*$_+$ (we_{g+}) conformation by more than 20 % relative to the combined MP2/aug-cc-pVQZ/CCSD(T)-F12/aug-cc-pVQZ calculations. The dispersion corrected B3LYP-D3 method by Grimme *et al.* [99] slightly overestimates the dissociation energy by 5 % (1.5 kJ·mol^{-1}) relative to the benchmark value of 26.50 at the MP2/aug-cc-pVTZ/CCSD(T)-F12/aug-cc-pVTZ level of theory. The harmonic zero-point vibrational energy of 8.3 kJ·mol^{-1} results in a dissociation energy D_0 of 18.2 kJ·mol^{-1} for the most stable conformation. In the most stable geometry of the mixed ethanol/water dimer, the ethanol subunit is forced from the *trans* global energy minimum conformation of the monomer to the less stable *gauche* conformation in the dimer. This is considered one of the most simple cases of adaptive aggregation where a non-rigid molecule is forced into a less stable conformation upon non-covalent interactions to optimize the combined interaction energy. The second most stable conformation of water with ethanol in *trans* conformation is likewise further stabilized by a secondary and weaker C-H $\cdots$ O hydrogen bond interaction. The difference in dissociation energy between the two most stable conformations depends on both the size of the basis set and the computational method. The B3LYP approach predicts an almost identical D_e, whereas the B3LYP-D3 method slightly overestimates the difference when compared to the benchmark value of 0.6 kJ·mol^{-1}. The effect of zero-point vibrational energies is thus critical for further discussion.

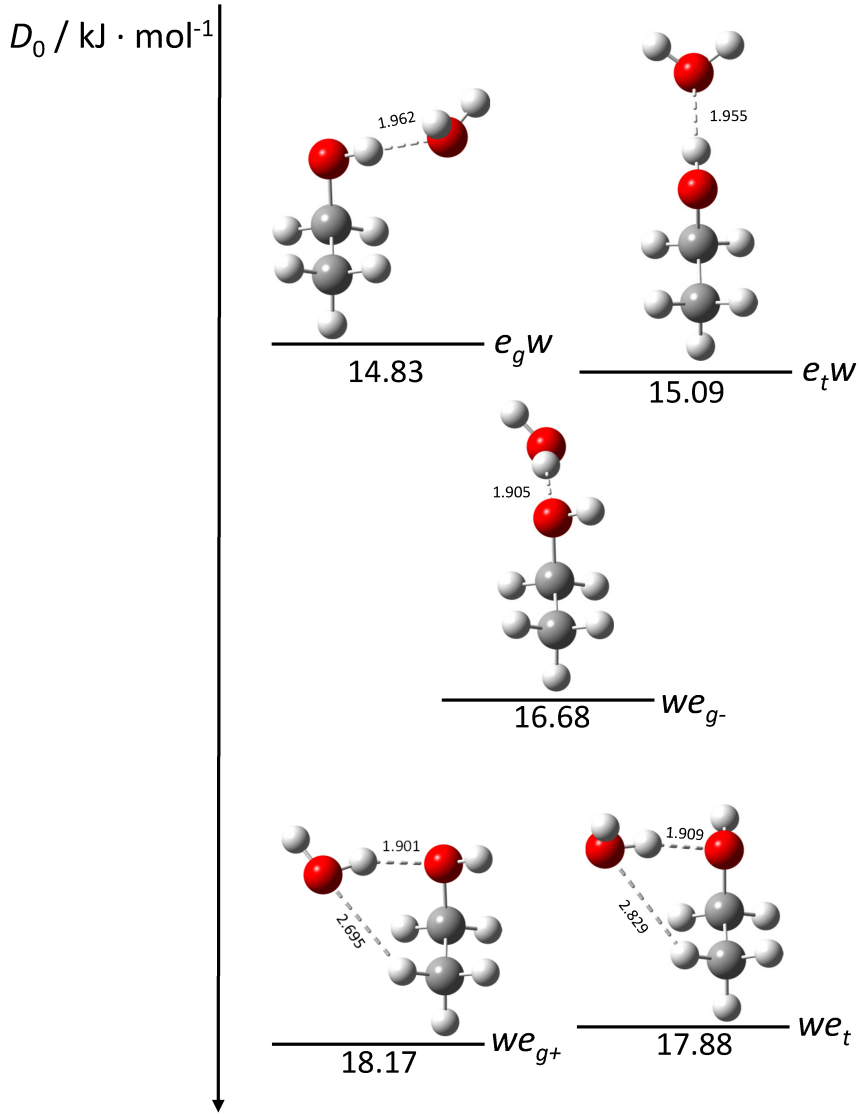

Figure 2.25: The energy landscape of ethanol/water dimers optimized at the MP2/aug-cc-pVQZ level of theory and further refined by CCSD(T)-F12/aug-cc-pVQZ calculations. The zero-point vibrational energy is determined at the MP2/aug-cc-pVTZ level of theory.

Table 2.19: The electronic dissociation energy D_e of the two most stable hydrogen bonded complex of water with ethanol in *trans* and *gauche+* conformations, and the difference of electronic dissociation energy between the two different conformers ΔE_e predicted from several combined quantum chemical methodologies for geometry and electronic energy calculations using Dunnings augmented correlation consistent triple zeta (aug-cc-pVTZ) or quadruple zeta (aug-cc-pVQZ) basis sets.

Geometry Optimization[a]	**Electronic Energy**	$\boldsymbol{D_e(we_t)}$/kJ·mol^{-1}	$\boldsymbol{D_e(we_{g+})}$/kJ·mol^{-1}	$\boldsymbol{\Delta E_e}$/kJ·mol^{-1}
B3LYP/aug-cc-pVTZ	B3LYP/aug-cc-pVTZ	20.96	20.99	0.03
B3LYP-CP/aug-cc-pVTZ[b]	B3LYP/aug-cc-pVTZ	20.66	20.69	0.04
B3LYP-CP/aug-cc-pVTZ[b]	CCSD(T)/aug-cc-pVTZ	26.30	26.33	0.03
B3LYP-D3/aug-cc-pVTZ	B3LYP-D3/aug-cc-pVTZ	27.40	28.02	0.61
B3LYP-D3-CP/aug-cc-pVTZ[b]	B3LYP-D3/aug-cc-pVTZ	27.06	27.68	0.62
B3LYP-D3-CP/aug-cc-pVTZ[b]	CCSD(T)/aug-cc-pVTZ	27.48	27.96	0.48
MP2/aug-cc-pVTZ	MP2/aug-cc-pVTZ	26.91	27.27	0.36
MP2-CP/aug-cc-pVTZ[b]	MP2/aug-cc-pVTZ	24.16	24.52	0.37
MP2-CP/aug-cc-pVTZ[b]	CCSD(T)/aug-cc-pVTZ	26.92	27.46	0.54
MP2-CP/aug-cc-pVTZ[b]	CCSD(T)-F12/aug-cc-pVTZ	26.43	27.01	0.58
MP2/aug-cc-pVQZ	MP2/aug-cc-pVQZ	26.20	26.61	0.41
MP2-CP/aug-cc-pVQZ[b]	MP2/aug-cc-pVQZ	24.84	25.24	0.40
MP2-CP/aug-cc-pVQZ[b]	CCSD(T)/aug-cc-pVDZ	28.03	28.48	0.45
MP2-CP/aug-cc-pVQZ[b]	CCSD(T)/aug-cc-pVTZ	26.97	27.50	0.53
MP2-CP/aug-cc-pVQZ[b]	CCSD(T)/aug-cc-pVQZ	26.05	26.63	0.58
MP2-CP/aug-cc-pVQZ[b]	CCSD(T)-F12/aug-cc-pVQZ	25.94	26.50	0.56
MP2-CP/aug-cc-pVQZ[b]	CCSD(T)/CBS	25.01	25.63	0.61

[a] RMS force criterion set to 10^{-6} (atomic units) for all geometry optimizations
[b] CP = Counterpoise Correction applied

The change in zero-point vibrational energy upon weak intermolecular interaction is highly complicated to predict by quantum chemical approaches. Especially the large-amplitude and anharmonic intermolecular vibrational modes are difficult to predict as illustrated for the water/methanol dimer and the methanol homodimer [40]. Harmonic and anharmonic (VPT2) predicted band origins for the two observed donor OH librational modes for the two most stable conformations of the ethanol/water complex are listed in Table 2.20.

Table 2.20: Harmonic and anharmonic VPT2 band origins (in units of cm^{-1}) for the two observed high-frequency out-of-plane and low-frequency in-plane librational modes for the we_{g+} and we_t conformers at the MP2/aug-cc-pVTZ level of theory.

	$\mathbf{we}_g+$		$\mathbf{we}_t$	
	$\nu_{\mathrm{lib,high}}$	$\nu_{\mathrm{lib,high}}$	$\nu_{\mathrm{lib,high}}$	$\nu_{\mathrm{lib,low}}$
MP2/aug-cc-pVTZ	653.6	372.9	660.1	379.4
VPT/aug-cc-pVTZ	548.8	320.1	543.4	318.5

The VPT2 method has previously shown to be able to predict excellent anharmonic band origins for both the methanol dimer and mixed complexes of methanol and water. The ordering of the harmonic band origins is in qualitative agreement with the previous experimental findings of the interaction of water with methanol and *t*-butanol. The ethanol/water interaction is stronger than the methanol/ water interaction but weaker than the *t*-butanol/water interaction. However, the second most stable dimer we_t conformation is predicted to have a higher band origin at 660 cm^{-1} than the most stable we_{g+} conformation at 654 cm^{-1} which is contradictory to the spectroscopic observables where the most stable conformation has the highest band origin. The anharmonic VPT2 predictions, however, reverse the order of the predicted band origins, and confirm the anharmonic contribution of approximate 15-20 % as previously observed for both the water/methanol dimer and the methanol homodimer. A complete treatment of the large-amplitude motions predicted at the VPT2 level of theory would stretch the reliability of this method and the zero-point vibrational energy is thus determined from harmonic frequency predictions at the MP2/aug-cc-pVTZ level of theory. The calculated dissociation energies D_0 for the two most stable conformers and isotopologues are listed in Table 2.21. The total change of the vibrational zero-point energy upon complexation varies between 6.4 and 8.3 $kJ{\cdot}mol^{-1}$ in the harmonic approximation. The sum of the donor OH librational modes account for as much as 5.2 $kJ{\cdot}mol^{-1}$ or roughly 60 % of the total zero-point vibrational energy. The difference between the two most stable conformers of ethanol and water translates into a smaller energy difference of 0.28 cm^{-1} $kJ{\cdot}mol^{-1}$ for the dissociation energy D_0. It is noteworthy that the small energy difference for the complexes of regular isotopes translate into an even smaller difference

Table 2.21: The electronic dissociation energy D_e (CCSD(T-F12/aug-cc-pVQZ[a]), the total change of harmonic vibrational zero-point energy upon complexation ΔZPE_{tot}^{calc} (MP2/aug-cc-pVTZ) and the resulting absolute dissociation energy D_0 for mixed isotopic hydrogen bonded donor-acceptor complexes together with the observed (anharmonic) contribution to the zero-point energy from the class of donor OH librational modes ΔZPE_{lib}^{exp} (all values in units of kJ·mol^{-1}).

	$\mathbf{we}_t$	$\mathbf{we}_t(\mathbf{d}_1)$	$\mathbf{we}_t(\mathbf{d}_6)$	$\mathbf{w(d}_2\mathbf{)e}_t$
D_e	25.94[a]	25.94[a]	25.94[a]	25.94[a]
ΔZPE_{tot}^{calc}	8.05	7.85	7.64	6.39
ΔZPE_{lib}^{exp}	**5.2**	**5.1**	**5.1**	[c]
D_0	17.89	18.09	18.30	19.55

	$\mathbf{we}_{g+}$	$\mathbf{we}_{g+}(\mathbf{d}_1)$	$\mathbf{we}_{g+}(\mathbf{d}_1)$	$\mathbf{w(d}_2\mathbf{)e}_{g+}$
D_e	26.50[a]	26.50[a]	26.50[a]	26.50[a]
ΔZPE_{tot}^{calc}	8.33	8.21	7.96	6.68
ΔZPE_{lib}^{exp}	**5.2**	**5.2**	**5.2**	**3.9**
D_0	18.17	18.29	18.54	19.82
$\Delta(D_0)$	0.28	0.20	0.24	0.27

[a] Electronic dissociation energies D_e calculated at the CCSD(T)/aug-cc-pVTZ level based on optimized geometries at the MP2/aug-cc-pVTZ level.

[b] Includes the observed band origin of the high-frequency donor OD librational mode and an anharmonically predicted band origin for the low-frequency donor OD librational mode.

[c] Not observed

for water/ethanol-d_1 of 0.20 kJ·mol^{-1} and 0.24 kJ·mol^{-1} for the water/ethanol-d_6 complexes. The smaller difference between the molecular complexes help to explain the fact that both conformations are observed in the recorded far-infrared absorption spectra. The H/D substitution of the water subunit results in a slight difference of 0.27 kJ·mol^{-1} between the D_0 values and possibly explains why only one conformation is observed.

The sharper bands for deuterated species in matrices help to explain the observation of both conformers for the water/ethanol-d_1 and water/ethanol-d_6 interactions. However, it does not explain why the high-frequency bands are overlapped and the low-frequency bands are separated. The normal mode pictures in Figure 2.21 reveal that the high-frequency out-of-plane donor OH librational mode is a localized motion of the bound hydrogen atom, while the low-frequency in-plane donor librational mode can be viewed as a hindered *c*-axis rotation. The high-frequency in-plane donor OH librational mode was previously determined to be an excellent probe for the strength of the primary O-H $\cdots$ O hydrogen bond, in similar fashion to the

Badger-Bauer relationship [14]. The low-frequency in-plane donor librational mode must thus be more affected by the weak secondary hydrogen bond interaction than the out-of-plane librational mode. In a series of quantum chemical calculations with fixed intermolecular hydrogen bond interactions, the effect of the secondary hydrogen bond interaction was investigated. By shortening and varying the length of the secondary hydrogen bond while keeping the primary hydrogen bond fixed, the effect can be seen in the resulting harmonic frequency predictions of the forced geometries. The change in predicted harmonic band origins of the in-plane donor OH librational mode, the out-of-plane donor OH librational mode and the donor OH stretching as a function of the displacement of the secondary hydrogen bond relative to the equilibrium value can be seen in Figure 2.26. The change of the harmonic band origin

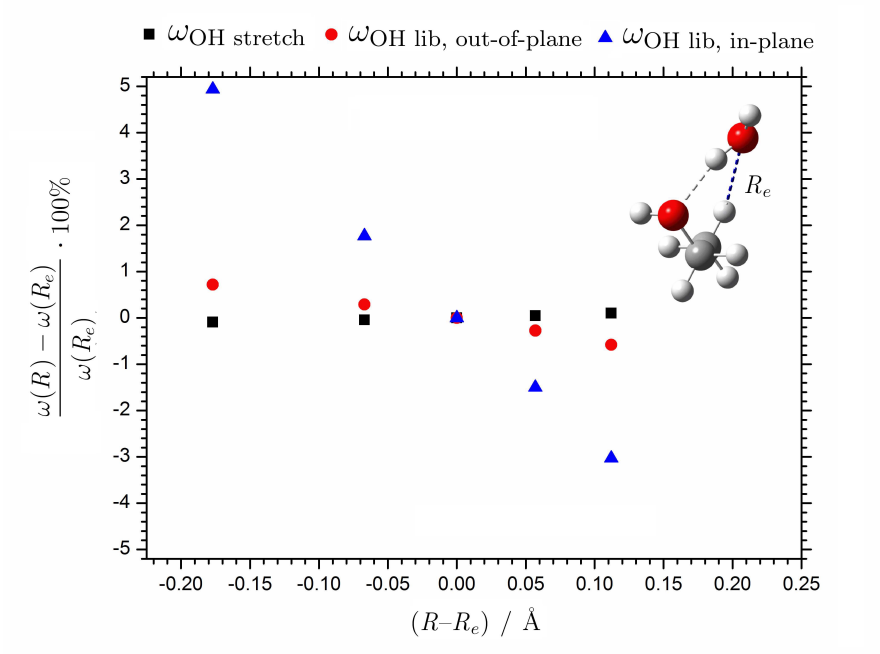

Figure 2.26: The predicted relative harmonic band origins at the MP2/aug-cc-pVTZ level of theory for the intramolecular OH stretching (black squares), the high-frequency out-of-plane (red circles) and the low-frequency in-plane (blue triangles) donor OH librational modes as a function of the displacement R-R_e from the intermolecular equilibrium O ···HC hydrogen bond distance for the most stable conformation of the water/ethanol dimer (we_{g+}).

of the donor OH stretching mode and the high-frequency out-of-plane donor OH li-

brational mode are predicted to be almost unaffected by a change in the secondary hydrogen bond distance. A shortening of the bond distance of 0.075 Å corresponds to a relative red-shift of less than 0.5 ‰ for the red-shifted donor OH stretching. The in-plane donor OH librational mode is more affected by the intermolecular O $\cdots$ HC hydrogen bond distance and a blue-shift of approximate 7.5 cm^{-1} is observed for a 0.075 Å shortened intermolecular distance. The blue-shift of 7.5 cm^{-1} corresponds to a change of 2.5 %. The relative blue-shift of the low-frequency in-plane donor OH librational mode is thus one order of magnitude larger than the relative spectral shifts for the red-shifted donor OH stretching fundamental. The significant dependence on the C-H $\cdots$ O hydrogen bond distance supports the assumption that the low-frequency in-plane donor OH librational mode provides an excellent probe for the weak secondary intermolecular interaction. The quantum chemical exploration provides a qualitative explanation of the proposed assignment of the two separated bands in the far-infrared spectrum for both ethanol-d_1 and ethanol-d_6 with water. The proposed assignment of the band at 320.9 cm^{-1} to the $we_{g+}(d_1)$ conformation seems reasonable as the intermolecular O $\cdots$ HC bond distance of 2.695 Å is shorter than the bond distance of 2.829 Å for the $we_t(d_1)$ conformer, as listed in Table 2.17.

To summarize, the most stable geometry of the water/ethanol dimer has been assigned by dual inlet neon matrix isolation experiments. In the most stable we_{g+} geometry a second cooperative hydrogen bond is formed between a terminal C-H group and an oxygen lone pair from water, forcing the ethanol into its less stable *gauche* conformation. The low-frequency in-plane donor OH librational band provides an excellent spectroscopic probe for the secondary hydrogen bond interactions.

2.4.4 Hydrogen Bonding between Isopropanol and Water

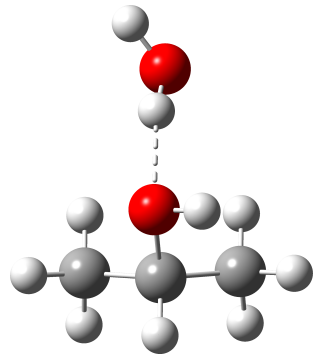

Figure 2.27: The MP2/aug-cc-pVTZ optimized geometry of the most stable hydrogen bonded conformation of the isopropanol/water complex

Isopropanol, the most simple secondary alcohol, is a commonly used chemical in the industry as a solvent. Despite the industrial importance very little attention has been given to the infrared [221–227], Raman [228] or the rotational [229–234] spectrum of isopropanol. Isopropanol can theoretically appear in several conformations as there is free rotation for the two methyl groups and the alcohol group, however, only two conformations are reported in the literature; a *gauche*- and a *trans* conformation [221, 227]. The hydrogen bond interaction between isopropanol and water is thus a subtle balance between the monomer conformation and the donor/acceptor relationship between alcohols and water, now well-established based on the observations between water and methanol, ethanol and *t*-butanol.

The far-infrared absorption spectrum of isopropanol reveals several strong transitions that can be assigned to torsional motions of the alcohol and methyl groups. The region below 300 cm^{-1} is omitted in figure 2.28 as this region is dominated by torsional motions of both the alcohol and methyl groups, and couplings between the different modes [223, 224]. In the spectrum above 300 cm^{-1} a skeletal C-C-O bending mode can be observed as a broad spectral feature with band center at 370.0 cm^{-1}, while the strong band at 416.6 cm^{-1} can be tentatively assigned to the first overtone transition of the alcohol torsion for which the fundamental is observed at 217.3 cm^{-1}. The broad feature at 485.2 cm^{-1} can be assigned to a skeletal C-C-C-O bending motion. The two weak bands at 468.6 cm^{-1} and 440.6 cm^{-1} can possibly be assigned to combination bands of the methyl and alcohol torsion modes. For matrices embedded with both water and isopropanol new bands appear in close vicinity of the spectral features observed for 1:1 hydrated molecular clusters of methanol, ethanol and *t*-butanol. The high-frequency out-of-plane donor OH librational mode is observed at 554.3 cm^{-1}, while the in-plane donor OH librational mode is observed at 317.3 cm^{-1}. The complete deuteration of the alcohol subunit results in a small and

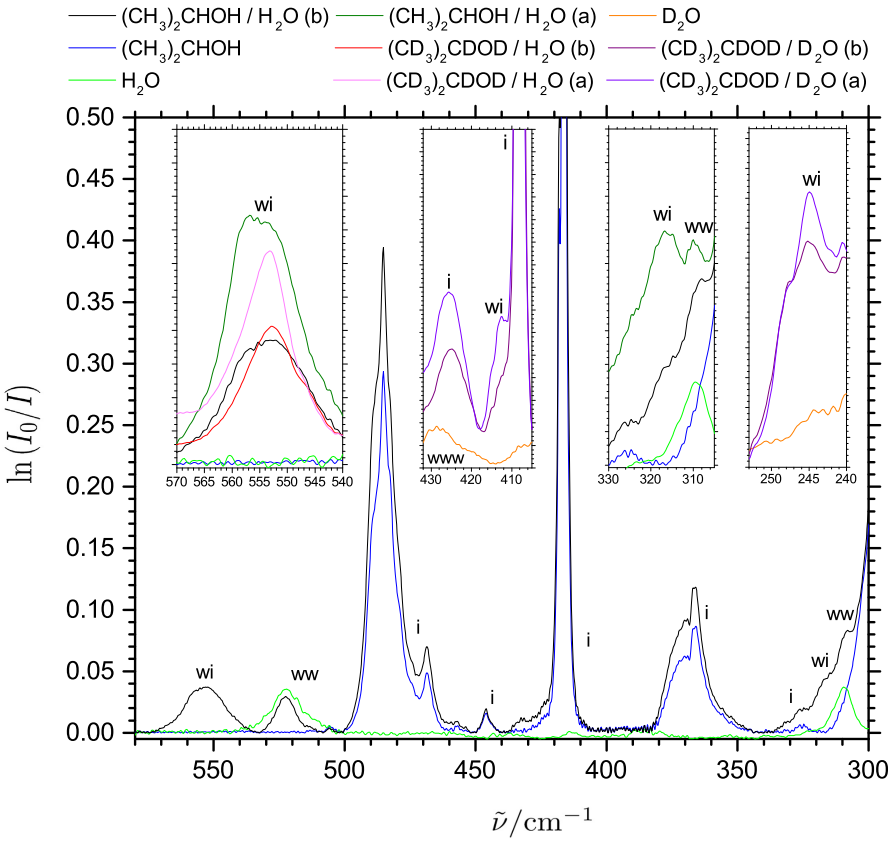

Figure 2.28: Far-infrared absorption spectra of 1.0 cm^{-1} resolution of cryogenic neon matrices doped with pure water (H_2O:Ne) = (1:2000), pure isopropanol with traces of H_2O (CH_3OH:H_2O:Ne)=(3:1:13000) and different isotopic water/isopropanol mixtures ($(CH_3)_2CHOH$:H_2O:Ne) = (3:2:6000) at 2.8 K

reproducible isotopic red-shift of 1.6 cm^{-1} for the high-frequency out-of-plane donor OH librational mode observed at 552.7 cm^{-1} for the water/isopropanol-d_8 complex. The low frequency in-plane donor librational mode for the water/isopropanol-d_8 complex cannot be assigned due to overlapping isopropanol-d_8 monomer fundamentals and combination bands. For experiments with isopropanol-d_8 and water-d_2 the high-frequency out-of-plane donor OD librational band can be observed at 412.7 cm^{-1}, while the in-plane donor OD librational band can be tentatively assigned at 244.9 cm^{-1}, with both bands reproduced by a concentration dependency series.

The quantum chemical predictions at the MP2/aug-cc-pVTZ level of theory for the isopropanol/water system are considered to assign the observed librational modes. A

Table 2.22: The electronic dissociation energy D_e of the most stable hydrogen bonded complex of water with isopropanol and the difference of electronic dissociation energy between the two different conformers ΔE_e predicted from several combined quantum chemical methodologies for geometry and electronic energy calculations using Dunnings augmented correlation consistent triple zeta (aug-cc-pVTZ) basis set.

Geometry Optimization[a]	Electronic Energy	D_e/kJ·mol^{-1}	ΔE_e/kJ·mol^{-1}
B3LYP	B3LYP	21.37	4.19
B3LYP-CP[b]	B3LYP	21.02	4.17
B3LYP-CP[b]	CCSD(T)	29.20	6.32
B3LYP-D3	B3LYP-D3	29.56	7.60
B3LYP-D3-CP[b]	B3LYP-D3	29.15	7.54
B3LYP-D3-CP[b]	CCSD(T)	29.14	6.32
MP2	MP2	29.16	6.62
MP2-CP[b]	MP2	25.99	5.95
MP2-CP[b]	CCSD(T)	29.19	6.40
MP2-CP[b]	CCSD(T)-F12	28.47	6.07

[a] RMS force criterion set to 10^{-6} (atomic units) for all geometry optimizations
[b] CP = Counterpoise Correction applied

Table 2.23: The electronic dissociation energy D_e (CCSD(T)-F12/aug-cc-pVTZ[a]), the total change of harmonic vibrational zero-point energy upon complexation ΔZPE(MP2/aug-cc-pVTZ) and the resulting absolute dissociation energy D_0 for mixed isotopic hydrogen bonded donor-acceptor complexes (all values in units of kJ·mol^{-1}) of isopropanol and water.

	D_e	ΔZPE	D_0
H_2O–$(CH_3)_2CHOH$	28.47[a]	8.49	19.98
$CH_3)_2CHOH$–H_2O	22.40[a]	6.27	16.13
H_2O–$(CD_3)_2CDOD$	28.47[a]	8.12	20.35
$CD_3)_2CDOD$–H_2O	22.40[a]	5.69	16.71

	D_e	ΔZPE^{calc}_{tot}	D_0
D_2O–$(CH_3)_2CHOH$	28.47[a]	6.86	21.61
$(CH_3)_2CHOH$–D_2O	22.40[a]	5.51	16.89
D_2O–$(CD_3)_2CDOD$	28.47[a]	6.48	21.99
$(CD_3)_2CDOD$–D_2O	22.40[a]	4.91	17.49

[a] Electronic dissociation energies D_e calculated at the CCSD(T)/aug-cc-pVTZ level based on optimized geometries at the MP2/aug-cc-pVTZ level.

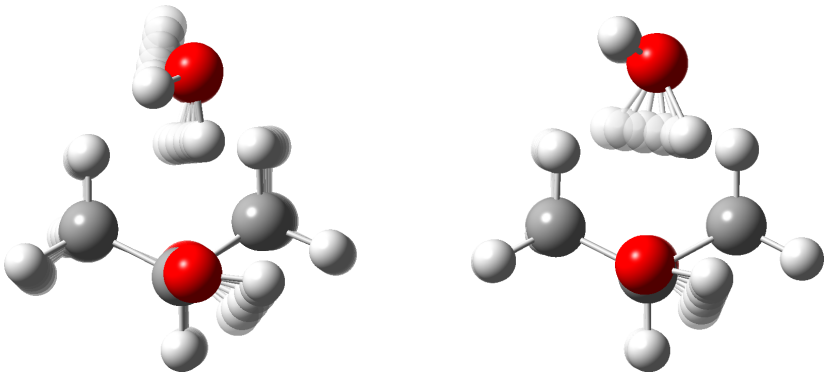

(a) The low-frequency in-plane donor OH librational mode

(b) The high-frequency out-of-plane donor OH librational mode

Figure 2.29: Normal mode illustrations of the two observed librational modes for the water/isopropanol dimer

single conformation of the water donor complex and a single conformation of the water acceptor complex were determined, both with isopropanol in *gauche* conformation. Even though the isopropanol monomer can exist in two conformers, no change in conformation is observed for the mixed dimer with water. The interaction between isopropanol and water, like the interaction between *t*-butanol and water, illustrates some of the challenges associated with the description of weak non-covalent intermolecular interactions. The interaction energy listed in 2.23 determined by B3LYP/aug-cc-pVTZ compared to the benchmark MP2/aug-cc-pVTZ/CCSD(T)-F12/aug-cc-pVTZ level of theory significantly underestimates the counterpoise corrected dissociation energy D_e for the most stable conformation by 7.1 kJ·mol^{-1}. MP2/aug-cc-pVTZ optimized geometry and the corresponding interaction energy is likewise underestimated by 2.5 kJ·mol^{-1} when compared to the interaction energy determined by CCSD(T)-F12/aug-cc-pVTZ for the MP2/aug-cc-pVTZ optimized geometry. The B3LYP-D3 functional with dispersion correction, however, overestimates the binding energy by 0.7 kJ·mol^{-1} relative to the benchmark level of theory.

The intermolecular hydrogen bond interaction between isopropanol and water follow the trend observed for the previous alcohol/water complexes. The small energy difference between the interaction of water with isopropanol or *t*-butanol and the related minor difference in the out-of-plane donor OH librational band origin indicates that there is just a minor extra inductive effect associated with the third methyl group of *t*-butanol. One might argue that the absolute value of the interaction between a saturated monohydric alcohol and water is close to the value of the interaction energy between *t*-butanol and water.

2.4.5 Hydrogen Bond Donor/Acceptor Switching upon Fluorination

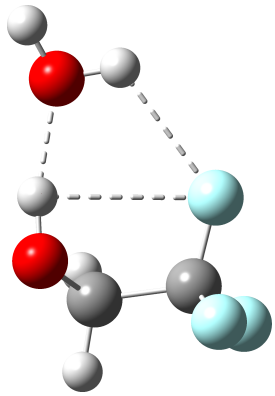

Figure 2.30: Global energy minimum structure of the dimer of 2,2,2-trifluoroethanol and water optimized at the MP2/aug-cc-pVTZ level of theory

Alcohol based solvents have been used to stabilize secondary structures in peptides and to denature proteins. Fluorinated alcohols such as 2,2,2-trifluoroethanol or 1,1,1,3,3,3-hexafluoroisopropanol have shown to be able to increase the population of α-helices and β-sheets in the secondary structure of proteins when added as a co-solvent at low concentrations, whereas higher concentrations of the fluorinated alcohols can denature proteins [235–238]. The low polarity weakens hydrophobic interactions that stabilize the compact native structure of proteins but simultaneously increases hydrogen bonding which stabilizes secondary structures [239]. The alcohol group of 2,2,2-trifluoroethanol becomes a much weaker hydrogen bond acceptor as the fluor atoms attract electron density.

Homodimers of the most simple fluorinated alcohol, 2,2,2-trifluoroethanol, and heterodimers with water have been studied theoretically [240, 241] and experimentally [218, 224, 242–250]. The geometry of the global energy minimum for the 2,2,2-trifluoroethanol monomer is a *gauche*-conformation in which an intramolecular hydrogen bond is formed between the alcohol group and one of the fluor atoms. This is contrary to the conformation of regular ethanol in which the global energy minimum is a *trans*-conformation.

The hydrogen bonding between 2,2,2-trifluoroethanol and water has previously been studied by rotational spectroscopy by Thomas and Xu [249] and a single potential energy minimum conformation with 2,2,2-trifluoroethanol as the hydrogen bond donor and water as the hydrogen bond acceptor has been reported. The experimental observations are supported by theoretical predictions by Senent *et al.* [241].

The far-infrared and terahertz spectrum of the 2,2,2-trifluoroethanol is dominated by skeletal motions, torsional motion of the alcohol group and torsional motion of the CF_3 group. The previous far-infrared and terahertz observations of Barnes *et al.* [224], of Durig and Larsen [218] and of Kollipost [251], eased the assignments of the fundamental vibrational modes associated with the 2,2,2-trifluoroethanol monomer in the global *gauche* energy minimum in cryogenic neon matrices at 2.8 K. The present combined far-infrared and terahertz absorption spectra of 2,2,2-trifluoroethanol embedded in several millimeter thick neon matrices (Ne:CF_3CH_2OH:H_2O) (4460:1:0) reveal a weak band at 129.8 cm^{-1} that is assigned to the CF_3 torsional mode. A medium strong band is observed at 225.2 cm^{-1} and assigned to the rocking mode of the CF_3 group. A very weak band with a band center of 257.8 cm^{-1} is assigned to the first overtone of CF_3 torsional band. Two very strong transitions at 280.6 cm^{-1} and 278.9 cm^{-1} are assigned to the OH torsional mode of the alcohol group. A medium band at 365.7 cm^{-1} is assigned to another CF_3 rocking mode. A medium strong band at 417.0 cm^{-1} is assigned to a C-C-O bending mode. Four bands at 472.0 cm^{-1}, 485.8 cm^{-1}, 491.8 cm^{-1} and 496.6 cm^{-1} cannot easily be assigned. These bands seem to be associated with the 2,2,2-trifluoroethanol monomer as no change in intensity is observed between pre- and post-annealing experiments which is expected for molecular cluster bands. Two bands are observed at 532.7 cm^{-1} and 546.7 cm^{-1} and are assigned to a deformation of the CF_3 group. A very distinct doublet feature at 666.7 cm^{-1} and 658.5 cm^{-1} is assigned to two CF_3 deformations.

The simultaneous deposition of 2,2,2-trifluoroethanol and water (Ne:CF_3CH_2OH:H_2O) = (2700:1:1) in several millimeter thick cryogenic neon matrices at 2.8 K reveals three new distinct bands in the terahertz region as shown in Figure 2.31. The bands observed at 111.6 cm^{-1}, 174.7 cm^{-1} and 211.5 cm^{-1}, are not associated with water clusters and depend on the concentration of both 2,2,2-trifluoroethanol and water in a stoichiometric 1:1 relationship. The intensity of all three bands scale together pre- and post-annealing, indicating that they belong to the same complex. In the far-infrared region, shown as an insert in Figure 2.31, a very broad feature is observed at 597.7 cm^{-1} with two shoulder bands at 611.2 cm^{-1} and 618.8 cm^{-1}. The relative intensity between the bands is constant and even appears at very low concentrations of water and 2,2,2-trifluoroethanol. The identical relative intensity of the bands are likewise reproduced pre- and post-annealing and can confidently be assigned to the 2,2,2-trifluoroethanol/water complex.

The intensity ratio between the three bands are likewise reproduced in the corresponding O-H stretching region of the same neon matrices where a triplet of bands are observed at 3519.7 cm^{-1}, 3508.1 cm^{-1} and 3493.8 cm^{-1}. The intensity of the triplet scales with the triplet of bands in the far-infrared region at 597.7 cm^{-1}, 611.2 and 618.8 cm^{-1}, with no relative intensity changes observed pre- and post-annealing. If the bands are related to a site splitting in the matrix they would disappear at higher temperatures due to a more flexible matrix, but the same intensity ratio before and af-

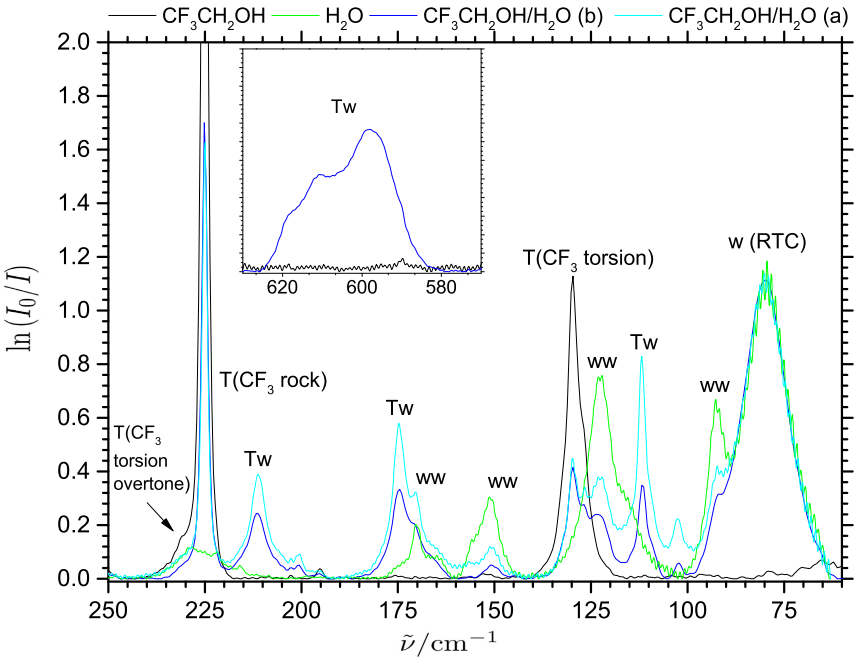

Figure 2.31: Terahertz absorption spectrum of 1.0 cm^{-1} resolution of 2,2,2-trifluoroethanol (Ne:CF_3CH_2OH:H_2O) (4460:1:0), water (1740:0:1) and 2,2,2-trifluoroethanol/water (2700:1:1) embedded in a cryogenic neon matrices at 2.8 K before (b) and after (a) annealing at 9 K. T denotes transitions of 2,2,2-trifluoroethanol, w of water, ww of the water dimer and Tw of 2,2,2-trifluoroethanol/water dimer.

ter annealing indicates that there are no site splittings in the matrix. The three bands could belong to three different conformations of the 2,2,2-trifluoroethanol/water interaction, which is a little surprising as only a single conformation has been observed in the combined theoretical and rotational spectroscopic study by Thomas and Xu [249] and in the supersonic jet expansions by Heger *et al.* [250]. The interaction energy can be directly correlated to the strength of the hydrogen bond interaction [6, 14], and it is thus surprising that the most intense OH-stretching band is the least red-shifted. The size of the blue-shift of the high-frequency out-of-plane donor OH librational mode can likewise be correlated to a stronger interaction as shown for the mixed alcohol/water complexes, but the most intense band is the least blue-shifted. It is thus a little contradictory that the most pronounced complex band is the least red-shifted in the OH-stretching region and the least blue-shifted donor librational mode, which makes it possible to confidently exclude the possibility of three different conformers. The bands could belong to larger mixed clusters, but that can be ruled out by the embedding of water and 2,2,2-trifluoroethanol in cryogenic neon matrices with larger

dopant concentrations.

The combined far-infrared and terahertz spectra of several millimeter thick cryogenic neon matrices embedded simultaneously with 2,2,2-trifluoroethanol and water-d_2 (Ne:CF_3CH_2OH:D_2O) = (2700:1:1) shown in Figure 2.32, likewise reveal three high-frequency out-of-plane OH donor librational bands at 585.3 cm^{-1}, 599.0 cm^{-1} and 609.6 cm^{-1}. The bands are red-shifted slightly relative to the regular 2,2,2-trifluoroethanol/water complex due to the higher reduced mass of water-d_2. A small red-shift of 12.4 cm^{-1} in the mixed complex with fully deuterated water confirms that 2,2,2-trifluoroethanol is the hydrogen bond donor. If water was the hydrogen bond donor, a much larger red-shift would have taken place as previously shown for the interaction between non-fluorinated alcohols and water. Again a constant relative concentration relationship between the three bands in the high-frequency out-of-plane donor OH librational region for the 2,2,2-trifluoroethanol/water-d_2 complex is observed pre- and post annealing, confirming that no site splittings occur in the neon matrix.

In the terahertz region a new complex band appears at 233.1 cm^{-1}. Pre- and post-annealing observations and a concentration dependency series show that this band should be assigned to the 2,2,2-trifluoroethanol/water-d_2 complex. Isotopic red-shifting is expected for H/D substitution of the water subunit, thus this band must belong to an intermolecular vibrational mode that has not been observed for the regu-lar complex. The three observed intermolecular vibrational acceptor modes for the regular complex are all expected to be red-shifted due to the higher reduced mass. The observed band at 211.5 cm^{-1} for the regular complex can be assigned at 168.6 cm^{-1} for the 2,2,2-trifluoroethanol/water-d_2 dimer, with an isotopic red-shift of 42.9 cm^{-1}. The band overlaps with a water-d_2 dimer band with a band center of 166 cm^{-1}. In the same region a new sharp spectral feature appears at 195.4 cm^{-1} belonging to the OD torsion for 2,2,2-trifluoroethanol-d_1 due to a small H/D exchange of the alcohol group with water-d_2. The OD torsion of 2,2,2-trifluoroethanol has previously been assigned by Durig and Larsen [218]. Another dimer band is observed at 132.3 cm^{-1} by pre- and post-annealing on the shoulder of the CF_3 torsional mode at 129.8 cm^{-1}, red-shifted by 42.4 cm^{-1} relative to the regular complex. A similar red-shift in the order of approximate 25 % for the observed isotopic red-shifts of the two observed bands of 2,2,2-trifluoroethanol/water and 2,2,2-trifluoroethanol/water-d_2 should be expected for the last acceptor mode, which would shift this band to approximate 80 cm^{-1} to a region that is dominated by strong rotation-translation coupling transitions for water-d_2 and water-d_1. The weaker secondary hydrogen bond interaction between water and fluor from the CF_3 group can be characterized for the intermolecular interactions between water-d_1 and 2,2,2-trifluoroethanol. The recorded far-infrared and terahertz spectra for several millimeter thick cryogenic neon matrices doped simultaneously with 2,2,2-trifluoroethanol, water, water-d_1 and water-d_2 (Ne:CF_3CH_2OH:H_2O:HDO:D_2O) = (4000:2:1:2:1) reveal a combination of mixed complexes between 2,2,2-trifluoroethanol and water, water-d_1 and water-d_2, and wa-

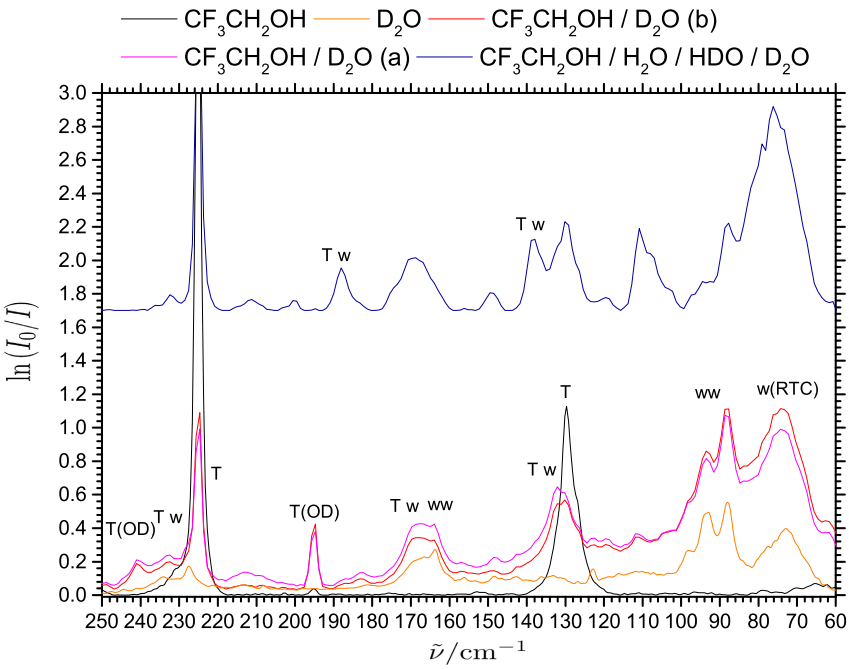

Figure 2.32: Terahertz absorption spectrum of 1.0 cm^{-1} resolution of water-d_2(Ne:D_2O) = (1500:1), 2,2,2-trifluoroethanol with water-d_2 (Ne:CF_3CH_2OH:D_2O) = (2700:1:1) and a mixture of water, water-d_1 and water-d_2 (Ne:CF_3CH_2OH:H_2O:HDO:D_2O) = (4000:2:1:2:1) embedded in cryogenic neon matrices at 2.8 K. T denotes transitions of 2,2,2-trifluoroethanol, T(OD) impurity of 2,2,2-trifluoroethanol-d_1, w of water, ww of the water dimer and Tw of 2,2,2-trifluoroethanol/water dimer.

ter complexes of the previously mentioned water isotopologues. A smaller red-shift is expected for the mixed dimer with water-d_1 than for 2,2,2-trifluoroethanol/water-d_2.

The far-infrared and terahertz regions of the several millimeter thick cryogenic neon matrices doped simultaneously with 2,2,2-trifluoroethanol and a mixture of water and water-d_2 reveals new bands belonging to the interaction of 2,2,2-trifluoroethanol and water-d_1. In the high-frequency out-of-plane donor OH librational region two possible bands can be tentatively assigned at 587.6 cm^{-1} and 601.1 cm^{-1}, as they appear as shoulders on previously assigned 2,2,2-trifluoroethanol and water/water-d_2 bands. The mid-infrared region of the same neon matrices reveal no new bands in the donor OH stretching region. The terahertz region reveals several new bands due to water complexes of mixed water isotopologues. An isotopic blue-shift is expected for the 233.1 cm^{-1} band observed for 2,2,2-trifluoroethanol and water-d_2, but no new bands could be assigned by a concentration dependency series and pre- and post-annealing

Table 2.24: Observed vibrational band origins (units of cm^{-1} for the mixed complexes of 2,2,2-trifluoroethanol (TFE) and water isotopologues embedded in cryogenic neon matrices at 2.8 K

	TFE–H_2O	**TFE–HDO**	**TFE–D_2O**
ν(OH)	3519.7	[a]	3516.7
	3508.1	[a]	3505.3
	3493.8	[a]	3488.5
ν(donor OH)	597.7	[a]	585.3
	611.2	[a]	599.0
	618.8	[a]	609.6
ν(acceptor $_1$)	[b]	[b]	233.1
ν(acceptor $_2$)	211.5	187.9	168.6
ν(acceptor $_3$)	174.7	138.3	132.3
ν(acceptor $_4$)	111.6	[c]	[c]

[a] Overlapped by 2,2,2-trifluoroethanol/water/water-d_2
[b] Overlapped by 2,2,2-trifluoroethanol
[c] Possible overlap with RTC transition for water monomer [67]

observations. Assuming that the intermolecular vibrational acceptor modes involve rotation of the water subunit, a new band should be expected in the region between the intermolecular vibrational modes with band center at 211.5 cm^{-1} for the regular complex and at 168.6 cm^{-1} for the water-d_2 complex as water-d_1 rotates faster than water-d_2 but slower than regular water. A new sharp band can be observed at 187.9 cm^{-1}, supported by pre- and post-annealing observations. Similarly, a new 2,2,2-trifluoroethanol/water-d_1 complex band can be observed at 138.3 cm^{-1} by pre- and post-annealing observation. A predicted red-shift in the order of 20% based on experi-mental red-shifts from the regular complex, is expected for the last intermolecular vibrational mode. The band observed at 111.6 cm^{-1} for the regular complex will thus be shifted to the region dominated by the rotation-translation coupling transitions of water. The observed intermolecular vibrational transitions are listed in Table 2.24 for the 2,2,2-trifluoroethanol/water dimer.

Harmonic frequency calculations are consulted to assign the observed vibrational transitions and to determine whether 2,2,2-trifluoroethanol interacts by a secondary O-H $\cdots$ F or O-D $\cdots$ F hydrogen bond. The harmonic frequency predictions at the MP2/aug-cc-pVTZ level of theory reveal a red-shifted donor OH stretching mode, a strong high-frequency out-of-plane donor OH librational mode, an acceptor mode that involves a hindered donor torsion and large-amplitude movement of the acceptor which is denoted acceptor mode$_1$, and three intermolecular acceptor modes denoted acceptor mode$_{2,3,4}$. Normal mode illustrations of the large-amplitude intermolecular

vibrational motions are shown in Figure 2.33, except for the acceptor mode$_1$.

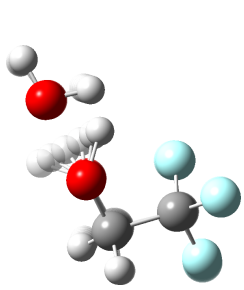

(a) out-of-plane donor OH librational mode

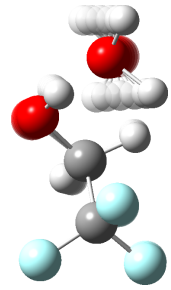

(b) acceptor mode$_2$

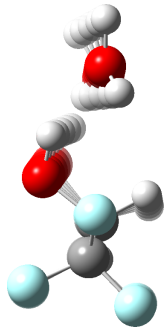

(c) acceptor mode$_3$

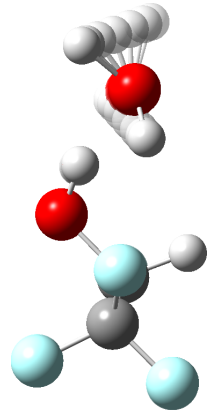

(d) acceptor mode$_4$

Figure 2.33: Normal mode illustrations of the observed librational modes for the 2,2,2-trifluoroethanol/water complex.

The harmonic frequency predicted band origins suggest straightforward assignment of the 597.7 cm^{-1} band to the high-frequency out-of-plane donor OH librational mode. The acceptor mode$_1$ is predicted to be red-shifted by just 5 cm^{-1} relative to the torsional mode of 2,2,2-trifluoroethanol and the complex band is thus most likely overlapped by the strong monomer transition, which explains this missing spectral feature in the observed terahertz spectrum. The observations at 211.5 cm^{-1}, 174.7 cm^{-1} and 111.6 cm^{-1} suggest straightforward assignments for the remaining three intermolecular acceptor vibrational modes. The harmonic frequency predictions for 2,2,2-trifluoroethanol with heavy water isotopologues are listed in Table 2.25. Small blue-shifts are predicted for the donor OH stretching fundamental, but otherwise isotopic red-shifts are predicted for the class of intermolecular vibrational modes. For the high-frequency out-of-plane donor OH librational mode a red-shift of 13.7 cm^{-1}

Table 2.25: Predicted vibrational transitions (units of cm^{-1}) for the dimers of 2,2,2-trifluoroethanol with water isotopologues

	TFE–H_2O	**TFE–HDO(D···F)**	**TFE–HDO(H···F)**	**TFE–D_2O**
ω(OH)	3658.6	3659.6	3659.3	3659.9
ω(lib d_1)	690.6	678.0	688.4	676.9
ω(lib a_1)	303.9	264.8	293.3	240.8
ω(lib a_2)	260.6	225.7	242.7	224.9
ω(lib a_3)	202.0	190.9	184.0	174.5
ω(lib a_4)	160.6	139.9	128.5	117.8

is predicted for the water-d_2 complex, which qualitatively agrees with the experimental isotopic red-shift of 12.4 cm^{-1}. The predicted isotopic red-shift from 308 cm^{-1} for the alcohol monomer to the mixed 2,2,2-trifluoroethanol/water-d_2 complex at 240.8 cm^{-1} of 67.2 cm^{-1} has experimentally been determined to be 46.9 cm^{-1}. The effect of isotopic substitution is thus overestimated slightly in the harmonic frequency calculations. Nevertheless, the harmonic frequency calculations qualitatively agree with the observed intermolecular vibrational band origins. The two observed intermolecular acceptor modes for the mixed 2,2,2-trifluoroethanol/water-d_1 complex are blue-shifted by 19.3 cm^{-1} for the second acceptor mode and 6.0 cm^{-1} for the third acceptor mode relative to the 2,2,2-trifluoroethanol/water-d_2 complex. The harmonic frequency prediction of the mixed 2,2,2-trifluoroethanol with water isotopologues indicates that the mixed complex of 2,2,2-trifluoroethanol/water-d_1 interacts by formation of a secondary H···F hydrogen bond. A complete unambiguous assignment based on the high-frequency out-of-plane donor OH librational mode and the red-shifted donor OH stretching is unreliable due to overlapping bands of 2,2,2-trifluoroethanol with water/water-d_2. *Direct* observation of the acceptor librational modes in the terahertz region thus provides a better probe for determination of the weaker, but important, secondary interaction and the conformation of the mixed 2,2,2-trifluoroethanol/water dimer, with 2,2,2-trifluoroethanol as the hydrogen bond donor.

The relatively high dissociation energy D_0 of 25.6 $kJ{\cdot}mol^{-1}$ compared to the alcohol/water complexes determined by harmonic frequency calculations at MP2/aug-cc-pVTZ level of theory and CCSD(T)/aug-cc-pVTZ calculation of the dissociation energy D_e, allows the high-frequency out-of-plane donor OH librational mode of the mixed 1:1 complex to be studied by far-infrared spectroscopy of the high-throughput supersonic jet expansions. The sensitivity of the supersonic jet spectrum is much lower than the high optical density of the matrix isolation. The low sensitivity can be explained by a single 60 cm optical path of gaseous sample that contains 1 % sample and 99 % helium. The far-infrared supersonic jet spectrum of mixed 2,2,2-trifluoroethanol/water samples at 3 cm^{-1} resolution is illustrated in Figure 2.34 and

compared to a matrix isolation spectrum.

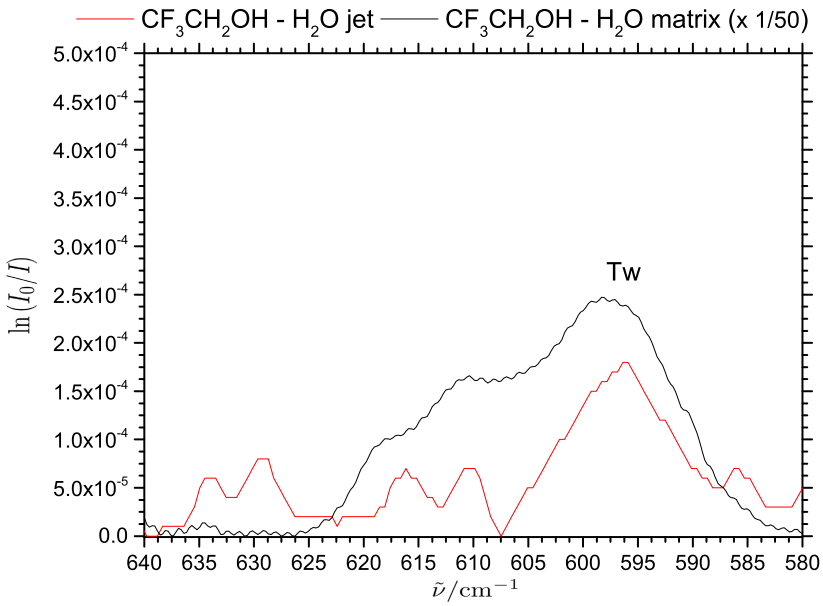

Figure 2.34: Far-infrared absorption spectrum of 2,2,2-trifluoroethanol and water (Ne:TFE:H_2O) (2700:1:1) in a cryogenic neon matrix of 1.0 cm^{-1} resolution at 2.8 K and in supersonic jet expansions of 3.0 cm^{-1} resolution.

Six bands are observed at 634 cm^{-1}, 629 cm^{-1}, 616 cm^{-1}, 611 cm^{-1}, 597 cm^{-1} and 586 cm^{-1} in the far-infrared jet spectrum. The three observed bands at 597 cm^{-1}, 611 cm^{-1} and 616 cm^{-1} scale with the concentration of 2,2,2-trifluoroethanol and water in a 1:1 stoichiometric fashion. The remaining bands at 634 cm^{-1}, 629 cm^{-1} and 586 cm^{-1} cannot be assigned the 2,2,2-trifluoroethanol monomer or dimer librational modes [251]. The appearance of two blue-shifted shoulder bands on the strong 597 cm^{-1} band at 611 cm^{-1} and 616 cm^{-1} in the observed jet spectrum, similar to the observed bands in the cryogenic neon matrix environments support the fact that there are no site splittings in the cryogenic neon matrices. The observation of the strong high-frequency out-of-plane donor OH librational band both in cryogenic neon matrices and in supersonic jet expansions reveals a spectral blue-shift of $\sim$1 cm^{-1} or less than 2 ‰. The jet-spectra will contain just as much trimer as dimer and it is reasonable to tentatively assign the doublet spectral feature at 634 cm^{-1} and 629 cm^{-1} to a mixed 2,2,2-trifluoroethanol/water trimer. The combined far-infrared observations do not provide an explanation for the triplet of bands for the donor OH stretching mode nor for the high-frequency out-of-plane donor OH librational mode, a physical explanation of the extra spectral features is thus still missing.

The observation of the high-frequency out-of-plane donor OH librational mode in both a cryogenic neon matrix environment and in supersonic jet expansions provide the first direct comparison of the large-amplitude motion of mixed alcohol/water complexes in the challenging far-infrared region. These observations are highly important for validating the effect of the matrix environment on observed band origins for the large-amplitude librational motions.

Table 2.26: Observed vibrational transitions (in units of cm^{-1}) for the 2,2,2-trifluoroethanol - water dimer embedded in cryogenic neon matrices at 2.8 K and isolated in supersonic jet expansions.

	TFE–H_2O_{matrix}	**TFE–H_2O_{jet}**
ν(OH)	3519.7	3529±3 [a]
	3508.1	
	3493.8	
ν(lib d_1)	597.7	597±3
	611.2	611±3
	618.8	616±3

[a] Ref. [250]

2.5 The Potential Energy Landscapes of the Hydrogen Bond Interactions Between Alcohols and Water

The combined mid- and far-infrared experimental observations indicates increasingly larger red-shifts of the intramolecular donor OH stretching bands of the mixed alcohol/water complexes when the alcohol group becomes larger. The increased red-shift of the donor OH stretching band indicate a stronger intermolecular interaction according to the Badger-Bauer relationship [14]. Together with the increased red-shifting bands of the donor OH stretching follow an increased blue-shifting of the intermolecular high-frequency out-of-plane donor OH librational bands. The increased absolute values for the band origins can be explained by stronger intermolecular interactions giving rise to higher barriers for the hindered internal rotational motion.

The spectroscopic observations of the hydrogen bond interaction of mixed alcohol/water complexes make it possible to compare the theoretical predictions with spectroscopic observations. The dissociation energy D_e has been predicted for the four different investigated water/alcohol complexes of methanol, ethanol, isopropanol and t-butanol for five different theoretical methodologies. The dissociation energies, D_e, for the most stable conformation of the mixed water/alcohol dimer have been calculated using B3LYP, B3LYP-D3 and MP2 levels of theory including the counterpoise correction scheme by Boys and Bernardi [105] and Dunnings aug-cc-pVTZ basis set. Subsequent CCSD(T) and CCSD(T)-F12 single point energy calculations have been performed for the MP2/aug-cc-pVTZ optimized geometries. The CCSD(T)/CBS value for the water/methanol dimer has been reached by an exponential fit on the basis of CCSD(T)/aug-cc-pVDZ, CCSD(T)/aug-cc-pVTZ, CCSD(T)/aug-cc-pVQZ and CCSD(T)/aug-cc-pV5Z calculations for the counterpoise corrected MP2/aug-cc-pVQZ optimized water/methanol geometries. The CCSD(T)/CBS value for the water/ethanol dimer in the most stable geometry has been reached by an exponential fit on the basis of CCSD(T)/aug-cc-pVDZ, CCSD(T)/aug-cc-pVTZ and CCSD(T)/aug-cc-pVQZ electronic energies for the counterpoise corrected MP2/aug-cc-pVQZ optimized geometry. The CCSD(T)/aug-cc-pV5Z level of theory is only accessible for the methanol/water interaction and the highest accuracy is obtained for this interaction. The predicted dissociation energies, D_e, are illustrated in Figure 2.35 for the most stable conformations of the different mixed alcohol/water complexes.

The predicted dissociation energy for the most stable geometry for all theoretical methodologies reveal that the dissociation energy D_e is smallest for the methanol/water dimer, and strongest for the water/t-butanol dimer. A difference of 3.31 kJ·mol^{-1} of D_e for the water/methanol dimer is evident for the B3LYP/aug-cc-pVTZ level of theory relative to the CCSD(T)/CBS. For the interaction of water with the larger alcohols, water/ethanol, water/isopropanol and water/t-butanol, there is an even larger

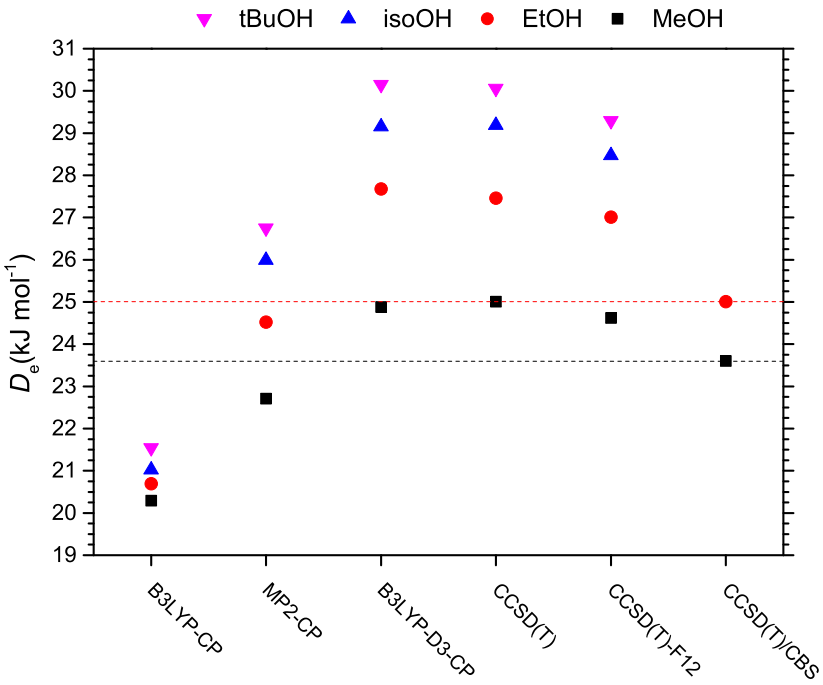

Figure 2.35: The electronic dissociation energy D_e for the most stable conformations of the mixed complexes of water methanol (MeOH), ethanol (EtOH), isopropanol (isoOH) and *t*-butanol (tBuOH) at different theoretical methodologies as described in the text.

difference between the B3LYP calculations and the MP2 calculations. This illustrates the challenges of describing the larger contribution from dispersion interactions for these systems relative to the smaller water/methanol dimer. One way to compensate for the poor description of dispersion interactions by B3LYP is to apply the dispersion correction developed by Grimme *et al.* [99]. The dispersion corrected B3LYP method (B3LYP-D3), however, overestimates the dissociation energies D_e for mixed alcohol/water complexes. The difference of 1.28 kJ·mol^{-1} for the water/methanol complex and 2.67 kJ·mol^{-1} of the water/ethanol complex for the B3LYP-D3 dissociation energy D_e relative to dissociation energy D_e at the CCSD(T)/CBS level of theory illustrates the increased overestimation. The dissociation energy difference between MP2/aug-cc-pVTZ and CCSD(T)/CBS for the water/methanol complex is 0.89 kJ·mol^{-1} and 0.49 kJ·mol^{-1} for the water/ethanol complex. The higher level of electron correlation with the *ab initio* MP2 method thus provide a more accurate description of the dissociation energy when compared with the density functional theory approach.

The CCSD(T)/aug-cc-pVTZ calculations with the explicit correlated CCSD(T)-F12 method and the same basis set demonstrate that the explicit correlated method converges faster towards the CCSD(T) method in the limit of a complete basis set. The difference between the CCSD(T) and CCSD(T)-F12 values increases with an increasing number of electrons as evident from a difference of 0.39 kJ·mol^{-1} for water/methanol, 0.45 kJ·mol^{-1} for water/ethanol, 0.72 kJ·mol^{-1} for water/isopropanol and 0.77 kJ·mol^{-1} for water/*t*-butanol. The dissociation energy D_e for the mixed water/methanol and water/ethanol complexes at the CCSD(T)-F12/aug-cc-pVTZ level of theory is overestimated by 1.02 kJ·mol^{-1} and 2.00 kJ·mol^{-1}, respectively, relative to the CCSD(T)/CBS value. The important difference between the dissociation energies of the investigated conformations of alcohol/water complexes are accurately described by the benchmark level of theory (CCSD(T)-F12/aug-cc-pVTZ) as evident from the calculations listed in Table 2.19 and Table 2.15.

The large increase in intensity [197] and spectral red-shift [14] for the intramolecular donor OH stretching vibrational modes for hydrogen bonded systems is a significant part of the description of a hydrogen bond. A just as sensitive but more *direct* probe for studying the hydrogen bond interaction is the highly localized large-amplitude high-frequency out-of-plane donor OH librational mode. The spectral band origins appear to be directly correlated with the dissociation energies of the alcohol/water complexes as illustrated in Figure 2.36, where the absolute experimental values of the high-frequency out-of-plane donor OH librational band and the experimental red-shift of the donor OH stretching band are shown as a function of the predicted theoretical dissociation energy, D_0, at the benchmark level of theory. The results are listed in Table 2.12. Raman spectroscopy of mixed water/ethanol clusters, isolated in supersonic jet expansions, has previously revealed that the donor OH stretching band for the we_t conformation of the ethanol/water complex is less red-shifted by 3 cm^{-1} rela-tive to the corresponding OH stretching band of the we_{g+} conformation [180]. The benchmark level of theory for D_0 predictions combines the benchmark level of theory for D_e predictions with harmonic MP2/aug-cc-pVTZ zero-point vibrational energies.

A trend between the dissociation energies D_0 at the benchmark level of theory and the observed red-shift for the donor OH symmetric stretching bands is evident for the most stable conformations of the mixed complexes of alcohol and water. The correlation between the absolute large-amplitude high-frequency out-of-plane donor OH librational bands and the dissociation energy D_0 is less convincing, but still clearly illustrates that the band origin of the librational mode correlates with the dissociation energy D_0. The donor OH out-of-plane librational mode can be envisioned as a very localized mode and should in principle be independent of the weak secondary interaction, but it is evident from Figure 2.37 that the water/ethanol dimer with ethanol in the *gauche*$_+$-conformation is the outlier. The cooperative effect of the stronger secondary C-H $\cdots$ O hydrogen bond in the we_{g+} conformation makes the we_t conformation a more suited candidate for this discussion of the empirical rela-

Table 2.27: The dissociation energy D_0 at the benchmark level of theory with MP2/aug-cc-pVTZ zero-point vibrational energies for the most stable conformations of the mixed complexes of water with methanol, ethanol, isopropanol or *t*-butanol (in units of kJ·mol^{-1}). Observed spectral red-shifts($\Delta\nu_{\mathrm{OH}}$) and the absolute band center for the out-of-plane donor OH librational mode origin(ν_{lib})(in units of cm^{-1}).

	$\boldsymbol{D}_0$	ν_{lib}	$\Delta\nu_{\mathbf{OH}}$
H_2O - CH_3OH	16.82	527.3	-109.1
H_2O - $CH_3CH_2OH_g$+	18.69	551.6	-127.1
H_2O - $CH_3CH_2OH_t$	18.38	545.4	-124.1[a]
H_2O - $(CH_3)_2CHOH$	19.98	554.3	-136.7
H_2O - $(CH_3)_3COH$	20.89	556.6	-142.0

[a] Ref [180]

tionship of the primary O-H $\cdots$ O hydrogen bond with the dissociation energy D_0. The larger number of large-amplitude intermolecular vibrational modes for larger alcohol/water complexes introduce a larger error to the harmonic frequency predictions of the zero-point vibrational energy that becomes larger for bigger alcohols, making it increasingly more difficult to obtain accurate dissociation energies D_0.

The results in Figure 2.37 are completely based on experimental observations, and are thus free of the errors in both the description of the dissociation energy D_e and the intermolecular zero-point vibrational energy. It appears that there is a correlation between the intramolecular donor OH stretching band red-shift and the high-frequency out-of-plane donor OH librational band. A theoretical physical model for the description of the empirical band center of the high-frequency out-of-plane donor OH librational mode as a function of the hydrogen bond interaction energy still remains to be addressed.

The inductive effect of an increasing number of methyl groups on the carbon atom adjacent to the alcohol is illustrated by the larger alcohols being better hydrogen bond acceptors, illustrated by a dissociation energy of 16.82 kJ·mol^{-1} for the water/methanol dimer to 20.89 kJ·mol^{-1} for the water/*t*-butanol dimer at the benchmark level of theory. The energy landscape of the investigated mixed alcohol/water dimers is illustrated in Figure 2.38, where the minimum energy structures and the dissociation energies D_0 of the different mixed alcohol/water conformers are shown. The mixed alcohol/water complexes, with alcohol as the hydrogen bond donor, likewise increase in stability from 15.39 kJ·mol^{-1} in methanol/water dimer to 16.43 kJ·mol^{-1} in the *t*-butanol/water dimer. However, the difference between the alcohol donor and alcohol acceptor dimers increase with the number of methyl groups illustrating

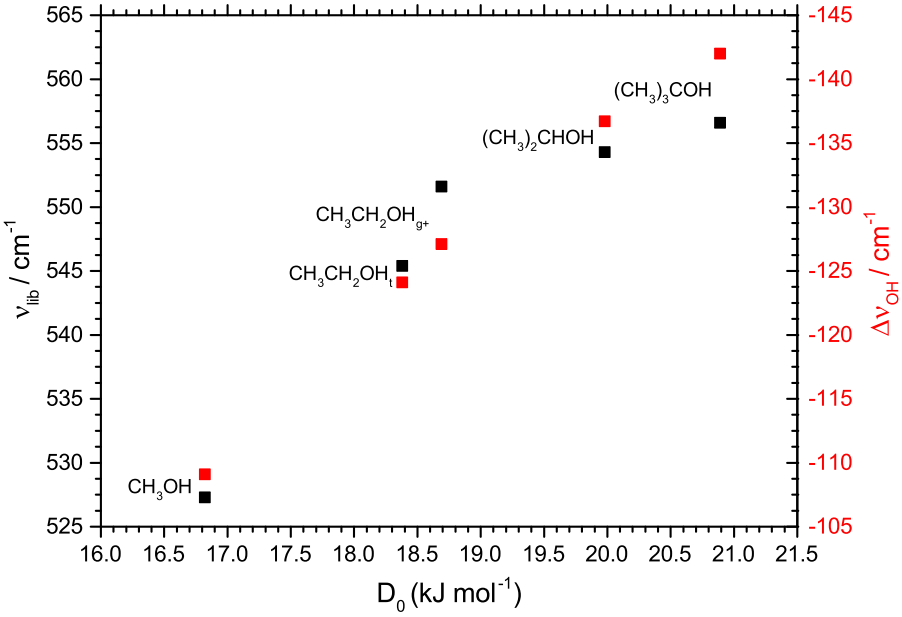

Figure 2.36: The observed absolute out-of-plane OH donor librational band origins (black dots) and donor OH symmetric stretching spectral red-shifts (red dots) (in units of cm^{-1}) compared to the dissociation energy D_0 (in units of kJ·mol^{-1}) predicted at the benchmark level of theory for the most stable conformations of the mixed complexes of water with methanol, ethanol, isopropanol and *t*-butanol.

that the alcohol subunit always is the hydrogen bond acceptor. These microscopic observations can be correlated with the macroscopic dissociation constant pK_a. For methanol, ethanol, isopropanol and *t*-butanol the pK_a values are determined to be 15.21, 15.85, 16.48 and 16.54 respectively [252]. The relative acidities illustrate how *t*-butanol is a much better acceptor given the lower preference for the donation of the alcohol proton and the macroscopic properties are thus directly correlated with the microscopic spectroscopic observables. In order to change the donor/acceptor properties of the alcohol/water interaction, the hydrogen bond acceptor character of the alcohol unit needs to be weakened. Substitution of a hydrogen atom with fluor in the methyl group leads to reversed hydrogen bond donor/acceptor properties [250], due to the electronegativity of fluor that weakens the hydrogen bond acceptor property. The mid-infrared spectroscopic study by Heger *et al.* revealed that a single substitution of hydrogen with fluor changed the hydrogen bond donor/acceptor properties for the mixed complexes of water and fluorinated alcohols. This reversed interaction is illustrated by the interaction between 2,2,2-trifluoroethanol and water, where the combined terahertz and far-infrared spectra *directly* reveal reversed donor/acceptor

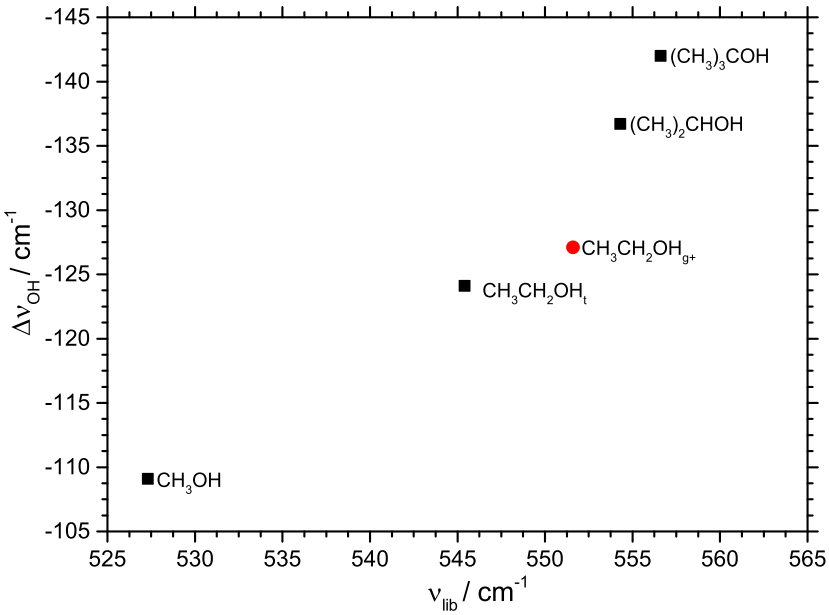

Figure 2.37: The observed out-of-plane OH donor librational band origin as a function of the spectral red-shift of the intramolecular donor OH symmetric stretching (in units of cm^{-1}) for the most stable conformations of the mixed complexes of water with methanol, ethanol, isopropanol and *t*-butanol.

roles relative to the regular alcohol/water interaction. The dissociation constant pK_a of 12.37 for 2,2,2-trifluoroethanol [253] illustrates that 2,2,2-trifluoroethanol is a worse hydrogen bond acceptor than water. The error margin for the harmonic frequency predictions increases as the alcohol subunit becomes bigger, which mainly is caused by several low-frequency large-amplitude intermolecular vibrational modes. Anharmonic treatment of the large-amplitude inter- and intramolecular vibrational mods can shed light on this problem, but VPT2 calculations for mixed alcohol/water complexes of isopropanol or *t*-butanol are not feasible and would definitely stretch the reliability of this theoretical approach. The large contribution to the zero-point vibrational energy from the class of intermolecular librational transitions are overestimated in the double harmonic approximation. From the out-of-plane donor OH librational mode an anharmonic contribution of 15-20 % is estimated from spectroscopic observations, contributing approximate 0.6 kJ·mol^{-1} to the intermolecular binding energy D_0.

The significant dataset of far-infrared and terahertz experimental band origins of large-amplitude intermolecular vibrational modes for mixed alcohol/water complexes as well as the weaker carbon dioxide, ethylene and acetylene interactions with water allow for accurate determination of the potential energy surfaces for non-covalent

weakly bound molecular clusters. The spectroscopic observations invite for validations of future high-level anharmonic predictions of vibrational band origins using approaches such vibrational coupled cluster theory for weakly bound cluster molecules.

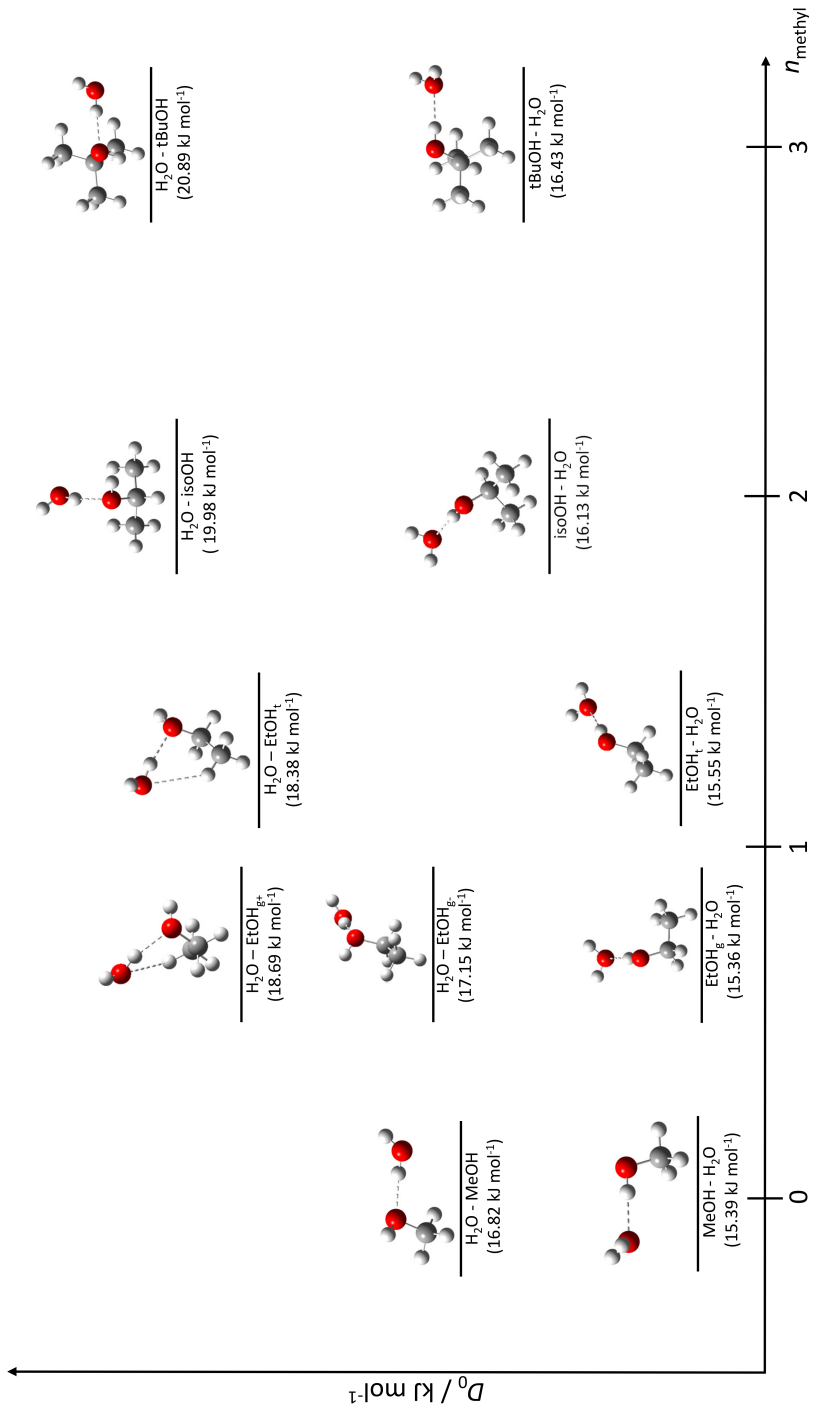

Figure 2.38: Potential energy landscape of the dissociation energy D_0 for the most stable conformations of the water/alcohol dimers at the benchmark level of theory (described in the text).

2.6 Alcohol Homodimers in Cryogenic Neon Matrices and Supersonic Jet Expansions

Observations and assignments of mixed alcohol/water complexes in the less sensitive supersonic jet approach are difficult in the far-infrared region, except for the strongly bound 2,2,2-trifluoroethanol/water dimer. For the purpose of determining the spectral shift from the matrix environment to the "real" gas phase, several more strongly bound alcohol dimers have been studied both in the supersonic jet expansion approach and in cryogenic neon matrix environments. The out-of-plane donor OH librational mode for the methanol dimer has been observed and assigned both in cryogenic neon matrices and in supersonic jet expansions, revealing a band origin of 560 $\pm$ 10 cm^{-1} in the gas phase [40] and 558 cm^{-1} in the cryogenic neon matrix environment. The far-infrared spectroscopic observations described here are tentative assignments of the high-frequency out-of-plane donor librational mode for the most stable geometry of the homodimers of ethanol, isopropanol and *t*-butanol. A complete study of the alcohol dimers, including many different conformations of the homodimers of ethanol and isopropanol are to be addressed at a later stage [254].

Theoretical studies of ethanol dimers [255–257] reveal that of nine different combinations of the ethanol monomer the six most stable dimer conformations primarily involve ethanol in the *trans* or *gauche* conformation. The global energy minimum conformation involves two *gauche* ethanol subunits, as shown by supersonic jet expansions in the mid infrared region [217, 256].

The far-infrared absorption spectrum of ethanol in supersonic jet expansions is shown as the red curve in Figure 2.39 together with a far-infrared absorption spectrum of ethanol embedded in a cryogenic neon matrices at 2.8 K as the pink curve. The jet spectrum reveals a strong band at 588 cm^{-1} and several bands from 633 cm^{-1} to 614 cm^{-1}. The bands increase in intensity at higher ethanol concentrations, supporting the previous assignment of these bands to ethanol trimers [251], which makes it possible to assign the 588 cm^{-1} band to a conformation of the ethanol dimer. The matrix isolation spectrum reveals a very broad feature with a band center of 589 cm^{-1} with shoulders at lower wavenumbers. After annealing the intensity of the strong band and the nearest shoulders increase, it is suggested that at least three conformations can be observed for the ethanol dimer in cryogenic neon matrices. Nevertheless, the band origin for the high-frequency donor OH librational mode for the most stable ethanol dimer conformation can be observed and assigned at 589 cm^{-1}, slightly blue-shifted relative to the gas phase band origin.

Snow *et al.* [232] predicted the nine most stable conformations of the isopropanol dimer at the MP2/6-311++G(d,p) level of theory. The counterpoise corrected dissociation energy D_0 revealed that the nine different combinations of isopropanol in the

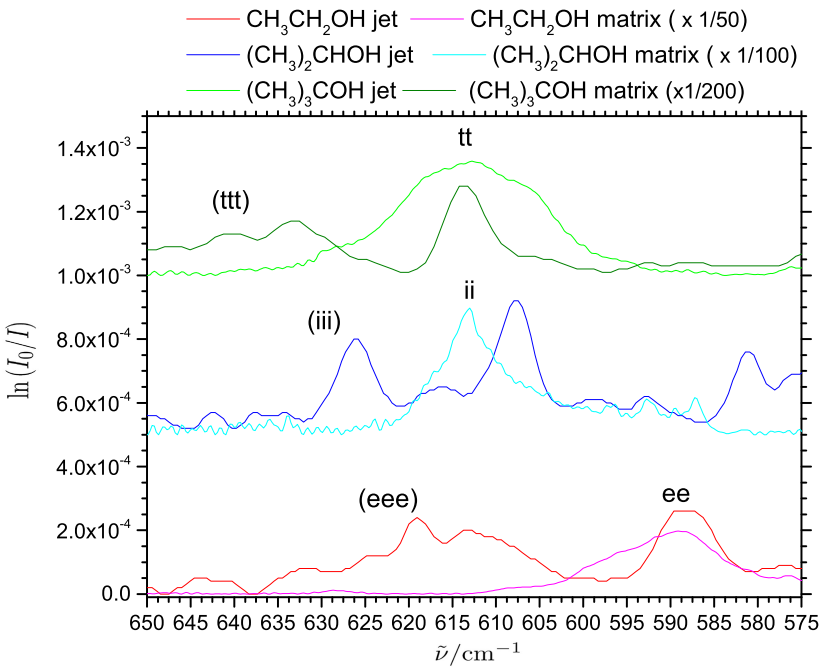

Figure 2.39: Far-infrared absorption spectrum of ethanol, isopropanol and *t*-butanol in supersonic jet expansions of 3.0 cm^{-1} resolution or embedded in cryogenic neon matrices at 2.8 K of 1.0 cm^{-1} resolution. The ethanol homodimer is denoted ee, while the assignment of the trimer is denoted (eee). Similar notations are used for isopropanol ii and (iii) and for *t*-butanol tt and (ttt).

trans or *gauche* conformation are within 1.1 $kJ{\cdot}mol^{-1}$ from the most stable to the least stable conformation. The three most stable conformations of the nine different predicted conformations are, however, within 0.2 $kJ{\cdot}mol^{-1}$ and several conformations are thus expected to be observed in both supersonic jet expansions and in matrix isolation experiments. This is further underlined by the observation of five different conformations of the homodimer of isopropanol by rotational spectroscopy [232]. The far-infrared spectra of isopropanol isolated in supersonic jet expansions, blue curve, and in cryogenic neon matrices can be seen in Figure 2.39. The far-infrared spectrum of isopropanol embedded in cryogenic neon matrix reveals a strong band at 613 cm^{-1}, that grows in intensity after annealing and by increasing concentration of isopropanol in matrix, which allows an assignment of this band to the high-frequency out-of-plane donor OH librational mode of the isopropanol homodimer, which involves two identical gauche conformations of the isopropanol subunits [232]. For the jet spectrum two bands are observed at 608 cm^{-1} and 626 cm^{-1}, both are reproducible but scale differently with the concentration of isopropanol in the jet. The lower lying band at

608 cm^{-1} is possible to observe at the lowest concentrations of isopropanol in the jet and can be assigned to the donor OH librational mode of the isopropanol dimer in supersonic jet expansions. The 626 cm^{-1} band grows in intensity at higher isopropanol concentrations suggesting that the band belongs to a larger cluster, most likely a trimer. Relative to the ethanol dimer observations the spectral shift is larger for the homodimer of isopropanol embedded in cryogenic neon matrices relative to the gas phase. The absolute spectral shift, although with an experimental uncertainty of the lower resolution of the supersonic jet expansions, of 5 cm^{-1} is still less than 1 %.

Supersonic jet expansions of *t*-butanol [258] and microwave rotational studies reveal that the homodimer of *t*-butanol only exists in one conformation [259]. The far-infrared spectrum of *t*-butanol has been studied in detail by Kollipost [251], who also provided the far-infrared jet spectrum [260].The far-infrared spectrum for *t*-butanol in supersonic jet expansions reveals one isolated band at 614 cm^{-1} and three overlapping bands from 632 cm^{-1} to 642 cm^{-1}. The isolated 614 cm^{-1} band has been assigned to the *t*-butanol dimer, while the overlapping bands have been assigned to a trimer of *t*-butanol [251]. The far-infrared spectrum of *t*-butanol embedded in cryogenic neon matrices at 2.8 K reveals a single and very broad spectral feature at 614 cm^{-1}. The concentration dependency series of *t*-butanol reveals that this band can be assigned to the high-frequency donor OH librational mode of the *t*-butanol homodimer embedded in cryogenic neon matrices.

The spectroscopic observations of homodimers of alcohols isolated in supersonic jet expansions and in cryogenic neon matrix environments allow for an investigation of the spectral shift between the matrix environment and the "real" gas phase value. The results illustrate how difficult it is to produce jet expansions with cluster sizes that are limited to monomers and dimers, and likewise also illustrate the much lower sensitivity in the supersonic jet expansions than in the cryogenic neon matrices that have a high optical density. It is likewise much easier to control the concentration in cryogenic neon matrices, thus avoiding buildup of larger alcohol clusters. In general, a small blue-shift of less than 1 % are estimated for the large-amplitude high-frequency out-of-plane donor OH librational modes for the investigated alcohol homodimers. A recent high-resolution study of the water dimer in gas phase reveals the out-of-plane donor OH librational mode at approximate 522 cm^{-1} [15], while the corresponding band is observed at 522.4 cm^{-1} in a cryogenic neon matrix [19]. The combined results, including the small and reproducible blue-shift of 0.7 cm^{-1} for the mixed complex of 2,2,2-trifluoroethanol and water, further emphasize that the neon matrix isolation technique can compete with the supersonic jet expansion approach for accurate characterization of the weakly bound molecular clusters.

Table 2.28: Observed donor OH librational bands (units of cm^{-1}) of a series of alcohol dimers isolated in supersonic jet expansions and embedded in cryogenic neon matrices.

	Jet Expansion	Neon matrix
$(CH_3OH)_2$	560±10 [a]	558
$(CH_3CH_2OH)_2$	588±3	589
$((CH_3)_2CHOH)_2$	608±3	613
$(C(CH_3)_3OH)_2$	614±3[b]	614

[a] Ref. [40] [b] Ref. [251]

2.7 The Cryogenic Matrix Environment

The method of trapping reactive species, ions, radicals and weakly bonded complexes in inert cryogenic matrices have been known since the 1950's when the method "Matrix Isolation" was coined by Pimentel and coworkers. The dilution of a sample with an inert gas and a low temperature of the cryogenic environment ensures that the sample molecules are isolated and relaxed into the vibrational ground state. The trapping of molecules in some inert environments has shown to quench the overall rotation of larger molecules, but still allows for rotational motion of small molecules such as water, hydrogen halides etc. More importantly, the cryogenic matrix environments allow free vibrational motion of the large-amplitude librational motion such as torsional motion of an alcohol or methyl group and large-amplitude intermolecular vibrational motions, such as the high-frequency out-of-plane donor OH librational mode of mixed alcohol/water complexes. The observed band positions can be significantly shifted in matrix environments, as evident by the estimated vibrational fundamentals of the water monomer in different matrix environments listed in Table 1.2. The most perturbing matrix environments of noble gases, krypton and xenon, introduce a significant red-shift for the monomer fundamentals, while the still very popular host material argon both introduces red-shifts and site splittings.

The more perturbing matrix environments of nitrogen have shown to quench the overall rotational of the water monomer [261], suggesting a strong interaction between the matrix environment and the guest molecule as well as a small confined space for the molecule to vibrate and rotate inside the matrix. The observed perturbations are similar to those of argon matrices, including site splittings. This is evident in the study by Zhang [136] where two conformations of the carbon dioxide/water dimer is observed experimentally in the carbon dioxide bending region. More importantly, nitrogen matrices significantly influence the donor/acceptor properties of weakly bound molecular complexes, as illustrated by the reversed donor/acceptor property of the methanol/water complex [49]. The unambiguous assignment of the

hydrogen bond donor/acceptor properties for the interaction between methanol and water in cryogenic neon matrices, supported by spectroscopic observations of three other alcohol/water complexes, clearly illustrate that nitrogen matrices have a significant impact on the determined intermolecular interactions, resulting in the least stable conformation being the most stable.

The less perturbing matrix environments of neon, helium and *para*-hydrogen differ in technique and the resulting spectral shifts. The best performing matrix environment is helium in the helium nanodroplet spectroscopy experiments. The embedding of guest molecules in superfluid helium nanodroplets allows for almost free rotation and vibration of molecules, although the rotational constants are smaller than the gas phase constants. The smaller rotational constants arise as helium atoms have to move in order for the guest molecule to rotate [262–265]. The vibrational resonance is observed indirectly by detecting a change in mass by mass spectrometry, and the available spectral region thus significantly depends on available lasers. This excludes *direct* observations of the large-amplitude intermolecular vibrational modes in the challenging far-infrared and terahertz spectral regions.

The *para*-hydrogen matrix environment was initially thought to be less perturbing than the best performing noble gas, neon, in matrix isolation experiments. However, the estimated vibrational band origins for the water monomer fundamentals indicate a slightly bigger interaction with the matrix environment for *para*-hydrogen experiments than for neon experiments.

The performance of vibrational motions observed in neon and *para*-hydrogen matrices are less clear when dealing with large-amplitude intermolecular vibrational motions in the challenging far-infrared and terahertz regions. For neon matrices water interacts with the matrix environment, which results in the appearance of the broad and strong rotation-translation coupling at 79.5 cm^{-1} [67]. The band arises as the molecule rotates around a center of interaction instead of the center of mass, which introduces a coupling between translational oscillations and the rotation of the molecule [92]. The coupling between rotation and translation does not appear in *para*-hydrogen matrices which suggests a larger volume for the molecules to rotate freely inside the confinement of the matrix. The recorded far-infrared and terahertz spectra of *para*-hydrogen matrices are disturbed by a very strong and sharp transition at 355.6 cm^{-1} [16, 20], caused by a forbidden $S_0(0)$ rotational transition of a *para*-hydrogen molecule in the matrix [20]. The band further couples with a phonon band for the quantum *para*-hydrogen crystal and disturbs the spectral region from 380 cm^{-1} to 500 cm^{-1}. However, a high-quality background of a very pure *para*-hydrogen sample should be able to compensate for this unwanted feature. The rotational band, however, allowed determination of the thickness of the cryogenic *para*-hydrogen matrix [20], which allowed an estimation of the thickness of the cryogenic neon matrices.

Comparison of the matrix materials are limited to the far-infrared and terahertz

observations of the water dimer embedded in neon, in *para*-hydrogen and isolated in gas phase. It is impossible to predict a trend from a single point, nevertheless, it provides a qualitative indication of the performance of the different matrix environments for the intermolecular large-amplitude donor OH librational motion. The far-infrared spectroscopic observations of the donor OH librational mode for the water dimer in supersonic jet expansions was determined around 522 cm^{-1} [15]. The far-infrared spectrum of water embedded in *para*-hydrogen reveals this band origin at 485 cm^{-1} [16], red-shifted by $\sim$ 37 cm^{-1} relative to the gas phase value. The band origin has been observed at 522.4 cm^{-1} [16,20] in cryogenic neon matrices, essentially at the gas phase value.

Astounding small spectral blue-shifts of less than 1 % are observed for the large-amplitude donor OH librational modes of alcohol homodimers embedded in cryogenic neon matrix environments relative to the observed band positions of the homodimers isolated in supersonic jet expansions. A small spectral blue-shift of less than 1% has likewise been observed for the mixed complex of 2,2,2-trifluoroethanol and water. The observed spectral shifts between supersonic jet expansions and cryogenic neon matrices are listed in Table 2.28. These combined results thus demonstrate that neon matrix isolation at 2.8 K can compete with supersonic jet expansions for accurate characterizations of weakly bound cluster molecules.

Chapter 3

Concluding Remarks

"If you want to find the secrets of the universe,
think in terms of energy, frequency and vibration."

Nikola Tesla (1856-1943)

In conclusion, weak non-covalent intermolecular interactions of small mixed hydrated molecular clusters have been investigated by combined infrared- and terahertz absorption spectroscopy by means of neon matrix isolation spectroscopy. The embedding of molecular clusters in solid cryogenic neon matrices at 2.8 K ensured a high sensitivity for *direct* observations of the large-amplitude intermolecular vibrational modes for a series of weakly bound molecular clusters in the challenging far-infrared and terahertz regions.

The spectroscopic detection of intermolecular vibrational modes for the weak van der Waals complex of carbon dioxide and water provided crucial observables for a characterization of the shallow intermolecular potential energy surface spanned by the two subunits. The combination of thick neon matrices and isotopic substitutions of the water subunit has proven crucial for observation of three large-amplitude intermolecular vibration modes; the in-plane rocking-, out-of-plane wagging- and torsional motions of the water subunit. The combination of high-level theoretical structure calculations and an almost empirical intermolecular zero-point vibrational energy enabled a semi-empirical dissociation energy D_0 of 738 $\pm$ 15 cm^{-1} was found for the weak van der Waals complex.

The weak intermolecular interactions between unsaturated hydrocarbons and water have been investigated by combined infrared and terahertz absorption spectroscopy studies. The hydrogen bond interaction of either C-H $\cdots$ O character or O-H $\cdots$ π character can be determined by the nature of the large-amplitude intermolecular vibrational modes. Two high-frequency librational modes for the water/ethylene

dimer reveal an O-H $\cdots$ π hydrogen bond, while the single intermolecular acceptor wagging mode for the acetylene/water dimer reveals a C-H $\cdots$ O hydrogen bond. A (semi)-empirical dissociation energy D_0 of 786 $\pm$ 25 cm^{-1} for the acetylene/water dimer and 589 $\pm$ 25 cm^{-1} for the water/ethylene dimer are obtained for these classes of weak hydrogen bonds.

The collapse of the spectroscopic selection rules in the matrix environment allowed confirmation of the vibrational ground state splitting of the methanol monomer of 6.7 cm^{-1} by dedicated annealing experiments. The far-infrared spectrum of methanol in neon matrices additionally allowed observation of the intermolecular hydrogen bond donor OH librational mode of the methanol dimer for the first time. This donor OH librational band is observed at 558 cm^{-1}, blue-shifted by more than 300 cm^{-1} relative to the torsional mode of the methanol monomer, while the perturbed torsional mode of the acceptor molecule is observed at 286 cm^{-1}. The neon matrix isolation experiments were supported by supersonic jet expansion approach, which confirmed a donor OH librational band origin of 560 $\pm$ 10 cm^{-1}.

The far-infrared spectroscopy study of the hydrogen bond interactions between alcohols and water, a combination of partial isotopic substitution of individual subunits and annealing of the neon matrix, allowed for the first time an unambiguous assignment of the intermolecular high-frequency out-of-plane donor OH librational modes and the low-frequency in-plane donor OH librational modes for the mixed hydrogen-bonded molecular complexes of water with methanol, ethanol, isopropanol or *t*-butanol. The vibrational assignments based on isotopic red-shifts confirm *directly* that water always acts as the hydrogen bond donor in the hydrogen bond interactions with aliphatic monohydric alcohols.

The study of ethanol and water represents one of the simplest cases of adaptive aggregation in which the conformation of a subunit is changed upon complexation. The partial H/D substitution of the ethanol subunit allowed the observation and assignment of the high-frequency out-of-plane donor OH librational modes and the low-frequency in-plane donor OH librational modes for two conformations of the water/ethanol complex, with water as the hydrogen bond donor. In the most stable conformation of the mixed ethanol/water dimer, water forces the ethanol subunit into its less stable *gauche*$_+$ conformation, due to a weak secondary C-H $\cdots$ O hydrogen bond between a terminal C-H group and a lone pair from the oxygen atom in the water molecule. The weaker secondary hydrogen bond interaction causes a significant blue-shift of the low-frequency in-plane donor OH librational band, which has proven an excellent spectroscopic probe for this interaction.

The experimental findings of the alcohol/water interactions are supported by MP2/aug-cc-pVTZ calculations for geometry optimization and harmonic zero-point vibrational energies and CCSD(T)-F12/aug-cc-pVTZ single point energies for determination of the dissociation energy D_0. The theoretical predictions allowed estimation of energy

differences for the investigated conformers of the alcohol/water complexes. The dissociation energies D_0 for the most stable geometry of the weakly bound alcohol/water complexes have been estimated at 16.8 kJ·mol^{-1} for water/methanol, 18.7 kJ·mol^{-1} for water/ethanol$_{g+}$, 20.0 kJ·mol^{-1} for water/isopropanol and 20.9 kJ·mol^{-1} for water/*t*-butanol. The inductive effect of substituting one hydrogen atom with a methyl group results in the alcohol being both a significantly better hydrogen bond acceptor and a slightly better donor. The strength of the hydrogen bond interaction manifests itself by the size of the red-shift of the intramolecular donor OH stretching mode as evident by the Badger-Bauer rule but also by the absolute band origin of the highly localized intermolecular high-frequency out-of-plane donor OH librational mode. The latter large-amplitude intermolecular mode turns out to be a direct probe for the strength of the hydrogen bond interaction.

The observed out-of-plane donor OH librational mode for the water/isopropanol dimer is slightly red-shifted relative to the water/*t*-butanol dimer, which is confirmed by a slightly smaller dissociation energy D_0 at the benchmark CCSD(T)-F12/aug-cc-pVTZ level of theory. The experimental results indicate that there is a maximum strength of the hydrogen bond interactions between water and aliphatic monohydric alcohols close to the value of *t*-butanol and water, as there is just a minor increased inductive effect of substituting a methyl group with an ethyl group. The harmonic frequency predictions at the MP2/aug-cc-pVTZ level of theory overestimate the high-frequency out-of-plane donor OH librational band origins by 15-20 % indicating an anharmonic contribution of this magnitude as shown for the observations and calculations for both the water/methanol dimer and the methanol homodimer.

The hydrogen bond donor/acceptor relationship of the alcohol/water interactions can be reversed by substituting hydrogens with fluorine atoms, as shown for the hydrogen bond interaction between the simplest fluorinated alcohol, 2,2,2-trifluoroethanol, and water. The nature of the intermolecular interaction has been settled by observing a high-frequency out-of-plane donor OH librational mode for 2,2,2-trifluoroethanol in the far-infrared region and four other intermolecular acceptor vibrational modes in the terahertz region. The "high" interaction energy of 25.6 kJ·mol^{-1} at the combined MP2/aug-cc-pVTZ/CCSD(T)/aug-cc-pVTZ level of theory for the most stable conformation of the mixed 2,2,2-trifluoroethanol/water dimer allows this weakly bound molecular cluster to be investigated by the less sensitive supersonic jet expansion approach. The latter experiments reveal a small spectral blue-shift from gas phase to the cryogenic neon matrix environment of less than 1 cm^{-1} for this large-amplitude donor OH librational mode.

The spectral shift from gas phase to the cryogenic neon matrix environment has been investigated by studying several alcohol homodimers embedded in cryogenic neon matrices and isolated in supersonic jet expansions. The observed high-frequency donor OH librational modes reveal small spectral blue-shifts of less than 1% from the gas phase band origins to the band origins in the cryogenic neon matrix environment for

homodimers of methanol, ethanol, isopropanol and *t*-butanol. Combined with the observations of the mixed 2,2,2-trifluoroethanol/water complex and a recently published vibrational-rotational tunneling terahertz study of the water dimer in molecular beams demonstrate that neon matrix isolation spectroscopy at 2.8 K can provide accurate spectroscopic observables of a series of weakly bound cluster molecules. The significant dataset of experimentally observed band origins of large-amplitude intermolecular vibrational modes in the challenging far-infrared and terahertz regions allow accurate determination of the potential energy surfaces for non-covalent weakly bound molecular clusters. The observed intermolecular vibrational band origins likewise allow for future validations of anharmonic predictions of vibrational band origins using approaches such as second order vibrational perturbation theory and vibrational coupled cluster theory for weakly bound molecular clusters.

Chapter 4

Bibliography

[1] J.-M. Lehn. Supramolecular chemistry - Scope and perspectives: Molecules - Supermolecules - Molecular devices. *Journal of inclusion phenomena* **1988**, *6*, 351–396.

[2] E. G. Robertson, J. P. Simons. Getting into shape: Conformational and supramolecular landscapes in small biomolecules and their hydrated clusters. *Phys. Chem. Chem. Phys.* **2001**, *3*, 1–18.

[3] G. R. Desiraju. Chemistry beyond the molecule. *Nature* **2001**, *412*, 397–400.

[4] J. N. Israelachvili, *Intermolecular and Surface forces: third edition*, Academic press, **2011**.

[5] N. O. B. Lüttschwager, T. N. Wassermann, R. A. Mata, M. A. Suhm. The last globally stable extended alkane. *Angewandte Chemie International Edition* **2013**, *52*, 463–466.

[6] E. Arunan, G. R. Desiraju, R. A. Klein, J. Sadlej, S. Scheiner, I. Alkorta, D. C. Clary, R. H. Crabtree, J. J. Dannenberg, P. Hobza, et al.. Definition of the hydrogen bond (IUPAC Recommendations 2011). *Pure and applied chemistry* **2011**, *83*, 1637–1641.

[7] K. Müller-Dethlefs, P. Hobza. Noncovalent interactions: A challenge for experiment and theory. *Chemical Reviews* **2000**, *100*, 143–168, PMID: 11749236.

[8] M. Cowan, B. D. Bruner, N. Huse, J. Dwyer, B. Chugh, E. Nibbering, T. Elsaesser, R. Miller. Ultrafast memory loss and energy redistribution in the hydrogen bond network of liquid H_2O. *Nature* **2005**, *434*, 199–202.

[9] B. Stevens, S. Bony. Water in the atmosphere. *Physics Today* **2013**, *66*, 29–34.

[10] R. Ludwig. Water: from clusters to the bulk. *Angewandte Chemie International Edition* **2001**, *40*, 1808–1827.

[11] T. R. Dyke, J. Muenter. Microwave spectrum and structure of hydrogen bonded water dimer. *The Journal of Chemical Physics* **1974**, *60*, 2929–2930.

[12] Z. Huang, R. Miller. High-resolution near-infrared spectroscopy of water dimer. *The Journal of Chemical Physics* **1989**, *91*, 6613–6631.

[13] R. H. Page, J. G. Frey, Y.-R. Shen, Y. Lee. Infrared predissociation spectra of water dimer in a supersonic molecular beam. *Chemical Physics Letters* **1984**, *106*, 373 – 376.

[14] R. M. Badger, S. H. Bauer. Spectroscopic studies of the hydrogen bond. II. The shift of the O–H vibrational frequency in the formation of the hydrogen bond. *The Journal of Chemical Physics* **1937**, *5*, 839–851.

[15] W. T. S. Cole, R. S. Fellers, M. R. Viant, C. Leforestier, R. J. Saykally. Far-infrared VRT spectroscopy of the water dimer: Characterization of the 20 μm out-of-plane librational vibration. *The Journal of Chemical Physics* **2015**, *143*, 154306.

[16] J. Ceponkus, P. Uvdal, B. Nelander. Observations of host guest interactions specific to molecular matrices: Water monomers and dimers in hydrogen matrices. *The Journal of Physical Chemistry A* **2011**, *115*, 7921–7927.

[17] J. Ceponkus, G. Karlström, B. Nelander. Intermolecular vibrations of the water trimer, a matrix isolation study. *The Journal of Physical Chemistry A* **2005**, *109*, 7859–7864.

[18] J. Ceponkus, A. Engdahl, P. Uvdal, B. Nelander. Structure and dynamics of small water clusters, trapped in inert matrices. *Chemical Physics Letters* **2013**, *581*, 1–9.

[19] J. Ceponkus, B. Nelander. Water dimer in solid neon. Far-infrared spectrum. *The Journal of Physical Chemistry A* **2004**, *108*, 6499–6502.

[20] J. Ceponkus, P. Uvdal, B. Nelander. Complex Formation of Small Molecules during Isolation in Low Temperature Matrices: Water Dimers in p-H_2 and Ne Matrices. *The Journal of Physical Chemistry A* **2010**, *114*, 6829–6831.

[21] Y. Bouteiller, J. Perchard. The vibrational spectrum of $(H_2O)_2$: Comparison between anharmonic ab initio calculations and neon matrix infrared data between 9000 and 90 cm^{-1}. *Chemical physics* **2004**, *305*, 1–12.

[22] Y. Bouteiller, B. Tremblay, J. Perchard. The vibrational spectrum of the water dimer: Comparison between anharmonic ab initio calculations and neon matrix infrared data between 14,000 and 90cm^{-1}. *Chemical Physics* **2011**, *386*, 29–40.

[23] A. Shank, Y. Wang, A. Kaledin, B. J. Braams, J. M. Bowman. Accurate ab initio and hybrid potential energy surfaces, intramolecular vibrational energies, and classical IR spectrum of the water dimer. *The Journal of Chemical Physics* **2009**, *130*, 144314.

[24] B. E. Rocher-Casterline, L. C. Ch'ng, A. K. Mollner, H. Reisler. Communication: Determination of the bond dissociation energy (D_0) of the water dimer, $(H_2O)_2$, by velocity map imaging. *The Journal of Chemical Physics* **2011**, *134*, 211101.

[25] S. S. Xantheas. Ab initio studies of cyclic water clusters $(H_2O)_n$, $n = 16$. II. Analysis of many-body interactions. *The Journal of Chemical Physics* **1994**, *100*, 7523–7534.

[26] J. M. Hollas, *Modern Spectroscopy 4th ed.*, John Wiley & Sons, Ltd, Chichester, UK, **2010**.

[27] W. Demtröder, *Atoms, Molecules and Photons*, Springer-Verlag, Berlin Heidelberg, Germany, **2006**.

[28] W. Demtröder, *Molecular Physics 1st ed.*, Wiley-VCH Verlag GmgH & Co. KGaA, Weinheim, Germany, **2005**.

[29] P. R. Bunker, P. Jensen, *Molecular symmetry and spectroscopy, Vol. 2*, NRC Research Press, **1998**.

[30] W. Caminati, *Microwave spectroscopy of large molecules and molecular complexes* in *Handbook of High-resolution Spectroscopy*, John Wiley & Sons, Ltd, **2011**.

[31] F. N. Keutsch, M. G. Brown, P. B. Petersen, R. J. Saykally, M. Geleijns, A. van der Avoird. Terahertz vibration - rotation - tunneling spectroscopy of water clusters in the translational band region of liquid water. *The Journal of Chemical Physics* **2001**, *114*, 3994–4004.

[32] M. Suhm, F. Kollipost. Femtisecond single-mole infrared spectroscopy of molecular clusters. *Physical Chemistry Chemical Physics* **2013**, *15*, 10702–10721.

[33] M. Snels, V. Horká-Zelenková, H. Hollenstein, M. Quack, *High-resolution FTIR and diode laser spectroscopy of supersonic jets* in *Handbook of High-resolution Spectroscopy*, John Wiley & Sons, Ltd, **2011**.

[34] J. Scherer, J. Paul, A. O'keefe, R. Saykally. Cavity ringdown laser absorption spectroscopy: history, development, and application to pulsed molecular beams. *Chemical reviews* **1997**, *97*, 25–52.

[35] A. Campargue, L. Biennier, A. Garnache, A. Kachanov, D. Romanini, M. Herman. High resolution absorption spectroscopy of the V 1= 2–6 acetylenic overtone bands of propyne: spectroscopy and dynamics. *J. Chem. Phys* **1999**, *111*, 7888–7903.

[36] G. Berden, R. Peeters, G. Meijer. Cavity ring-down spectroscopy: Experimental schemes and applications. *International Reviews in Physical Chemistry* **2000**, *19*, 565–607.

[37] M. D. Brookes, C. Xia, J. Tang, J. A. Anstey, B. G. Fulsom, K.-X. A. Yong, J. M. King, A. McKellar. Tunable diode laser spectrometer for pulsed supersonic jets: application to weakly-bound complexes and clusters. *Spectrochimica Acta Part A: Molecular and Biomolecular Spectroscopy* **2004**, *60*, 3235–3242.

[38] R. W. Larsen, M. A. Suhm. Cooperative organic hydrogen bonds: the librational modes of cyclic methanol clusters. *The Journal of Chemical Physics* **2006**, *125*, 154314–154314.

[39] R. W. Larsen, M. Suhm. The benefits of alternation and alkylation: large amplitude hydrogen bond librational modes of alcohol trimers and tetramers. *Physical Chemistry Chemical Physics* **2010**, *12*, 8152–8157.

[40] F. Kollipost, J. Andersen, D. Mahler, J. Heimdal, M. Heger, M. A. Suhm, R. Wugt Larsen. The effect of hydrogen bonding on torsional dynamics: A combined far-infrared jet and matrix isolation study of methanol dimer. *Journal of Chemical Physics* **2014**.

[41] T. Häber, U. Schmitt, M. A. Suhm. FTIR-spectroscopy of molecular clusters in pulsed supersonic slit-jet expansions. *Physical Chemistry Chemical Physics* **1999**, *1*, 5573–5582.

[42] N. Borho, M. A. Suhm, K. Le Barbu-Debus, A. Zehnacker. Intra- vs. intermolecular hydrogen bonding: dimers of alpha-hydroxyesters with methanol. *Phys. Chem. Chem. Phys.* **2006**, *8*, 4449–4460.

[43] E. D. Becker, G. C. Pimentel. Spectroscopic studies of reactive molecules by the matrix isolation method. *The Journal of Chemical Physics* **1956**, *25*, 224–228.

[44] E. Whittle, D. A. Dows, G. C. Pimentel. Matrix isolation method for the experimental study of unstable species. *The Journal of Chemical Physics* **1954**, *22*, 1943–1943.

[45] G. C. Pimentel. The promise and problems of the matrix isolation method for spectroscopic studies. *Spectrochimica Acta* **1958**, *12*, 94 – 96.

[46] I. Norman, G. Porter. Trapped atoms and radicals in a glass 'cage'. *Nature* **1954**, *174*, 508–509.

[47] A. S. Engdahl, *Intermolecular interactions in hydrogen bonded 1:1 molecular complexes*, Ph.D. thesis, University of Lund, **1997**.

[48] A. Barnes, W. Orville-Thomas, A. Müller, R. Gaufrès, *Matrix Isolation Spectroscopy*, D. Reidel Publishing Company, **1981**.

[49] S. Coussan, P. Roubin, J. Perchard. Hydrogen Bonding in ROH: R'OH (R, R'= H, CH_3, C_2H_5) Heterodimers: Matrix-Dependent Structure and Infrared-Induced Isomerization. *The Journal of Physical Chemistry A* **2004**, *108*, 7331–7338.

[50] M. Nedic, T. N. Wassermann, R. W. Larsen, M. A. Suhm. A combined Raman- and infrared jet study of mixed methanol-water and ethanol-water clusters. *Phys. Chem. Chem. Phys.* **2011**, *13*, 14050–14063.

[51] J. Andersen, J. Heimdal, R. W. Larsen. The influence of large-amplitude librational motion on the hydrogen bond energy for alcohol-water complexes. *Phys. Chem. Chem. Phys* **2015**, *17*, 23761–23769.

[52] R. White, *Chromatography/Fourier transform infrared spectroscopy and its applications, Vol. 10*, CRC Press, **1989**.

[53] A. F. Vilela, P. R. Barreto, R. Gargano, C. R. Cunha. Ab initio studies of hydrogen-bonded complexes: The H_2O dimer, trimer and H_2O – CO. *Chemical Physics Letters* **2006**, *427*, 29–34.

[54] X. Huang, B. J. Braams, J. M. Bowman. Ab initio potential energy and dipole moment surfaces of $(H_2O)_2$. *The Journal of Physical Chemistry A* **2006**, *110*, 445–451.

[55] I. Gurtubay, R. Needs. Dissociation energy of the water dimer from quantum Monte Carlo calculations. *The Journal of Chemical Physics* **2007**, *127*, 124306.

[56] G. S. Tschumper, M. L. Leininger, B. C. Hoffman, E. F. Valeev, H. F. Schaefer III, M. Quack. Anchoring the water dimer potential energy surface with explicitly correlated computations and focal point analyses. *The Journal of Chemical Physics* **2002**, *116*, 690–701.

[57] J. A. Anderson, G. S. Tschumper. Characterizing the potential energy surface of the water dimer with DFT: failures of some popular functionals for hydrogen bonding. *The Journal of Physical Chemistry A* **2006**, *110*, 7268–7271.

[58] N. Goldman, R. Fellers, M. Brown, L. Braly, C. Keoshian, C. Leforestier, R. Saykally. Spectroscopic determination of the water dimer intermolecular potential-energy surface. *The Journal of Chemical Physics* **2002**, *116*, 10148–10163.

[59] F. N. Keutsch, L. B. Braly, M. G. Brown, H. A. Harker, P. B. Petersen, C. Leforestier, R. J. Saykally. Water dimer hydrogen bond stretch, donor torsion overtone, and in-plane bend vibrations. *The Journal of Chemical Physics* **2003**, *119*, 8927–8937.

[60] C. Leforestier, F. Gatti, R. S. Fellers, R. J. Saykally. Determination of a flexible (12D) water dimer potential via direct inversion of spectroscopic data. *The Journal of Chemical Physics* **2002**, *117*, 8710–8722.

[61] N. Goldman, C. Leforestier, R. Saykally. A first principles potential energy surface for liquid water from VRT spectroscopy of water clusters. *Philosophical Transactions of the Royal Society of London A: Mathematical, Physical and Engineering Sciences* **2005**, *363*, 493–508.

[62] K. Szalewicz, C. Leforestier, A. Van Der Avoird. Towards the complete understanding of water by a first-principles computational approach. *Chemical Physics Letters* **2009**, *482*, 1–14.

[63] H. Harker, F. Keutsch, C. Leforestier, Y. Scribano, J.-X. Han, R. Saykally. Refinements in the description of excited VRT states of the water dimer. *Molecular Physics* **2007**, *105*, 513–527.

[64] R. Bentwood, A. Barnes, W.-J. Orville-Thomas. Studies of intermolecular interactions by matrix isolation vibrational spectroscopy: Self-association of water. *Journal of Molecular Spectroscopy* **1980**, *84*, 391–404.

[65] J. Perchard. Anharmonicity and hydrogen bonding. III. Analysis of the near infrared spectrum of water trapped in argon matrix. *Chemical Physics* **2001**, *273*, 217–233.

[66] J. Perchard. Anharmonicity and hydrogen bonding: II–A near infrared study of water trapped in nitrogen matrix. *Chemical Physics* **2001**, *266*, 109–124.

[67] J. Ceponkus, P. Uvdal, B. Nelander. The coupling between translation and rotation for monomeric water in noble gas matrices. *The Journal of Chemical Physics* **2013**, *138*, 244305.

[68] S. Hirabayashi, K. M. T. Yamada. Infrared spectra of water clusters in krypton and xenon matrices. *The Journal of Chemical Physics* **2005**, *122*, 244501.

[69] S. Hirabayashi, K. M. Yamada. Infrared spectra and structure of water clusters trapped in argon and krypton matrices. *Journal of Molecular Structure* **2006**, *795*, 78–83.

[70] M. Van Thiel, E. D. Becker, G. C. Pimentel. Infrared Studies of Hydrogen Bonding of Water by the Matrix Isolation Technique. *The Journal of Chemical Physics* **1957**, *27*, 486–490.

[71] A. J. Tursi, E. R. Nixon. Matrix-Isolation Study of the Water Dimer in Solid Nitrogen. *The Journal of Chemical Physics* **1970**, *52*, 1521–1528.

[72] K. Ohno, M. Okimura, N. Akai, Y. Katsumoto. The effect of cooperative hydrogen bonding on the OH stretching-band shift for water clusters studied by matrix-isolation infrared spectroscopy and density functional theory. *Physical Chemistry Chemical Physics* **2005**, *7*, 3005–3014.

[73] J. Ceponkus, P. Uvdal, B. Nelander. Intermolecular vibrations of different isotopologs of the water dimer: Experiments and density functional theory calculations. *The Journal of Chemical Physics* **2008**, *129*, 194306.

[74] J. Ceponkus, P. Uvdal, B. Nelander. Acceptor switching and axial rotation of the water dimer in matrices, observed by infrared spectroscopy. *The Journal of Chemical Physics* **2010**, *133*, 074301.

[75] D. Forney, M. Jacox, W. Thompson. The mid- and near-infrared spectra of water and water dimer isolated in solid neon. *Journal of Molecular Spectroscopy* **1993**, *157*, 479 – 493.

[76] M. E. Fajardo, S. Tam, M. E. DeRose. Matrix isolation spectroscopy of H_2O, D_2O, and HDO in solid parahydrogen. *Journal of Molecular Structure* **2004**, *695*, 111–127.

[77] K. E. Kuyanov, M. N. Slipchenko, A. F. Vilesov. Spectra of the ν_1 and ν_3 bands of water molecules in helium droplets. *Chemical Physics Letters* **2006**, *427*, 5 – 9.

[78] R. Fröchtenicht, M. Kaloudis, M. Koch, F. Huisken. Vibrational spectroscopy of small water complexes embedded in large liquid helium clusters. *The Journal of chemical physics* **1996**, *105*, 6128–6140.

[79] C. J. Burnham, S. S. Xantheas, M. A. Miller, B. E. Applegate, R. E. Miller. The formation of cyclic water complexes by sequential ring insertion: Experiment and theory. *The Journal of Chemical Physics* **2002**, *117*, 1109–1122.

[80] M. N. Slipchenko, K. E. Kuyanov, B. G. Sartakov, A. F. Vilesov. Infrared intensity in small ammonia and water clusters. *The Journal of Chemical Physics* **2006**, *124*, 241101.

[81] W. Benedict, N. Gailar, E. K. Plyler. The Vibration-Rotation Spectrum of HDO. *The Journal of Chemical Physics* **1953**, *21*, 1302–1303.

[82] W. Benedict, N. Gailar, E. K. Plyler. Rotation-vibration spectra of deuterated water vapor. *The Journal of Chemical Physics* **1956**, *24*, 1139.

[83] F. Matsushima, H. Nagase, T. Nakauchi, H. Odashima, K. Takagi. Frequency Measurement of Pure Rotational Transitions of $H_2{}^{17}O$ and $H_2{}^{18}O$ from 0.5 to 5 THz. *Journal of Molecular Spectroscopy* **1999**, *193*, 217 – 223.

[84] N. M. Gailar, F. P. Dickey. The vibration-rotation band ν_2 of HDO vapor. *Journal of Molecular Spectroscopy* **1960**, *4*, 1 – 15.

[85] F. Huisken, M. Kaloudis, A. Kulcke. Infrared spectroscopy of small size-selected water clusters. *The Journal of Chemical Physics* **1996**, *104*, 17–25.

[86] J. Paul, R. Provencal, C. Chapo, K. Roth, R. Casaes, R. Saykally. Infrared cavity ringdown spectroscopy of the water cluster bending vibrations. *The Journal of Physical Chemistry A* **1999**, *103*, 2972–2974.

[87] F. N. Keutsch, R. J. Saykally. Water clusters: untangling the mysteries of the liquid, one molecule at a time. *Proceedings of the National Academy of Sciences* **2001**, *98*, 10533–10540.

[88] J. Paul, R. Provencal, C. Chapo, A. Petterson, R. Saykally. Infrared cavity ringdown spectroscopy of water clusters: O–D stretching bands. *The Journal of Chemical Physics* **1998**, *109*, 10201–10206.

[89] K. E. Otto, Z. Xue, P. Zielke, M. A. Suhm. The Raman spectrum of isolated water clusters. *Physical Chemistry Chemical Physics* **2014**, *16*, 9849–9858.

[90] L. Braly, K. Liu, M. Brown, F. Keutsch, R. Fellers, R. Saykally. Terahertz laser spectroscopy of the water dimer intermolecular vibrations. II.$(H_2O)_2$. *Journal of Chemical Physics* **2000**, *112*, 10314–10326.

[91] S. A. Nizkorodov, M. Ziemkiewicz, D. J. Nesbitt, A. E. Knight. Overtone spectroscopy of H_2O clusters in the νOH=2 manifold: infrared-ultraviolet vibrationally mediated dissociation studies. *Journal of Chemical Physics* **2005**, *122*, 194316–194316.

[92] H. Friedmann, S. Kimel. Rotation - Translation Coupling Spectrum of Matrix-Isolated Diatomic Molecules in the Near and Far Infrared. *The Journal of Chemical Physics* **1966**, *44*, 4359–4360.

[93] A. D. Becke. Density functional thermochemistry. III. The role of exact exchange. *The Journal of Chemical Physics* **1993**, *98*, 5648–5652.

[94] C. Lee, W. Yang, R. G. Parr. Development of the Colle-Salvetti correlation-energy formula into a functional of the electron density. *Physical Review B* **1988**, *37*, 785.

[95] P. J. Stephens, F. J. Devlin, C. F. Chabalowski, M. J. Frisch. Ab initio calculation of vibrational absorption and circular dichroism spectra using density functional force fields. *The Journal of Physical Chemistry* **1994**, *98*, 11623–11627.

[96] L. F. Holroyd, T. van Mourik. Insufficient description of dispersion in B3LYP and large basis set superposition errors in MP2 calculations can hide peptide conformers. *Chemical Physics Letters* **2007**, *442*, 42 – 46.

[97] M. D. Wodrich, C. Corminboeuf, P. von Ragué Schleyer. Systematic errors in computed alkane energies using B3LYP and other popular DFT functionals. *Organic Letters* **2006**, *8*, 3631–3634, PMID: 16898778.

[98] M. Koné, B. Illien, J. Graton, C. Laurence. B3LYP and MP2 calculations of the enthalpies of hydrogen-bonded complexes of methanol with neutral bases and anions: Comparison with experimental Data. *The Journal of Physical Chemistry A* **2005**, *109*, 11907–11913, PMID: 16366642.

[99] S. Grimme, J. Antony, S. Ehrlich, H. Krieg. A consistent and accurate ab initio parametrization of density functional dispersion correction (DFT-D) for the 94 elements H-Pu. *The Journal of Chemical Physics* **2010**, *132*, 154104.

[100] C. Møller, M. S. Plesset. Note on an Approximation Treatment for Many-Electron Systems. *Physical Review* **1934**, *46*, 618–622.

[101] T. H. Dunning, Jr. Gaussian basis sets for use in correlated molecular calculations. I. The atoms boron through neon and hydrogen. *The Journal of Chemical Physics* **1989**, *90*, 1007–1023.

[102] D. E. Woon, T. H. Dunning, Jr. Gaussian basis sets for use in correlated molecular calculations. IV. Calculation of static electrical response properties. *The Journal of Chemical Physics* **1994**, *100*, 2975–2988.

[103] K. A. Peterson, D. E. Woon, T. H. Dunning, Jr. Benchmark calculations with correlated molecular wave functions. IV. The classical barrier height of the $H+H_2 \rightarrow H_2+H$ reaction. *The Journal of Chemical Physics* **1994**, *100*, 7410–7415.

[104] B. J. Ransil. Studies in Molecular Structure. IV. Potential Curve for the Interaction of Two Helium Atoms in Single-Configuration LCAO MO SCF Approximation. *The Journal of Chemical Physics* **1961**, *34*, 2109–2118.

[105] S. Boys, F. Bernardi. The calculation of small molecular interactions by the differences of separate total energies. Some procedures with reduced errors. *Molecular Physics* **1970**, *19*, 553–566.

[106] J. A. Pople, M. Head-Gordon, K. Raghavachari. Quadratic configuration interaction. A general technique for determining electron correlation energies. *The Journal of Chemical Physics* **1987**, *87*, 5968–5975.

[107] K. Raghavachari, G. W. Trucks, J. A. Pople, M. Head-Gordon. A fifth-order perturbation comparison of electron correlation theories. *Chemical Physics Letters* **1989**, *157*, 479 – 483.

[108] T. B. Adler, H.-J. Werner. An explicitly correlated local coupled cluster method for calculations of large molecules close to the basis set limit. *The Journal of Chemical Physics* **2011**, *135*, 144117.

[109] J. Vázquez, J. F. Stanton. Simple(r) algebraic equation for transition moments of fundamental transitions in vibrational second-order perturbation theory. *Molecular Physics* **2006**, *104*, 377–388.

[110] V. Barone, M. Biczysko, J. Bloino, M. Borkowska-Panek, I. Carnimeo, P. Panek. Toward anharmonic computations of vibrational spectra for large molecular systems. *International Journal of Quantum Chemistry* **2012**, *112*, 2185–2200.

[111] H. H. Nielsen. The vibration-rotation energies of molecules. *Reviews of Modern Physics* **1951**, *23*, 90.

[112] V. Barone. Anharmonic vibrational properties by a fully automated second-order perturbative approach. *The Journal of Chemical Physics* **2005**, *122*, 014108.

[113] V. Barone, J. Bloino, C. A. Guido, F. Lipparini. A fully automated implementation of VPT2 Infrared intensities. *Chemical Physics Letters* **2010**, *496*, 157 – 161.

[114] M. J. Frisch, G. W. Trucks, H. B. Schlegel, G. E. Scuseria, M. A. Robb, J. R. Cheeseman, G. Scalmani, V. Barone, B. Mennucci, G. A. Petersson, H. Nakatsuji, M. Caricato, X. Li, H. P. Hratchian, A. F. Izmaylov, J. Bloino, G. Zheng, J. L. Sonnenberg, M. Hada, M. Ehara, K. Toyota, R. Fukuda, J. Hasegawa, M. Ishida, T. Nakajima, Y. Honda, O. Kitao, H. Nakai, T. Vreven, J. A. Montgomery, Jr., J. E. Peralta, F. Ogliaro, M. Bearpark, J. J. Heyd, E. Brothers, K. N. Kudin, V. N. Staroverov, R. Kobayashi, J. Normand, K. Raghavachari, A. Rendell, J. C. Burant, S. S. Iyengar, J. Tomasi, M. Cossi, N. Rega, J. M. Millam, M. Klene, J. E. Knox, J. B. Cross, V. Bakken, C. Adamo, J. Jaramillo, R. Gomperts, R. E. Stratmann, O. Yazyev, A. J. Austin, R. Cammi, C. Pomelli, J. W. Ochterski, R. L. Martin, K. Morokuma, V. G. Zakrzewski, G. A. Voth, P. Salvador, J. J. Dannenberg, S. Dapprich, A. D. Daniels, . Farkas, J. B. Foresman, J. V. Ortiz, J. Cioslowski, D. J. Fox, *Gaussian09 Revision D.01*, **2009**, Gaussian Inc. Wallingford CT.

[115] *TURBOMOLE V6.2*, **2010**, a development of University of Karlsruhe and Forschungszentrum Karlsruhe GmbH, 1989-2007, TURBOMOLE GmbH, since 2007; available from `http://www.turbomole.com`.

[116] R. Ahlrichs, M. Bär, M. Häser, H. Horn, C. Kölmel. Electronic structure calculations on workstation computers: The program system turbomole. *Chemical Physics Letters* **1989**, *162*, 165–169.

[117] F. Furche, R. Ahlrichs, C. Hättig, W. Klopper, M. Sierka, F. Weigend. Turbomole. *Wiley Interdisciplinary Reviews: Computational Molecular Science* **2014**, *4*, 91–100.

[118] M. T. Nguyen, M. H. Matus, V. E. Jackson, V. T. Ngan, J. R. Rustad, D. A. Dixon. Mechanism of the Hydration of Carbon Dioxide: Direct Participation of H_2O versus Microsolvation. *The Journal of Physical Chemistry A* **2008**, *112*, 10386–10398.

[119] R. R. Gamache, A. L. Laraia, J. Lamouroux. Half-widths, their temperature dependence, and line shifts for the HDO-CO_2 collision system for applications to CO_2-rich planetary atmospheres. *Icarus* **2011**, *213*, 720–730.

[120] Y. Abashkin, N. Mele, F.and Russo, M. Toscano. Density-functional treatment of water carbon-dioxide van-der-Waals complex. *International Journal of Quantum Chemistry* **1994**, *52*, 1011–1015.

[121] J. Altmann, T. Ford. Ab initio calculations of some weakly bound dimers and complexes: II. The complexes of carbon dioxide with water and hydrogen sulphide. *Journal of Molecular Structure* **2007**, *818*, 85–92.

[122] R. J. Wheatley, A. H. Harvey. Intermolecular potential energy surface and second virial coefficients for the water–CO_2 dimer. *The Journal of Chemical Physics* **2011**, *134*, 134309.

[123] J. Sadlej, P. Mazurek. Ab-initio calculations on the water-carbon dioxide system. *Journal of Molecular Structure* **1995**, *337*, 129–138.

[124] J. Sadlej, J. Makarewicz, G. Chalasinski. Ab initio study of energy, structure and dynamics of the water-carbon dioxide complex. *The Journal of Chemical Physics* **1998**, *109*, 3919–3927.

[125] C. N. Ramachandran, E. Ruckenstein. Water clustering in the presence of a CO_2 molecule. *Computational and Theoretical Chemistry* **2011**, *966*, 84–90.

[126] K. M. de Lange, J. R. Lane. Explicit correlation and intermolecular interactions: Investigating carbon dioxide complexes with the CCSD(T)-F12 method. *The Journal of Chemical Physics* **2011**, *134*, 034301.

[127] M. Kieninger, O. Ventura. Equilibrium structure of the carbon dioxide water complex in the gas phase: An ab initio and density functional study. *Journal of Molecular Structure* **1997**, *390*, 157–167.

[128] Y. Danten, T. Tassaing, M. Besnard. Ab initio investigation of vibrational spectra of water-$(CO_2)_n$ Complexes (n = 1,2). *The Journal of Physical Chemistry A* **2005**, *109*, 3250–3256.

[129] A. S. Tulegenov. On the interaction in the watercarbon dioxide complex. *Chemical Physics Letters* **2011**, *505*, 71–74.

[130] J. Makarewicz, T. Ha, A. Bauder. Potential energy surface and large amplitude motions of the water-carbon dioxide complex. *The Journal of Chemical Physics* **1993**, *99*, 3694–3699.

[131] J. Makarewicz. Intermolecular potential energy surface of the water-carbon dioxide complex. *The Journal of Chemical Physics* **2010**, *132*, 234305.

[132] K. I. Peterson, W. Klemperer. Structure and internal rotation of H_2O–CO_2, HDO–CO_2, and D_2O–CO_2 van der Waals complexes. *The Journal of Chemical Physics* **1984**, *80*, 2439–2445.

[133] G. Columberg, A. Bauder, N. Heineking, W. Stahl, J. Makarewicz. Internal rotation effects and hyperfine structure in the rotational spectrum of a water-carbon dioxide complex. *Molecular Physics* **1998**, *93*, 215–228.

[134] L. Fredin, B. Nelander, G. Ribbegard. Matrix-isolation study of interaction between water and carbon–dioxide. *Chemica Scripta* **1975**, *7*, 11–13.

[135] A. Schriver, L. Schriver-Mazzuoli, P. Chaquin, E. Dumont. FTIR and ab initio study of the 1/1 complex between water and carbon dioxide in solid nitrogen. *The Journal of Physical Chemistry A* **2006**, *100*, 51–56.

[136] X. Zhang, S. P. Sander. Infrared absorption spectra of the CO_2/H_2O complex in a cryogenic nitrogen matrix-detection of a new bending frequency. *The Journal of Physical Chemistry A* **2011**, *115*, 9854–9860.

[137] L. Wan, L. Wu, A.-W. Liu, S.-M. Hu. Neon matrix isolation spectroscopy of CO_2 isotopologues. *Journal of Molecular Spectroscopy* **2009**, *257*, 217 – 219.

[138] A. Schriver, L. Schriver-Mazzuoli, A. A. Vigasin. Matrix isolation spectra of the carbon dioxide monomer and dimer revisited. *Vibrational Spectroscopy* **2000**, *23*, 83 – 94.

[139] L. Andrews, R. T. Arlinghaus, G. L. Johnson. Infrared spectrum of the CO_2-HCl complex in solid argon at 12 K. *The Journal of Chemical Physics* **1983**, *78*, 6353–6357.

[140] I. Suzuki. General anharmonic force constants of carbon dioxide. *Journal of Molecular Spectroscopy* **1968**, *25*, 479 – 500.

[141] J. Vázquez, J. F. Stanton. Treatment of Fermi resonance effects on transition moments in vibrational perturbation theory. *Molecular Physics* **2007**, *105*, 101–109.

[142] J. Andersen, J. Heimdal, D. W. Mahler, B. Nelander, R. W. Larsen. Communication: THz absorption spectrum of the CO_2H_2O complex: Observation and assignment of intermolecular van der Waals vibrations. *The Journal of Chemical Physics* **2014**, *140*, 091103.

[143] R. Bukowski, J. Sadlej, B. Jeziorski, P. Jankowski, K. Szalewicz, S. Kucharski, H. Williams, B. Rice. Intermolecular potential of carbon dioxide dimer from symmetry-adapted perturbation theory. *The Journal of Chemical Physics* **1999**, *110*, 3785–3803.

[144] L. Fredin, B. Nelander, G. Ribbegård. On the dimerization of carbon dioxide in nitrogen and argon matrices. *Journal of Molecular Spectroscopy* **1974**, *53*, 410 – 416.

[145] A. A. Vigasin, L. Schriver-Mazzuoli, A. Schriver. An Attempt To Systematize the Vibrational Shifts in CO_2 Monomers and Dimers Trapped in Various Matrices. *The Journal of Physical Chemistry A* **2000**, *104*, 5451–5456.

[146] W. Blokzijl, J. B. F. N. Engberts. Hydrophobic effects. Opinions and facts. *Angewandte Chemie International Edition in English* **1993**, *32*, 1545–1579.

[147] N. Muller. Search for a realistic view of hydrophobic effects. *Accounts of Chemical Research* **1990**, *23*, 23–28.

[148] S. Otto, J. B. F. N. Engberts. Hydrophobic interactions and chemical reactivity. *Org. Biomol. Chem.* **2003**, *1*, 2809–2820.

[149] I. G. Economou, M. D. Donohue. Equations of state for hydrogen bonding systems. *Fluid Phase Equilibria* **1996**, *116*, 518 – 529.

[150] I. G. Economou, C. Tsonopoulos. Associating models and mixing rules in equations of state for water/hydrocarbon mixtures. *Chemical Engineering Science* **1997**, *52*, 511 – 525.

[151] W. Klemperer. Intermolecular interactions. *Science* **1992**, *257*, 887–888.

[152] A. Engdahl, B. Nelander. A matrix isolation study of the ethylene-water interaction. *Chemical Physics Letters* **1985**, *113*, 49–55.

[153] A. Engdahl, B. Nelander. A matrix isolation study of the benzene–water interaction. *The Journal of Physical Chemistry* **1985**, *89*, 2860–2864.

[154] A. Engdahl, B. Nelander. Water–olefin complexes. A matrix isolation study. *The Journal of Physical Chemistry* **1986**, *90*, 4982–4987.

[155] F. A. Baiocchi, J. H. Williams, W. Klemperer. Molecular beam studies of hexafluorobenzene, trifluorobenzene, and benzene complexes of hydrogen fluoride. The rotational spectrum of benzene–hydrogen fluoride. *The Journal of Physical Chemistry* **1983**, *87*, 2079–2084.

[156] L. Andrews, G. L. Johnson, S. R. Davis. Infrared spectrum of the benzene–hydrogen fluoride complex in solid argon. *The Journal of Physical Chemistry* **1985**, *89*, 1706–1709.

[157] L. Andrews, G. L. Johnson, B. J. Kelsall. Infrared spectra of the hydrogen-bonded pi complex C_2H_4-HF in solid argon. *The Journal of Chemical Physics* **1982**, *76*, 5767–5773.

[158] J. E. D. Bene. Molecular orbital theory of the hydrogen bond. π electrons as proton acceptors. *Chemical Physics Letters* **1974**, *24*, 203 – 207.

[159] M. Heger, R. A. Mata, M. A. Suhm. Soft hydrogen bonds to alkenes: the methanol-ethene prototype under experimental and theoretical scrutiny. *Chem. Sci.* **2015**, *6*, 3738–3745.

[160] C. A. Hunter, J. K. M. Sanders. The nature of π–π interactions. *Journal of the American Chemical Society* **1990**, *112*, 5525–5534.

[161] F. Meyer-Wegner, H.-W. Lerner, M. Bolte. CH - π interactions in cocrystals of bis (trimethylsilyl) acetylene and diphenylacetylene with benzene. *Acta Crystallographica Section C: Crystal Structure Communications* **2010**, *66*, 182–184.

[162] A. Engdahl, B. Nelander. The acetylene–water complex. A matrix isolation study. *Chemical Physics Letters* **1983**, *100*, 129–132.

[163] K. I. Peterson, W. Klemperer. Water-hydrocarbon interactions: Rotational spectroscopy and structure of the water-acetylene complex. *The Journal of Chemical Physics* **1984**, *81*, 3842–3845.

[164] P. A. Block, M. D. Marshall, L. G. Pedersen, R. E. Miller. Wide amplitude motion in the water–carbon dioxide and water–acetylene complexes. *The Journal of Chemical Physics* **1992**, *96*, 7321–7332.

[165] D. Tzeli, A. Mavridis, S. S. Xantheas. A first principles study of the acetylene-water interaction. *The Journal of Chemical Physics* **2000**, *112*, 6178–6189.

[166] M. J. Frisch, J. A. Pople, J. E. Del Bene. Hydrogen bonds between first-row hydrides and acetylene. *The Journal of Chemical Physics* **1983**, *78*, 4063–4065.

[167] A. M. Andrews, R. L. Kuczkowski. Microwave spectra of C_2H_4–H_2O and isotopomers. *The Journal of Chemical Physics* **1993**, *98*, 791–795.

[168] K. I. Peterson, W. Klemperer. Water-hydrocarbon interactions: Structure and internal rotation of the water-ethylene complex. *The Journal of Chemical Physics* **1986**, *85*, 725–732.

[169] P. Tarakeshwar, H. S. Choi, S. J. Lee, J. Y. Lee, K. S. Kim, T.-K. Ha, J. H. Jang, J. G. Lee, H. Lee. A theoretical investigation of the nature of the π-H interaction in ethene-H_2O, benzene-H_2O, and benzene-$(H_2O)_2$. *The Journal of Chemical Physics* **1999**, *111*, 5838–5850.

[170] P. Tarakeshwar, H. S. Choi, , K. S. Kim. Olefinic vs aromatic πH interaction: A theoretical investigation of the nature of interaction of first-row hydrides with ethene and benzene. *Journal of the American Chemical Society* **2001**, *123*, 3323–3331, PMID: 11457068.

[171] D. B. DuPré, M. C. Yappert. Cooperative hydrogen- and πH-bonded interactions involving water and the ethylenic double bond. *The Journal of Physical Chemistry A* **2002**, *106*, 567–574.

[172] M. C. Chan, P. A. Block, R. E. Miller. Structure of the ethylene dimer from rotationally resolved nearinfrared spectroscopy: A quadruple hydrogen bond. *The Journal of Chemical Physics* **1995**, *102*, 3993–3999.

[173] Y. N. Kalugina, V. N. Cherepanov, M. A. Buldakov, N. Zvereva-Loëte, V. Boudon. Theoretical investigation of the ethylene dimer: Interaction energy and dipole moment. *Journal of Computational Chemistry* **2012**, *33*, 319–330.

[174] M. G. K. Thompson, E. G. Lewars, J. M. Parnis. Observation of the $\pi \cdots$ H hydrogen-bonded ternary complex, $(C_2H_4)_2H_2O$, using matrix isolation infrared spectroscopy. *The Journal of Physical Chemistry A* **2005**, *109*, 9499–9506, PMID: 16866400.

[175] F. t. Franks, D. Ives. The structural properties of alcohol–water mixtures. *Quarterly Reviews, Chemical Society* **1966**, *20*, 1–44.

[176] G. L. Bertrand, F. J. Millero, C.-h. Wu, L. G. Hepler. Thermochemical investigations of the water-ethanol and water-methanol solvent systems. I. Heats of mixing, heats of solution, and heats of ionization of water. *The Journal of Physical Chemistry* **1966**, *70*, 699–705.

[177] J. Larkin. Thermodynamic properties of aqueous non-electrolyte mixtures I. Excess enthalpy for water+ ethanol at 298.15 to 383.15 K. *The Journal of Chemical Thermodynamics* **1975**, *7*, 137–148.

[178] J.-P. Grolier, E. Wilhelm. Excess volumes and excess heat capacities of water+ ethanol at 298.15 K. *Fluid Phase Equilibria* **1981**, *6*, 283–287.

[179] G. C. Benson, O. Kiyohara. Thermodynamics of aqueous mixtures of nonelectrolytes. I. Excess volumes of water-n-alcohol mixtures at several temperatures. *Journal of Solution Chemistry* **1980**, *9*, 791–804.

[180] M. Nedić, T. N. Wassermann, Z. Xue, P. Zielke, M. A. Suhm. Raman spectroscopic evidence for the most stable water/ethanol dimer and for the negative mixing energy in cold water/ethanol trimers. *Physical Chemistry Chemical Physics* **2008**, *10*, 5953–5956.

[181] G. Matisz, A.-M. Kelterer, W. Fabian, S. Kunsagi-Mate. Structural properties of methanol–water binary mixtures within the quantum cluster equilibrium model. *Physical Chemistry Chemical Physics* **2015**, *17*, 8467–8479.

[182] E. E. Fileti, P. Chaudhuri, S. Canuto. Relative strength of hydrogen bond interaction in alcoholwater complexes. *Chemical Physics Letters* **2004**, *400*, 494 – 499.

[183] P. Maksyutenko, O. V. Boyarkin, T. R. Rizzo, D. S. Perry. Conformational dependence of intramolecular vibrational redistribution in methanol. *The Journal of Chemical Physics* **2007**, *126*, 044311–044311.

[184] R. Lees, L.-H. Xu, J. Johns, B. Winnewisser, M. Lock. Rotation–torsion–vibration term-value mapping for CH_3OH: Torsion-mediated doorways and corridors for intermode population transfer. *Journal of Molecular Spectroscopy* **2007**, *243*, 168–181.

[185] A. D. Mackerell. Empirical force fields for biological macromolecules: overview and issues. *Journal of Computational Chemistry* **2004**, *25*, 1584–1604.

[186] U. Liddel, E. D. Becker. Infra-red spectroscopic studies of hydrogen bonding in methanol, ethanol, and t–butanol. *Spectrochimica Acta* **1957**, *10*, 70 – 84.

[187] F. Lovas, S. Belov, M. Tretyakov, W. Stahl, R. Suenram. The a-Type K = 0 Microwave Spectrum of the Methanol Dimer. *Journal of Molecular Spectroscopy* **1995**, *170*, 478 – 492.

[188] C. L. Lugez, F. Lovas, J. T. Hougen, N. Ohashi. Global Analysis of a-, b-, and c-Type Transitions Involving Tunneling Components of K= 0 and 1 States of the Methanol Dimer. *Journal of Molecular Spectroscopy* **1999**, *194*, 95–112.

[189] A. J. Barnes, H. E. Hallam. Infra-red cryogenic studies. Part 4.-Isotopically substituted methanols in argon matrices. *Trans. Faraday Soc.* **1970**, *66*, 1920–1931.

[190] M. A. Hoffbauer, C. F. Giese, W. R. Gentry. Infrared photodissociation of methanol dimers. *The Journal of Physical Chemistry* **1984**, *88*, 181–184.

[191] F. Huisken, M. Stemmler. Infrared photodissociation of small methanol clusters. *Chemical Physics Letters* **1988**, *144*, 391–395.

[192] A. Bizzarri, S. Stolte, J. Reuss, J. V. D. van De Rijdt, F. V. Duijneveldt. Infrared excitation and dissociation of methanol dimers and trimers. *Chemical Physics* **1990**, *143*, 423 – 435.

[193] U. Buck, X. Gu, C. Lauenstein, A. Rudolph. Infrared photodissociation of size-selected methanol clusters. *The Journal of Chemical Physics* **1990**, *92*, 6017–6029.

[194] J. P. LaCosse, J. M. Lisy. Vibrational predissociation spectroscopy of methanol dimers [$(CH_3OD)_2$ and $(CH_3OH)(CH_3OD)$] in the 9.6 μm region. *The Journal of Physical Chemistry* **1990**, *94*, 4398–4400.

[195] U. Buck, F. Huisken. Infrared spectroscopy of size-selected water and methanol clusters. *Chemical Reviews* **2000**, *100*, 3863–3890.

[196] M. Heger, M. A. Suhm, R. A. Mata. Communication: Towards the binding energy and vibrational red shift of the simplest organic hydrogen bond: Harmonic constraints for methanol dimer. *The Journal of Chemical Physics* **2014**, *141*, 101105.

[197] A. Iogansen. Direct proportionality of the hydrogen bonding energy and the intensification of the stretching ν(XH) vibration in infrared spectra. *Spectrochimica Acta Part A: Molecular and Biomolecular Spectroscopy* **1999**, *55*, 1585 – 1612.

[198] F. Huisken, A. Kulcke, C. Laush, J. M. Lisy. Dissociation of small methanol clusters after excitation of the O–H stretch vibration at 2.7 μ. *The Journal of Chemical Physics* **1991**, *95*, 3924–3929.

[199] R. Provencal, J. Paul, K. Roth, C. Chapo, R. Casaes, R. Saykally, G. Tschumper, H. Schaefer III. Infrared cavity ringdown spectroscopy of methanol clusters: Single donor hydrogen bonding. *The Journal of Chemical Physics* **1999**, *110*, 4258–4267.

[200] H.-L. Han, C. Camacho, H. A. Witek, Y.-P. Lee. Infrared absorption of methanol clusters $(CH_3OH)_n$ with n=2–6 recorded with a time-of-flight mass spectrometer using infrared depletion and vacuum-ultraviolet ionization. *The Journal of Chemical Physics* **2011**, *134*, 144309.

[201] R. W. Larsen, P. Zielke, M. A. Suhm. Hydrogen-bonded OH stretching modes of methanol clusters: A combined IR and Raman isotopomer study. *The Journal of Chemical Physics* **2007**, *126*, 194307.

[202] F. Kollipost, K. Papendorf, Y.-F. Lee, Y.-P. Lee, M. A. Suhm. Alcohol dimers - how much diagonal OH anharmonicity? *Phys. Chem. Chem. Phys.* **2014**, *16*, 15948–15956.

[203] Y.-P. Lee, Y.-J. Wu, R. Lees, L.-H. Xu, J. T. Hougen. Internal rotation and spin conversion of CH_3OH in solid para-hydrogen. *Science* **2006**, *311*, 365–368.

[204] J. Perchard. The torsion-vibration spectrum of methanol trapped in neon matrix. *Chemical Physics* **2007**, *332*, 86–94.

[205] J. Perchard, F. Romain, Y. Bouteiller. Determination of vibrational parameters of methanol from matrix-isolation infrared spectroscopy and ab initio calculations. Part 1–Spectral analysis in the domain 11000–200cm^{-1}. *Chemical Physics* **2008**, *343*, 35–46.

[206] P. A. Stockman, G. A. Blake, F. J. Lovas, R. D. Suenram. Microwave rotation-tunneling spectroscopy of the water–methanol dimer: Direct structural proof for the strongest bound conformation. *The Journal of Chemical Physics* **1997**, *107*, 3782–3790.

[207] L. Evangelisti, W. Caminati. Internal dynamics in complexes of water with organic molecules. Details of the internal motions in tert–butylalcohol–water. *Physical Chemistry Chemical Physics* **2010**, *12*, 14433–14441.

[208] N. Bakkas, Y. Bouteiller, A. Loutellier, J. Perchard, S. Racine. The water–methanol complexes. I. A matrix isolation study and an abinitio calculation on the 1–1 species. *The Journal of Chemical Physics* **1993**, *99*, 3335–3342.

[209] N. Bakkas, Y. Bouteiller, A. Loutellier, J. Perchard, S. Racine. The water-methanol complexes. Matrix induced structural conversion of the 1–1 species. *Chemical Physics Letters* **1995**, *232*, 90–98.

[210] J. Korppi-Tommola. Tert–butyl alcohol-matrix ir spectra and vibrational assignment. *Spectrochimica Acta Part A: Molecular Spectroscopy* **1978**, *34*, 1077–1085.

[211] J. W. Moskowitz, Z. Bačić, A. Sarsa, K. E. Schmidt. Relative stabilities of the two isomers of the methanol-water dimer: The effects of the internal rotations of the hydroxyl and methyl groups of methanol. *The Journal of Chemical Physics* **2001**, *114*, 10294–10299.

[212] A. Engdahl, B. Nelander. On the structure of the water trimer. A matrix isolation study. *The Journal of Chemical Physics* **1987**, *86*, 4831–4837.

[213] A. J. Barnes, H. E. Hallam. Infra-red cryogenic studies. Part 5.-Ethanol and ethanol-d argon matrices. *Trans. Faraday Soc.* **1970**, *66*, 1932–1940.

[214] I. A. Finneran, P. B. Carroll, M. A. Allodi, G. A. Blake. Hydrogen bonding in the ethanol-water dimer. *Phys. Chem. Chem. Phys.* **2015**, –.

[215] S. Coussan, Y. Bouteiller, J. Perchard, W. Zheng. Rotational isomerism of ethanol and matrix isolation infrared spectroscopy. *The Journal of Physical Chemistry A* **1998**, *102*, 5789–5793.

[216] J. Durig, W. Bucy, C. Wurrey, L. Carreira. Raman spectra of gases. XVI. Torsional transitions in ethanol and ethanethiol. *The Journal of Physical Chemistry* **1975**, *79*, 988–993.

[217] T. N. Wassermann, M. A. Suhm. Ethanol monomers and dimers revisited: A Raman study of conformational preferences and argon nanocoating effects. *The Journal of Physical Chemistry A* **2010**, *114*, 8223–8233.

[218] J. Durig, R. Larsen. Torsional vibrations and barriers to internal rotation for ethanol and 2,2,2-trifluoroethanol. *Journal of Molecular Structure* **1990**, *238*, 195–222.

[219] J. C. Pearson, C. S. Brauer, B. J. Drouin. The asymmetric top–asymmetric frame internal rotation spectrum of ethyl alcohol. *Journal of Molecular Spectroscopy* **2008**, *251*, 394–409.

[220] M. L. Senent Díez, Y. Smeyers, R. Domínguez Gómez, M. Villa, et al.. Ab initio determination of the far infrared spectra of some isotopic varieties of ethanol. *Journal of Chemical Physics* **2000**, *112*, 5809–5819.

[221] H. Schaal, T. Häber, , M. A. Suhm. Hydrogen bonding in 2-propanol. The effect of fluorination. *The Journal of Physical Chemistry A* **2000**, *104*, 265–274.

[222] F. Inagaki, I. Harada, T. Shimanouchi. Far-infrared spectra and barriers to internal rotation of isopropyl alcohol and alkyl mercaptans. *Journal of Molecular Spectroscopy* **1973**, *46*, 381 – 396.

[223] J. R. Durig, C. M. Player, Y. S. Li, J. Bragin, C. W. Hawley. Low frequency vibrations in molecular solids. XVIII. Torsional modes and barriers to internal rotation of some isopropyl compounds. *The Journal of Chemical Physics* **1972**, *57*, 4544–4555.

[224] A. J. Barnes, H. E. Hallam, D. Jones. Vapour phase infrared studies of alcohols. I. Intramolecular interactions and self-association. *Proceedings of the Royal Society of London A: Mathematical, Physical and Engineering Sciences* **1973**, *335*, 97–111.

[225] B. V. D. Veken, P. Coppens. Conformer assignment of O–H stretches in ethanol and isopropanol. *Journal of Molecular Structure* **1986**, *142*, 359 – 362, Proceedings of the {XVIIth} European Congress on Molecular Spectroscopy,.

[226] J. C. Dobrowolski, S. Ostrowski, R. Koos, M. H. Jamróz. Ar-matrix {IR} spectra of 2-propanol and its OD, D_7 and D_8 isotopologues. *Vibrational Spectroscopy* **2008**, *48*, 82 – 91.

[227] H. L. Fang, D. A. Compton. Vibrational overtones of gaseous alcohols. *The Journal of Physical Chemistry* **1988**, *92*, 6518–6527.

[228] D. Schiel, W. Richter. The OH-stretching vibrational raman profile and isomer assignment of 2-propanol. *Chemical Physics Letters* **1987**, *142*, 345 – 348.

[229] A. Adilov, J. Jafarov, C. Qajar, S. Musayev. Spectra of the gauche-conformer of isopropyl alcohol in the millimeter and submillimeter wavelength regions. *Journal of Applied Spectroscopy* **2008**, *75*, 669–675.

[230] A. Maeda, I. R. Medvedev, F. C. D. Lucia, E. Herbst. The millimeter- and submillimeter-wave spectrum of iso-propanol [$(CH_3)_2CHOH$]. *The Astrophysical Journal Supplement Series* **2006**, *166*, 650.

[231] O. Ulenikov, A. Malikova, C. Qagar, S. Musaev, A. Adilov, M. Mehtiev. On the analysis of the gauche-form microwave spectrum of the isopropyl alcohol molecule. *Journal of Molecular Spectroscopy* **1991**, *145*, 262 – 269.

[232] M. S. Snow, B. J. Howard, L. Evangelisti, W. Caminati. From transient to induced permanent chirality in 2-Propanol upon dimerization: A rotational study. *The Journal of Physical Chemistry A* **2011**, *115*, 47–51, PMID: 21142179.

[233] S. Kondo, E. Hirota. Microwave spectrum and internal rotation of isopropyl alcohol. *Journal of Molecular Spectroscopy* **1970**, *34*, 97 – 107.

[234] E. Hirota. Internal rotation in isopropyl alcohol studied by microwave spectroscopy. *The Journal of Physical Chemistry* **1979**, *83*, 1457–1465.

[235] D. Roccatano, G. Colombo, M. Fioroni, A. E. Mark. Mechanism by which 2,2,2-trifluoroethanol/water mixtures stabilize secondary-structure formation in peptides: A molecular dynamics study. *Proceedings of the National Academy of Sciences* **2002**, *99*, 12179–12184.

[236] M. Buck. Trifluoroethanol and colleagues: cosolvents come of age. Recent studies with peptides and proteins. *Quarterly reviews of biophysics* **1998**, *31*, 297–355.

[237] F. D. Sonnichsen, J. E. V. Eyk, R. S. Hodges, B. D. Sykes. Effect of trifluoroethanol on protein secondary structure: an NMR and CD study using a synthetic actin peptide. *Biochemistry* **1992**, *31*, 8790–8798, PMID: 1390666.

[238] M. Matsugami, R. Yamamoto, T. Kumai, M. Tanaka, T. Umecky, T. Takamuku. Hydrogen bonding in ethanolwater and trifluoroethanolwater mixtures studied by NMR and molecular dynamics simulation. *Journal of Molecular Liquids* **2015**, –.

[239] D.-P. Hong, M. Hoshino, R. Kuboi, Y. Goto. Clustering of fluorine-substituted alcohols as a factor responsible for their marked effects on proteins and peptides. *Journal of the American Chemical Society* **1999**, *121*, 8427–8433.

[240] M. Senent, A. Perez-Ortega, A. Arroyo, R. Domnguez-Gómez. Theoretical investigation of the torsional spectra of 2,2,2-trifluoroethanol. *Chemical Physics* **2001**, *266*, 19 – 32.

[241] M. L. Senent, A. Niño, C. Muñoz-Caro, Y. G. Smeyers, , R. Domínguez-Gómez, J. M. Orza. Theoretical study of the effect of hydrogen-bonding on the stability and vibrational spectrum of isolated 2,2,2-trifluoroethanol and its molecular complexes. *The Journal of Physical Chemistry A* **2002**, *106*, 10673–10680.

[242] L.-H. Xu, G. T. Fraser, F. J. Lovas, R. D. Suenram, C. W. Gillies, H. E. Warner, J. Z. Gillies. The microwave spectrum and OH internal rotation dynamics of *gauche*-2,2,2-trifluoroethanol. *The Journal of Chemical Physics* **1995**, *103*, 9541–9548.

[243] J. Marco, J. Orza. Vapor phase FTIR study of H-bonded complexes of 2,2,2-Trifluoroethanol and its deuterated derivatives. *Journal of Molecular Structure* **1992**, *267*, 33 – 38.

[244] J. Marco, J. Orza, J.-L. Abboud. Fourier transform infrared study of gas phase H-bonding: Absorptivities and formation equilibrium constants of fluoroalcohol complexes. *Vibrational spectroscopy* **1994**, *6*, 267–283.

[245] V. F. Kalasinsky, H. V. Anjaria. Vibrational spectra and conformations of 2,2,2-trifluoroethylamine and 2,2,2-trifluoroethanol. *The Journal of Physical Chemistry* **1980**, *84*, 1940–1944.

[246] T. Scharge, T. Häber, M. A. Suhm. Quantitative chirality synchronization in trifluoroethanol dimers. *Phys. Chem. Chem. Phys.* **2006**, *8*, 4664–4667.

[247] T. Scharge, C. Cezard, P. Zielke, A. Schutz, C. Emmeluth, M. A. Suhm. A peptide cosolvent under scrutiny: self-aggregation of 2,2,2-trifluoroethanol. *Phys. Chem. Chem. Phys.* **2007**, *9*, 4472–4490.

[248] M. Perttilä. Vibrational spectra and normal coordinate analysis of 2,2,2-trichloroethanol and 2,2,2-trifluoroethanol. *Spectrochimica Acta Part A: Molecular Spectroscopy* **1979**, *35*, 585–592.

[249] J. Thomas, Y. Xu. Structure and tunneling dynamics in a model system of peptide co-solvents: Rotational spectroscopy of the 2,2,2-trifluoroethanol· · ·water complex. *The Journal of Chemical Physics* **2014**, *140*, 234307.

[250] M. Heger, T. Scharge, M. A. Suhm. From hydrogen bond donor to acceptor: the effect of ethanol fluorination on the first solvating water molecule. *Phys. Chem. Chem. Phys.* **2013**, *15*, 16065–16073.

[251] F. Kollipost, *Schwingungsdynamik in O–H · · · O-verbrückten Aggregaten: FTIR-Spektroskopie vom Nah- bis zum Ferninfraroten*, Ph.D. thesis, Georg-August-Universität Göttingen, **2015**.

[252] W. Reeve, C. M. Erikson, P. F. Aluotto. A new method for the determination of the relative acidities of alcohols in alcoholic solutions. The nucleophilicities and competitive reactivities of alkoxides and phenoxides. *Canadian Journal of Chemistry* **1979**, *57*, 2747–2754.

[253] W. Haynes, *CRC Handbook of Chemistry and Physics, 96th Edition*, CRC Press, **2015**.

[254] J. Andersen, F. Kollipost, M. Heger, M. A. Suhm, R. Wugt Larsen, *To be submitted*, **2016**.

[255] V. Dyczmons. Dimers of Ethanol. *The Journal of Physical Chemistry A* **2004**, *108*, 2080–2086.

[256] C. Emmeluth, V. Dyczmons, T. Kinzel, P. Botschwina, M. A. Suhm, M. Yanez. Combined jet relaxation and quantum chemical study of the pairing preferences of ethanol. *Phys. Chem. Chem. Phys.* **2005**, *7*, 991–997.

[257] A. Vargas-Caamal, F. Ortiz-Chi, D. Moreno, A. Restrepo, G. Merino, J. Cabellos. The rich and complex potential energy surface of the ethanol dimer. *Theoretical Chemistry Accounts* **2015**, *134*, 16.

[258] D. Zimmermann, T. Häber, H. Schaal, M. A. Suhm. Hydrogen bonded rings, chains and lassos: the case of t-butyl alcohol clusters. *Molecular Physics* **2001**, *99*, 413–425.

[259] S. Tang, I. Majerz, W. Caminati. Sizing the Ubbelohde effect: the rotational spectrum of a tert-butylalcohol dimer. *Physical Chemistry Chemical Physics* **2011**, *13*, 9137–9139.

[260] F. Kollipost, Private communication, **2015**.

[261] A. J. Tursi, E. R. Nixon. Matrix-isolation study of the water dimer in solid nitrogen. *The Journal of Chemical Physics* **1970**, *52*, 1521–1528.

[262] C. Callegari, K. K. Lehmann, R. Schmied, G. Scoles. Helium nanodroplet isolation rovibrational spectroscopy: Methods and recent results. *The Journal of Chemical Physics* **2001**, *115*, 10090–10110.

[263] J. P. Toennies, A. F. Vilesov. Superfluid helium droplets: A uniquely cold nanomatrix for molecules and molecular complexes. *Angewandte Chemie International Edition* **2004**, *43*, 2622–2648.

[264] M. Hartmann, R. E. Miller, J. P. Toennies, A. F. Vilesov. High-resolution molecular spectroscopy of van der Waals clusters in liquid helium droplets. *Science* **1996**, *272*, 1631–1634.

[265] M. Y. Choi, G. E. Douberly, T. M. Falconer, W. K. Lewis, C. M. Lindsay, J. M. Merritt, P. L. Stiles, R. E. Miller. Infrared spectroscopy of helium nanodroplets: novel methods for physics and chemistry. *International Reviews in Physical Chemistry* **2006**, *25*, 15–75.

Appendix A

Peer-Reviewed Journal Publications

A.1 Communication: THz absorption spectrum of the CO_2-H_2O complex: Observation and assignment of intermolecular van der Waals vibrations

Communication: THz absorption spectrum of the CO_2H_2O complex: Observation and assignment of intermolecular van der Waals vibrations
J. Andersen, J. Heimdal, D. W. Mahler, B. Nelander, and R. Wugt Larsen
The Journal of Chemical Physics 140, 091103 (2014)

THE JOURNAL OF CHEMICAL PHYSICS **140**, 091103 (2014)

Communication: THz absorption spectrum of the CO_2–H_2O complex: Observation and assignment of intermolecular van der Waals vibrations

J. Andersen,[1] J. Heimdal,[2] D. W. Mahler,[1] B. Nelander,[2] and R. Wugt Larsen[1,a)]
[1]*Department of Chemistry, Technical University of Denmark, Kemitorvet 206, 2800 Kgs. Lyngby, Denmark*
[2]*MAX-IV Laboratory, Lund University, P. O. Box 118, 22100 Lund, Sweden*

(Received 4 February 2014; accepted 25 February 2014; published online 7 March 2014)

Terahertz absorption spectra have been recorded for the weakly bound CO_2–H_2O complex embedded in cryogenic neon matrices at 2.8 K. The three high-frequency van der Waals vibrational transitions associated with out-of-plane wagging, in-plane rocking, and torsional motion of the isotopic H_2O subunit have been assigned and provide crucial observables for benchmark theoretical descriptions of this systems' flat intermolecular potential energy surface. A (semi)-empirical value for the zero-point energy of 273 ± 15 cm^{-1} from the class of intermolecular van der Waals vibrations is proposed and the combination with high-level quantum chemical calculations provides a value of 726 ± 15 cm^{-1} for the dissociation energy D_0. © *2014 AIP Publishing LLC*. [http://dx.doi.org/10.1063/1.4867901]

The intermolecular interaction between CO_2 and H_2O plays a major role for a variety of phenomena in physics, chemistry, and biology including the radiative transfer through the Earth's and other planetary atmospheres,[1] the early stages in carbonic acid formation[2] and the transportation of dissolved CO_2 in the tissues of biological organisms. The prototypical binary mixed van der Waals complex of CO_2 and H_2O has been intensively investigated by both theory and experiment. Numerous quantum-chemical studies of the systems' intermolecular potential energy surface (IPES) have been reported.[3–13] High level of electron correlation, extensive basis sets, and inclusion of basis set superposition errors prove mandatory as the IPES is extremely flat near the global potential energy minimum. A recent comprehensive work reports a complete 5D *ab initio* IPES composed of 23 000 high level single-point energies in configuration space and settles that the global potential energy minimum has a planar and T-shaped geometry of C_{2v} symmetry with the oxygen atom of H_2O bound to the C atom and the H atoms pointing away from the CO_2 molecule[14] (Fig. 1). This global potential energy minimum geometry has independently been confirmed experimentally by a variety of spectroscopic studies[15–17,27] whereas other works have suggested the existence of other higher energy configurations.[18,19] The most important observable is the dissociation energy D_0 which requires reliable band origins for the system's complete set of fundamental vibrational transitions and in particular for the class of five intermolecular van der Waals vibrational transitions addressed in the present work.

Neon (L'Air Liquide, 99.5%) doped with CO_2 (Matheson, 99.9%) and degassed samples of H_2O, $H_2{}^{18}O$ (Sigma Aldrich, 99.0% ^{18}O) and D_2O (Sigma Aldrich, 99.5% D) with mixing ratios of ≃0.5‰ to 5‰ were deposited with a flow rate of 0.02 mol/h at 3.6 K on a gold-plated oxygen-free high thermal conductivity (OFHC) copper mirror inside an immersion helium cryostat (IHC-3) modified for matrix isolation spectroscopy at MAX-lab.[20] A 3-mm deep cavity with 10-mm diameter and a flat bottom has been drilled into the mirror centre to allow deposition of several millimeter thick matrices doped with weak absorbers. The mirror temperature was monitored by a Lake Shore silicon diode and maintained stable at 2.8 ± 0.1 K before and after deposition employing resistive heaters and feedback electronics. The sample mount was equipped with interchangeable CsI and polymethylpentene (TPX) windows and combined IR and THz single-beam spectra were collected by a Bruker IFS 120 FTIR spectrometer employing a globar lamp as radiation source. A HgCdTe detector combined with a Ge/KBr beam splitter and a Si-bolometer operating at 4.2 K combined with a 6 μm multilayer Mylar beam splitter were employed for the IR and THz spectral regions, respectively. Spectral resolutions of 0.1–1 cm^{-1} were selected depending on the observed bandwidths.

Figure 2 shows a series of THz absorption spectra collected for several millimeter thick cryogenic neon matrices doped with CO_2 (CO_2:H_2O:Ne)=(1:0:800), H_2O (0:1:4000), and mixtures of CO_2 and H_2O (3:1:4000), respectively. A

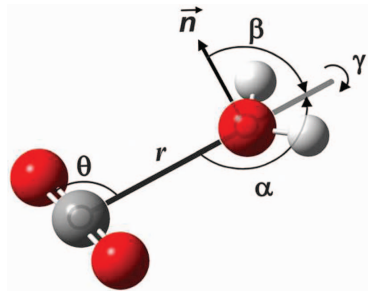

FIG. 1. The five intermolecular coordinates (r,α,β,γ,θ) specifying the configuration of the CO_2–H_2O van der Waals complex.

a)Author to whom correspondence should be addressed. Electronic mail: rewl@kemi.dtu.dk

dominant spectral feature observed for the matrices doped with regular H_2O is observed at 79.5 cm^{-1}. This band has previously been assigned to a rotational-translation-coupling (RTC) transition of H_2O monomer in neon[21] and helps to monitor the H_2O monomer concentration. At higher H_2O concentrations, signs of hydrogen-bonded dimers of water started to show up. The strongest intermolecular hydrogen bond vibrations of $(H_2O)_2$ observed in the THz region, the acceptor torsional and acceptor wagging modes, have previously been observed and assigned in neon matrices at 116.0 cm^{-1} and 122.2 cm^{-1}.[20,22–24] THz spectra recorded for neon matrices doped solely with CO_2 showed no signs of CO_2-containing cluster entities in agreement with high-level theoretical studies of the weakly bound $(CO_2)_2$ system.[25] As shown in Fig. 2 the simultaneous use of CO_2 and H_2O as dopants allowed the identification of two new distinct bands located at 101.6 and 166.6 cm^{-1}; the latter band being a factor of 3–4 less intense. The intensity of these bands increased similarly with the CO_2 and H_2O concentration suggesting the assignments to a mixed $(CO_2)_n$–$(H_2O)_n$ complex. A stoichiometric 1:1 relationship could be confirmed at the low sample concentrations and by the complementary IR spectral series. THz spectra collected for neon matrices doped with CO_2 and isotopically enriched samples of $H_2{}^{18}O$ and D_2O/HDO are useful to validate the proposed assignments further. An illustrative spectrum obtained for $CO_2/H_2{}^{18}O$ doped neon matrices is shown in Fig. 2. The small isotopic shifts upon ^{18}O-substitution have been reported previously both for the monomeric RTC transition[21] and the strongest dimeric hydrogen bond vibrations of water.[20] The observed spectral shifts caused by the ^{18}O-substitution are also very small for both the proposed CO_2–H_2O bands. The band at 101.6 cm^{-1} seems to be rather unaffected by the ^{18}O-substitution. The upper band has a small but significant reproducible isotopic red-shift of 1.9 cm^{-1} as indicated by arrows in Fig. 2. The effect of deuteration has a much larger impact on the recorded THz spectra since both the monomeric and dimeric water spectral features have significant isotope shifts not to mention that mixed isotopic entities start to build up. Both the D_2O and HDO as well as the mixed deuterated dimeric entities of water have been extensively studied previously and the complete list of spectral assignments is given in Table I. In the further spectral analysis of the isotopically enriched spectral signatures we consult quantum chemical predictions.

As described and cited in the introduction, a variety of high-level quantum chemical calculations have been performed to describe the accurate IPES of the CO_2–H_2O complex in great detail. In Table II, we have listed harmonic MP2/aug-cc-pVQZ predictions for the global potential energy

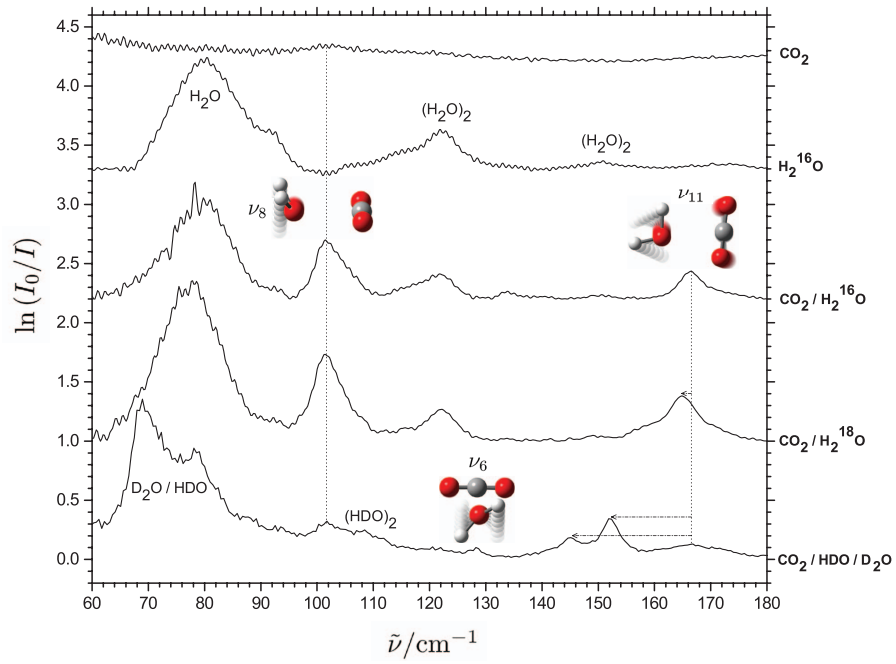

FIG. 2. A series of THz absorption spectra of 1.0 cm^{-1} resolution collected for cryogenic neon matrices doped with CO_2, H_2O, and 3:1 mixtures of CO_2 and isotopically enriched samples of H_2O at 2.8 K. The CO_2–H_2O assignments are indicated by animated normal vibrations.

TABLE I. The assigned transitions (units of cm^{-1}) for the recorded THz absorption spectra of $CO_2/H_2{}^{16}O$, $CO_2/H_2{}^{18}O$, CO_2/HDO, and CO_2/D_2O embedded in neon matrices at 2.8 K.

$CO_2/H_2{}^{16}O$	$CO_2/H_2{}^{18}O$	CO_2/HDO	CO_2/D_2O	Assignment
79.5[a]	77.8[a]		73.1[a]	H_2O monomer, RTC transition[a]
101.6[b]	**101.4**[b]			**CO_2–H_2O complex, H_2O wagging**
116.0[c]	116.0[c]			$(H_2O)_2$ complex, acceptor torsion
122.2[c]	122.0[c]	106.0[c]	93.3[c]	$(H_2O)_2$ complex, acceptor wagging
		128.4[b]		**CO_2–H_2O complex, H_2O torsion**
150.6[c]	149.7[c]	135.0[c]	123.1[c]	$(H_2O)_2$ complex, acceptor twist
166.6[b]	**164.7**[b]	**152.1**[b]	**145.1**[b]	**CO_2–H_2O complex, H_2O rocking**

[a]Rotation-translation-coupling transition (see Ref. 21).
[b]Present work.
[c]Reference 20.

minimum with C_{2v} symmetry. These predictions are in accordance with the study by Makarewicz[14] and specify the class of five intermolecular van der Waals vibrational transitions. The out-of-plane H_2O wagging mode ν_8 (B_1) described by the intermolecular coordinate β (Fig. 1) has a high intensity whereas the in-plane rocking of H_2O ν_{11} (B_2) described by α and the CO_2 librational rocking mode of ν_{12} (B_2) described by θ both have medium intensity. The H_2O torsional mode ν_6 (A_2) described by γ is strictly IR-forbidden for the regular CO_2–H_2O complex and the intermolecular O···C stretching mode ν_5 (A_1) described by r has a very low intensity. A convincing correlation immediately appears between the harmonic predictions and the observation of the two distinct bands at 101.6 and 166.6 cm^{-1} for THz spectra of neon matrices doped simultaneously with CO_2 and H_2O. This excellent agreement between experiment and theory suggests straightforward assignments for the out-of-plane H_2O wagging mode ν_8 at 101.6 cm^{-1} and the in-plane H_2O rocking mode ν_{11} at 166.6 cm^{-1} for the regular CO_2–H_2O complex. This agreement could partly be due to some kind of fortunate cancelation of smaller spectral shifts in opposite directions originating from anharmonicity effects and minor matrix perturbations which shall be discussed below. Small isotopic red-shifts are expected upon ^{18}O-substitution on the water subunit since both these intermolecular vibrational modes involve hindered rotational motion of H_2O. The harmonic calculations for the enriched CO_2–$H_2{}^{18}O$ system predict a very small red-shift of 0.9 cm^{-1} for the H_2O wagging mode ν_8 and a more pronounced red-shift of 2.2 cm^{-1} for the H_2O rocking mode ν_{11} (Table III). These red-shift predictions are convincingly close to the observations within the experimental reproducibility. The predicted relative harmonic band intensity agrees qualitatively with the experimental findings. The rotational motion of D_2O is much slower relative to H_2O and rather large isotopic spectral red-shifts for both the D_2O wagging and rocking modes are expected. The harmonic calculations for CO_2–D_2O accordingly predict red-shifts of 24.3 and 19.1 cm^{-1} with factors of 2 and 3 smaller harmonic band intensities, respectively, for these intermolecular van der Waals modes (Table III). The band origin for the strongest D_2O wagging mode is expected at 77.4 cm^{-1} and thereby unavoidably overlapped with the strong RTC transitions for H_2O, HDO, and D_2O (Table I). The band origin for the D_2O rocking mode with medium intensity is predicted at 148.5 cm^{-1} but the threefold loss of band intensity (8.5 km/mol) and the experimental challenge with isotopic H/D exchange and formation of HDO in the matrix inlet system was expected to blur this spectral signature. Nevertheless, a series of THz spectra recorded for neon matrices doped with CO_2/HDO/D_2O mixtures reproduces a medium strong band at 145.1 cm^{-1} which we assign to the D_2O rocking transition of the CO_2–D_2O complex as indicated in Fig. 2. The rotational motion of HDO is slower relative to H_2O but faster relative to D_2O and smaller predicted isotopic spectral red-shifts for the H_2O wagging and rocking modes of 18.1 and 11.6 cm^{-1}, respectively, for CO_2–HDO relative to CO_2–H_2O are both expected. The harmonic band intensities are both predicted to be a factor of 2 smaller for this isotopic variant of the complex. The band origin for the stronger HDO wagging mode predicted at 83.6 cm^{-1} cannot be observed unambiguously due to the overlapping RTC transitions of H_2O, HDO, and D_2O. The red-shifted HDO rocking mode predicted at 156.0 cm^{-1} with 14.5 km/mol intensity is easily observed and assigned at 152.1 cm^{-1} for the CO_2/HDO/D_2O doped neon matrices.

TABLE II. MP2/aug-cc-pVQZ predictions in the double harmonic approximation of vibrational band origins (units of cm^{-1}) and corresponding infrared band strengths (units of km/mol, in parenthesis) for the weakly bound CO_2–H_2O complex of C_{2v} symmetry.

Mode	Description	Origin (Int.)	Mode	Description	Origin (Int.)
ν_1 (A_1)	Sym. H_2O stretch	3836.3 (10)	ν_7 (B_1)	Out-of-plane CO_2 bend	667.2 (22)
ν_2 (A_1)	In-plane H_2O bend	1630.2 (76)	ν_8 (B_1)	Intermol. H_2O wagging	101.7 (228)
ν_3 (A_1)	Sym. CO_2 stretch	1334.7 (0.2)	ν_9 (B_2)	Antisym. H_2O stretch	3962.3 (87)
ν_4 (A_1)	In-plane CO_2 bend	653.2 (39)	ν_{10} (B_2)	Antisym. CO_2 stretch	2415.3 (564)
ν_5 (A_1)	Intermol. O···C stretch	111.2 (0.4)	ν_{11} (B_2)	Intermol. H_2O rocking	167.6 (25)
ν_6 (A_2)	Intermol. H_2O torsion	151.2 (0.0)	ν_{12} (B_2)	Intermol. CO_2 libration	16.8 (29)

TABLE III. Harmonic MP2/aug-cc-pVQZ predictions of vibrational band origins (units of cm^{-1}) and corresponding infrared band strengths (units of km/mol, in parenthesis) for the H_2O wagging, rocking, and torsional modes of different CO_2–H_2O isotopomers (the labeling refers to CO_2–$H_2{}^{16}O$).

Mode	Description	CO_2–$H_2{}^{16}O$	CO_2–$H_2{}^{18}O$	CO_2/HDO	CO_2/D_2O
ν_6 (A_2)	Intermol. H_2O torsion (γ)	151.2 (0)	151.2 (0)	135.9 (43)	108.3 (0)
ν_8 (B_1)	Intermol. H_2O wagging (β)	101.7 (228)	100.8 (225)	83.6 (133)	77.4 (125)
ν_{11} (B_2)	Intermol. H_2O rocking (α)	167.6 (25)	165.4 (25)	156.0 (14)	148.5 (9)

This assignment is indicated in Fig. 2 for an experiment with a CO_2:D_2O:HDO:H_2O composition of (18:6:6:1). The harmonic calculations of CO_2–HDO predict that the HDO torsional mode becomes IR-active. A band origin for the IR-forbidden H_2O torsional mode is predicted at 151.2 cm^{-1} for regular CO_2–H_2O and red-shifted to 135.9 cm^{-1} with significant intensity for the isotopic CO_2–HDO variant of C_s symmetry. The spectral series of CO_2/HDO/D_2O doped neon matrices confirms another weaker band at 128.4 cm^{-1} (Fig. 2) which does not show up in neon matrices doped solely with HDO/D_2O. This indirect and so far tentative assignment for the IR-forbidden H_2O torsional mode ν_6 for the regular CO_2–H_2O complex requires extra attention in the discussion of this transition's contribution to the zero-point energy.

The present experimental findings for the weakly bound CO_2–H_2O system enable us to provide a (semi)-empirical estimate of the system's zero-point energy. The weakly bound nature of the CO_2–H_2O system results in rather small perturbations of the intramolecular vibrational transitions. The total shift of the zero-point energy contribution to D_0 caused by perturbations of intramolecular vibrational transitions is in the order of 5 cm^{-1}.[14] A reliable determination of the system's zero-point energy thus relies completely on accurate band origins for the set of five intermolecular van der Waals vibrational transitions introduced by complex formation. According to our harmonic MP2 predictions, the three observed transitions constitute about 75% of the total intermolecular vibrational zero-point energy contribution to the dissociation energy D_0. The contributions from the H_2O wagging mode ν_8 observed at 101.6 cm^{-1} and the H_2O rocking mode ν_{11} observed at 166.6 cm^{-1} are clear. In order to establish the contribution from the IR-forbidden H_2O torsional mode ν_6 we consider the effect of H/D substitution on this kind of motion. The torsional mode can be described as a hindered rotation of H_2O around the C_2 symmetry axis which also has the role of the principal *b*-axis for an isolated H_2O molecule. The torsional mode can as such be described as an almost genuine *b*-type rotation of H_2O although this motion is hindered in the complex. In the harmonic approximation the ratio of the two harmonic torsional band origins is thus proportional to the square root of the ratio of the *B* rotational constants for the two isotopic water molecules in question. In this way, the use of experimental *B*-values[26] predicts an isotopic harmonic red-shift of 21% for the band origin upon a single H/D-substitution. The model predicts a blue-shift of the proposed HDO torsional band origin at 128.4 cm^{-1} to 162.1 cm^{-1} for the corresponding IR-forbidden mode of the regular CO_2–H_2O system where our MP2 predictions provide a band origin close of 151.2 cm^{-1}. A complete unambiguous assignment of the HDO torsional cannot be justified solely by this crude model although the model provides a convincing argument. In our estimate for the zero-point energy we add a contribution of 75 ± 5 cm^{-1} from this IR-forbidden mode. The band origin of the medium intense CO_2 librational mode ν_{12} predicted to 16.8 cm^{-1} is close to the optical bandpass of our experimental setup and cannot be observed. In consequence, the zero-point energy contributions from this transition and the weak intermolecular O···C stretching transition ν_5 are based on the theoretical values listed in Table II. We estimate a total (semi)-empirical contribution to the zero-point energy from the class of intermolecular van der Waals transitions to 273 ± 15 cm^{-1} based on the present findings. A total zero-point energy contribution of 278 ± 15 cm^{-1} is achieved by inclusion of the predicted contribution caused by perturbations of the intramolecular vibrational transitions.[14]

The excellent agreement between our harmonic MP2 predictions and the observed band origins of CO_2–H_2O embedded in solid neon matrices is rather surprising. Harmonic predictions usually overshoot the actual (anharmonic) band origins for large-amplitude vibrational modes associated with intermolecular van der Waals transitions of weakly bound cluster molecules. A recent review addressing complexes of H_2O embedded in neon matrices reports that large-amplitude intermolecular vibrational transitions tend to be slightly blue-shifted relative to the gas phase although numerous red-shifts have been reported as well.[21] These small blue-shifts of large-amplitude vibrations are ascribed as minor repulsive steric effects originating from the congested neon host environment. These combined arguments could suggest that both our harmonic predictions and observed neon matrix band origins are slightly higher than expected gas-phase values. The present experimental findings thus invite for future high-level anharmonic theoretical investigations of the large-amplitude vibrational CO_2–H_2O motion which may shed light on the subtle balance of potential neon matrix blue-shifts and anharmonicity effects for this weakly bound system. We consider as such our current (semi)-empirical estimate of 273 ± 15 cm^{-1} as an upper limit for the intermolecular part of the zero-point energy. In the recent comprehensive theoretical study of the CO_2–H_2O system the highest level of theory including the almost complete electron correlation effects captured by the CCSD(T) approach and basis set superposition errors predicts an equilibrium dissociation energy D_e of 1004 cm^{-1}.[14] The combination with the present experimental findings thus provides a lower limit of 726 ± 15 cm^{-1} for the dissociation energy D_0 for this prototypical van der Waals interaction.

We appreciate the help and discussions with B. Brink, K. L. Feilberg, J. Ceponkus, A. Engdahl, and P. Uvdal. R.W.L.

acknowledges financial support from the Danish Council for Independent Research's Sapere Aude Programme (Grant No. 12-125248).

[1] R. R. Gamache, A. L. Laraia, and J. Lamouroux, Icarus **213**(2), 720–730 (2011).
[2] M. T. Nguyen, M. H. Matus, V. E. Jackson, V. T. Ngan, J. R. Rustad, and D. A. Dixon, J. Phys. Chem. A **112**(41), 10386–10398 (2008).
[3] Y. Abashkin, F. Mele, N. Russo, and M. Toscano, Int. J. Quantum Chem. **52**(4), 1011–1015 (1994).
[4] J. Altmann and T. Ford, J. Mol. Struct. **818**(1–3), 85–92 (2007).
[5] R. J. Wheatley and A. H. Harvey, J. Chem. Phys. **134**(13), 134309 (2011).
[6] J. Sadlej and P. Mazurek, J. Mol. Struct. **337**(2), 129–138 (1995).
[7] J. Sadlej, J. Makarewicz, and G. Chalasinski, J. Chem. Phys. **109**(10), 3919–3927 (1998).
[8] C. N. Ramachandran and E. Ruckenstein, Comput. Theor. Chem. **966**(1–3), 84–90 (2011).
[9] K. M. de Lange and J. R. Lane, J. Chem. Phys. **134**(3), 034301 (2011).
[10] M. Kieninger and O. Ventura, J. Mol. Struct. **390**, 157–167 (1997).
[11] Y. Danten, T. Tassaing, and M. Besnard, J. Phys. Chem. A **109**(14), 3250–3256 (2005).
[12] A. S. Tulegenov, Chem. Phys. Lett. **505**(21–23), 71–74 (2011).
[13] J. Makarewicz, T.-K. Ha, and A. Bauder, J. Chem. Phys. **99**(5), 3694–3699 (1993).
[14] J. Makarewicz, J. Chem. Phys. **132**(23), 234305 (2010).
[15] K. I. Peterson and W. Klemperer, J. Chem. Phys. **80**(6), 2439–2445 (1984).
[16] G. Columberg, A. Bauder, N. Heineking, W. Stahl, and J. Makarewicz, Mol. Phys. **93**(2), 215–228 (1998).
[17] L. Fredin, B. Nelander, and G. Ribbegard, Chem. Scr. **7**(1), 11–13 (1975).
[18] A. Schriver, L. Schriver-Mazzuoli, P. Chaquin, and E. Dumont, J. Phys. Chem. A **110**(1), 51–56 (2006).
[19] X. Zhang and S. P. Sander, J. Phys. Chem. A **115**(35), 9854–9860 (2011).
[20] J. Ceponkus, P. Uvdal, and B. Nelander, J. Chem. Phys. **129**(19), 194306 (2008).
[21] J. Ceponkus, A. Engdahl, P. Uvdal, and B. Nelander, Chem. Phys. Lett. **581**, 1–9 (2013).
[22] J. Ceponkus and B. Nelander, J. Phys. Chem. A **108**(31), 6499–6502 (2004).
[23] J. Ceponkus, P. Uvdal, and B. Nelander, J. Chem. Phys. **133**(7), 074301 (2010).
[24] J. Ceponkus, P. Uvdal, and B. Nelander, J. Phys. Chem. A **114**(25), 6829–6831 (2010).
[25] R. Bukowski, J. Sadlej, B. Jeziorski, P. Jankowski, K. Szalewicz, S. Kucharski, H. Williams, and B. Rice, J. Chem. Phys. **110**(8), 3785–3803 (1999).
[26] W. Benedict, N. Gailar, and E. K. Plyler, J. Chem. Phys. **24**(6), 1139 (1956).
[27] Y. Zhu, S. Li, P. Sun, and C. Duan, J. Mol. Spectrosc. **283**, 7–9 (2013).

A.2 The effect of hydrogen bonding on torsional dynamics: A combined far-infrared jet and matrix isolation study of methanol dimer

Reprinted with permission from
The effect of hydrogen bonding on torsional dynamics: A combined far-infrared jet and matrix isolation study of methanol dimer
F. Kollipost, J. Andersen, D. W. Mahler, J. Heimdal, M. Heger, M. A. Suhm, and R. Wugt Larsen
The Journal of Chemical Physics 141, 174314 (2014)

THE JOURNAL OF CHEMICAL PHYSICS **141**, 174314 (2014)

The effect of hydrogen bonding on torsional dynamics: A combined far-infrared jet and matrix isolation study of methanol dimer

F. Kollipost,[1] J. Andersen,[2] D. W. Mahler,[2] J. Heimdal,[3] M. Heger,[1] M. A. Suhm,[1] and R. Wugt Larsen[2,a)]

[1]*Institut für Physikalische Chemie, Universität Göttingen, Tammannstr. 6, D-37077 Göttingen, Germany*
[2]*Department of Chemistry, Technical University of Denmark, Kemitorvet 206, DK-2800 Kgs. Lyngby, Denmark*
[3]*MAX-IV Laboratory, Lund University, P. O. Box 118, SE-22100 Lund, Sweden*

(Received 22 September 2014; accepted 22 October 2014; published online 6 November 2014)

The effect of strong intermolecular hydrogen bonding on torsional degrees of freedom is investigated by far-infrared absorption spectroscopy for different methanol dimer isotopologues isolated in supersonic jet expansions or embedded in inert neon matrices at low temperatures. For the vacuum-isolated and Ne-embedded methanol dimer, the hydrogen bond OH librational mode of the donor subunit is finally observed at ∼560 cm^{-1}, blue-shifted by more than 300 cm^{-1} relative to the OH torsional fundamental of the free methanol monomer. The OH torsional mode of the acceptor embedded in neon is observed at ∼286 cm^{-1}. The experimental findings are held against harmonic predictions from local coupled-cluster methods with single and double excitations and a perturbative treatment of triple excitations [LCCSD(T)] and anharmonic. VPT2 corrections at canonical MP2 and density functional theory (DFT) levels in order to quantify the contribution of vibrational anharmonicity for this important class of intermolecular hydrogen bond vibrational motion.
 [http://dx.doi.org/10.1063/1.4900922]

I. INTRODUCTION

Methanol is one of the most important flexible molecules for the study of internal rotation or torsional motion, a class of large-amplitude vibrational motion in which two parts of the same molecule rotate with respect to each other over distances comparable to chemical bond lengths. In the case of methanol, the methyl group can counter-rotate with respect to the hydroxy group around the C–O bond axis. The coupling between large-amplitude torsional motion and other vibrational motions of a molecule is known to accelerate the transfer of energy internally among the vibrational modes via intramolecular vibrational redistribution (IVR).[1,2] These energy transfer processes are particularly important in order to understand the quantum control of chemical reactions via laser-induced bond breaking by torsion-mediated IVR relaxation in molecules containing a methyl rotor.[3] More generally, the torsional degrees of freedom are of critical importance in the development of molecular force fields for flexible molecules.[4]

In cyclic methanol clusters, the torsional motion of all the subunits is affected significantly by intermolecular hydrogen bonding, and the resulting hydrogen bond librational motion is effectively decoupled from the methyl group rotation.[5,6] The librational motion should not be described as torsional or rotational, but more or less as a genuine localized displacement of the hydrogen-bonded H atoms. As such, this displacement probes a substantial range of the anharmonic hydrogen bond potential and may be regarded as one of the most sensitive markers of hydrogen bonding. The role of librational motion in intermolecular energy transfer processes of condensed phases is currently being discussed.[7] Recent quantum chemical studies of the methanol dimer (Fig. 1) show that the incorporation of the donor OH librational mode is essential in order to capture the physics of the predissociation pathway that follows OH stretching excitation[8] since it has been shown to effectively absorb the initially deposited energy. This fits the results from ultra-fast pump-probe experiments of the hydrogen bond breaking dynamics.[9]

The spectroscopy of the hydrogen-bonded methanol dimer has been studied intensely. The rotational spectrum of several methanol dimer isotopologues isolated in molecular beams has been obtained by Lovas *et al.* and its analysis showed that the methanol dimer exhibits a linear hydrogen bond.[10,11] The first experimental study of methanol dimer was reported by Hoffbauer *et al.* who investigated the infrared photodissociation spectrum in the CO stretching region.[12] The observation and assignment of one single C–O stretching band was updated by Huisken and Stemmler who observed two well-separated bands in this region at 1026.5 and 1051.6 cm^{-1}.[13] This observation has been confirmed by subsequent experimental works and supported by theoretical studies.[14–16] The red-shifted dimer band has been assigned to the free CO stretching mode of the acceptor subunit whereas the latter more intense and blue-shifted band has been assigned to the CO stretching mode of the more perturbed H-atom donor molecule. The red-shift originates from an elongation of the acceptor C–O bond distance in the attractive hydrogen bond and the blue-shift results from a stronger force constant and coupling to the OH stretching mode which compresses the C–O bond distance.[17]

A particularly sensitive probe for the hydrogen bond interaction in methanol dimer is the OH stretching mode of the donor subunit. A significant elongation of its O–H

a)Author to whom correspondence should be addressed. Electronic mail: rewl@kemi.dtu.dk

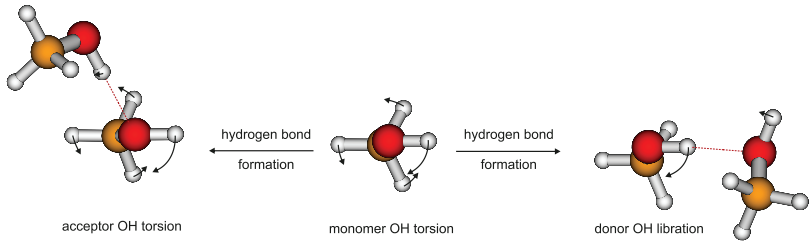

FIG. 1. The normal mode description of the acceptor OH torsional mode and the hydrogen-bonded donor OH librational mode of the methanol dimer.

bond distance upon hydrogen bonding together with a significantly increased OH transition dipole moment provides both a pronounced red-shift and infrared band intensity gain of this chromophore. A variety of independent experimental approaches – infrared photodissociation,[18] cavity ring-down,[19] IR-UV photoionization,[20] spontaneous Raman and direct absorption FTIR spectroscopies[21,22] in supersonic jet expansions – have settled the band origin at around 3575 cm^{-1} with a red-shift of ∼111 cm^{-1} from the monomer band origin, although slight ambiguities exist in the interpretation of the exact monomer reference due to its complicated band structure. Recently, this red-shift has been decomposed into a harmonic contribution[23] of about 121 cm^{-1} and a diagonal anharmonicity correction of 26 cm^{-1},[24] leaving only about −36 cm^{-1} for the combined coupling of all other modes to the hydrogen-bonded OH stretching vibration. The free OH stretching mode of the acceptor subunit has been located around 3684 cm^{-1}[17] and also somewhat lower in wavenumber[20] but in any case close to the monomer band origin.

The most valuable among the technologically accessible spectroscopic observables for the intermolecular potential energy landscape spanned by two interacting methanol molecules is the donor OH librational mode induced by the hydrogen bond. The observation and assignment of this large-amplitude mode provides direct benchmarks for theoretical descriptions of anisotropy and anharmonicity for the hydrogen bond. To the best of our knowledge, the only attempts to explore this crucial observable in the challenging far-infrared region of the electromagnetic spectrum have employed the medium of cryogenic matrices of nitrogen, argon, and carbon monoxide.[25–28] These matrix hosts are known to cause significant matrix-induced perturbations and potential site effects. In nitrogen matrices, up to four different isomers or differently trapped species have been reported with donor OH librational band origins between 572 and 624 cm^{-1} and perturbed acceptor OH torsional band origins between 325 and 386 cm^{-1} relative to the monomer OH torsional band at 304 cm^{-1}.[25] In the present work, we are revisiting these far-infrared spectral signatures of methanol dimer by detecting them in supersonic jet expansions and in less perturbative cryogenic neon matrices.

To discuss the anharmonicity of and the cross-talk between the different vibrational modes, we make use of the simple second-order perturbation theory relationship[29–31] between anharmonic fundamental transitions $\tilde{\nu}_i$ and harmonic normal modes ω_i in the presence of all other modes j

$$\tilde{\nu}_i = \omega_i + 2x_{ii} + \frac{1}{2}\sum_j x_{ij}, \tag{1}$$

where x_{ii} and x_{ij} are diagonal and off-diagonal anharmonicity constants, respectively. While the former can be easily extracted from overtone transitions, the latter are obtainable from combination bands. Neither of these are accessible in the present experimental work for the methanol dimer OH librational modes, but we can still draw important conclusions from benchmark calculations in the recent literature,[23,24] which have been made available to us by the authors and are mostly contained in the corresponding electronic supplements.

II. EXPERIMENTAL DETAILS

The infrared absorption spectra of jet-cooled methanol clusters were obtained by the high-throughput FTIR jet apparatus at Universität Göttingen described in detail elsewhere.[32] Helium gas pulses on the order of 0.5 mol doped with traces of CH_3OH (99.9% atom, VWR) were expanded through a 600 mm long and 0.2 mm wide pulsed slit nozzle into a 23 m^3 vacuum buffer dilution volume. The resulting supersonic jet expansions were synchronously probed by single 2–4 cm^{-1} resolution scans of a rapid-scan Bruker IFS 66v/S FTIR spectrometer. The buffer dilution volume was continuously evacuated by a series of Roots blowers at a pump speed of 2500 m^3 h^{-1} with time intervals of ∼50 s between the pulses to prevent any Mach disk interference by shock waves. The stagnation pressure in the gas reservoir from which the pulsed expansions emerge was 0.8 bar with sample concentrations in the range of 0.3%–0.8%. The mid-infrared spectra were obtained employing a conventional globar radiation source combined with CaF_2 beamsplitter and optics and a liquid nitrogen cooled InSb detector. The far-infrared spectra (190–650 cm^{-1}) were recorded employing a 6 μm multilayer Mylar beam splitter, CsI optics, and a liquid-helium cooled Si bolometer from Infrared Labs, Inc. Scans of approximately 400 pulses were collected and averaged for each sample concentration.

For the matrix isolation experiments, neon gas (L'Air Liquide, 99.996%) was deposited via a liquid nitrogen precooled inlet tube with a flow rate of 0.02 mol/h at 3.6 K on a

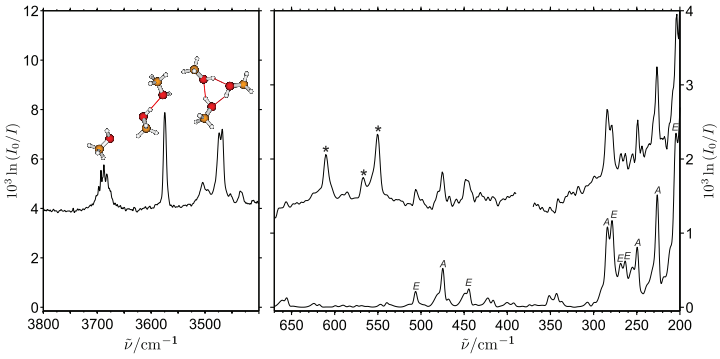

FIG. 2. The combined mid-infrared OH-stretching (upper left trace) and far-infrared (upper right trace) absorption spectrum recorded for supersonic jet expansions of helium doped with methanol together with a simulated rovibrational far-infrared spectrum of methanol monomer based on observations reported in Ref. 42 (lower trace, $T_{\mathrm{rot}} = 25$ K). The methanol cluster bands observed in the far-infrared region are marked with asterisks whereas the Q-branches of the torsional fundamental of methanol monomer are labeled by the symmetry species.

gold-plated oxygen-free high thermal conductivity (OFHC) copper mirror inside an immersion helium cryostat (IHC-3) modified for matrix isolation spectroscopy[33] at MAX-lab. Degassed samples of CH_3OH (Sigma-Aldrich, 99.9% atom) or CH_3OD (Sigma-Aldrich, 98%) were deposited simultaneously with the matrix gas by a separate inlet tube, giving mixing ratios of $\simeq$0.5–5 permille. The sample temperature at the mirror was monitored by a Lake Shore silicon diode and was kept stable at 2.8 $\pm$ 0.1 K before and after the matrix deposition employing resistive heaters and feedback electronics. In most cases, the doped neon matrices were afterwards annealed up to 9 K for the study of temperature effects. The sample mount was equipped with interchangeable CsI and TPX windows, and combined mid-infrared and THz single-beam spectra were collected by a Bruker IFS 120 FTIR spectrometer employing a globar lamp as radiation source. Broadband HgCdTe and InSb detectors combined with a Ge/KBr beam splitter and a Si-bolometer operating at 4.2 K combined with a 6 μm multilayer Mylar beam splitter were employed for the IR and THz spectral regions, respectively. A spectral resolution between 0.1 and 1 cm^{-1} was applied depending on the observed band widths.

III. METHANOL ISOLATED IN SUPERSONIC JET EXPANSIONS

The OH stretching region helps to monitor the size distribution of clusters in the supersonic jet expansions[19,21,22] (see Fig. 2, upper left trace). A reported band origin of 3681.5 cm^{-1} for the monomer OH stretching band based on the center of gas-phase Q-branches[34,35] has been employed in a range of cluster studies.[19,21,35–38] A band origin at 3686 cm^{-1} has subsequently been established by complementary Raman and infrared studies of jet-cooled methanol.[22,39] This value corresponds to the high-frequency component of the jet-Raman spectrum[39] and the absorption maximum in the jet-FTIR spectrum[22] and agrees well with the band origin of 3685 cm^{-1} obtained from a high-resolution rovibrational analysis of this strongly coupled torsion-vibration system.[40] In addition, the spacing of $\sim$2.6 cm^{-1} between the two observed Q-branches in the jet-Raman spectrum[39] agrees perfectly with the difference in tunneling splitting between the vibrational ground state and the excited OH stretching state.[41] The red-shifted donor OH stretching band origin of 3575 cm^{-1} for the methanol dimer has been established by complementary jet-cooled Raman and FTIR observations whereas the free acceptor OH stretching band overlaps with the rotational structures and torsional tunneling splittings of the monomer band.[21,22] The complicated OH stretching jet spectrum of the cyclic methanol trimer has been shown to involve a vibrational Franck-Condon effect[22] and consists of two near-degenerate strong bands at 3469 cm^{-1} and 3474 cm^{-1}. These two strong bands are accompanied by five weaker sub-bands and no hydrogen-bond isomerism of methanol trimer has to be invoked to understand these jet spectral features.

The upper right trace in Fig. 2 shows the far-infrared absorption spectrum of jet-cooled methanol down to the CsI cut-off close to 200 cm^{-1}. In the region around 370 cm^{-1}, the 6 μm multilayer Mylar beam splitter has a strong dip in the throughput and thereby causes an artifact in the generated absorption spectrum. In the lower far-infrared region, the absorption spectrum reproduces a very rich structure caused by multiple rovibrational sub-bands associated with the torsional fundamental band of the methanol monomer. The large-amplitude torsional motion of methanol is coupled to the overall rotational motion and the other vibrational modes of the molecule. The analysis of these couplings have been described in detail elsewhere.[43] The lower right trace of Fig. 2 shows a rovibrational simulation based on previously assigned Q-branch structures reported in the methanol atlas of Moruzzi *et al.*[42] The room temperature (T_1) spectra were converted to spectra at cold temperatures T_2 by the following

relationship:

$$\frac{S_{nm}(T_1)}{S_{nm}(T_2)} = \frac{e^{-\frac{E_m}{kT_1}}\left(1 - e^{-\frac{hc\tilde{\nu}_{nm}}{kT_1}}\right)}{e^{-\frac{E_m}{kT_2}}\left(1 - e^{-\frac{hc\tilde{\nu}_{nm}}{kT_2}}\right)} \quad (2)$$

employing the line strength S_{nm} and wavenumber $\tilde{\nu}_{nm}$ of a transition from a lower state m to an upper state n and the energy E_m of the m level. The simulated far-infrared spectrum in Fig. 2 is plotted as an overlay of Gaussian curves with 4 cm^{-1} full widths at half maximum matching the spectral resolution of the jet experiment. It was found that a simulated spectrum at $T_2 = 25$ K yields the best match with the experimental jet spectra. Non-equilibrium effects in the jet expansion concerning the population of the A and E states[44] were ignored, because these are not significant at 25 K.

The most distinct spectral features observed in the lower far-infrared absorption spectrum are located around 205 cm^{-1}, 226 cm^{-1}, 278 cm^{-1}, and 284 cm^{-1} with decreasing intensity for the transitions at higher wavenumbers. These have previously been attributed to Q-branches of different A–A (226 and 284 cm^{-1}) and E–E (205 and 278 cm^{-1}) sub-bands with $\Delta K = \pm 1$ and $K'' \leq 1$ associated with the torsional fundamental.[42] Another observed series of distinct spectral features has previously been attributed to other, less intense A–A (249 cm^{-1}) and E–E (263 and 269 cm^{-1}) torsional sub-bands with $\Delta K = \pm 1$ and $K'' \leq 2$.[42] The convincing agreement between the observed jet spectra and the simulated rovibrational spectrum of the monomer in the low far-infrared spectral region does not at first sight point at any potential methanol dimer contributions.

In the upper far-infrared region above the beam splitter artifact, another three distinct spectral features are reproduced with band origins around 448 cm^{-1}, 475 cm^{-1}, and 507 cm^{-1}. These spectral features can be assigned to three different sub-bands or Q-branches associated with the first torsional overtone of the methanol monomer which are included in the simulated rovibrational spectrum shown in Fig. 2. The Q-branches observed around 448 and 507 cm^{-1} have previously been assigned to the E–E transitions corresponding to $K = -1 \rightarrow -2$ and $K = -1 \rightarrow 0$, respectively, whereas the Q-branch observed around 475 cm^{-1} has previously been assigned to the A–A transition corresponding to $K = 0 \rightarrow +1$.[42] The simulated rovibrational spectrum shown in Fig. 2 includes a total of 17 previously assigned sub-bands with $K'' \leq 3$ associated with the first torsional overtone of methanol in the range from 343 cm^{-1} to 656 cm^{-1}. None of the 14 weaker torsional overtone Q-branches of the monomer are observed clearly in the present far-infrared jet-spectra. The strong spectral features observed in the range from 520 cm^{-1} to 650 cm^{-1} must therefore be assigned to jet-cooled clusters of methanol.

The mid-infrared OH stretching spectral signatures have previously guided the assignment of a number of hydrogen-bonded OH librational modes of jet-cooled methanol trimers and tetramers in the upper far-infrared region.[6,22] Assisted by dedicated concentration-dependence spectral series, direct comparisons with the corresponding OH stretching spectra and quantum-chemical predictions, we have previously assigned the observed band at 613 cm^{-1} to the most IR-active OH librational mode of the methanol trimer (see Fig. 2, upper right trace).[5] In addition, two bands have been assigned to the librational modes of the cyclic methanol tetramer: a highly IR-active doubly degenerate mode at 760 cm^{-1}, and a lower-wavenumber mode at 695 cm^{-1} with lower infrared activity (not shown).[5] Subsequently, an upgraded configuration of the experimental jet-FTIR apparatus including a liquid helium cooled Si-bolometer detector revealed the existence of a band centered around 551 cm^{-1} which we tentatively assigned to the lowest-wavenumber OH librational mode of the cyclic trimer,[6] although quantum-chemical calculations have predicted an overlap with the donor OH librational band of the methanol dimer[5] and the relative intensity is indeed higher than predicted. In the present work, featuring an improved signal-to-noise performance in the lower far-infrared region,[45] the existence of the 551 cm^{-1} band is easily confirmed with a reproducible high-wavenumber shoulder at 567 cm^{-1} and an overall higher intensity than the 613 cm^{-1} band as seen in Fig. 2. However, a completely unambiguous size assignment of the 551 cm^{-1} band cannot be obtained by dedicated jet experiments from the concentration dependency alone. Trimer formation cannot be effectively suppressed once dimer formation is favored in the earlier stages of the expansions, and extreme dilutions are not compatible with signal-to-noise limitations in this spectral region. A dimer OH librational fundamental below 551 cm^{-1} or above 567 cm^{-1} can be safely ruled out from the jet experiments, but there could be one or more spectral features attributed to this band in this interval. Therefore, we consult a more sensitive matrix isolation approach where the discrimination between dimer and trimer spectral fingerprints is easier.

IV. METHANOL EMBEDDED IN NEON MATRICES

In previous studies of methanol embedded in solid matrices of para-H_2[46] and neon,[47,48] these inert matrix environments have been shown to completely forbid the overall rotational motion of methanol but still allow for large-amplitude internal torsional motion which is just slightly hindered relative to the gas phase. The torsion-vibration splittings into A and E sub-levels by torsional tunneling therefore persist in the inert neon matrix environment, but their standard A–A and E–E selection rules have been shown not to apply anymore.[47] The torsional fundamental of the methanol monomer accordingly gives rise to four different sub-bands (see Fig. 3). In cryogenic neon matrices, the splitting of the ground state of the torsional vibration is reduced from the gas phase value of 9.1 cm^{-1} to 6.7 cm^{-1}, whereas the splitting of the first excited state is reduced from the gas phase value of 86.5 cm^{-1} to 56.2 cm^{-1}.[47] Both of these vibrational splittings can be revealed by dedicated annealing experiments. Fig. 3 shows the observed far-infrared absorption spectrum of methanol embedded in neon at 2.8 K together with the corresponding spectra after subsequent annealing the matrix to 6 K and 9 K and relaxing it back to 3 K. It appears that the higher population of the A sub-level of the vibrational ground state at 2.8 K favors the two A–E and A–A transitions observed at

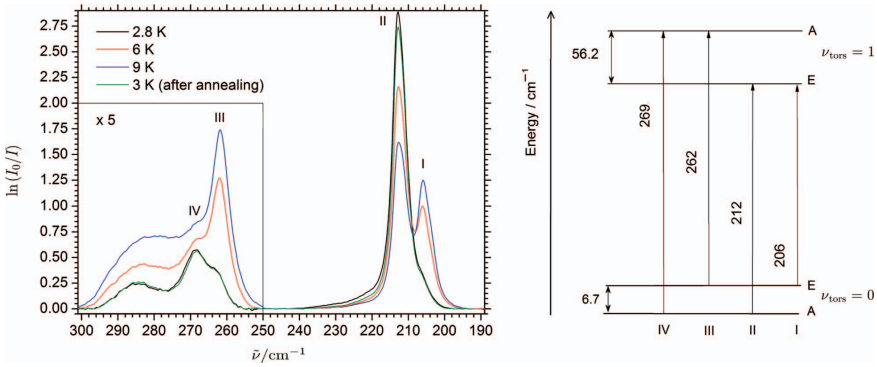

FIG. 3. The temperature dependence of the observed far-infrared absorption spectrum of methanol embedded in neon annealed from 2.8 K to 6 K and 9 K and relaxed back to 3 K (left). The assignments of the four different observed components I, II, III, and IV for the torsional fundamental ($\upsilon_{tors} = 0 \rightarrow 1$) of methanol monomer are indicated together with a corresponding torsional energy diagram illustrating the different *A*/*E* transitions (right).

212 cm^{-1} (denoted II) and 269 cm^{-1} (denoted IV), respectively. The slow, step-wise annealing reveals the emergence of the two torsional *E*–*E* and *E*–*A* transitions originating from the *E* sub-level of the vibrational ground state which gradually becomes more populated with increasing temperature. These bands, observed at 206 cm^{-1} (denoted I) and 262 cm^{-1} (denoted III), are red-shifted by the vibrational ground-state splitting of 6.7 cm^{-1} relative to the "cold" transitions (II and IV). In the matrix isolation spectra recorded at 2.8 K where the "cold" sub-bands dominate, another band is reproduced at 286 cm^{-1}. The concentration dependency of this band, although somewhat distorted by the overlap with the 269 cm^{-1} feature (IV), is steeper than observed for the four monomer sub-bands, which points at a dimer origin. This is supported by the blue-shifted position relative to the monomer band system and the fact that it collapses into a single band. The methanol:neon mixing ratios in the permille region rule out any methanol trimer assignments which is also supported by the lack of any corresponding trimer absorption in the OH stretching region (not shown).

Fig. 4 shows the entire far-infrared absorption spectrum of methanol embedded in neon at 2.8 K from 200 cm^{-1} up to the high-wavenumber cut-off of the cold optical filter inside the Si bolometer around 600 cm^{-1}. In the upper far-infrared region, a strong band is observed at 446 cm^{-1} even at the smallest methanol:neon mixing ratios, pointing at a monomer origin. This slightly broadened band has previously been observed by Perchard for very diluted methanol doped neon matrices.[47] At higher methanol:neon mixing ratios, another weak band appears at 507 cm^{-1} with the same concentration dependency. The intensity of these two bands also decreases by the same amount upon annealing of the neon matrices. A detailed assignment of these monomer transitions is difficult. However, we cannot reject Perchard's tentative assignment of the strong 446 cm^{-1} band to a torsional overtone transition originating from the *A* sub-level of the vibrational ground state.[47] In some matrix experiments, another weak band with varying intensity is observed at 527 cm^{-1} in methanol-doped neon matrices. This band is attributed to water/methanol dimers which shall not be discussed further in the present contribution. At higher methanol:neon mixing ratios, a sharp band with one or more high-wavenumber shoulders appears at 558 cm^{-1}. This band has a steep concentration dependency which qualitatively matches the behavior of the broader proposed acceptor OH torsional mode at 286 cm^{-1}. As mentioned above, the latter band overlaps with the neighboring monomer feature which complicates a solid quantitative intensity analysis. Nevertheless, the two dimer bands in question appear to have almost the same integrated intensity at low methanol concentrations. This is supported by harmonic MP2 and B3LYP frequency calculations[5] which predict an almost 1:1 intensity ratio of these bands. These predictions

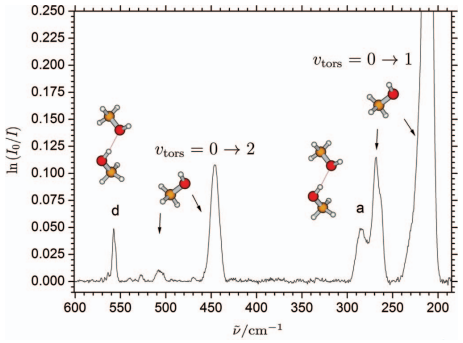

FIG. 4. The observed far-infrared absorption spectra of methanol embedded in neon matrices at 2.8 K. The components of the torsional fundamental ($\upsilon_{tors} = 0 \rightarrow 1$) and first torsional overtone ($\upsilon_{tors} = 0 \rightarrow 2$) transitions of the monomer as well as of the acceptor OH torsional ("a") and donor OH librational ("d") transitions of the dimer are assigned by minimum structures.

suggest a straightforward assignment of the 558 cm^{-1} band to the missing donor OH librational band of methanol dimer.

The matrix band position lines up between the strong 551 cm^{-1} band and the weaker 567 cm^{-1} band observed in the jet spectra. A recent review article addressing water clusters embedded in neon matrices reports that large-amplitude intermolecular vibrational transitions tend to become slightly blue-shifted relative to the gas phase.[49] These small blue-shifts of large-amplitude vibrational modes are ascribed as minor repulsive steric effects originating from the neon host environment. This provides a qualitative argument in support for a dimer assignment of the 551 cm^{-1} band in the far-infrared jet spectrum. On the other hand, the predicted 1:1 intensity relationship mentioned above together with the lack of strong dimer absorptions at lower wavenumbers in the jet spectrum provide a counter-argument for an assignment of the weaker 567 cm^{-1} band to the librational mode in question. In the jet experiments, it is furthermore possible that the librational intensity is distributed over several $\Delta K = \pm 1$ sub-branches or affected by rovibrational couplings, similar to but less pronounced than in the case of the HF dimer.[50] In addition, the blue-shift observations cited above are not a strict indicator, since numerous red-shifts have been observed under similar conditions as well. Further, our previous quantum-chemical predictions[5] point at a possible overlap between the donor OH librational mode of the dimer and the lowest-wavenumber OH librational mode of the trimer. The far-infrared jet spectral series is thus less conclusive than the neon matrix isolation data, and we can only suggest a band origin interval of 560±10 cm^{-1} for the OH librational mode of the methanol dimer when not affected by a neon matrix environment.

In order to verify the proposed methanol dimer assignment further, we explore the isotopic spectral shifts associated with H/D substitution on the hydroxy group. Fig. 5 shows the full far-infrared absorption spectrum of methanol-OD embedded in neon at 2.8 K (red trace) together with the corresponding far-infrared spectrum of regular methanol (black trace) at a similar methanol:neon mixing ratio. H/D exchange processes on the very large surface of the matrix inlet tubing are inevitable, preventing higher purities than 80%–85% of methanol-OD in the deposited neon matrices. The traces of regular methanol can be monitored most clearly by the isolated torsional overtone sub-band observed at 447 cm^{-1}. The torsion-vibration splittings of the ground and excited torsional states are smaller for methanol-OD, owing to the slower torsional tunneling of D relative to H. Two major bands are reproduced at 187.5 cm^{-1} and 205.5 cm^{-1}; the latter being overlapped by the two torsional *E*–*E* and *A*–*E* sub-bands of regular methanol. These two bands have previously been observed by Perchard for very diluted methanol-OD doped neon matrices and assigned to the "cold" torsional sub-bands originating from the *A* sub-level of the vibrational ground state.[47] The two remaining torsional sub-bands originating from the *E* sub-level could not be observed by dedicated annealing experiments. The vibrational ground state splitting of methanol-OD in the gas phase is 2.6 cm^{-1} and might be even smaller in neon matrices.[51] The splitting of the excited torsional state of methanol-OD must therefore be very close to the wavenumber difference of ∼18 cm^{-1} between the "cold" torsional sub-bands.

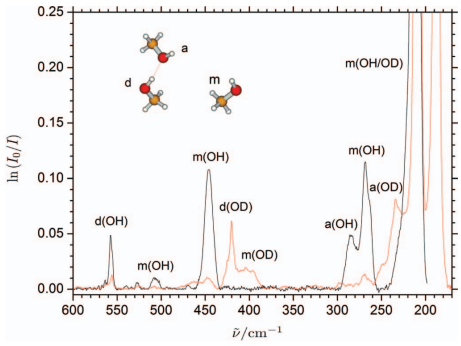

FIG. 5. The observed far-infrared absorption spectra of methanol (black trace) and methanol-OD (∼80%, red trace) embedded in neon matrices at 2.8 K. The assignments for the torsional fundamental and the first torsional overtone of the monomers (denoted "m(. . .)") as well as the acceptor OH/OD torsional (denoted "a") and donor OH/OD librational modes of the hydrogen-bonded methanol dimers (denoted "d") are shown (see text).

In the regions of the proposed dimer assignments for regular methanol, we also observe small traces of deuterated dimeric species. A closer inspection of the region for the proposed donor OH librational band reveals a rather small red shift of ∼1–2 cm^{-1} relative to the band origin of 558 cm^{-1}. This small isotopic wavenumber shift points at a OH librational mode and could originate from mixed methanol dimers where regular methanol acts as a donor and methanol-OD acts as the acceptor. A red-shift of the same size is also observed for the mixed water/methanol dimer band around 527 cm^{-1} which shall not be discussed further in the present contribution. A series of previous cluster studies have shown that D-bonded complexes in general are more stable than the corresponding H-bonded complexes due to smaller zero-point energies.[52] Accordingly, the mixed methanol dimer where methanol-OD acts as the donor should be more abundant. In the region of the proposed acceptor OH torsional mode of the methanol dimer, we observe a rather weak and very broad spectral feature overlapped by the torsional *E*–*A* and *A*–*A* sub-bands of regular methanol. This broad spectral feature must have a contribution from mixed methanol dimers where regular methanol acts as acceptor instead of donor, but a quantitative analysis of the relative abundance of mixed methanol dimers is not possible even at higher mixing ratios.

The inevitable H/D exchange does not prevent a large excess of methanol-OD and clear absorption by the methanol-OD dimer. The donor OD librational mode is easily assigned as a rather sharp band at 420 cm^{-1}. The somewhat broad spectral feature observed below the sharp donor OD-librational band around 400 cm^{-1} appears to have a similar concentration dependency as the torsional sub-bands of methanol-OD and might originate from a monomeric torsional overtone sub-band. The acceptor OD torsional mode appears clearly as a high-wavenumber shoulder on the torsional *A*–*A* sub-band of methanol-OD at 234 cm^{-1}. This acceptor OD torsional

TABLE I. The observed band origins (in cm^{-1}) for the acceptor OH/OD torsional mode and the donor OH/OD librational mode of different hydrogen-bonded methanol dimer isotopologues isolated in supersonic jet expansions and embedded in cryogenic neon matrices at 2.8 K.

Species	Jet	Neon matrix
$(CH_3OH)_2$ acceptor OH torsion	Not assigned	286
$(CH_3OH)_2$ donor OH libration	560 ± 10	558
$(CH_3OD)_2$ acceptor OD torsion	Not assigned	234
$(CH_3OD)_2$ donor OD libration	Not assigned	420

band must be overlapped by mixed methanol dimers where methanol-OD acts as the acceptor and regular methanol as the donor which can explain the apparent larger band intensity relative to the acceptor OH torsional band of regular methanol dimer. The resulting OD/OH isotope ratios of 0.75–0.82 are significantly larger than $1/\sqrt{2}$ as expected for strongly anharmonic potential energy wells. The complete set of methanol dimer assignments from the combined jet and neon matrix isolation experiments is summarized in Table I.

V. HARMONIC LOCAL-CORRELATION COUPLED CLUSTER AND ANHARMONIC PREDICTIONS

Harmonic predictions for the donor OH stretching red-shift of the methanol dimer have been available for some time from MP2 and Density Functional Theory (DFT) calculations.[22] These predictions demonstrate a red-shift on the order of 150 cm^{-1}, much more than the experimental anharmonic value of 111 cm^{-1}. A recent study has now applied harmonic Coupled-Cluster methods in a local correlation framework (prefix L) to the problem,[23] providing a full normal-mode analysis at the optimized structures while being essentially free of basis set superposition error (BSSE). The exaggerated MP2 red-shifts were traced to an underestimation of the O–H bond strength of the donor molecule in the dimer, which is only partially compensated by likewise underestimated intermolecular electron correlation effects. A combination of local and explicit electron correlation beyond second-order perturbation theory placed the harmonic donor OH stretching red-shift close to 121 cm^{-1}.

Harmonic transition wavenumbers for the acceptor OH torsional and the donor OH librational modes were obtained at the same levels[23] and are reproduced in Table II. We augment these data with MP2/cc-pVTZ, B2PLYP-D3/cc-pVTZ, and B3LYP-D3BJ/6-311+G(2d,p) calculations making use of Grimme's empirical dispersion correction (D3)[53] and Becke-Johnson damping (BJ),[54] both in the harmonic approximation (Table II) and applying a standard second-order perturbational (VPT2) anharmonic treatment as implemented in the Gaussian 09 program,[29] carried out and reported in Ref. 24 and summarized in Table III. For brevity, we shorten the 6-311+G(2d,p) basis set to "6311"and cc-pVTZ to "VTZ." The VPT2 calculations avoided diffuse functions on all hydrogen atoms (6311) or even altogether (VTZ), improving numerical stability in the finite-displacement steps of the VPT2 treatment. The highest level of theory in Ref. 23 with an optimized geometry and harmonic frequencies is explicitly correlated

TABLE II. Harmonic wavenumbers ω (units of cm^{-1}) for the OH torsional ("tors") mode of the methanol monomer ("mon") and corresponding donor OH librational ("lib") and acceptor torsional ("tors") modes of the dimer ("dim"), reproduced from Refs. 24 and 23.

	$\omega_{\text{tors}}^{\text{mon}}$	$\omega_{\text{lib}}^{\text{dim}}$	$\omega_{\text{tors}}^{\text{dim}}$
MP2/VTZ	309	699	317
B3LYP-D3BJ/6311	294	708	355
B2PLYP-D3/VTZ	304	694	308
MP2/A′VTZ[a]	294	695	331
LMP2/A′VTZ	293	660	319
LCCSD(T0)/A′VTZ(int)	294	647	320
Benchmark[b]	294	660	322

[a]Diffuse functions omitted for CH_3 hydrogens.
[b]LCCSD(T*)-F12a/VDZ-F12(int).

LCCSD(T)-F12/cc-pVDZ-F12(int), with the intermolecular interactions ("int") treated at the same high level of theory. Comparison with larger basis sets showed that these results were very close to the Complete Basis Set (CBS) limit. We can therefore regard these data as the harmonic benchmark for all other calculations henceforth.

The harmonic OH librational wavenumbers are overestimated in the canonical MP2 and DFT calculations by 30–50 cm^{-1}. This correlates with overestimated OH stretching shifts, indicative of a too anisotropic hydrogen bond. The good performance of LMP2 is a result of error compensation and does not extend to the OH stretching shift.[23]

Advancing to the anharmonic VPT2 results which are restricted to lower electronic structure levels (Table III), the donor OH librational mode exhibits a pronounced negative diagonal anharmonicity, red-shifting the fundamental transition by about 90 cm^{-1}. This corresponds to a sub-linear increase of the restoring force due to the directional hydrogen bond. The off-diagonal couplings to all other modes are predicted to slightly increase this red-shift when taken together, but a distinct positive coupling to the donor OH stretching vibration can be identified. This coupling reflects the fact that

TABLE III. Calculated VPT2 spectroscopic constants (units of cm^{-1}) for the donor OH librational mode of methanol dimer (from Ref. 24 and by personal communication of the computer outputs through its authors). The 20 anharmonic coupling cross-terms not given in the table are somewhat smaller and their overall sum is very close to 0.

	MP2/VTZ	B3LYP-D3BJ/6311	B2PLYP-D3/VTZ
ω_{lib}[a]	699	708	694
$2x_{\text{lib, lib}}$[b]	−92	−91	−85
$\frac{1}{2}x_{\text{lib, }\nu(\text{OH})_b}$[c]	+30	+30	+30
$\frac{1}{2}x_{\text{lib,}\delta(\text{OH})_b}$[d]	−9	−8	−8
$\frac{1}{2}x_{\text{lib,tors}}$[e]	−7	−11	−7
$\frac{1}{2}\sum_{1}^{6} x_{\text{lib,intermol}}$[f]	−31	−31	−21
$\tilde{\nu}_{\text{lib}}$[g]	589	595	603

[a]The harmonic wavenumber.
[b]The anharmonic contribution from diagonal anharmonicity.
[c]The anharmonic contribution from the coupling to the donor OH stretching mode.
[d]The anharmonic contribution from the coupling to the donor OH bending mode.
[e]The anharmonic contribution from the coupling to the acceptor OH torsional mode.
[f]The anharmonic contribution from the coupling to the six intermolecular modes.
[g]The anharmonic wavenumber.

TABLE IV. Calculated VPT2 spectroscopic constants (units of cm^{-1}) for the acceptor OH torsional mode of methanol dimer (from Ref. 24 and by personal communication of the computer outputs through its authors).

	MP2/VTZ	B3LYP-D3BJ/6311	B2PLYP-D3/VTZ
ω_{tors} [a]	317	355	308
$2x_{tors,\,tors}$ [b]	−66	−61	−73
$\frac{1}{2}\sum_{j}^{29} x_{tors,j}$ [c]	+31	−9	+11
$\tilde{\nu}_{tors}$ [d]	282	285	246

[a]The harmonic wavenumber.
[b]The anharmonic contribution from diagonal anharmonicity.
[c]The anharmonic contribution from the sum of all coupling cross-terms to the other 29 vibrational modes.
[d]The anharmonic wavenumber.

the OH librational mode is ultimately of dissociative nature, and its excitation tends to restore the higher monomer value for the OH stretching frequency. The magnitude of this coupling is remarkably consistent among the calculations, independent of variations in the absolute harmonic wavenumbers for the OH librational and stretching modes. The positive $x_{lib,\nu(OH)_b}$ coupling is key responsible for the fact that the harmonic OH stretching red-shift of methanol dimer is larger than the experimental one despite opposing diagonal anharmonic OH stretching effects. Indeed, from the experimental constraints outlined in the Introduction,[23,24] one can estimate the order of magnitude of $\frac{1}{2}x_{lib,\nu(OH)_b}$ around 36 cm^{-1}, if all other off-diagonal contributions to the OH stretching shift are assumed to approximately cancel. All this lends some credibility to the VPT2 corrections despite their limited electronic structure level and the relatively large amplitude motion in the OH librational mode, which probably challenges the applicability of the VPT2 approximations.

The overall sum of anharmonic corrections to the librational fundamental transition is on the order of $-(100 \pm 10)$ cm^{-1}. Adding this to the benchmark harmonic wavenumber of 660 cm^{-1}, a prediction of 560 cm^{-1} is obtained which is fully consistent with the present experimental value of (560 ± 10) cm^{-1}. A similar analysis of the acceptor OH torsional mode of methanol dimer is likely to stretch the reliability of VPT2 calculations, but we note that the best harmonic estimate of 322 cm^{-1} (Table II) in combination with the average VPT2 correction of (50 ± 20) cm^{-1} (Table IV) is not too far from the experimental value of 286 cm^{-1} obtained in this work.

We finally note that the overtone of the hydrogen-bonded librational mode is predicted remarkably close to the CO stretching fundamentals of methanol dimer[13] based on the results of the present work, potentially complicating their quantitative analysis.

VI. CONCLUSIONS

For the first time, the fundamental hydrogen bond librational mode of the smallest organic hydrogen-bonded dimer has been confidently assigned experimentally near 560 cm^{-1} with an accuracy which allows for rigorous benchmarking of theory. The remaining experimental uncertainty of at most ± 10 cm^{-1} is due to spectral overlap with methanol trimer (in the gas phase) or residual matrix influence (in the cryogenic neon matrix). The 100 cm^{-1} or 15% gap to the benchmark harmonic prediction can be rationalized mostly by anharmonicity along the librational coordinate. Off-diagonal coupling terms are significant, in particular to the bound OH stretching mode, but they are largely canceled by opposing coupling cross-terms from the intermolecular modes. The experimental result is corroborated by results for O-deuterated methanol dimer (420 cm^{-1}) and the even larger amplitude acceptor OH (OD) torsional mode of the dimer is observed at 286 cm^{-1} (234 cm^{-1}) in the neon matrices. Thus, two orthogonal degrees of freedom of the hydrogen bonded (and free) OH groups in methanol dimer as well as their mutual coupling are now rather well established by infrared vibrational spectroscopy. Sensitivity limits of supersonic jet spectroscopy in the far infrared and environmental effects in neon matrices are seen to be surmountable by a combination of both techniques. Quantitative studies of sub-picosecond intermolecular energy flow in organic hydrogen bonds can profit from these reference values. It would be valuable to confirm some of the conclusions on off-diagonal coupling cross-terms by direct observation of weak OH stretching-libration combination bands of methanol dimer.

ACKNOWLEDGMENTS

We appreciate help from and discussions with A. Engdahl, B. Nelander, and R. Mata. R.W.L. acknowledges financial support from the Danish Council for Independent Research's Sapere Aude Programme (Grant Ref. No. 12-125248). The work was supported by the Fonds der Chemischen Industrie and by the German Research Foundation (DFG) (Su 121/4-1).

[1]P. Maksyutenko, O. Boyarkin, T. Rizzo, and D. Perry, J. Chem. Phys. **126**, 044311 (2007).
[2]R. M. Lees, L.-H. Xu, J. W. C. Johns, B. P. Winnewisser, and M. Lock, J. Mol. Spectrosc. **243**, 168–181 (2007).
[3]D. J. Nesbitt, J. Phys. Chem. **100**, 12735–12756 (1996).
[4]A. D. Mackerell, Jr., J. Comput. Chem. **25**, 1584–1604 (2004).
[5]R. Wugt Larsen and M. A. Suhm, J. Chem. Phys. **125**, 154314 (2006).
[6]R. Wugt Larsen and M. A. Suhm, Phys. Chem. Chem. Phys. **12**, 8152–8157 (2010).
[7]T. Yagasaki, J. Ono, and S. Saito, J. Chem. Phys. **131**, 164511 (2009).
[8]R. Jiang and E. L. Sibert, J. Phys. Chem. A **113**, 7275–7285 (2009).
[9]R. Jiang and E. L. Sibert, J. Chem. Phys. **136**, 224104 (2012).
[10]C. L. Lugez, F. J. Lovas, J. T. Hougen, and N. Ohashi, J. Mol. Spectrosc. **194**, 95–112 (1999).
[11]F. J. Lovas, S. P. Belov, M. Y. Tretyakov, W. Stahl, and R. Suenram, J. Mol. Spectrosc. **170**, 478–492 (1995).
[12]M. A. Hoffbauer, C. F. Giese, and W. R. Gentry, J. Phys. Chem. **88**, 181–184 (1984).
[13]F. Huisken and M. Stemmler, Chem. Phys. Lett. **144**, 391–395 (1988).
[14]U. Buck, X. J. Gu, C. Lauenstein, and J. Rudolph, J. Chem. Phys. **92**, 6017 (1990).
[15]J. P. La Cosse and J. M. Lisy, J. Phys. Chem. **94**, 4398–4400 (1990).
[16]A. Bizzarri, S. Stolte, J. Reuss, J. Van Duijneveldt-van De Rijdt, and F. Van Duijneveldt, Chem. Phys. **143**, 423–435 (1990).
[17]U. Buck and F. Huisken, Chem. Rev. **100**, 3863–3890 (2000).
[18]F. Huisken and A. Kulcke, J. Chem. Phys. **95**, 3924–3929 (1991).
[19]R. A. Provencal, J. B. Paul, K. Roth, C. Chapo, R. N. Casaes, R. J. Saykally, G. S. Tschumper, and H. F. Schaefer III, J. Chem. Phys. **110**, 4258–4267 (1999).

[20]H. Han, C. Camacho, H. Witek, and Y.-P. Lee, J. Chem. Phys. **134**, 144309 (2011).
[21]T. Häber, U. Schmitt, and M. A. Suhm, Phys. Chem. Chem. Phys. **1**, 5573–5582 (1999).
[22]R. Wugt Larsen, P. Zielke, and M. A. Suhm, J. Chem. Phys. **126**, 194307 (2007).
[23]M. Heger, M. A. Suhm, and R. A. Mata, J. Chem. Phys. **141**(10), 101105 (2014); Supplementary material is available at ftp://ftp.aip.org/epaps/journ_chem_phys/E-JCPSA6-141-034436.
[24]F. Kollipost, K. Papendorf, Y.-F. Lee, Y.-P. Lee, and M. A. Suhm, Phys. Chem. Chem. Phys. **16**, 15948–15956 (2014); Supplementary material is available at http://pubs.rsc.org/en/Content/ArticleLanding/2014/CP/c4cp01418a.
[25]J. Murto, M. Räsänen, A. Aspiala, and E. Kemppinen, Acta Chem. Scand. A **37a**, 323–335 (1983).
[26]S. Coussan, Y. Bouteiller, A. Loutellier, J. P. Perchard, S. Racine, A. Peremans, W. Q. Zheng, and A. Tadjeddine, Chem. Phys. **219**, 221–234 (1997).
[27]S. Coussan, A. Loutellier, J. P. Perchard, S. Racine, A. Peremans, A. Tadjeddine, and W. Q. Zheng, Chem. Phys. **223**, 279–292 (1997).
[28]J. P. Perchard and Z. Mielke, Chem. Phys. **264**, 221–234 (2001).
[29]V. Barone, J. Chem. Phys. **122**(1), 014108 (2005).
[30]I. M. Mills, *Vibration-rotation Structure in Asymmetric- and Symmetric-top Molecules in Molecular Spectroscopy: Modern Research*, edited by N. Rao and C. W. Mathews (Academic, 1972), Vol. I, pp. 115–140.
[31]G. Amat, H. Nielsen, and G. Tarrago, *Rotation-vibration Spectra of Molecules* (Marcel Dekker, New York, 1971).
[32]M. A. Suhm and F. Kollipost, Phys. Chem. Chem. Phys. **15**, 10702–10721 (2013).
[33]J. Andersen, J. Heimdal, D. W. Mahler, B. Nelander, and R. Wugt Larsen, J. Chem. Phys. **140**, 091103 (2014).
[34]A. Serrallach, R. Meyer, and H. H. Günthard, J. Mol. Spectrosc. **52**, 94–129 (1974).
[35]J. R. Dixon, W. O. George, F. Hossain, R. Lewis, and J. M. Price, J. Chem. Soc., Faraday Trans. **93**, 3611–3618 (1997).
[36]F. Huisken, M. Kaloudis, M. Koch, and O. Werhahn, J. Chem. Phys. **105**, 8965–8968 (1996).
[37]U. Buck, J.-G. Siebers, and R. J. Wheatley, J. Chem. Phys. **108**, 20–32 (1998).
[38]Y. Liu, M. Weimann, and M. A. Suhm, Phys. Chem. Chem. Phys. **6**, 3315–3319 (2004).
[39]P. Zielke and M. A. Suhm, Phys. Chem. Chem. Phys. **8**, 2826–2830 (2006).
[40]R. H. Hunt, W. N. Shelton, F. A. Flaherty, and W. B. Cook, J. Mol. Spectrosc. **192**, 277–293 (1998).
[41]B. Fehrensen, D. Luckhaus, M. Quack, M. Willeke, and T. R. Rizzo, J. Chem. Phys. **119**, 5534–5544 (2003).
[42]G. Moruzzi, M. Winnewisser, B. P. Winnewisser, I. Mukhopadhyay, and F. Strumia, *Microwave, Infrared, and Laser Transitions of Methanol Atlas of Assigned Lines from 0 to 1258 cm^{-1}* (CRC Press, Inc., 1995).
[43]D. G. Burkhard and D. M. Dennison, J. Mol. Spectrosc. **3**, 299 (1959).
[44]M. Hepp, I. Pak, K. Yamada, E. Herbst, and G. Winnewisser, J. Mol. Spectrosc. **166**, 66–78 (1994).
[45]F. Kollipost, R. Wugt Larsen, A. V. Domanskaya, M. Noerenberg, and M. A. Suhm, J. Chem. Phys. **136**, 151101 (2012).
[46]Y.-P. Lee, Y.-J. Wu, R. M. Lees, L.-H. Xu, and J. T. Hougen, Science **311**, 365–368 (2006).
[47]J. P. Perchard, Chem. Phys. **332**, 86–94 (2007).
[48]J. P. Perchard, F. Romain, and Y. Bouteiller, Chem. Phys. **343**, 35–46 (2008).
[49]J. Ceponkus, A. Engdahl, P. Uvdal, and B. Nelander, Chem. Phys. Lett. **581**, 1–9 (2013).
[50]M. Quack and M. A. Suhm, Theor. Chim. Acta **93**, 61–65 (1996).
[51]I. Mukhopadhyay, Spectrochim. Acta **54**, 1325 (1998).
[52]A. Engdahl and B. Nelander, J. Chem. Phys. **86**, 1819 (1987).
[53]S. Grimme, J. Antony, S. Ehrlich, and H. Krieg, J. Chem. Phys. **132**, 154104 (2010).
[54]S. Grimme, S. Ehrlich, and L. Goerigk, J. Comput. Chem. **32**, 1456–1465 (2011).

A.3 The influence of large-amplitude librational motion on the hydrogen bond energy for alcohol-water complexes

Reprinted with permission from
The Influence of large-amplitude librational motion on the hydrogen bond energy for alcohol-water Complexes
J. Andersen, J. Heimdal, and R. Wugt Larsen,
Physical Chemistry Chemical Physics 17, 23761–23769 (2015)

PCCP

PAPER

Cite this: *Phys. Chem. Chem. Phys.*, 2015, **17**, 23761

The influence of large-amplitude librational motion on the hydrogen bond energy for alcohol–water complexes†

J. Andersen,[a] J. Heimdal[b] and R. Wugt Larsen*[a]

Received 23rd July 2015,
Accepted 17th August 2015

DOI: 10.1039/c5cp04321b

www.rsc.org/pccp

The far-infrared absorption spectra have been recorded for hydrogen-bonded complexes of water with methanol and *t*-butanol embedded in cryogenic neon matrices at 2.8 K. The partial isotopic substitution of individual subunits enabled by a dual inlet deposition procedure provides for the first time unambiguous assignments of the intermolecular high-frequency out-of-plane and low-frequency in-plane donor OH librational modes for mixed alcohol–water complexes. The vibrational assignments confirm directly that water acts as the hydrogen bond donor in the most stable mixed complexes and the tertiary alcohol is a superior hydrogen bond acceptor. The class of large-amplitude donor OH librational motion is shown to account for up to 5.1 kJ mol^{-1} of the destabilizing change of vibrational zero-point energy upon intermolecular OH···O hydrogen bond formation. The experimental findings are supported by complementary electronic structure calculations at the CCSD(T)-F12/aug-cc-pVTZ level of theory.

1. Introduction

Intermolecular hydrogen bonding between alcohols and water is of general interest ranging from various fundamental microscopic aspects related to conformational isomerism, hydrogen bond donor/acceptor preferences and the large-amplitude and highly anharmonic hydrogen bond vibrational motion introduced upon complexation to more applied macroscopic aspects related to hydrophobic effects and the optimization of experimental separation technologies of bulk alcohol/water mixtures and bio-fuels. It has previously been demonstrated that the intermolecular interactions responsible for thermodynamic anomalies[1] such as negative heats of mixing[2,3] and negative excess volumes[4,5] of bulk alcohol/water mixtures can be addressed qualitatively by combined infrared and Raman spectroscopic investigations of hydrogen-bonded jet-cooled alcohol–water clusters.[6,7] These thermodynamic anomalies depend strongly on the relative hydrogen bond energies of mixed alcohol–water complexes *versus* the pure complexes of alcohols and water.[8]

The amount of experimental spectroscopic data reported in the literature for isolated mixed binary alcohol–water complexes is surprisingly limited. One explanation for this sparsity of spectroscopic data might be the absence of any suitable UV chromophores in these systems which would otherwise enable sensitive electronic double-resonance spectroscopy investigations.[9] A series of pure rotational spectroscopic studies of adiabatically cooled mixed complexes of water with methanol[10] and *t*-butanol[11] has unraveled the structure of the conformers where the water subunit acts as the hydrogen bond donor. The other conformations with the alcohol subunit acting as the hydrogen bond donor were not detected under the cold conditions of the seeded molecular beam studies. In terms of vibrational spectroscopy, a sensitive probe for intermolecular hydrogen bond formation is the OH-stretching manifold of the subunits[12] and recent combined infrared and Raman investigations have monitored bathochromic OH-stretching spectral shifts for vacuum-isolated mixed complexes of water with both methanol and ethanol.[6,7] The observed vibrational spectral signatures support the hydrogen bond donor/acceptor relationships found in the cited microwave studies. The ethanol–water complex furthermore represents one of the simplest mixed hydrogen-bonded molecular systems where internal conformational degrees of freedom influence the hydrogen bond formation. In the mixed ethanol–water complex, the ethanol subunit prefers the *gauche* conformation as the hydrogen bond acceptor although the *trans* conformation is the most stable for an isolated ethanol molecule. This is considered as one of the most elementary cases of adaptive aggregation, where a flexible molecule is forced into a less stable conformation upon non-covalent binding to a hydrogen bond donor molecule to optimize the mutual interaction energy.[6,7] A few other experimental studies of this vibrational OH-stretching manifold have been

[a] *Department of Chemistry, Technical University of Denmark, Kemitorvet 206, 2800 Kgs. Lyngby, Denmark. E-mail: rewl@kemi.dtu.dk*
[b] *MAX-IV Laboratory, Lund University, P. O. Box 118, 22100 Lund, Sweden*

† Electronic supplementary information (ESI) available: The calculated absolute electronic energies employing the B3LYP, B3LYP-D3, MP2, CCSD(T) and CCSD(T)-F12 methodologies with the aug-cc-pVTZ and aug-cc-pVQZ basis sets and the calculated harmonic vibrational zero-point energy corrections employing the MP2/aug-cc-pVTZ method. See DOI: 10.1039/c5cp04321b

reported for mixed water complexes with methanol and ethanol embedded in cryogenic matrices of nitrogen and argon.[13,14] In the most perturbing matrix environment of nitrogen a reversed donor/acceptor relationship has been observed although severe site effects blurred the OH-stretching signatures of the alcohol donor subunits. This opposite donor/acceptor relationship observed in cryogenic nitrogen matrices has been explained by weak cooperative attractive interactions between the OH groups and the N_2 host molecules.[15] In the mixed complexes where the alcohol molecule acts as the hydrogen bond donor both dangling OH groups of the water acceptor subunit might interact with N_2 host molecules and thereby increasing the acceptor character of the O nuclei on the water molecule. This effect could strengthen the intermolecular hydrogen bond to the alcohol molecule and overcome the energy barrier between the water–alcohol conformers.[15]

In the present work it is demonstrated how the strength, directionality and anharmonicity of these important intermolecular hydrogen bonding motifs can be probed directly *via* large-amplitude intermolecular OH librational modes of mixed isotopically substituted alcohol–water complexes. These direct spectroscopic observables detected in the challenging far-infrared region of the electromagnetic spectrum have been shown to enable an accurate characterization of the intermolecular potential energy landscape between identical hydrogen bond partners.[16–19] In a recent combined far-infrared supersonic jet and neon matrix isolation study of methanol dimer, the large-amplitude intermolecular donor OH librational transition was unambiguously assigned for the first time.[18] This study demonstrated that this large-amplitude OH librational motion is basically unhindered in an inert neon matrix environment at 2.8 K and allowed for a rigorous benchmarking of theory. The present work shows the potential to detect these important spectroscopic observables in the far-infrared region for mixed alcohol–water complexes embedded in neon by a dual inlet deposition procedure. The mixed water complexes with the simplest primary alcohol, methanol, and the simplest tertiary alcohol, *t*-butanol, are the systems of choice since conformational isomerism of the *t*-butanol monomer is absent.

2. Experimental

Several millimeter thick matrices of pre-cooled neon (L'Air Liquide, 99.999%) doped with ''freeze–pump–thaw'' purified CH_3OH (Sigma Aldrich, 99.9%), $C(CH_3)_3OH$ (Sigma Aldrich, 99.9%) and H_2O (Milli-Q) samples and isotopically substituted CH_3OH-d1 (Sigma Aldrich, 99.0% D), CH_3OH-d4 (Sigma Aldrich, 99.0% D), $C(CH_3)_3OH$-d1 (Sigma Aldrich, 99.0% D), $C(CH_3)_3OH$-d10 (Sigma Aldrich, 99.0% D) and D_2O (Sigma Aldrich, 99.5% D) samples with mixing ratios of $\simeq$0.25 to 2.5 permille have been deposited with a flow rate of 0.02 mole on a gold-plated oxygen-free high thermal conductivity (OFHC) copper mirror at 3.6 K inside an immersion helium cryostat (IHC-3) modified for matrix isolation spectroscopy.[19,20] The pre-cooling of neon significantly reduces the heat load on the copper mirror and enables a total deposition time of less than 1 hour per experiment. A dual inlet deposition procedure enabled studies of individual deuterium-enriched samples without the risk of H/D exchange before deposition. The combination of resistive heaters and feedback electronics has been employed to maintain a stable mirror temperature at 2.8 $\pm$ 0.1 K before and after the depositions. The cold head was equipped with interchangeable CsI and polymethylpentene (TPX) windows and the combined mid- and far-infrared single-beam sample spectra have been collected by a Bruker IFS 120 FTIR spectrometer employing tungsten and globar lamps as radiation sources. Liquid nitrogen cooled HgCdTe and InSb detectors combined with Ge/KBr and CaF_2 beam splitters, respectively, were employed for the spectral region above 600 cm^{-1}. A Si-bolometer operating at 4.2 K combined with a 6 μm multi-layer Mylar beam splitter was employed for the 30–650 cm^{-1} spectral region. In most cases the doped neon matrices have been annealed up to 9 K and relaxed back to 3 K for the study of temperature effects. Single-beam background spectra were subsequently collected of the evacuated warm cryostat. A spectral resolution ranging from 0.1 to 1.0 cm^{-1} was selected depending on observed band widths.

3. Vibrational assignments for the mixed methanol/water complex

Fig. 1 shows a series of far-infrared absorption spectra (200–600 cm^{-1}) collected for several millimeter thick cryogenic neon matrices doped with pure water (H_2O : Ne) = (1 : 2000), pure methanol with traces of H_2O (CH_3OH : H_2O : Ne) = (3 : 1 : 13 000) and different isotopic water/methanol mixtures (CH_3OH : H_2O : Ne) = (3 : 2 : 6000) at 2.8 K. In previous studies of methanol embedded in solid matrices of *para*-H_2[21] and neon,[18,22,23] the torsional-vibrational splittings into *A* and *E* sub-levels by torsional tunneling have been shown to persist although the standard *A*–*A* and *E*–*E* selection rules do not apply in the inert matrix environments. The torsional fundamental of methanol embedded in cryogenic neon matrices thus gives rise to four different sub-bands in the far-infrared region; the pair of ''cold'' *A*–*E* and *A*–*A* transitions observed at 212 and 269 cm^{-1} and the pair of ''hot'' *E*–*E* and *E*–*A* transitions observed at 206 and 262 cm^{-1}.[18,22] The sub-bands observed at 447 and 507 cm^{-1} have previously been assigned to components of the first torsional overtone transition for methanol monomer.[22] In terms of pure methanol complexes, a combined far-infrared jet and neon matrix isolation study has recently revealed the donor OH librational transition at 557.7 cm^{-1} as well as the acceptor OH torsional transition at 286 cm^{-1} of the methanol dimer for the first time.[18] In addition, the far-infrared absorption from pure complexes of water embedded in neon matrices have been explored previously.[19,24–27] In the spectral region above 200 cm^{-1} the strong intermolecular high-frequency out-of-plane and low-frequency in-plane donor OH librational bands of the water dimer embedded in neon matrices have previously been assigned at 522.4 cm^{-1} and 309.1 cm^{-1}, respectively.[24]

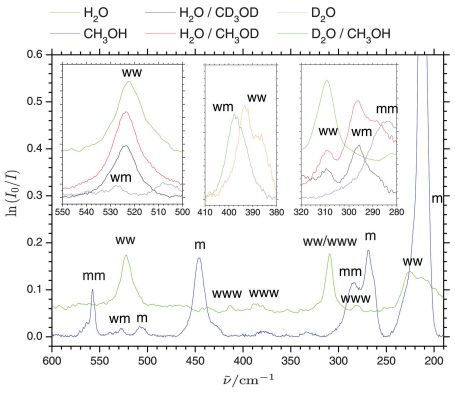

Fig. 1 The observed far-infrared absorption spectra of pure water (denoted w), pure methanol (denoted m) and different isotopic methanol/water mixtures embedded in neon matrices at 2.8 K with proposed vibrational assignments. The inserts show close-ups of the spectral regions belonging to the out-of-plane OH (left), out-of-plane OD (center) and in-plane OH (right) donor librational modes of the hydrogen-bonded complexes (ww: water dimer, wm: 1 : 1 methanol–water complex, mm: methanol dimer, *etc.*).

The broad band observed around 226 cm^{-1} has previously been attributed dimeric water absorption although the nature of this far-infrared transition is not yet understood in detail as the four other intermolecular fundamental modes have all been assigned at lower frequencies.[24] The in-plane donor OH librational band is slightly overlapped with the strong *c*-axis librational mode of cyclic water trimer previously assigned at 310.8 cm^{-1}. Five combination bands have previously been assigned the cyclic water trimer where the strongest are observed at 280.0, 386.8 and 414.1 cm^{-1}.[25]

The assignment of the band observed at 527.3 cm^{-1} (Fig. 1) was at first not possible even by dedicated methanol concentration series. In some annealing experiments at 9 K the intensity of this band increased significantly without any subsequent relaxation upon repeated cooling to 3 K. This observation pointed at an irreversible build-up of molecular complexes driven by diffusion in the soft matrix. The combined findings suggested the assignment to a mixed methanol–water complex as minor traces of water are always present in various amounts in the inlet system. The severe band overlap with the out-of-plane donor OH librational modes of water dimer assigned at 522.4 cm^{-1} suggested that water takes the role as the hydrogen bond donor in the most stable mixed complex and possesses almost an identical donor OH librational motion as for the lass stable water dimer. An unambiguous identification of the hydrogen bond donor/acceptor relationship in the cryogenic neon environment could be settled by partial isotopic H/D substitution of the individual subunits enabled by the dual inlet deposition procedure. The three inserts of Fig. 1 show the spectral regions belonging to the donor OH (OD) librational modes. The H/D substitution on the water subunit introduces a significant red-shift from 527.3 cm^{-1} to 397.6 cm^{-1} confirming that water acts as hydrogen bond donor. The observed band origin ratio of 1.33 is close to the theoretical value of $\sqrt{2}$ expected for a genuine harmonic hydrogen motion and supports an assignment to the out-of-plane donor OD librational mode for the complex of D_2O with methanol. The latter band origin is furthermore slightly larger than the corresponding out-of-plane donor OD librational band origin of $(D_2O)_2$ reported previously as expected.[19] The H/D substitution on the OH group of methanol introduces only a minor red-shift of 4 cm^{-1} for the out-of-plane donor OH librational mode confirming a hydrogen bond acceptor role of the methanol subunit. In terms of the in-plane donor OH librational bands, the isotopic H/D substitution on the OH group of methanol induces a more pronounced red-shift of around 13 cm^{-1}. A closer look at the normal mode pictures reveals that whereas the out-of-plane OH librational mode exhibits an almost localized genuine motion of the bound hydrogen atom not involving the dangling OH group on the water molecule, the in-plane OH librational mode can be pictured as a hindered overall *c*-axis rotation of the water subunit. The latter large-amplitude in-plane OH librational motion of the whole water molecule thus has a more significant effect on the center of mass and is more affected by isotopic substitution of the methanol subunit as summarized in Table 1.

4. Vibrational assignments for the mixed *t*-butanol/water complex

Fig. 2 shows far-infrared absorption spectra (300–600 cm^{-1}) collected for several millimeter thick cryogenic neon matrices doped with pure water (H_2O : Ne) = (1 : 2000), *t*-butanol with small traces of H_2O ($C(CH_3)_3OH$: H_2O : Ne) = (4 : 1 : 4000) and

Table 1 The observed high-frequency out-of-plane and low-frequency in-plane donor OH (OD) librational band origins (cm^{-1}) for isotopic water complexes and isotopic mixed complexes of water with methanol/*t*-butanol embedded in neon matrices at 2.8 K

Donor–acceptor	$\nu_{lib,out\text{-}of\text{-}plane}$	$\nu_{lib,in\text{-}plane}$	Donor–acceptor	$\nu_{lib,out\text{-}of\text{-}plane}$	$\nu_{lib,in\text{-}plane}$
H_2O–H_2O	522.4[a]	309.1[a]	D_2O–D_2O	393.2[a]	233.5[a]
H_2O–CH_3OH	527.3	[b]	D_2O–CH_3OH	397.6	[c]
H_2O–CH_3OD	523.7	296.2	D_2O–CH_3OD	395.0	[c]
H_2O–CD_3OD	523.9	295.9	D_2O–CD_3OD	[c]	[c]
H_2O–$C(CH_3)_3OH$	556.6	318.2	D_2O–$C(CH_3)_3OH$	427.7	[d]
H_2O–$C(CH_3)_3OD$	548.9	298.1	D_2O–$C(CH_3)_3OD$	[e]	242.4
H_2O–$C(CD_3)_3OD$	549.0	[f]			

[a] Ceponkus *et al.*[19] [b] Overlapped with $(H_2O)_2$. [c] Overlapped with $(D_2O)_2$. [d] Overlapped with $C(CH_3)_3OH$. [e] Overlapped with $C(CH_3)_3OD$. [f] Overlapped with $C(CD_3)_3OD$.

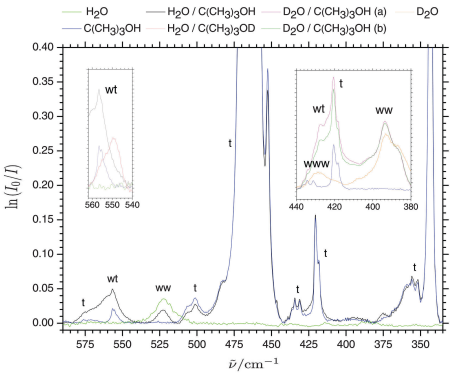

Fig. 2 The observed far-infrared absorption spectra of water (denoted w), *t*-butyl alcohol (denoted *t*) with small traces of water and different isotopic *t*-butanol/water mixtures embedded in neon matrices at 2.8 K with proposed vibrational assignments. The inserts show close-ups of the spectral regions belonging to the out-of-plane OH (left) and OD (right) donor librational modes of the hydrogen-bonded complexes (ww: water dimer, www: water trimer, wt: 1 : 1 *t*-butanol–water complex, *etc.*). The latter insert shows the far-infrared spectra recorded for *t*-butanol/D_2O doped matrices before (b) and after (a) annealing to 9 K.

different isotopic *t*-butanol/water mixtures ($C(CH_3)_3OH : H_2O : Ne$) = (5 : 2 : 3000) at 2.8 K. The spectral region below 300 cm^{-1} (not shown) is dominated by complex torsional–vibrational coupling components of the monomer OH and methyl torsional motion which shall be considered in details elsewhere. In addition, the monomer of regular *t*-butanol in contrast to methanol exhibits several intramolecular skeletal fundamental transitions in the far-infrared spectral region.[28] In the cryogenic neon matrices doped solely with *t*-butanol the two overlapping CCC bending fundamental bands are assigned at 343.4 cm^{-1} and 356.0 cm^{-1}, the symmetric CCO bending fundamental is assigned at 420.2 cm^{-1} and the two stronger asymmetric CCO bending fundamentals are assigned between 450 and 475 cm^{-1}. A higher ($Ne : C(CH_3)_3OH$) mixing ratio relative to ($Ne : CH_3OH$) was employed to study the mixed *t*-butanol–water complexes but any formation of mixed *t*-butanol–water trimers could be excluded by the inspection of the corresponding mid-infrared absorption spectra recorded for all neon matrices.

For the neon matrices doped simultaneously with small concentrations of water and *t*-butanol, two new bands appear in close vicinity to the donor OH librational modes of water dimer. This observation indicates that the water subunit also acts as the hydrogen bond donor in the mixed complex with *t*-butanol and supports the findings of the previous microwave molecular beam study where only this conformer was assigned.[11] A band observed at 556.6 cm^{-1} is shifted by almost 35 cm^{-1} relative to the water dimer transition and is assigned to the out-of-plane donor OH librational mode of the mixed complex. A lower band appears as a shoulder on the corresponding water dimer transition around 318.2 cm^{-1} and is assigned to the in-plane OH librational band of the mixed complex. The unambiguous assignments could again be supported by partial isotopic H/D substitution of the individual subunits enabled by the dual inlet deposition procedure. Both the isotopic H/D substitution on the alcohol group alone and the full H/D substitution on *t*-butanol introduce a minor red-shift of around 7.5 cm^{-1} for the 556.6 cm^{-1} band indicating the hydrogen bond acceptor role of *t*-butanol. Unfortunately, the high-frequency donor OD librational band for the complex of D_2O with regular *t*-butanol accordingly is expected in the region of the symmetric CCO bending fundamental band around 420.2 cm^{-1} assuming the band origin ratio of 1.33 observed for the methanol–water complex. In this spectral region the high-frequency out-of-plane OD libration of $(D_2O)_2$ is also located at 397.6 cm^{-1} [19] and the shear librational band of $(D_2O)_3$ is located around 428 cm^{-1}.[25] However, the far-infrared spectrum of *t*-butanol/D_2O doped matrices of neon nevertheless reveals a new distinct spectral feature at 427.7 cm^{-1} on the high-frequency shoulder of the symmetric CCO bending fundamental band of *t*-butanol (see trace b) of Fig. 2. The intensity of this spectral feature at 427.7 cm^{-1} clearly increases upon annealing of the matrix to 9 K without any subsequent relaxation upon repeated cooling to 3 K as witnessed by trace a of Fig. 2. The annealing is expected to enable the diffusion of the D_2O molecules in the neon matrix and trigger the formation of mixed complexes of D_2O with *t*-butanol more than the formation of $(D_2O)_2$ as the bulky *t*-butanol molecules are more likely collision partners in the matrices. The significant intensity increase of the 427.7 cm^{-1} band relative to the $(D_2O)_2$ band at 397.6 cm^{-1} upon annealing to 9 K thus supports an assignment to the high-frequency donor OD librational band for the mixed complex of D_2O with *t*-butanol. The observed band origin ratio of 1.3 for the proposed OH/OD librational bands is furthermore rather close to the theoretical value of $\sqrt{2}$ expected for a genuine harmonic hydrogen motion. The two inserts of Fig. 2 show the spectral regions belonging to the donor OH (OD) librational modes of the mixed isotopic complexes of water with *t*-butanol. The proposed assignment of the low-frequency in-plane OH librational mode is furthermore supported by an isotopic red-shift of 20.1 cm^{-1} upon *O*-deuteration of *t*-butanol. In addition, a tentatively assignment of the in-plane low-frequency OD librational transition at is 242.4 cm^{-1} is proposed for the mixed complex of D_2O with *t*-butanol-d1 as summarized in Table 1. Whereas the high-frequency out-of-plane donor OH/OD librational modes are highly localized, the low-frequency in-plane OH/OD librational motion might couple slightly to the intramolecular skeletal motion of the *t*-butanol subunits.

The observed donor OH librational spectral signatures point at a stronger hydrogen bond interaction between water and *t*-butanol than between water and methanol. An inductive effect of the bulky alkyl groups of *t*-butanol improves the acceptor quality of the oxygen atom in the tertiary alcohol group. This inductive effect stiffens the intermolecular hydrogen bond and the more hindered internal rotational motion raises the band origins for the donor OH librational modes when the hydrogen bond acceptor changes from water to methanol and finally *t*-butanol. A far-infrared jet study has previously demonstrated that alkylation strengthens and stiffens the intermolecular

hydrogen bonding between alcohol molecules.[17] This was also reflected in increased average OH librational band origins for the clusters of *t*-butanol relative to methanol although these observations could not be captured by density functional methods lacking electron correlation available for such bulky alcohol clusters containing 30 to 60 atoms.[17]

5. Exploratory quantum chemical calculations

The smaller size of the water complexes with methanol and even *t*-butanol allows for rigorous *ab initio* computations including high degrees of electron-correlation of the electronic dissociation energy D_e which may be compared to results from both canonical and dispersion-corrected density functional theory. The quantum chemical software packages Gaussian09 (Rev. D.01)[29] and Turbomole (ver. 6.6)[30,31] have been employed for the present *ab initio* molecular orbital and DFT calculations. The geometries of the monomers and the mixed hydrogen-bonded complexes were all optimized and the resulting electronic energies calculated employing the canonical B3LYP level,[32] the dispersion-corrected B3LYP-D3 approach[33] and the second-order Möller–Plesset MP2 methodology[34,35] coupled with Dunning's augmented correlation-consistent polarized triple-zeta (aug-cc-pVTZ) and quadruple-zeta (aug-cc-pVQZ) basis sets.[36] The root-mean-square force criterion has been set to 10^{-6} (atomic units) for all the geometry optimizations. The electronic energies for these optimized geometries were subsequently furthermore calculated employing both the coupled-cluster approach with single and double excitations and perturbative treatment of triple excitations CCSD(T)[37] and the explicitly-correlated CCSD(T)-F12 methodology[38] to optimize the level of electron correlation combined with the same basis sets. In the electronic energy calculations for the mixed alcohol–water complexes, the effects of the basis set superposition errors[39] have been accounted for by the counterpoise method.[40] The harmonic frequencies and overall ZPE contributions of the monomers and hydrogen-bonded complexes have been calculated in the doubly harmonic approximation whereas the anharmonic frequencies have been calculated employing the vibrational second-order perturbation theory (VPT2) approach[41] as implemented in Gaussian09 (Rev. D.01).[29]

6. Discussion

Table 2 shows the electronic dissociation energy D_e of the most stable methanol–water conformer and the energy difference ΔE_e between the two different conformers predicted from combined quantum chemical methodologies employed for geometry optimization and subsequent single-point electronic energy calculations. The potential energy minimum structures for the different conformers of the alcohol–water complexes are illustrated in Fig. 3. The benchmark level of theory available for both alcohol–water complexes employs the MP2/aug-cc-pVTZ[34–36] level for geometry optimization and the CCSD(T)-F12/aug-cc-pVTZ level[36,38] for the electronic dissociation energy D_e. The benchmark D_e-value of 24.62 kJ mol^{-1} for the most stable methanol–water conformer and the energy difference of 2.65 kJ mol^{-1} between the two conformers agree with the highest level of methodology employing a combined MP2/aug-cc-pVQZ/CCSD(T)-F12/aug-cc-pVQZ approach within 0.42 and 0.03 kJ mol^{-1}, respectively. The benchmark approach is thus expected to provide reliable dissociation energies for the two different conformers of the more bulky water complexes with *t*-butanol as listed in Table 3.

The benchmark CCSD(T)-F12/aug-cc-pVTZ predictions confirm that *t*-butyl alcohol is a superior hydrogen bond acceptor than methanol. The electronic dissociation energy D_e of the most stable mixed water complex with *t*-butanol is predicted to be 4.67 kJ mol^{-1} larger than for the corresponding mixed complex with methanol. The predictions listed in Table 2 show that the canonical B3LYP functional[32] underestimate the binding energies for the mixed complexes of water with methanol by more than 15% whereas the B3LYP-D3 approach including Grimme and

Table 2 The electronic dissociation energy D_e for the most stable hydrogen-bonded complex of water with methanol and the difference of electronic dissociation energy between the two different conformers ΔE_e predicted from several combined quantum chemical methodologies for geometry and electronic energy calculations

Geometry optimization[a]	Electronic energy	D_e/kJ mol^{-1}	ΔE_e/kJ mol^{-1}
B3LYP/aug-cc-pVTZ	B3LYP/aug-cc-pVTZ	20.58	2.18
B3LYP-CP/aug-cc-pVTZb	B3LYP/aug-cc-pVTZ	20.29	2.16
B3LYP-CP/aug-cc-pVTZb	CCSD(T)/aug-cc-pVTZ	24.64	2.53
B3LYP-D3/aug-cc-pVTZ	B3LYP-D3/aug-cc-pVTZ	25.18	3.03
B3LYP-D3-CP/aug-cc-pVTZ[b]	B3LYP-D3/aug-cc-pVTZ	24.88	3.02
B3LYP-D3-CP/aug-cc-pVTZ[b]	CCSD(T)/aug-cc-pVTZ	24.92	2.74
MP2/aug-cc-pVTZ	MP2/aug-cc-pVTZ	25.06	3.10
MP2-CP/aug-cc-pVTZ[b]	MP2/aug-cc-pVTZ	22.71	2.88
MP2-CP/aug-cc-pVTZ[b]	CCSD(T)/aug-cc-pVTZ	25.01	2.82
MP2-CP/aug-cc-pVTZ[b]	CCSD(T)-F12/aug-cc-pVTZ	24.62	2.65
MP2/aug-cc-pVQZ	MP2/aug-cc-pVQZ	24.54	3.06
MP2-CP/aug-cc-pVQZ[b]	MP2/aug-cc-pVQZ	23.36	2.91
MP2-CP/aug-cc-pVQZ[b]	CCSD(T)/aug-cc-pVTZ	24.74	2.82
MP2-CP/aug-cc-pVQZ[b]	CCSD(T)-F12/aug-cc-pVTZ	24.66	2.65
MP2-CP/aug-cc-pVQZ[b]	CCSD(T)-F12/aug-cc-pVQZ	24.20	2.68

[a] RMS force criterion set to 10^{-6} (atomic units) for all geometry optimizations. [b] CP = counterpoise correction applied.

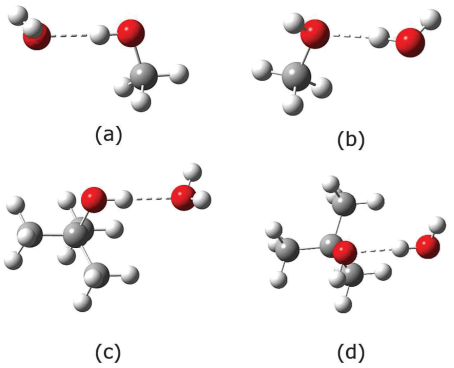

Fig. 3 Illustration of the predicted potential energy minima structures of the different alcohol–water conformers. The most stable conformers (b and d) have water as the hydrogen bond donor whereas the less stable conformers have the alcohol subunit as hydrogen bond donor (a and c).

co-worker's dispersion corrections[33] reproduce the predictions by the highest level of methodology within 0.25 kJ mol^{-1}. However, the dissociation energies for the more electron-rich mixed complexes of water with *t*-butanol are strongly underestimated by 7.4 kJ mol^{-1} (*ca.* 25%) by the B3LYP functional and slightly overestimated 1.3 kJ mol^{-1} (*ca.* 5%) by the dispersion-corrected B3LYP-D3 predictions (Table 3). In the context of relative hydrogen bond donor/acceptor capabilities we note that the benchmark theoretical CCSD(T)-F12 predictions (in strong contrast to the canonical B3LYP predictions) indicate that *t*-butanol has a slightly higher interaction energy of 0.8 kJ mol^{-1} with water than methanol when the alcohols act as the hydrogen bond donor. This increased interaction energy may be ascribed to the increased dispersion forces between the water molecule and the electron-rich *t*-butyl alcohol molecule. The effect of the zero-point energy (ZPE) contributions and in particular the influence of the donor OH librational motion on the electronic dissociation energy must be considered before reaching further conclusions.

The change of vibrational ZPE upon intermolecular hydrogen bond formation is notoriously difficult to predict computationally, in particular for the observed large-amplitude and highly anharmonic intermolecular hydrogen bond librational motion. In a recent combined jet and neon matrix isolation far-infrared study of methanol dimer, the donor OH librational band was observed and assigned for the first time at 560 cm^{-1}.[18] This study predicted an overall sum of anharmonic contributions to the OH donor librational fundamental transition of 100 cm^{-1} by vibrational second-order perturbation theory.[41] In combination with a benchmark harmonic band origin of 660 cm^{-1} predicted at the LCCSD(T)-F12 level, the anharmonic predicted band origin of 560 cm^{-1} was in excellent agreement with the experimental findings. A similar detailed analysis of the mixed water complexes with methanol and *t*-butanol is beyond the scope of the present predominantly experimental work. However, standard vibrational frequency calculations at the MP2/aug-cc-pVTZ level in the doubly harmonic approximation provide harmonic band origins of 630, 647 and 669 cm^{-1} for the high-frequency out-of-plane and 360, 375 and 388 cm^{-1} for the low-frequency in-plane donor OH librational transitions for the pure water complex and the most stable mixed complexes of water with methanol and *t*-butanol, respectively. The ordering of these harmonic predictions is in qualitative agreement with the present experimental findings and the anharmonicity contributions seem to be in the order of 15–20% as found for the recent methanol dimer study.[18] An anharmonic VPT2 analysis[41] for the mixed complex of water with methanol at the MP2/aug-cc-pVTZ level predicts an overall anharmonicity of 18% for the high-frequency donor OH librational transition. This VPT2 calculation is not feasible for the multi-dimensional mixed complex of water and *t*-butanol. A similar analysis of the low-frequency in-plane donor OH librational transitions and the other intermolecular large-amplitude vibrational transitions for these non-rigid hydrogen-bonded complexes would be to stretch the reliability of the VPT2 approach. Table 4 thus provides the change of harmonic vibrational ZPE for the isotopic mixed complexes of water with methanol and *t*-butanol predicted at the common feasible MP2/aug-cc-pVTZ level.

The incorporation of the computed vibrational ZPE contributions has an enormous impact as evidenced by the resulting absolute

Table 3 The electronic dissociation energy D_e of the most stable hydrogen-bonded complex of water with *t*-butanol and the difference of electronic dissociation energy between the two different conformers ΔE_e predicted from several combined quantum chemical methodologies for geometry and electronic energy calculations

Geometry optimization[a]	Electronic energy	D_e/kJ mol^{-1}	ΔE_e/kJ mol^{-1}
B3LYP/aug-cc-pVTZ	B3LYP/aug-cc-pVTZ	21.93	5.57
B3LYP-CP/aug-cc-pVTZ[b]	B3LYP/aug-cc-pVTZ	21.54	5.52
B3LYP-CP/aug-cc-pVTZ[b]	CCSD(T)/aug-cc-pVTZ	28.80	5.95
B3LYP-D3/aug-cc-pVTZ	B3LYP-D3/aug-cc-pVTZ	30.59	8.41
B3LYP-D3-CP/aug-cc-pVTZ[b]	B3LYP-D3/aug-cc-pVTZ	30.15	8.34
B3LYP-D3-CP/aug-cc-pVTZ[b]	CCSD(T)/aug-cc-pVTZ	30.03	6.64
MP2/aug-cc-pVTZ	MP2/aug-cc-pVTZ	30.09	6.90
MP2-CP/aug-cc-pVTZ[b]	MP2/aug-cc-pVTZ	26.75	6.31
MP2-CP/aug-cc-pVTZ[b]	CCSD(T)/aug-cc-pVTZ	30.06	6.65
MP2-CP/aug-cc-pVTZ[b]	CCSD(T)-F12/aug-cc-pVTZ	29.29	6.52

[a] RMS force criterion set to 10^{-6} (atomic units) for all geometry optimizations. [b] CP = counterpoise correction applied.

Table 4 The electronic dissociation energy D_e (CCSD(T)-F12/aug-cc-pVTZ[a]), the total change of harmonic vibrational zero-point energy upon complexation ΔZPE_{tot}^{calc} (MP2/aug-cc-pVTZ) and the resulting absolute dissociation energy D_0 for mixed isotopic hydrogen-bonded donor–acceptor complexes together with the observed (anharmonic) contribution to the zero-point energy from the class of donor OH librational modes ΔZPE_{lib}^{exp} (all values in units of kJ mol^{-1})

	H_2O–CH_3OH	CH_3OH–H_2O	H_2O–CD_3OD	CD_3OD–H_2O	D_2O–CH_3OH	CH_3OH–D_2O
D_e	24.62[a]	21.98[a]	24.62[a]	21.98[a]	24.62[a]	21.98[a]
ΔZPE_{tot}^{calc}	7.80	6.59	7.52	5.90	6.25	5.85
ΔZPE_{lib}^{exp}	**5.0**		**4.9**		[**3.8**][b]	
D_0	16.82	15.39	17.10	16.08	18.37	16.13
	H_2O–$C(CH_3)_3OH$	$C(CH_3)_3OH$–H_2O	H_2O–$C(CD_3)_3OD$	$C(CD_3)_3OD$–H_2O	D_2O–$C(CH_3)_3OH$	$C(CH_3)_3OH$–D_2O
D_e	29.29[a]	22.77[a]	29.29[a]	22.77[a]	29.29[a]	22.77[a]
ΔZPE_{tot}^{calc}	8.40	6.34	8.06	5.74	6.77	5.57
ΔZPE_{lib}^{exp}	**5.2**		**5.1**		[**4.0**][b]	
D_0	20.89	16.43	21.23	17.04	22.52	17.20

[a] Electronic dissociation energies D_e calculated at the CCSD(T)-F12/aug-cc-pVTZ level based on optimized geometries at the MP2/aug-cc-pVTZ level. [b] Includes the observed band origin of the high-frequency donor OD librational mode and an anharmonically predicted band origin for the low-frequency donor OD librational mode.

ground-state dissociation energies D_0 of the mixed alcohol–water complexes listed in Table 4. The total vibrational ZPE account for between 5.6 and 8.4 kJ mol^{-1} for the mixed water complexes with *t*-butanol in the harmonic approximation depending on the isotopic variant and the hydrogen donor/acceptor roles. The sum of the experimental anharmonic ZPE contributions from the donor OH librational motion alone accounts for up to 5.2 kJ mol^{-1} or minimum 60% of the total anharmonic vibrational ZPE when water acts as hydrogen bond donor. This conformer has a significantly higher vibrational ZPE contribution owing to the two different donor OH librational modes. The conformer with the alcohol as hydrogen bond donor only has one single donor OH librational mode. The alcohol OH librational mode of this latter conformer is significantly blue-shifted relative to the free alcohol torsional mode but this blue-shift still introduces a smaller vibrational ZPE introduced upon intermolecular hydrogen bond formation. The benchmark energy difference prediction ΔE_e of 6.5 kJ mol^{-1} for the two conformers of the water complex with *t*-butanol is accordingly translated into a significantly smaller 4.2 to 5.3 kJ mol^{-1} difference between the resulting D_0-values depending on the isotopic variants when the ZPE contributions are incorporated. In terms of the more simple mixed complexes of water and methanol, the total harmonic vibrational ZPE account for between 5.9 and 7.8 kJ mol^{-1} for the conformers of the mixed water complexes with methanol depending on the isotopic variant. For these simpler systems the sum of the experimental anharmonic ZPE contributions from the donor OH librational motion alone accounts for up to 5.0 kJ mol^{-1} *i.e.* minimum 65% of the total anharmonic vibrational ZPE for the conformer where water acts as hydrogen bond donor. The present benchmark energy difference prediction ΔE_e of 2.65 kJ mol^{-1} between the methanol–water conformers also translates into a smaller 1.0 to 2.2 kJ mol^{-1} difference between the resulting D_0-values depending on the isotopic substitutions. A diffusion quantum Monte Carlo study has previously predicted a difference of these D_0-values between 0.3 to 1.3 kJ mol^{-1} for the regular isotopic methanol–water conformers depending on the exact theoretical treatment of the large-amplitude intermolecular vibrational motion.[42] H/D isotopic substitutions on the methanol subunit further translated the resulting difference between D_0-values into the 0.04 to 1.2 kJ mol^{-1} interval.

The effect of the large-amplitude intermolecular donor OH librational motion on the absolute intermolecular hydrogen bond energy D_0 for mixed alcohol–water complexes demonstrated by the present experimental findings has been explored previously for the pure complexes of water.[19,43] These far-infrared studies have shown that D-bonded water complexes are more stable than the H-bonded counterparts due to the difference in the total vibrational ZPEs. In particular, the distinct observation and vibrational assignments for the deuterium-bonded configuration of the mixed isotopic $(HDO)_2$ complex embedded at low temperatures have verified the strong preference for intermolecular deuterium bonds experimentally. Of the twelve possible H/D isotopologues of the water dimer only six of these have been detected in observable amounts in cryogenic neon matrices doped with $H_2O/HDO/D_2O$ mixtures.[19] The major explanation for these experimental findings could be found in the significant isotopic spectral red-shift of 129 m^{-1} for the high-frequency out-of-plane donor OH librational mode of the pure water complex upon H/D substitution. This mode alone thus provide a stabilizing decrease of the vibrational ZPE upon complex formation by *ca.* 0.8 kJ mol^{-1} for the D-bonded complexes.

7. Conclusions

To conclude is that the large-amplitude donor OH librational modes of partial isotopically substituted mixed complexes of water with aliphatic alcohols in the challenging far-infrared region have now been observed and assigned enabled by a dual inlet matrix deposition approach and supported by quantum chemical calculations. The far-infrared spectroscopic findings have demonstrated that water acts as the hydrogen bond donor upon complexation with aliphatic alcohols as methanol and *t*-butanol and the sum of the contributions from the class of donor OH librational motion alone has been quantified to be

5.0–5.2 kJ mol^{-1}. It's nature as a localized genuine motion of the bound hydrogen atom makes the high-frequency out-of-plane donor OH librational mode an excellent probe for the intermolecular hydrogen bond strength in a similar fashion as the often discussed Badger–Bauer relationship associated with the bathochromic shift of the hydrogen-bonded intramolecular OH stretching band origin.[44] A stronger intermolecular hydrogen bond results in a more hindered internal rotational motion and the increase of the band origin for this high-frequency hydrogen bond donor vibration. In the mixed complexes of water with aliphatic alcohols the donor OH librational spectral signatures thus act as a measure of the hydrogen bond acceptor strength of the alcohol molecule. The electron donating inductive effect of the alkyl groups of *t*-butanol transforms the oxygen atom into a significant better hydrogen bond acceptor than the oxygen atom on methanol which can be qualitatively read from the relative band origins of the donor OH librational modes. The isotopic H/D substitution furthermore allows for a manipulation of the overall vibrational ZPE due to significant spectral red-shift of these donor OH librational modes upon H/D substitution. Quantum chemical calculations predict that the full H/D isotopic substitution of the alcohol subunit introduces the largest difference of the vibrational ZPE between the two different alcohol–water conformers. The present experimental findings show that even this full H/D substitution of the methanol and *t*-butanol subunits cannot overcome the differences of the electronic dissociation energy D_0 between the alcohol–water conformers. It will be interesting to see how future anharmonic theoretical methodologies will perform in the predictions of these intermolecular force fields spanned by water and the studied prototypical alcohols of increasing structural complexity.

Acknowledgements

The authors appreciate discussions with D. W. Mahler, J. Ceponkus, B. Nelander, A. Engdahl and K. L. Feilberg. The authors acknowledge Centre for Scientific and Technical Computing (LUNARC) at Lund University for the generous allocation of computational resources for the Turbomole calculations. RWL acknowledges financial support from the Danish Council for Independent Research's Sapere Aude Programme (Grant Ref.: 12-125248).

References

1 F. Franks and D. J. G. Ives, *Q. Rev., Chem. Soc.*, 1966, **20**, 1–44.
2 G. L. Bertrand, F. J. Millero, C.-H. Wu and L. G. Hepler, *J. Phys. Chem.*, 1966, **70**, 699–705.
3 J. A. Larkin, *J. Chem. Thermodyn.*, 1975, **7**, 137–148.
4 J.-P. E. Grolier, *Fluid Phase Equilib.*, 1981, **6**, 283–287.
5 G. C. Benson and O. Kiyohara, *J. Solution Chem.*, 1980, **9**, 791–804.
6 M. Nedić, T. N. Wassermann, Z. Xue, P. Zielke and M. A. Suhm, *Phys. Chem. Chem. Phys.*, 2008, **10**, 5953–5956.
7 M. Nedić, T. N. Wassermann, R. Wugt Larsen and M. A. Suhm, *Phys. Chem. Chem. Phys.*, 2011, **13**, 14050–14063.
8 G. Matisz, A.-M. Kelterer, W. M. F. Fabiand and S. Kunsagi-Mate, *Phys. Chem. Chem. Phys.*, 2015, **17**, 8467–8479.
9 C. J. Gruenloh, F. C. Hagemeister, J. R. Carney and T. S. Zwier, *J. Chem. Phys.*, 1999, **103**, 503–513.
10 P. A. Stockman, G. A. Blake, F. J. Lovas and R. D. Suenram, *J. Chem. Phys.*, 1997, **107**, 3782–3790.
11 L. Evangelisti and W. Caminati, *Phys. Chem. Chem. Phys.*, 2010, **12**, 14433–14441.
12 R. Wugt Larsen, P. Zielke and M. A. Suhm, *J. Chem. Phys.*, 2007, **126**, 194307.
13 N. Bakkas, Y. Bouteiller, A. Loutellier, J. P. Perchard and S. Racine, *J. Chem. Phys.*, 1993, **99**, 3335–3342.
14 N. Bakkas, Y. Bouteiller, A. Loutellier, J. P. Perchard and S. Racine, *Chem. Phys. Lett.*, 1995, **232**, 90–98.
15 S. Coussan, P. Roubin and J. P. Perchard, *J. Phys. Chem. A*, 2004, **108**, 7331–7338.
16 R. Wugt Larsen and M. A. Suhm, *J. Chem. Phys.*, 2006, **125**, 154314.
17 R. Wugt Larsen and M. A. Suhm, *Phys. Chem. Chem. Phys.*, 2010, **12**, 8152–8157.
18 F. Kollipost, J. Andersen, D. W. Mahler, J. Heimdal, M. Heger, M. A. Suhm and R. Wugt Larsen, *J. Chem. Phys.*, 2014, **141**, 174314.
19 J. Ceponkus, P. Uvdal and B. Nelander, *J. Chem. Phys.*, 2008, **129**(19), 194306.
20 J. Andersen, J. Heimdal, D. W. Mahler, B. Nelander and R. Wugt Larsen, *J. Chem. Phys.*, 2014, **140**, 091103.
21 Y.-P. Lee, Y.-J. Wu, R. M. Lees, L.-H. Xu and J. T. Hougen, *Science*, 2006, **311**, 365–368.
22 J. P. Perchard, *Chem. Phys.*, 2007, **332**, 86–94.
23 J. P. Perchard, F. Romain and Y. Bouteiller, *Chem. Phys.*, 2008, **343**, 35–46.
24 J. Ceponkus and B. Nelander, *J. Phys. Chem. A*, 2004, **108**(31), 6499–6502.
25 J. Ceponkus, G. Karlstrom and B. Nelander, *J. Phys. Chem. A*, 2005, **109**, 7859–7864.
26 J. Ceponkus, P. Uvdal and B. Nelander, *J. Chem. Phys.*, 2010, **133**(7), 074301.
27 J. Ceponkus, P. Uvdal and B. Nelander, *J. Phys. Chem. A*, 2010, **114**(25), 6829–6831.
28 J. Korppi-Tommola, *Spectrochim. Acta*, 1978, **34**, 1077–1085.
29 M. J. Frisch, G. W. Trucks, H. B. Schlegel, G. E. Scuseria, M. A. Robb, J. R. Cheeseman, G. Scalmani, V. Barone, B. Mennucci, G. A. Petersson, H. Nakatsuji, M. Caricato, X. Li, H. P. Hratchian, A. F. Izmaylov, J. Bloino, G. Zheng, J. L. Sonnenberg, M. Hada, M. Ehara, K. Toyota, R. Fukuda, J. Hasegawa, M. Ishida, T. Nakajima, Y. Honda, O. Kitao, H. Nakai, T. Vreven, J. A. Montgomery, Jr., J. E. Peralta, F. Ogliaro, M. Bearpark, J. J. Heyd, E. Brothers, K. N. Kudin, V. N. Staroverov, R. Kobayashi, J. Normand, K. Raghavachari, A. Rendell, J. C. Burant, S. S. Iyengar, J. Tomasi, M. Cossi, N. Rega, J. M. Millam, M. Klene, J. E. Knox, J. B. Cross, V. Bakken, C. Adamo, J. Jaramillo, R. Gomperts, R. E. Stratmann, O. Yazyev, A. J. Austin, R. Cammi, C. Pomelli, J. W. Ochterski, R. L. Martin, K. Morokuma, V. G. Zakrzewski, G. A. Voth, P. Salvador, J. J. Dannenberg, S. Dapprich, A. D. Daniels, O. Farkas, J. B.

Foresman, J. V. Ortiz, J. Cioslowski and D. J. Fox, *Gaussian09 Revision D.01*, 2009.
30 R. Ahlrichs, M. Baer, M. Haeser, H. Horn and C. Koelmel, *Chem. Phys. Lett.*, 1989, **162**, 165–169.
31 F. Furche, R. Ahlrichs, C. Haettig, W. Klopper, M. Sierka and F. Weigend, *Wiley Interdiscip. Rev. Comput. Mol. Sci.*, 2014, **4**, 91–100.
32 A. D. Becke, *J. Chem. Phys.*, 1993, **98**, 5648–5652.
33 S. E. S. Grimme, J. Antony and H. Krieg, *J. Chem. Phys.*, 2010, **132**, 154104.
34 C. Møller and M. Plesset, *Phys. Rev.*, 1934, **46**, 618.
35 K. Raghavachari and J. A. Pople, *Int. J. Quantum Chem.*, 1978, **14**, 91.
36 R. A. Kendall, J. T. H. Dunning and R. J. Harrison, *J. Chem. Phys.*, 1992, **96**, 6796–6806.
37 J. A. Pople, M. Head-Gordon and K. Raghavachari, *J. Chem. Phys.*, 1987, **87**, 5968.
38 T. B. Adler and H.-J. Werner, *J. Chem. Phys.*, 2011, **135**, 144117.
39 B. J. Ransil, *J. Chem. Phys.*, 1961, **34**, 2109.
40 S. F. Boys and F. Bernardi, *Mol. Phys.*, 1970, **19**, 553–566.
41 V. Barone, *J. Chem. Phys.*, 2005, **122**, 14108.
42 J. W. Moskowitz, Z. Bacic, A. Sarsa and K. E. Schmidt, *J. Chem. Phys.*, 2001, **114**, 10294.
43 A. Engdahl and B. Nelander, *J. Chem. Phys.*, 1987, **86**, 1819.
44 S. H. Bauer and R. M. Badger, *J. Chem. Phys.*, 1937, **5**, 837.

A.4 Spectroscopic identification of ethanol-water conformers by large-amplitude hydrogen bond librational modes

Reprinted with permission from
Spectroscopic identification of ethanol-water conformers by large-amplitude hydrogen bond librational modes
J. Andersen, J. Heimdal, and R. Wugt Larsen,
The Journal of Chemical Physics, accepted (2015)

Spectroscopic Identification of Ethanol-Water Conformers By Large-Amplitude Hydrogen Bond Librational Modes

[a]J. Andersen, [b]J. Heimdal and [a]R. Wugt Larsen*

[a]*Department of Chemistry, Technical University of Denmark, Kemitorvet 206, 2800 Kgs. Lyngby, Denmark*

[b]*MAX-IV Laboratory, Lund University, P. O. Box 118, 22100 Lund, Sweden*

November 22, 2015

The far-infrared absorption spectra have been recorded for hydrogen-bonded complexes of water with ethanol embedded in cryogenic neon matrices at 2.8 K. The partial isotopic H/D-substitution of the ethanol subunit enabled by a dual inlet deposition procedure enables the observation and unambiguous assignment of the intermolecular high-frequency out-of-plane and the low-frequency in-plane donor OH librational modes for two different conformations of the mixed binary ethanol/water complex. The resolved donor OH librational bands confirm directly previous experimental evidence that ethanol acts as the O···HO hydrogen bond acceptor in the two most stable conformations. In the most stable conformation the water subunit forces the ethanol molecule into its less stable *gauche* configuration upon dimerization owing to a cooperative secondary weak O···HC hydrogen bond interaction evidenced by a significantly blue-shift of the low-frequency in-plane donor OH librational band origin. The strong correlation between the low-frequency in-plane donor OH librational motion and the secondary intermolecular O···HC hydrogen bond is demonstrated by electronic structure calculations. The experimental findings are further supported by CCSD(T)-F12/aug-cc-pVQZ calculations of the conformational energy differences together with second-order vibrational perturbation theory (VPT2) calculations of the large-amplitude donor OH librational band origins.

Keywords

CH···O Hydrogen-Bonding, Ethanol-Water Complex, OH Librational Modes, Large-Amplitude Motion, Far-Infrared Spectroscopy, Neon Matrix Isolation

*Corresponding Author: rewl@kemi.dtu.dk

1. Introduction

A long-standing challenge for the physical sciences is to accurately describe how remarkable macroscopic properties of condensed phases, biological systems and materials emerge from the interplay between the different classes of non-covalent intermolecular interactions such as directional hydrogen bonding, long-range London dispersion interactions and short-range steric repulsion between molecules. These different classes of non-covalent interactions are both responsible for the thermodynamic anomalies associated with bulk liquid mixtures, the three-dimensional folding dynamics for biological macromolecules and the mechanical properties of many functional materials.

In the context of biological systems the interplay between multiple intermolecular organic hydrogen bond interactions ranging from weak O$\cdots$HC and $\pi\cdots$HO ($<$5–20 kJ$\cdot$mol^{-1}) to stronger classical O$\cdots$HO ($\sim$20–60 kJ$\cdot$mol^{-1}) hydrogen bonds often governs the functionality of many biological macromolecules as these directional intermolecular interactions are able to control the formation of specific enzyme-substrate complexes. For this reason mixed hydrogen-bonded molecular complexes involving the simplest flexible alcohols are particular interesting model systems since both strong intermolecular O$\cdots$HO hydrogen bonds and weak secondary intermolecular O$\cdots$HC hydrogen bond interactions are realized simultaneously. The binary mixed complex of the simplest flexible alcohol, ethanol, with water can be regarded as a prototypical target system which is still amenable to high levels of theoretical *ab initio* methodologies. This 1:1 ethanol/water complex has turned out to represent one of the simplest mixed hydrogen-bonded molecular complexes of a flexible subunit where the intermolecular hydrogen bond formation affects the internal conformational degrees of freedom. The isolated ethanol molecule exists both in a *trans* (denoted t) and in two enantiomeric *gauche* configurations (denoted g^+ and g^-) being $\approx$ 0.5 kJ$\cdot$mol^{-1} higher in electronic energy.[1–4] Upon complexation with water several studies have suggested that the ethanol molecule is forced into the less stable *gauche* configuration.

A sensitive and well-established spectroscopic probe for hydrogen-bonded molecular complexes is the vibrational OH-stretching manifold of the donor subunits[5,6] and a recent combined infrared and Raman investigation has monitored the donor OH-stretching spectral red-shifts for mixed 1:1 complexes of water with methanol and ethanol adiabatically cooled in supersonic jet expansions.[7,8] The vibrational assignments confirmed microwave molecular beam studies[9] that water acts as the hydrogen bond donor in the most stable conformations of both mixed alcohol/water complexes.[7] Based on the lower limit of the effective conformational temperature in the supersonic jet expansions of 10 K, the energy difference between the two most stable conformations of the mixed ethanol/water complex has been estimated to be higher than 0.2 kJ$\cdot$mol^{-1} from dedicated collisional relaxation experiments.[8] However, a recent microwave molecular beam work[9] has only identified the single conformation with ethanol as the hydrogen bond acceptor in the g^+ configuration and more experimental evidence has been welcomed to shed more light on this internal conformational isomerism issue.

In a recent work it was demonstrated how the strength, directionality and anharmonicity of mixed alcohol/water complexes can be probed more *directly* via the large-amplitude intermolecular donor OH librational modes. These direct spectroscopic observables detected in the challenging far-infrared spectral region between 300 and 600 cm^{-1} have been shown to enable an accurate characterization of the intermolecular potential energy landscape between the hydrogen bond partners.[10–13] Its nature as a localized motion of the donor hydrogen atom makes the high-frequency out-of-plane donor OH librational mode an excellent probe for the intermolecular hydrogen bond interaction in a similar fashion as the Badger-Bauer relationship associated with the bathochromic shift of the intramolecular donor vibrational OH-stretching mode.[14] A stronger intermolecular hydrogen bond results in a more hindered internal rotational motion and an increase of the band origin for this high-frequency hydrogen bond donor mode. In the mixed complexes of water with aliphatic alcohols these donor OH librational spectral signatures thus act as a measure of the hydrogen bond acceptor strength of the alcohol molecule. In the present work we demonstrate how the low-frequency in-plane donor OH librational mode of mixed ethanol/water complexes, essentially a hindered overall *c*-axis rotation of the water subunit, provides an excellent probe for the cooperative secondary O$\cdots$HC hydrogen bond interactions, which allows for a rigorous benchmarking of theory.

2. Experimental

A pre-cooled (77 K) gas flow of neon (L'Air Liquide, 99.999%) was deposited with a flow rate of 0.02 mol/h on a gold-plated oxygen-free high thermal conductivity (OFHC) copper mirror at 3.6 K inside an immersion helium cryostat (IHC-3) modified for matrix isolation spectroscopy.[13,15] The pre-cooling of neon significantly reduces the heat load on the copper mirror and enables a total deposition time of 1–2 hour per experiment. The pre-cooled neon gas flow was subsequently doped with "freeze-pump-thaw" purified C_2H_5OH (Sigma Aldrich, 99.9%) and H_2O (Milli-Q) samples and isotopically substituted C_2H_5OH-d1 (Sigma Aldrich, 99.0% D), C_2H_5OH-d6 (Sigma Aldrich, 99.0% D) and D_2O (Sigma Aldrich, 99.5% D) samples via separate inlet tubes with mixing ratios of $\simeq$0.5 to 5 permille. The combination of resistive heaters and feedback electronics was employed to maintain a stable mirror temperature at 2.8$\pm$0.1 K before and after the neon matrix depositions. The cold head was mounted with interchangeable CsI and polymethylpentene (TPX) windows and combined IR and THz single-beam sample spectra were collected by a Bruker IFS 120 FTIR spectrometer employing tungsten and globar lamps as the radiation sources. Liquid nitrogen cooled HgCdTe (broadband) and InSb detectors combined with Ge/KBr and CaF_2 beam splitters, respectively, were employed for the spectral region above 600 cm^{-1}. A Si-bolometer operating at 4.2 K combined with a 6 μm multilayer Mylar beam splitter was employed for the 30–650 cm^{-1} spectral region. In all experiments the doped neon matrices were annealed up to 9 K for the study of temperature effects. Single-beam background spectra were subsequently collected of the evacuated cryostat. A spectral resolution in the range from 0.1 to 1.0 cm^{-1} was selected depending on the observed band widths.

3. Vibrational Assignments for the Mixed Ethanol/Water Complex

Fig. 1 and 2 show selected spectral regions from a series of far-infrared absorption spectra (200–600 cm^{-1}) collected for several millimeter thick cryogenic neon matrices doped with pure water (H_2O:Ne)=(1:1700), pure ethanol (C_2H_5OH:Ne)=(1:1200) and different isotopically substituted ethanol/water mixtures (C_2H_5OH:H_2O:Ne)=(2:1:1700) at 2.8 K. In previous far-infrared matrix isolation studies of water embedded in neon the pure complexes of water have been explored extensively.[13,16–19] In the spectral region above 300 cm^{-1} the strong intermolecular high-frequency out-of-plane and low-frequency in-plane donor OH librational bands of the water dimer embedded in neon matrices have previously been assigned at 522.4 cm^{-1} and 309.1 cm^{-1} (Fig. 1), respectively.[16] The low-frequency donor in-plane OH librational band is slightly overlapped with the *c*-axis librational band of cyclic water trimer previously assigned at 310.8 cm^{-1}. In addition, a number of five combination bands have previously been observed for the cyclic water trimer where the strongest transitions have been assigned at 280.0, 386.8 and 414.1 cm^{-1}.[17]

The absorption spectrum of ethanol below 300 cm^{-1} has been widely studied by both experiment and theory owing to the *trans-gauche* isomerism and the proximity and the large vibrational amplitudes for the OH and CH_3 torsional motion of this molecule.[1,2,20–24] A previous work has addressed the complex asymmetric top-asymmetric frame internal rotation spectrum of the flexible ethanol monomer and cites the numerous previous microwave investigations employed to characterize the vibrational ground state and the conformational *trans-gauche* isomerism of ethanol.[22] We also refer to this comprehensive work for further details about the excited energy sub-levels of ethanol associated with the large-amplitude OH and CH_3 torsional degrees of freedom which has been complemented by far-infrared gas-phase absorption spectroscopy[1,21] and more recently by Raman jet spectroscopy.[23] The gas-phase absorption study assigned a single band observed at 202.6 cm^{-1} to the fundamental OH torsional transition of the *trans* conformation and two other bands observed at 195.8 and 243.1 cm^{-1} to the *gauche* conformation ($g^+ \leftarrow g^-$ and $g^- \leftarrow g^+$ transitions, respectively). The Raman jet study assigned two other bands observed at 199.1 cm^{-1} ($g^+ \leftarrow g^+$) and 240 cm^{-1} ($g^- \leftarrow g^-$).[23] The far-infrared absorption spectrum of ethanol embedded in cryogenic argon matrices has previously just revealed two strong transitions observed at 211 and 264 cm^{-1} besides the strong CCO bending fundamental transition at 416.5 cm^{-1}.[20] In the present far-infrared spectra of ethanol embedded in more inert cryogenic neon matrices, a series of weak, medium-intensity and strong bands are observed besides the strong CCO bending fundamental transition at 419.9 cm^{-1} (Fig. 1). A strong sharp transition appears at 208.9 cm^{-1} with two less intense shoulders observed at 206.5 cm^{-1} and 202.4 cm^{-1}. The spectra further reveal a broad medium-intense band at 287.4 cm^{-1}, a medium-intense band structure around 258 cm^{-1} and a weaker band structure around 243 cm^{-1}. These observed spectral features are in qualitative agreement with the coupled OH and CH_3 torsional sub-bands predicted previously from a two-dimensional *ab initio* Hamiltonian.[24] A more detailed interpretation of the observed spectral features is beyond the scope of the present work concerned with the donor OH librational modes of the mixed ethanol/water

complex. Both the partial and complete H/D substitution of ethanol red-shifts the disturbing torsional sub-band component at 287.4 cm^{-1} to below 200 cm^{-1} and thereby paves the way for the spectral region between 300 and 600 cm^{-1}.

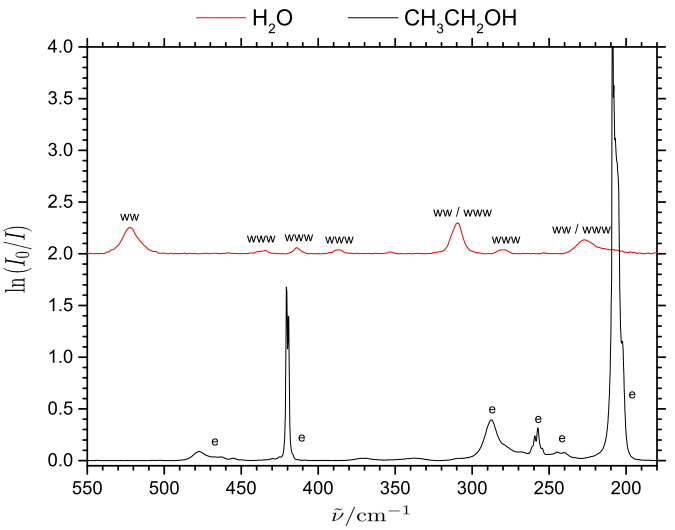

Figure 1: The observed far-infrared absorption spectra (200-550 cm^{-1}) of pure water and pure ethanol embedded in neon matrices at 2.8 K. The vibrational assignments for the ethanol monomer is denoted *e* and the vibrational assignments for the water complexes are denoted *ww* (dimer) and *www* (trimer), respectively.

The far-infrared spectra recorded for neon matrices doped with regular ethanol and regular water simultaneously at moderate concentrations reveal new distinct bands in the close vicinity to the high-frequency out-of-plane and low-frequency in-plane donor OH librational bands of water dimer. A weak band seems to emerge around 320 cm^{-1} on the shoulder of the in-plane donor OH librational band of water dimer at 309.1 cm^{-1} (Fig. 2, right insert). This spectral region is still affected by the broad torsional sub-band component of ethanol observed in the neon matrices at 287.4 cm^{-1}. In addition, a stronger and more distinct but somewhat broader band clearly emerges in the spectrum at 551.6 cm^{-1} for neon matrices doped with ethanol and water (Fig. 2, left insert). Both observed bands and in particular the latter band at 551.6 cm^{-1} are thus blue-shifted relative to the established donor OH librational transitions of the water dimer (Table 1). This observation supports the trend from the previous investigation of mixed binary complexes of water with methanol and *t*-butanol embedded in cryogenic neon matrices.[25] This previous work has established that water acts as the hydrogen bond donor in the most stable binary mixed complexes with methanol and *t*-butanol. This hydrogen bond

donor/acceptor relationship gives rise to similar out-of-plane and in-plane donor OH librational motions for the mixed alcohol/water complexes as observed for the donor subunit in the water dimer. The animated donor OH librational normal mode pictures are shown for the mixed ethanol/water complex in Fig. 3. The high-frequency out-of-plane donor OH libration can be described as a localized motion of the "bound" hydrogen atom. This localized mode turns out to be an excellent probe for the intermolecular hydrogen bond interaction[10,11,25] in the same way as the pronounced red-shift of the intramolecular donor OH-stretching mode. The observed high-frequency out-of-plane OH librational band origin of 551.6 cm^{-1} thus indicates a significantly stronger intermolecular hydrogen bond for the mixed ethanol/water complex than the corresponding mixed methanol/water complex having band origin of 527.5 cm^{-1} but a slightly weaker hydrogen bond than for the mixed *t*-butanol/water complex having a band origin of 556.6 cm^{-1}.[25] These preliminary and entirely spectroscopic interpretations about the relative hydrogen bond energies shall be supported with predictions from exploratory quantum chemical calculations in the theoretical section. A few other experimental studies for mixed water complexes with methanol and ethanol embedded in cryogenic matrices of nitrogen and argon have been reported in the literature.[26,27] In the most perturbing matrix environment of nitrogen a reversed hydrogen bond donor/acceptor relationship for the alcohol/water complexes has been observed although severe site effects blurred the observed spectral signatures. This has been explained by weak cooperative attractive interactions between the OH groups and the N_2 host molecules.[28] In the mixed complexes where the alcohol molecule acts as the hydrogen bond donor both dangling OH groups of the water acceptor subunit might interact with N_2 host molecules and thereby increasing the acceptor character of the O nuclei on the water molecule. This effect might strengthen the intermolecular interaction to the alcohol subunit and overcome the energy barrier between the different alcohol-water conformers.[28]

The dual inlet deposition procedure designed for partial isotopic H/D substitutions of the individual subunits enables the unambiguous identification of the proposed hydrogen bond donor/acceptor roles in the cryogenic neon environment. The H/D substitution on the water subunit introduces a significant red-shift from 551.6 cm^{-1} to 412.5 cm^{-1} which further confirms that water acts as hydrogen bond donor (Fig. 2, central insert). The observed OH/OD band origin ratio of 1.34 is rather close to the theoretical value of $\sqrt{2}$ expected for a genuine harmonic hydrogen motion and supports an assignment to the out-of-plane donor OD librational mode for the complex of D_2O with ethanol. This band origin is slightly larger than the corresponding donor OD librational band origin assigned previously at 397.6 cm^{-1} for the less stable mixed complex of methanol with D_2O embedded in neon.[25] The low-frequency in-plane donor OD librational mode is shifted into the congested spectral region belonging to the coupled OH and methyl torsional modes of ethanol making the assignment of this band difficult although a tentative assignment can be proposed at 239.6 cm^{-1} (not shown). A similar partial H/D substitution on ethanol deposited with regular water introduces solely a small red-shift of 6 cm^{-1} for the high-frequency donor OH librational band supporting the proposed hydrogen bond acceptor role of the ethanol subunit (Fig. 2, left insert). The far-infrared spectra for

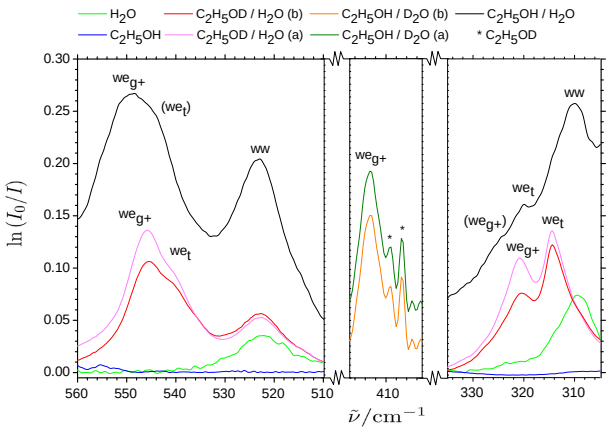

Figure 2: The observed far-infrared absorption spectra of pure water, pure ethanol and different isotopic ethanol/water mixtures embedded in neon matrices at 2.8 K before annealing b) and after annealing a) to 9 K in the spectral regions belonging to the out-of-plane OH (left), out-of-plane OD (center) and in-plane OH (right) donor librational modes. The proposed vibrational assignments for the mixed isotopic complexes of water (w) and ethanol (e) in the *trans* and *gauche+* conformations are denoted we_t and we_{g+}, respectively (see text), whereas the vibrational assignments for the water dimer is denoted *ww*. The asterisks denote traces of ethanol-d1 impurities.

ethanol-d1/water mixtures doped in neon, however, all seem to contain two distinct bands at 545.6 cm^{-1} and 541.1 cm^{-1} in this spectral region. These observations are supported by subsequent annealing experiments where the mirror temperature is raised to 9 K to allow the guest molecules to diffuse within the soft neon matrices. The annealing in particular favors the diffusion of the smaller water molecules in the soft neon matrices and the excess of ethanol should thereby trigger the formation of mixed ethanol/water complexes. The recorded post-annealing spectrum recorded after subsequent cooling to 3 K reveals a significant increase of both band intensities whereas the high-frequency out-of-plane donor OH librational band of water dimer at 522.9 cm^{-1} is almost unaffected by annealing (Fig. 2, left insert). The post-annealing intensity of the band observed at 545.6 cm^{-1} is significantly larger than the post-annealing intensity of the other band observed at 541.1 cm^{-1}. This observation suggests that these overlapped bands originate from two conformations of the mixed ethanol-d1/water complex with the band at 545.6 cm^{-1} assigned to the most stable conformation. The partial H/D substitution on the ethanol sample turns out to have an even more pronounced effect on the low-frequency

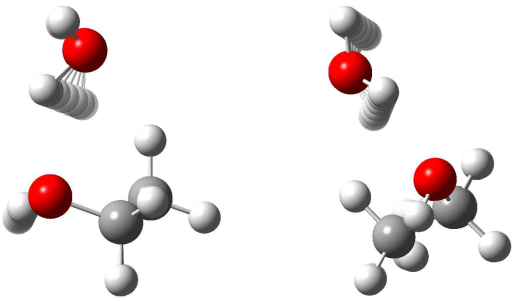

Figure 3: Normal mode pictures of the large-amplitude high-frequency out-of-plane (left) and low-frequency in-plane (right) donor OH librational modes of the most stable conformation of the mixed hydrogen-bonded ethanol/water complex (see text).

in-plane donor OH librational signature where two completely separated bands are observed at 320.9 cm^{-1} and 314.7 cm^{-1}, respectively (Fig. 2, right insert). The post-annealing spectra again reveal a changed relative intensity compared to the pre-annealing spectra. The more significant post-annealing intensity increase of the band observed at 320.9 cm^{-1} suggests an assignment to the most stable conformation of the mixed ethanol-d1/water complex. In the same fashion the complete H/D substitution on the ethanol sample enables the identification of two conformations of the mixed ethanol-d6/water complex with band origins red-shifted by less than 1 cm^{-1} relative to the ethanol-d1/water conformations (see Table 1). In order to shed further light on the proposed assignments and clarify the observation of two conformations of the ethanol-d1/water and ethanol-d6/water complexes, we consult exploratory electronic structure calculations.

5. Exploratory Quantum Chemical Calculations

The quantum chemical software packages Gaussian09 (Rev. D.01)[29] and Turbomole (ver. 6.6)[30,31] have both been employed for *ab initio* molecular orbital and supplementary density functional theory (DFT) calculations. The equilibrium geometries of the water and ethanol subunits and the different conformations of the mixed ethanol-water complexes were all optimized and the corresponding electronic energies calculated employing the canonical B3LYP level,[32] the dispersion-corrected B3LYP-D3 approach[33] and the second order Möller-Plesset MP2 methodology[34,35] coupled with Dunning's augmented correlation-consistent triple-zeta (aug-cc-pVTZ) and quadruple-zeta (aug-cc-pVQZ) basis sets.[36] The root-mean-square force

Table 1: The observed high-frequency out-of-plane and low-frequency in-plane donor OH (OD) librational band origins (cm^{-1}) for the water dimer and the two most stable isotopic complexes of water (w) and ethanol (e) in the *trans* (denoted we_t) and *gauche*$^+$ (denoted we_{g+}) conformations embedded in neon matrices at 2.8 K.

Donor-Acceptor	$\nu_{\text{lib,out-of-plane}}$	$\nu_{\text{lib,in-plane}}$	Donor-Acceptor	$\nu_{\text{lib,out-of-plane}}$	$\nu_{\text{lib,in-plane}}$
ww	522.4[a]	309.1[a]	w(d2)w(d2)	393.2[a]	233.5[a]
we_{g+}	551.6	324.7	w(d2)e_{g+}	412.5	239.6
we_t	(545.4)[b]	(320.4)[b]	w(d2)e_t	[c]	[c]
we_{g+}(d1)	545.6	320.9	w(d2)e_{g+}(d1)	[d]	238.2
we_t(d1)	541.1	314.7	w(d2)e_t(d1)	[c]	[c]
we_{g+}(d6)	545.6	320.9			
we_t(d6)	540.1	313.9			

[a] Ceponkus *et al.*[13]

[b] Tentative assignments due to strong overlaps with we_{g+}.

[c] Not observed.

[d] Overlap with the CCO bending mode of ethanol-d1.

criterion has been set to 10^{-6} (atomic units) for all the equilibrium geometry optimizations. The electronic energies for these optimized equilibrium geometries were subsequently calculated employing both the canonical and the explicitly-correlated coupled-cluster approaches with single and double with perturbative triple excitations, CCSD(T)[37] and CCSD(T)-F12,[38] in order to optimize the extent of electron correlation in combination with the same Dunning basis sets. The basis set superposition errors[39] have been accounted for by the counterpoise method of Boys and Bernadi.[40] The harmonic vibrational frequencies and overall vibrational zero-point energy (ZPE) contributions for the monomers and ethanol-water complexes have been calculated employing the doubly harmonic approximation whereas the anharmonic frequencies have been calculated using the vibrational second-order perturbation theory (VPT2) approach[41] as implemented in Gaussian09 (Rev. D.01).[29] In a series of calculations the secondary CH$\cdots$O hydrogen bond contact between the terminal CH on the ethanol subunit and the lone pair of the water subunit was kept fixed (Keyword=ModRedundant) in the geometry optimization in order to investigate the dependence of the donor OH-stretching and donor OH librational frequencies on this intermolecular CH$\cdots$O contact strength.

6. Discussion

6.1. Hydrogen-Bonded Conformations of the Mixed Ethanol/Water Complex

In line with previous theoretical predictions of the intermolecular potential energy landscape for the binary ethanol/water complex[7,9] five distinguishable conformations have been investigated. Fig. 4 illustrates the relative electronic binding energy D_0 calculated with the

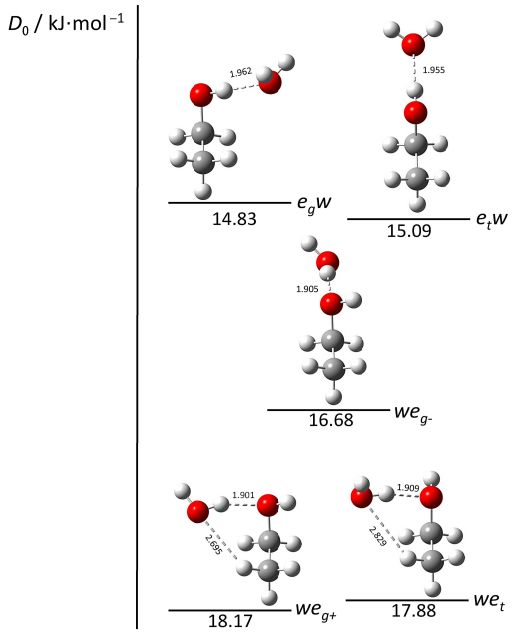

Figure 4: The intermolecular potential energy landscape including the most stable conformations of the mixed 1:1 complex of ethanol and water in terms electronic binding energy D_0 calculated employing the CCSD(T)-F12/aug-cc-pVQZ approach for the five most stable conformations optimized at the MP2/aug-cc-pVQZ level of theory (see text).

CCSD(T)-F12/aug-cc-pVQZ approach for these five most stable conformations optimized at the MP2/aug-cc-pVQZ level of theory. The changes of the harmonic vibrational zero-point energy upon complexation (ΔZPE) have been calculated at the MP2/aug-cc-pVTZ level of theory. This combined methodology is regarded as the benchmark level of theory as illustrated by the series of predictions of the electronic binding energy D_e for the most stable mixed complex of water with ethanol listed in Table 2. The listed predictions provide the results from combined quantum chemical methodologies employed for the geometry optimizations and subsequent single-point electronic energy calculations. These computations show that the canonical B3LYP functional[32] underestimates the binding energy D_e for the most stable mixed complex of water with ethanol by ca. 20% (5.5 kJ·mol^{-1}) whereas the B3LYP-D3 approach including Grimme and co-worker's dispersion corrections[33] slightly overestimate this binding

Table 2: The electronic dissociation energy D_e of the two most stable conformations of the ethanol/water complex (denoted we_{g+} and we_t) and the difference of electronic dissociation energy between the conformations $\Delta E_e = D_e(we_{g+})$–$D_e(we_t)$ predicted from combined quantum chemical methodologies for the geometry optimization and electronic energy calculations employing Dunning's augmented correlation-consistent triple zeta (aug-cc-pVTZ) and quadruple zeta (aug-cc-pVQZ) basis sets.

Optimization[a]	Electronic Energy	$D_e(we_{g+})$/ kJ·mol^{-1}	ΔE_e/ kJ·mol^{-1}
B3LYP/aug-cc-pVTZ	B3LYP/aug-cc-pVTZ	20.99	0.03
B3LYP-CP/aug-cc-pVTZ[b]	B3LYP/aug-cc-pVTZ	20.69	0.04
B3LYP-CP/aug-cc-pVTZ[b]	CCSD(T)/aug-cc-pVTZ	26.33	0.03
B3LYP-D3/aug-cc-pVTZ	B3LYP-D3/aug-cc-pVTZ	28.02	0.61
B3LYP-D3-CP/aug-cc-pVTZ[b]	B3LYP-D3/aug-cc-pVTZ	27.68	0.62
B3LYP-D3-CP/aug-cc-pVTZ[b]	CCSD(T)/aug-cc-pVTZ	27.96	0.48
MP2/aug-cc-pVTZ	MP2/aug-cc-pVTZ	27.27	0.36
MP2-CP/aug-cc-pVTZ[b]	MP2/aug-cc-pVTZ	24.52	0.37
MP2-CP/aug-cc-pVTZ[b]	CCSD(T)/aug-cc-pVTZ	27.46	0.54
MP2-CP/aug-cc-pVTZ[b]	CCSD(T)-F12/aug-cc-pVTZ	27.01	0.58
MP2/aug-cc-pVQZ	MP2/aug-cc-pVQZ	26.61	0.41
MP2-CP/aug-cc-pVQZ[b]	MP2/aug-cc-pVQZ	25.24	0.40
MP2-CP/aug-cc-pVQZ[b]	CCSD(T)/aug-cc-pVQZ	26.63	0.58
MP2-CP/aug-cc-pVQZ[b]	CCSD(T)-F12/aug-cc-pVQZ	26.50	0.56

[a] RMS force criterion set to 10^{-6} (atomic units) for all geometry optimizations

[b] CP = Counterpoise Correction applied

energy by ca. 5% (1.5 kJ·mol^{-1}) relative to the benchmark D_e-value of 26.5 kJ·mol^{-1}. This predicted electronic binding energy is significantly larger than the predicted binding energy for the mixed methanol/water complex but slightly smaller than the predicted binding energy for the *t*-butanol/water complex as expected.[25] The harmonic ΔZPE-correction of 8.3 kJ·mol^{-1} then translates this value into an absolute electronic binding energy D_0 of 18.2 kJ·mol^{-1} for the most stable conformation of the ethanol/water complex as shown in Fig. 2.

In the three most stable conformations the water subunit acts as the hydrogen bond donor. These three structures are denoted *we* whereas the remaining two structures having ethanol as the hydrogen bond donor are denoted denoted *ew*. In the three most stable forms having water as the hydrogen bond donor, not only the conformation (*trans* or *gauche*) of the ethanol subunit is relevant, but also the choice of the acceptor lone pair on ethanol. In the *gauche*$^+$ conformation the O-H bond is rotated clockwise by 120 degrees relative to the *trans* conformation in the perspective along the O-C bond employing a Newman projection. In the conformations of the mixed complex of ethanol with water as the hydrogen bond donor, a new asymmetric center emerges at the oxygen atom of the alcohol subunit due to the two

potential acceptor oxygen lone pairs and two potential enantiomeric conformations. Looking again along the O-C bond vector, the lone pair in a clockwise direction from the OH bond is denoted the right lone pair as shown in Fig. 4 in line with previous works.[7,9] In the case of two non-distinguishable enantiomeric conformations, we discuss the conformation where this right lone pair is engaged in the hydrogen bond. As illustrated in Fig. 4, the we_{g+} conformation with a hydrogen bond to the right lone pair of ethanol is predicted to be the most stable and compact conformation of the mixed ethanol/water complex at the benchmark level. In contrast to the third most stable we_{g-} conformation, the we_{g+} conformation is further stabilized by a cooperative secondary hydrogen bond interaction between the terminal CH group on ethanol and the oxygen lone pair on the water subunit with a contact distance predicted to 2.695 Å at the MP2/aug-cc-pVQZ level (see Fig. 4), although this weaker secondary interaction bends the primary O$\cdots$HO hydrogen bond slightly from a linear arrangement. In the most stable conformation the water subunit thus forces the ethanol hydrogen bond partner into its less stable *gauche* conformation upon complexation although the *trans* conformation is the most stable for an isolated ethanol molecule. This is considered as one of the most elementary cases together with hydroxyacetone[42] of adaptive aggregation, where a non-rigid molecule is forced into a less stable conformation upon non-covalent binding to a hydrogen bond donor molecule to optimize the mutual interaction energy. The second most stable conformation of the mixed complex having water as the hydrogen bond donor and the acceptor ethanol subunit in its *trans* configuration is also further stabilized by a cooperative secondary O$\cdots$HC contact. However, this secondary interaction is less strong with a contact distance predicted to 2.829 Å at the MP2/aug-cc-pVQZ level (see Fig. 4). The small difference of electronic dissociation energy between these two most stable conformations $\Delta E_e = D_e(we_{g+}) – D_e(we_t)$ listed in Table 2 seems to depend on the computational methodology. The canonical B3LYP approach predicts almost identical electronic dissociation energies whereas the dispersion-corrected B3LYP-D3 approach slightly overestimate this difference in the electronic dissociation energy relative to the benchmark CCSD(T)-F12/aug-cc-pVQZ value of 0.56 kJ·mol^{-1} for ΔE_e. The effect of the zero-point energy (ZPE) contributions and in particular the influence of the donor OH librational motion on the electronic dissociation energy must be considered before reaching any further conclusions.

6.2. Vibrational Zero-Point Energy Contributions

The change of vibrational ZPE upon intermolecular hydrogen bond formation is notoriously complicated to predict by quantum chemical methods in particular for the large-amplitude and highly anharmonic intermolecular hydrogen bond librational motions. In a previous combined jet and neon matrix isolation far-infrared study of methanol dimer, the similar high-frequency out-of-plane donor OH librational band was observed and assigned at 560 cm^{-1}.[12] This study reported an overall sum of anharmonic contributions to this out-of-plane donor OH librational fundamental transition in the order of 100 cm^{-1} by employing vibrational second-order perturbation theory (VPT2).[41] In the combination with the benchmark harmonic band origin of 660 cm^{-1} predicted at the LCCSD(T)-F12 level, the anharmonic predicted band origin of 560

Table 3: The electronic dissociation energy D_e (CCSD(T)-F12/aug-cc-pVQZ[a]), the total change of harmonic vibrational zero-point energy upon complexation ΔZPE (MP2/aug-cc-pVTZ) and the resulting absolute dissociation energy D_0 for the two most stable we_{g+} and we_t conformations of the mixed isotopic ethanol/water complex (units of kJ·mol^{-1}).

	we_{g+}	we_{g+}(d1)	we_{g+}(d6)	w(d2)e_{g+}
D_e	26.50	26.50	26.50	26.50
ΔZPE	8.33	8.21	7.96	6.68
D_0	18.17	18.29	18.54	19.82
	we_t	we_t(d1)	we_t(d6)	w(d2)e_t
D_e	25.94	25.94	25.94	25.94
ΔZPE	8.05	7.85	7.64	6.39
D_0	17.89	18.09	18.30	19.55

[a] Electronic dissociation energies D_e calculated at the CCSD(T)-F12/aug-cc-pVQZ level based on optimized geometries at the MP2/aug-cc-pVQZ level.

cm^{-1} turned out to be in excellent agreement with the experimental neon matrix findings. In a previous investigation of the mixed methanol/water complex, a similar anharmonic VPT2 analysis[41] at the MP2/aug-cc-pVTZ level also suggested anharmonicity contributions in the order of 15-20% for the corresponding high-frequency out-of-plane donor OH librational transition.[25] In this previous work standard vibrational frequency calculations at the MP2/aug-cc-pVTZ level provided harmonic band origins of 647 and 669 cm^{-1} for the high-frequency out-of-plane donor OH librational transitions for the mixed complexes of water with methanol and *t*-butanol, respectively.[25] The ordering of these harmonic values is in qualitative agreement with the previous experimental findings suggesting that similar harmonic predictions for the ethanol/water complex should fit into this picture. The harmonic calculations for the out-of-plane donor OH librational modes of the two most stable ethanol/water conformations at the MP2/aug-cc-pVTZ level indeed predict these band origins between 647 and 669 cm^{-1} as expected. However, the harmonic band origin for the most stable we_{g+} conformation is predicted at 654 cm^{-1} with the harmonic band origin for the less stable we_t conformation predicted at 660 cm^{-1} in contrast to our proposed experimental assignments based on evident annealing effects (see Table 1). An anharmonic VPT2 analysis at the MP2/aug-cc-pVTZ level, however, reverse the order of predicted band origins (549 cm^{-1} for the we_{g+} conformation and 543 cm^{-1} for the we_t conformation) and confirm anharmonicity contributions of 15-20%. A similar analysis of the low-frequency in-plane donor OH librational modes and the entire sets of large-amplitude intermolecular vibrational transitions for the non-rigid hydrogen-bonded ethanol/water complex would be to stretch the reliability of the VPT2 approach. Table 3 thus provides the harmonic vibrational ZPE contribution for mixed isotopic complexes of water with ethanol predicted at the feasible MP2/aug-cc-pVTZ level of theory.

The incorporation of the calculated vibrational ZPE contributions has a large impact as evidenced by the resulting absolute ground-state dissociation energies D_0 of the different we_t and we_{g+} conformations listed in Table 3. The total change of vibrational ZPE upon complexation accounts for between 6.4 and 8.3 kJ·mol^{-1} in the harmonic approximation depending on the isotopic substitutions and the hydrogen donor/acceptor roles. In terms of the the two most stable we_t and we_{g+} conformations the benchmark dissociation energy difference prediction $D_e(we_{g+})$–$D_e(we_t)$ of 0.56 kJ·mol^{-1} is translated into a smaller 0.28 kJ·mol^{-1} difference between the resulting absolute D_0-values. A smaller difference of 0.20 kJ·mol^{-1} between the resulting absolute D_0-values for the two most stable conformations of the ethanol-d1/water complex is predicted. These predictions help to explain the fact that both conformations are clearly observed in the far-infrared neon matrix isolation spectra recorded for ethanol-d1/water mixtures.

6.3. The Effects of Weak Secondary CH···O Hydrogen Bonding

A closer look at these two normal mode pictures reveals that whereas the out-of-plane donor OH librational mode exhibits an almost localized motion of the bound hydrogen atom almost independent of the dangling OH group on the water molecule, the in-plane mode donor OH librational mode can essentially be pictured as a hindered overall c-axis rotation of the water subunit. The latter large-amplitude in-plane OH librational motion of the entire water molecule is therefore expected to be affected more by the weaker secondary O···HC hydrogen bond interaction between the terminal CH group on ethanol and the oxygen lone pair on the water subunit. This has been observed previously for OH librational motion of hydroxy-group containing molecules in crystalline phases.[43] In a series of electronic structure calculations at the MP2/aug-cc-pVTZ level, the secondary O···HC hydrogen bond contact of the we_{g+} conformation has been kept as a fixed parameter in the geometry optimizations and subsequent harmonic force field calculations. The predicted harmonic band origins for the intramolecular donor OH-stretching band origin and the two intermolecular donor OH librational band origins versus the displacement R–R_e from the equilibrium value of the intermolecular CH···O hydrogen bond distance are shown in Fig. 5.

The predicted harmonic band origin of the intramolecular donor OH-stretching mode is lowered by less than 1.5 cm^{-1} when the O···HC hydrogen bond distance is shortened by 0.075 Å relative to the equilibrium configuration. This small predicted red-shift of the intramolecular OH-stretching band origin corresponds to a relative spectral shift of less than 0.05%. This almost non-existent dependence of O···HC contact is expected as this vibrational mode is highly localized into the intramolecular O-H bond of the water subunit involved in the primary OH···O hydrogen bond. The absolute harmonic band origin of the intermolecular large-amplitude out-of-plane donor OH librational mode, on the other hand, is predicted to increase by ca. 2 cm^{-1} when the secondary O···HC hydrogen bond distance is shortened by 0.075 Å. The relative blue-shift for this out-of-plane OH librational mode of 0.4 % confirms the nature of a highly lo-

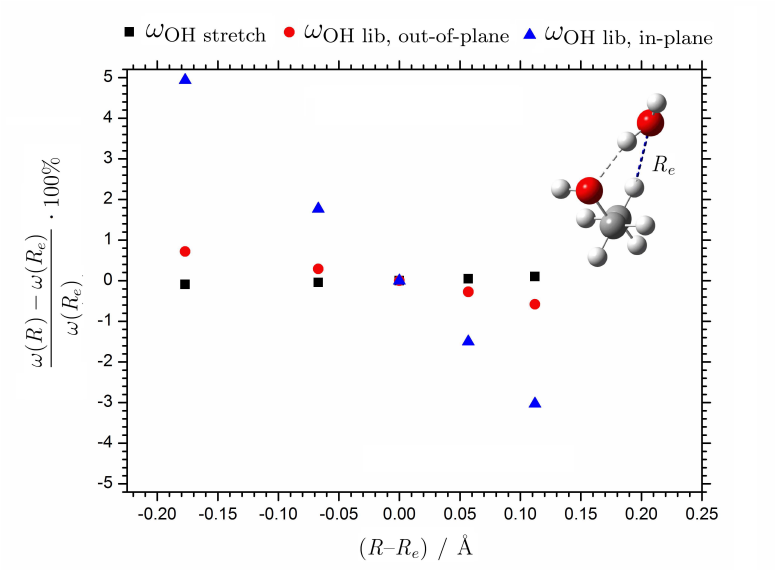

Figure 5: The predicted relative harmonic band origins (cm^{-1}) of the intramolecular donor OH-stretching mode (black squares) and the high-frequency out-of-plane (red circles) and low-frequency in-plane (blue triangles) donor OH librational modes at the MP2/aug-cc-pVTZ level as a function of the displacement R–R_e (Å) away from the intermolecular equilibrium O···HC hydrogen bond distance for the most stable we_{g+} conformation.

calized vibrational mode associated mainly with the primary intermolecular OH···O hydrogen bond. The intermolecular large-amplitude in-plane donor OH librational band origin, however, is predicted to depend much more significantly with the intermolecular O···HC hydrogen bond distance. The harmonic band origin of this hindered overall c-axis rotation of the water subunit is predicted to increase by ca. 7.5 cm^{-1} and thereby relatively blue-shifted by 2.5% when the O···HC interaction is shortened by 0.075 Å. This more significant dependence on the O···HC hydrogen bond distance supports the assumption that the large-amplitude in-plane donor OH librational mode involving the entire water subunit provides an excellent far-infrared spectroscopic probe for the secondary intermolecular hydrogen bond interaction. The proposed assignments of the bands observed at 320.9 cm^{-1} and 314.7 cm^{-1} to the we_{g+}-d1 and we_t-d1 conformations of the ethanol-d1/water complex, respectively, thus seem reasonable in view of the shorter secondary O···HC hydrogen bond distance in the most stable conformation.

7. Conclusions

The class of large-amplitude intermolecular donor OH librational modes for the mixed ethanol-water complex has been observed and unambiguously assigned in the challenging far-infrared spectral region enabled by a dual inlet neon matrix deposition approach and explorative electronic structure calculations. These far-infrared spectroscopic observables confirm *directly* electronic structure calculations showing that water acts as the hydrogen bond donor in the two most stable conformations of the mixed complex with ethanol. In the most stable and most compact we_{g+} conformation, electronic structure calculations predict that an intermolecular primary O$\cdots$HO hydrogen bond is formed between the water subunit and a lone pair of the oxygen atom on the ethanol subunit with a secondary cooperative hydrogen bond interaction between the terminal CH group on ethanol and the oxygen lone pair on water. In this most stable conformation the water subunit forces the ethanol hydrogen bond partner into its less stable *gauche* conformation upon complexation although the *trans* conformation is the most stable conformation for an isolated ethanol molecule. The second most stable we_t conformation of the mixed complex having water as the hydrogen bond donor and the acceptor ethanol subunit in its *trans* configuration is also further stabilized by a weaker intermolecular O$\cdots$HC hydrogen bond. Its nature as a localized motion of the "bound" hydrogen atom makes the high-frequency out-of-plane donor OH librational mode an excellent spectroscopic probe for the primary intermolecular O$\cdots$HO hydrogen bond energy in a similar fashion as the well-known Badger-Bauer relationship associated with the bathochromic shift of the intramolecular donor OH stretching band.[14] The low-frequency in-plane donor OH librational mode of the mixed ethanol/water complex, essentially a hindered overall *c*-axis rotation of the water subunit, has proven a valuable spectroscopic probe for the secondary intermolecular hydrogen bond interactions as supported by electronic structure calculations. The present findings thus indicate that these large-amplitude donor OH librational motions in general may be helpful for far-infrared spectroscopic detection of conformations for more complex biological systems where the interplay between multiple intermolecular organic hydrogen bond interactions defines the multidimensional conformational potential energy landscapes of the systems.

Supplemental Material

The calculated absolute electronic energies employing the B3LYP, B3LYP-D3, MP2, CCSD(T) and CCSD(T)-F12 methodologies with the aug-cc-pVTZ and aug-cc-pVQZ basis sets and the calculated harmonic vibrational zero-point energy corrections employing the MP2/aug-cc-pVTZ method are given as electronic supplemental material.

Acknowledgements

The authors acknowledge Center for Scientific and Technical Computing at Lund University (LUNARC) for the generous allocation of computational resources and the DTU Computing Center (DCC) for access to the High Performance Computing (HPC) services. RWL acknowl-

edges financial support from the Danish Council for Independent Research's Sapere Aude Programme (Grant Ref.: 12-125248).

References

[1] J. R. Durig and R. A. Larsen, *J. Mol. Struc.*, 1989, **238**, 195–222.

[2] J. C. Pearson, K. V. L. N. Sastry, E. Herbst, and F. de Lucia, *J. Mol. Spectrosc.*, 1996, **175**, 246–261.

[3] E. E. Fileti and S. Canuto, *Int. J. Quantum Chem.*, 2005, **104**, 808–815.

[4] E. E. Fileti, M. A. Castro, and S. Canuto, *Chem. Phys. Lett.*, 2008, **452**, 54–58.

[5] C. Cézard, C. A. Rice, and M. A. Suhm, *J. Phys. Chem. A*, 2006, **110**, 9839–9848.

[6] R. Wugt Larsen, P. Zielke, and M. A. Suhm, *J. Chem. Phys.*, 2007, **126**, 194307.

[7] M. Nedić, T. N. Wassermann, R. Wugt Larsen, and M. A. Suhm, *Phys. Chem. Chem. Phys.*, 2011, **13**, 14050–14063.

[8] M. Nedić, T. N. Wassermann, Z. Xue, P. Zielke, and M. A. Suhm, *Phys. Chem. Chem. Phys.*, 2008, **10**, 5953–5956.

[9] I. A. Finneran, P. B. Carroll, M. A. Allodi, and G. A. Blake, *Phys. Chem. Chem. Phys.*, 2015, **17**, 24210–24214.

[10] R. Wugt Larsen and M. A. Suhm, *J. Chem. Phys.*, 2006, **125**, 154314.

[11] R. Wugt Larsen and M. A. Suhm, *Phys. Chem. Chem. Phys.*, 2010, **12**, 8152–8157.

[12] F. Kollipost, J. Andersen, D. W. Mahler, J. Heimdal, M. Heger, M. A. Suhm, and R. Wugt Larsen, *J. Chem. Phys.*, 2014, **141**, 174314.

[13] J. Ceponkus, P. Uvdal, and B. Nelander, *J. Chem. Phys.*, 2008, **129**(19), 194306.

[14] S. H. Bauer and R. M. Badger, *J. Chem. Phys.*, 1937, **5**, 837.

[15] J. Andersen, J. Heimdal, D. W. Mahler, B. Nelander, and R. Wugt Larsen, *J. Chem. Phys.*, 2014, **140**, 091103.

[16] J. Ceponkus and B. Nelander, *J. Phys. Chem. A*, 2004, **108**(31), 6499–6502.

[17] J. Ceponkus, G. Karlstrom, and B. Nelander, *J. Phys. Chem. A*, 2005, **109**, 7859–7864.

[18] J. Ceponkus, P. Uvdal, and B. Nelander, *J. Chem. Phys.*, 2010, **133**(7), 074301.

[19] J. Ceponkus, P. Uvdal, and B. Nelander, *J. Phys. Chem. A*, 2010, **114**(25), 6829–6831.

[20] A. J. Barnes and H. E. Hallam, *Trans. Faraday Soc.*, 1970, **66**, 1932–1940.

[21] J. R. Durig, W. E. Bucy, C. J. Wurrey, and L. A. Carreira, *J. Phys. Chem.*, 1975, **79**, 988–993.

[22] J. C. Pearson, C. S. Brauer, and B. J. Drouin, *J. Mol. Spectrosc.*, 2008, **251**, 394–409.

[23] T. N. Wassermann and M. A. Suhm, *J. Phys. Chem. A.*, 2010, **114**, 8223–8233.

[24] M. L. Senent, Y. G. Smeyers, R. Dominguez Gomez, and M. Villa, *J. Chem. Phys.*, 2000, **112**, 5809–5819.

[25] J. Andersen, J. Heimdal, and R. Wugt Larsen, *Phys. Chem. Chem. Phys.*, 2015, **17**, 23761–23769.

[26] N. Bakkas, Y. Bouteiller, A. Loutellier, J. P. Perchard, and S. Racine, *J. Chem. Phys.*, 1993, **99**, 3335–3342.

[27] N. Bakkas, Y. Bouteiller, A. Loutellier, J. P. Perchard, and S. Racine, *Chem. Phys. Lett.*, 1995, **232**, 90–98.

[28] S. Coussan, P. Roubin, and J. P. Perchard, *J. Phys. Chem. A*, 2004, **108**, 7331–7338.

[29] M. J. Frisch, G. W. Trucks, H. B. Schlegel, G. E. Scuseria, M. A. Robb, J. R. Cheeseman, G. Scalmani, V. Barone, B. Mennucci, G. A. Petersson, H. Nakatsuji, M. Caricato, X. Li, H. P. Hratchian, A. F. Izmaylov, J. Bloino, G. Zheng, J. L. Sonnenberg, M. Hada, M. Ehara, K. Toyota, R. Fukuda, J. Hasegawa, M. Ishida, T. Nakajima, Y. Honda, O. Kitao, H. Nakai, T. Vreven, J. A. Montgomery, Jr., J. E. Peralta, F. Ogliaro, M. Bearpark, J. J. Heyd, E. Brothers, K. N. Kudin, V. N. Staroverov, R. Kobayashi, J. Normand, K. Raghavachari, A. Rendell, J. C. Burant, S. S. Iyengar, J. Tomasi, M. Cossi, N. Rega, J. M. Millam, M. Klene, J. E. Knox, J. B. Cross, V. Bakken, C. Adamo, J. Jaramillo, R. Gomperts, R. E. Stratmann, O. Yazyev, A. J. Austin, R. Cammi, C. Pomelli, J. W. Ochterski, R. L. Martin, K. Morokuma, V. G. Zakrzewski, G. A. Voth, P. Salvador, J. J. Dannenberg, S. Dapprich, A. D. Daniels, O. Farkas, J. B. Foresman, J. V. Ortiz, J. Cioslowski, and D. J. Fox, Gaussian09 Revision D.01, 2009.

[30] R. Ahlrichs, M. Baer, M. Haeser, H. Horn, and C. Koelmel, *Chem. Phys. Lett.*, 1989, **162**, 165–169.

[31] F. Furche, R. Ahlrichs, C. Haettig, W. Klopper, M. Sierka, and F. Weigend, *WIREs Comput. Mol. Sci.*, 2014, **4**, 91–100.

[32] A. D. Becke, *J. Chem. Phys.*, 1993, **98**, 5648–5652.

[33] S. E. S. Grimme, J. Antony and H. Krieg, *J. Chem. Phys.*, 2010, **132**, 154104.

[34] C. Møller and M. Plesset, *Phys. Rev*, 1934, **46**, 618.

[35] K. Raghavachari and J. A. Pople, *Int. J. Quantum Chem.*, 1978, **14**, 91.

[36] R. A. Kendall, J. T. H. Dunning, and R. J. Harrison, *J. Chem. Phys.*, 1992, **96**, 6796–6806.

[37] J. A. Pople, M. Head-Gordon, and K. Raghavachari, *J. Chem. Phys.*, 1987, **87**, 5968.

[38] T. B. Adler and H.-J. Werner, *J. Chem. Phys.*, 2011, **135**, 144117.

[39] B. J. Ransil, *J. Chem. Phys.*, 1961, **34**, 2109.

[40] S. F. Boys and F. Bernardi, *Mol. Phys.*, 1970, **19**, 553–566.

[41] V. Barone, *J. Chem. Phys.*, 2005, **122**, 14108.

[42] A. Sharma, I. Reva, R. Fausto, S. Hesse, M. A. Suhm, S. K. Nayak, R. Sathiskumar, R. Pal, and T. N. G. Row, *J. Am. Chem. Soc.*, 2011, **133**, 20194.

[43] S. Jarmelo, I. Reva, M. Rozenberg, M. Ramos Silva, A. M. Matos Beja, and R. Fausto, *J. Phys. Chem. B*, 2008, **112**, 8032–8041.

Appendix B

List of Chemicals

Table B.1: List of chemicals applied in this study

Chemical	Supplier	Purity
Neon	L'Air Liquide	99.999 %
Water-d_2	Sigma-Aldrich	99.5 %D
^{18}O - water	Sigma-Aldrich	99.0 % ^{18}O
Carbon dioxide	Matheson	99.9%
^{13}C-carbon dioxide	Sigma-Aldrich	99 % ^{13}C, <3 % ^{18}O
Ethylene	Matheson	99.95 %
Acetylene	Matheson	99.6 %
Methanol	Sigma-Aldrich	99.9 %
Methanol-d_1	Sigma-Aldrich	99.0 % D
Methanol-d_3	Sigma-Aldrich	99.8 % D
Methanol-d_4	Sigma-Aldrich	99.0 % D
t-butanol	Sigma-Aldrich	99.9 %
t-butanol-d_1	Sigma-Aldrich	99.0 % D
t-butanol-d_10	Sigma-Aldrich	99.0 % D
Ethanol	Sigma-Aldrich	99.9 %
Ethanol-d_1	Sigma-Aldrich	99.0% D
Ethanol-d_6	Sigma-Aldrich	99.0% D
Isopropanol	Sigma-Aldrich	99.9 %
Isopropanol-d_8	Sigma-Aldrich	99.0 %D
2,2,2-trifluoroethanol	Sigma-Aldrich	99.0 %

Appendix C

Non-Project Related Publications

Non-Project Related Publications

1. **Selective Synthesis of Clinoatacamite ($Cu_2(OH)_3Cl$ and Tenorite CuO Nanoparticles by pH control**, C. Engelbrekt, P. Malcho, J. Andersen, L. Zhang, K. Ståhl, B. Li, J. Hu and J. Zhang, *Journal of Nanoparticle Research, 16:2562 (2014)*

Patent Applications

1. **A Method for Effective Conversion of Saccharides to Furfural Compounds**, P. Malcho, J. Andersen, A. J. Kunov-Kruse, K. Ståhl, A. Riisager, and R. Fehrmann, *PCT/EP2014/064942*

The aim of the PhD thesis 'Far-Infrared Spectroscopy of Weakly Bound Hydrated Cluster Molecules' has been to investigate intermolecular interactions of prototypical medium sized molecular clusters by means of far-infrared and terahertz neon matrix isolation spectroscopy.

Department of Chemistry
Technical University of Denmark
Kemitorvet, Building 207
DK-2800 Kgs. Lyngby

www.kemi.dtu.dk